Optical properties of tin oxide

Reddaway, S. F.

Optical Properties of Tin Oxide

by

S.F. Reddaway

Department of Applied Physics,
Durham University

JANUARY 1968.

ACKNOWLEDGEMENTS

The author would like to thank his supervisor, Professor Wright, for his help and encouragement, and also the rest of the staff of the Applied Physics Department, especially Dr. Hearn for many helpful discussions. D.F. Morgan is thanked for cooperation, especially on some of the crystal growing. Dr. D.M. Eagles of the P.O. Research Department, Dollis Hill, London gave a lot of help with the theory.

The workshop staff under F. Spence are thanked for their willing help.

The author's present employers, English Electric Computers, are thanked for giving encouragement for the completion of the thesis.

Mrs. D. Pratt and Miss M. Johnson are thanked for doing most of the typing.

CONTENTS

Introduction

The programme of work for this thesis was originally to study the thermo-electric properties of SnO_2, with possible energy conversion applications in mind. The programme started in November 1962, with the only previous work at Durham on SnO_2 having been the demonstration a few months earlier of the feasibility of single crystal growth.

For about the first year the work followed three lines: crystal growing, conductivity measurements and optical transmission measurements. The latter was started to learn something of the band structure, and developed into being the main part of the work. The electrical measurements, which were not showing good results due to non-reproducibility, were taken over by another research student, D.F. Morgan, who also took over an increasing fraction of the crystal growing effort.

At the start of the work the literature on SnO_2 was not large, and consisted mostly of thin film work. This reflected the main applications of SnO_2 which had been as thin film resistors and transparent conducting films. It was probably the good conductivity of these (doped) films that led most authors in the literature, and ourselves at first, to too great a reliance on semi-conductor theory worked out for elemental and III-V semi-conductors, rather than theory developed for ionic materials such as the alkali halides. In our case this was probably reinforced by the semi-conductor orientation of the department, and it was only realised after about $2\frac{1}{2}$ years that polaron effects (which arise from the ionicity) are crucial to the interpretation of many of

the properties of SnO_2. Since starting the work many more papers on SnO_2 have been published, many of them on single crystals. During this period polaron theory, also, has made major advances which have facilitated the interpretation of several properties of SnO_2.

Compared with, say, silicon or germanium both the amount of work on, and the understanding of the properties of, SnO_2 is slight. As mentioned above, the ionicity of SnO_2 means that new theories, or strongly modified ones, are required, and so it is perhaps not surprising that much remains to be learnt about SnO_2. It is hoped that this thesis is a contribution to the understanding of SnO_2.

The organisation of the thesis is not perfect, partly due to the order in which the sections were actually written. The general layout, however, is that background theory is in chapter two, theory specifically developed for SnO_2 (this includes drawing on experimental results) is in chapter three, experimental methods are in chapter four, results are in chapter five, interpretation in chapter six and a short discussion in chapter seven. For some purposes it may be best to follow a topic from chapter to chapter; for example the absorption edge is considered in 2.5, 3.5, 5.1 and 6.1.

A more complete set of references to work on SnO_2 is contained in Morgan (1966 C).

2.1 Semi-conductor Theory

The basis of semi-conductor theory is the band theory of solids which is dealt with in many text books. There are two complementary ways of qualitatively understanding how the bands arise.

The first is the tight binding approach, in which the individual atoms in a solid are first considered to be separated by large distances. Each atom will then have its own electron levels; these levels have been extensively studied by means of optical and X-ray atomic spectra. As the atoms are brought closer together the energy levels become split by "resonance", i.e. the wave functions overlap slightly and electron states of the whole system can be formed by mixing the atomic wave functions with many different phase combinations. These differently mixed wave functions have slightly different energies. To take the simplest case, if two atoms with equivalent wave functions Ψ_A and Ψ_B are brought together to form a diatomic molecule then the two possible states, $\Psi_A + \Psi_B$ and $\Psi_A - \Psi_B$ will have different energies. The number of combined states in a solid of N identical atoms is N per original level, so each level has been broadened into a 'band' of N states. To be a true eigenstate of the system each wave must be orthogonal to all others; i.e. $\int \Psi_n \Psi_m d\underline{r} = 0$. Bloch showed in 1928 that for a large solid all states must have a periodicity, which can be characterised by a wave vector $\underline{k}$. The energy levels of the states are then usually thought of in $\underline{k}$ space. If the same states are not to be considered twice, $\underline{k}$ must be restricted to the first Brillouin zone. This is a region around $\underline{k} = 0$ on whose boundary the states $\underline{k}$ and $-\underline{k}$ are identical.

On a crystal axis this boundary is given by $k = \pm \frac{\pi}{a}$ where a is the lattice vector for that axis. The tight binding approach is most useful when the atomic electron overlap is not very large, such as for ionic solids and for the core electrons of all solids. These bands are fairly narrow, and for such bands a first approximation to the band shape in $\underline{k}$ space is a cosine wave with a period $\frac{2\pi}{a}$, for $\underline{k}$ along an axis. On this simplified picture $\underline{k}=o$ is a minimum, because the 'velocity' of the electron is zero. This model becomes more complicated when several atoms to a unit cell and degeneracy are considered. When the overlap is large, producing wide bands, mixing of different atomic states is very important.

The second approach is the "free electron" model. In this the electrons are first considered to be free particles in a large box. The wave functions are still periodic in nature and so can be represented in $\underline{k}$ space. They form a parabola centred on $\underline{k}=o$. If the electrons are not quite free but are moving in the periodic potential produced by the atomic cores, then the states for small $\underline{k}$ are not much affected. If, however, $\underline{k}$ is comparable to an integral multiple of $\frac{\pi}{a}$, then the electrons are "diffracted" by the lattice. It can be shown that the effect of this is to lower or raise the energy of the states according to whether $\underline{k}$ is just less or more than an integral multiple of $\frac{\pi}{a}$. The gradient of E is zero at these zone boundaries. This is shown in fig. 1. Gaps are thus created in the energy spectrum. The first gap occurs at the boundary of the first Brillouin zone, and, as mentioned above, states outside

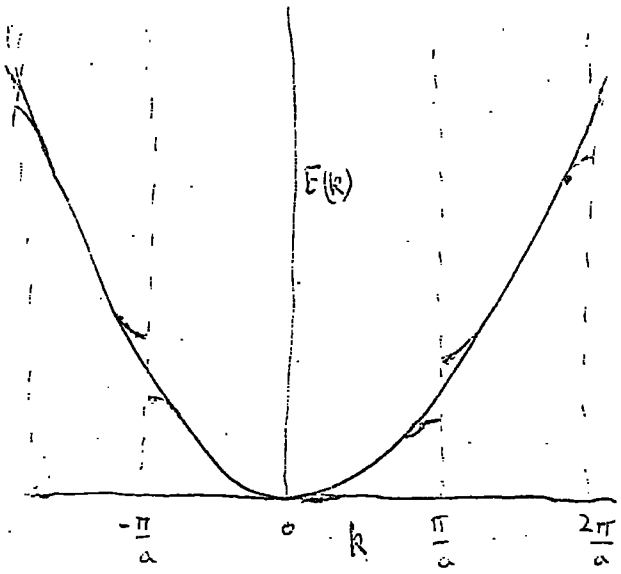

Fig 2.1.1.

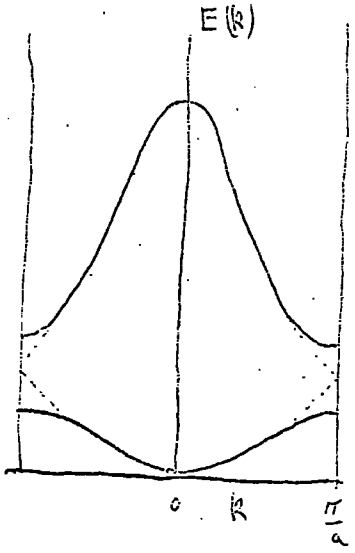

Fig 2.1.2.

this zone can also be represented inside it. This is achieved for $\underline{k}$ on an axis and $\frac{\pi}{a} < k \leq 2\frac{\pi}{a}$ by subtracting $\frac{2\pi}{a}$, and similarly for other states. The result is shown in fig. 2. It can be seen that a band maximum can occur at $\underline{k} = o$ (This is not so easy to show with the tight binding model).

We can now understand the difference between metals, insulators, semi-conductors and semi-metals. If there is an odd number of electrons per unit cell (not per atom), then the material is a metal. This is because if spin degeneracy is included each band holds 2N electrons, and so every band cannot be either completely full or empty.

If the number of electrons per unit cell is even, the material can still be a metal if the relevant bands overlap in energy. These materials are often referred to as semi metals. If, however, the material contains only full or empty bands, then it is either a semi-conductor or an insulator. More subtle distinctions between the two are possible, but the simplest is to consider materials with a large band gap as insulators and smaller band gaps as semi-conductors.

Two distinguishing features of semi-conductors are that especially for pure material the (low) conductivity rises rapidly with temperature, and that their electrical properties are very strongly dependent on small quantities of impurities. The reason for the latter can be seen most easily by considering a substitutional impurity which has one more electron and nuclear charge than the atom it replaces. The extra nuclear charge will cause bound states to be formed from the conduction band which will be situated in the forbidden gap. These states will somewhat resemble hydrogenic states except that the coulomb

attraction at large distances is modified by a dielectric constant of the material, and the electron does not have its free mass but an "effective" mass (see below). To maintain overall electrical neutrality there must be an extra electron in the vicinity. At low temperatures this is likely to be in the lowest bound state, but at higher temperatures it is likely to be "free". If there are several impurities these "free" electrons will drastically change the electrical conductivity and the absorption of light in the 1.R.

The term "effective mass" was mentioned above. In the free electron model, which can be applied most directly to atoms or ions with a band corresponding to the first electron outside a full shell of the periodic table, the first approximation is for the lowest minimum to have the free electron mass. The periodic potential of the cores may affect even that mass, and the minima due to the diffraction of electrons might well not even approximately have the free electron mass. It is, however, a general property that the minima and maxima are parabolic in shape. When this is so, an effective mass can be defined. This can be applied both to electrons near the bottom of an empty band and to "holes" near the top of a full band. In group IV and in III-V compounds bands are formed from electrons involved in covalent bonding. This situation is not well covered by either the free electron or tight binding models, and sometimes very small effective masses result.

The narrow bands that occur in the tight binding model correspond to large effective masses because of the shallow curvature.

It seems to be a fairly general property of valence bands that their maxima occur at (or near, if a centre of symmetry is absent) $\underline{k}=o$. The reason for this is not clear to the author, but it is presumed to apply in SnO_2 in this thesis.

Electrons obey Fermi-Dirac statistics because they belong to the class of particle that obey the exclusion principle. This states that each state can only be occupied by at the most one electron. (If spin is ignored the number is two). If the electron and hole effective masses are equal, then the probability of a state being occupied at the edge of the forbidden band in a pure semi-conductor is

$$\frac{1}{\exp\left(\frac{\pm Eg}{2kT}\right)+1} \quad ,$$

the + is for the conduction band and the - for the valence band. Eg is the band gap. It can be seen that if $Eg >> kT$ the probability of a conduction band state being occupied is very small and the probability of a velence band state not being occupied is equally small. Thus pure SnO_2 is expected to be a very poor conductor at normal temperatures, but as the temperature rises the conductivity should rise very rapidly. In practise impurity effects will mask this at lower temperatures.

2.2 Phonons

2.2.1 Basic Theory

Qualitatively phonons can be approached in several ways. One way is to consider a large crystal of N unit cells, and (as in SnO_2) 6 atoms to a unit cell. To describe the position of all the atoms would then require 18N independent coordinates. If the system is linear there will then be 18N normal modes of vibration, i.e. modes without coupling to any other modes and therefore with a definite frequency of vibration. These normal modes are not the motions of individual atoms because interatomic forces would couple them to their neighbours. Exactly what the normal modes are, depends on the details of the boundary conditions, but by arguing that the boundary conditions will only have a minor effect, special boundary conditions are assumed for mathematical convenience. Normal modes in the form of travelling waves are then obtained. Each of these waves has a wave vector, $\underline{k}$, and the density of modes in k space is uniform and proportional to N. The simplest types of mode are the acoustic modes, which form three sheets, or branches, in k space. (They are sometimes degenerate). The acoustic modes for small k are merely sound waves, and all the atoms in a unit cell move virtually as a body, with only slight overall compression or expansion. If certain symmetry conditions are met, of the 3 acoustic branches, two are transverse and one is longitudinal. A transverse mode has the atomic movement perpendicular to the direction of phase motion (i.e. the direction of $\underline{k}$) and a longitudinal mode has parallel motion.

As the value of $\underline{k}$ is increased for the acoustic modes, the wavelength, equal to $2\pi/k$, becomes comparable to a unit cell dimension. If $\underline{k}$ is along the a axis and equals $\frac{\pi}{a} + \varkappa$, then this mode turns out to be identical to the mode with k equal to $-\frac{\pi}{a} + \varkappa$. This makes the number of modes finite. The total number of acoustic modes turns out to be 3N. Other phonon branches exist however, and these in addition to the large scale motion indicated by $\underline{k}$ have a relative motion of atoms within the unit cell. Of course all motions of a particular mode have the same frequency, as this is a fundamental property of normal modes. The internal motion can only have $(6-1)x3 = 15$ independent vairables; the -1 corresponds to the position of a reference point and can be thought of as the acoustic mode. Each motion can be associated with any value of $\underline{k}$, so these 15"optical" branches complete the 18N modes. (The motions may gradually change with changing $\underline{k}$). An important property of these 15 branches is that because of the internal motion they have a fixed non-zero frequency around $\underline{k} = o$, whereas the acoustic modes tended linearly to zero.

In many respects the phonon branches are like electron bands in the band theory of solids. As in that theory, generally the branches become horizontal at the edge of the first Brillouin zone. This means, e.g., that at the energy where this flattening occurs, there is a certain type of discontinuity in the phonon density of states function against energy. In simple cases the optical branches are comparatively flat, i.e. cover a relatively small

frequency range. In many theories they are assumed to be flat.

A lot can be learnt by a study of the symmetry properties of optical phonons. The 15 optical branches can each be given a symmetry type in group theory. From this it can be shown e.g. that only certain branches couple with I.R. radiation of the correct energy. (Each normal mode is of course quantised in units of $\hbar\omega$). Also in certain symmetry conditions a branch, or part of a branch, can be classified as transverse or longitudinal. If this can be done for all branches for a particular polarisation, then there are two transverse branches for every longitudinal branch. When this can be done, the transverse branches are degenerate because the phase variation being perpendicular to the polarisation results in there being no depolarising field. The frequency of these branches is determined by atomic force constants. A condition for pure (I.R. active) longitudinal phonons is that the dielectric constant should equal zero. This condition is particularly useful when there are several I.R. active phonons, and is the basis of the phonon analysis used in 3.2.

2.2.2 Statistics

Phonons obey Bose - Einstein statistics, because any number of phonons can occupy a particular state. The phonon occupation number is thus

$$n = \frac{1}{\exp(\hbar\omega/kT)-1}$$

2.2.3 Harmonic Approximation

If the system is not linear, i.e. the harmonic approximation is not valid classicly, the natural vibration frequencies depend on the amplitude of the vibration. This was studied by Cowley (1963) in the alkali halides, and shown to have a considerable smearing effect on phonon frequencies and to produce some absorption in quite new parts of the spectrum. These effects are tentatively suggested as the cause of some phenomena discussed in 3.2.

2.3 Optical Constants

2.3.1 Basic Constants

There are several different optical constants which are used to describe the optical properties of a substance. Some of them are: the relative dielectric constant ϵ, the conductivity σ, the complex refractive index $\underline{n} = \underline{n} - ik$, the absorption coefficient K, the reflection coefficient R. All of them depend on the angular frequency ω, (or the free space wavelength λ), and there are certain relationships between them. In this section we shall derive some of these relationships, and give some properties of simplified models for dealing with phonon absorption. Anisotropy will also be dealt with.

From the electromagnetic point of view the basic constants are ϵ and σ. For isotropic media they are simply scalars, but for anisotropic media they are tensors. The solutions of Maxwell's equations are given in many books, and the result of looking for a plane wave solution of the form

$$V_x = V_o e^{i\omega(t - \frac{x\underline{n}}{c})}$$

(where V stands for either the electric or the magnetic field and c is the velocity of light in vacuo) is to obtain $(\underline{n})^2 = \mu\epsilon - i\sigma\mu/\omega\epsilon_o$ $(=(n - ik)^2)$, (2.3.1)

where μ is the relative permeability (almost = 1 in most materials) and ϵ_0 is the dielectric constant of free space. Here ϵ is real, but in some cases a complex $\underline{\epsilon}$ is used with an imaginary part equal to $-\frac{\sigma}{\omega \epsilon_0}$, and then $(\underline{n})^2 = \mu\underline{\epsilon}$.

From (1) we obtain

$$n^2 - k^2 = \epsilon \qquad 2nk = \sigma/\omega\epsilon_0 \qquad (2.3.2)$$

where we have put $\mu = 1$. k is sometimes known as the absorption index. (2.3.2) can be solved for n and k in terms of ϵ, σ and ω. In frequency ranges where k is small, $n^2 \rightarrow \epsilon$.

Absorption measurements most conveniently measure the absorption coefficient, K, defined as the reciprocal of the distance in which the energy in the wave falls by a factor of e. K is related to k by

$$K = \frac{2\omega k}{c} = \frac{4\pi k}{\lambda}$$

2.3.2 Reflection

Reflection is important in absorption experiments, interference experiments and is specifically measured to help obtain optical constants in highly absorbing regions.

The reflection and transmission coefficients for energy are usually represented by R and T, and for amplitude by r and t where r and t may be complex. $R = rr^*$ and $T = tt^*$ where * means complex conjugate. Reflection coefficients may be found by applying appropriate boundary conditions. We are mostly concerned with surfaces than are normal to the travelling waves, and for this case for a single surface between two media, one of which is free space, we have

$$R = \frac{(n-1)^2 + k^2}{(n+1)^2 + k^2} \qquad (2.3.3)$$

If the free space is replaced by a non-absorbing media of index n^1,

then n and k in (2.3.3) must be divided by n^1. For two absorbing media the expression is more complicated. (2.3.3) forms a family of circles of constant R on an n versus k graph, and these are drawn on p.6 of Moss (1961).

2.3.3 Interference

Because light is composed of electromagnetic waves which possess phase as well as magnitude, two or more waves can interfere, that is increase or reduce intensity depending on their phase relationship. It is the electric and magnetic fields which add or substract, and the energy, (or intensity), varies as the square of the field amplitudes. It follows that, e.g., two waves when interfering can have four times the intensity of a single one.

Two or more wavefronts coincide when light is passed through a medium with two paralled surfaces. We are most interested in the simple case when there is air on both sides. Let the amplitude reflection coefficient for a single surface for light passing out of the medium be γ_1, and the transmission coefficient be t_1. Let the corresponding coefficients for light passing into the medium be γ_2 and t_2, and let the total reflection and transmission coefficients of the film as a whole be γ and t. Because of boundary conditions we have

$$\gamma_1 = -\gamma_2 = \frac{n-1}{n+1}, \quad t_1 = 1 + \gamma_1, \quad t_2 = 1 + \gamma_2 = 1 - \gamma_1$$

The phase change on one traversal of the film is

$$\delta = \frac{2\pi}{\lambda} nd \cos\varphi$$

where d is the thickness of the medium and φ is the angle of incidence. Therefore r and t can be obtained as an infinite series, which can then be summed. Hence for a non-absorbing film

$$r = -r_1 + t_1 t_2 r_1 e^{-2i\delta} + t_1 t_2 r_1^3 e^{-4i\delta} + \ldots$$

$$= -r_1 + \frac{(1-r_1^2) r_1 e^{-2i\delta}}{1 - r_1^2 e^{-2i\delta}}$$

and similarly

$$t = \frac{(1-r_1^2) e^{-i\delta}}{1 - r_1^2 e^{-2i\delta}}$$

The energy coefficients are

$$T = tt^* = \frac{(1-r_1^2)^2}{1 + r_1^4 - 2 r_1^2 \cos 2\delta} \qquad 2.3.4$$

$$R = 1 - T$$

It can be seen that if $\delta = N\pi$ (i.e. $2nd\cos\varphi = N\lambda$) then $T_{max} = 1$. If $\delta = (N+\frac{1}{2})\pi$, $T_{min} = \frac{(1-r^2)}{(1+r^2)}$. If $2r_1^2 \ll 1$, (2.3.4) T varies approximately sinusiodally with λ^{-1}, but otherwise the peaks are sharp and narrow and the valleys are broad, flat and with small T. In SnO_2 $n \approx 2$, so $r_1 = \frac{1}{3}$, $T_{min} = .64$ and the sinusoidal approximation is fair. An interesting indication of how good the

approximation is, is obtained by looking at the average transmission for unresolved fringes. This is $\frac{1-\gamma_1^2}{1+\gamma_1^2}$, and for n = 2 this equals 0.8, while

$\frac{T_{max}+T_{min}}{2} = 0.82.$

With anisotropic crystals the incident light is best thought of as being resolved into two components with polarisations perpendicular to each other and related to the optic axes of the crystal. These two components can then be considered to produce independent interference patterns whose intensities are finally added together. The only exception to this occurs when some optical anisotropy occurs in the path of the light after the crystal, in which case a new set of optic axes may be defined and the two original components may interfere. An example of this was observed and is discussed in 4.7.

2.3.4 Interference Including Absorption

Absorption can be allowed for by making δ complex, e.g. $\delta + i\beta$, where $\beta = \frac{1}{2} Kd = 2\pi kd/\lambda$.

We now obtain

$$T = tt^* = \frac{(1-\gamma_1^2)(1+k^2/n^2)}{(e^{\beta} - \gamma_1^2 e^{-\beta})^2 + 4\gamma_1^2 \sin^2(\delta+\Psi)} \qquad 2.3.5$$

where $\tan \Psi = \frac{2k}{n^2 + k^2 - 1}$

If $k \ll n$, the fringe contrast, $\frac{T_{max}}{T_{min}}$, is $\left(\frac{1+\gamma_1^2 e^{-2\beta}}{1-\gamma_1^2 e^{-2\beta}}\right)^2$, and

if $\gamma_1^2 \ll 1$, this $\simeq 1+4\gamma_1^2 e^{-2\beta}$. If n is known this can provide a check on K and vice versa. If the fringes are not resolved (2.3.5) averages out to

$$\frac{(1-r_1^2)^2\,(1+k^2/n^2)\,e^{-Kd}}{1-r_1^4 e^{-2Kd}} \qquad (2.3.6)$$

Generally $k << n$ for absorption experiments, and often $R^2 e^{-2Kd} << 1$, In that case (2.3.6) becomes $(1-r_1^2)^2\ e^{-Kd}$. However the denominator in (2.3.6) can significantly affect calculations, and we retained it for our data analysis.

2.3.5 Dispersion Theory

Quantum mechanical treatments (e.g. Nozieres and Pines 1958) show that classical dispersion relations can be retained with only minor changes in interpretation. These dispersion relations show that optical constants are not as independent of each other as might be imagined.

The classical treatment starts by considering a bound electron oscillating about its equilibrium position with a natural frequency ω_o and with damping represented by g. By solving the equation of motion, the complex dielectric constant is found to be

$$(n-ik)^2 = \frac{Ne^2/m\epsilon_o}{\omega_o^2-\omega^2+i\omega g} + 1 \qquad (2.3.7)$$

where N is the density of electrons, m the electron mass and e the electron charge. (2.3.7) yields

$$n^2-k^2-1 = (Ne^2/m\,\epsilon_o)\,\frac{(\omega_o^2-\omega^2)}{(\omega_o^2-\omega^2)^2+\omega^2 g^2} \qquad (2.3.8)$$

$$\text{and } 2nk = (Ne^2/m\epsilon_o)\,\frac{\omega g}{(\omega_o^2-\omega^2)^2+\omega^2 g^2} \qquad (2.3.9)$$

Several oscillators lead to a sum of similar terms with different ω_o, and in quantum mechanics there are an infinity of such terms because "fractions of an electron are allowed". Each

oscillator corresponds to an allowed transition. The I.R. lattice phonon spectrum of an ionic solid is represented quite well by a sum of such terms, with one term for each I.R. active phonon brandh, together with a term to represent the electronic absorption. The latter plus unity will approximate to ϵ_∞, loosely defined as what the dielectric constant would be at zero frequency if the lattice absorption did not exist.

The contribution of each oscillator to the static dielectric constant is

$$Ne^2 f/m\epsilon_o w_o^2 \qquad (2.3.10)$$

where f is the factor, known as the oscillator strength, inserted to allow for "fractions of an electron", or in the case of the I.R. phonon spectrum it is an indication of the polarisation associated with the particular optical phonon involved. (2.3.10) is also known as $4\pi\rho$ in work dealing with the analysis of I.R. phonon spectra (e.g. in 5.6).

Moss (1961) derives a number of properties of (2.3.8) (with $\epsilon_\infty - 1$ added to the R.H.S.) and (2.3.9). These properties are of varying applicability in SnO_2, one of the causes of trouble being the multiplicity of optically active phonons. Two of the properties are:-

(i) ω_o is the frequency for which $2nk\omega$ (the conductivity) is a maximum.

(ii) The maximum of k, which is more likely to be measured than $2nk\omega$, is at a frequency ω given approximately by $\omega - \omega_o = 0.29g$.

Moss should be consulted for further details. Even though in SnO_2 the situation in the majority of cases is too complicated to use many of these properties in accurate work, they help build up a qualitative picture.

By generalising (2.3.8) and (2.3.9) to an infinity of oscillators, and performing some mathematical manipulation, it can be shown in general that if just one "optical" parameter of an isotropic substance is known at all frequencies, then all the others can be derived. Intuitively this result is somewhat surprising because at any one frequency two "optical" constants are required to define the "optical" properties. Moss (1961) derives a number of such relations. Perhaps the simplest and most useful is that between refractive index at any particular frequency and absorption at all frequencies:

$$n_a - 1 = \frac{1}{2\pi^2} \int_0^\infty \frac{Kd\lambda}{1-(\lambda/\lambda_a)^2} \qquad (2.3.11)$$

where n_a is the refractive index at a wavelength λ_a. In practise an integration is only required over a comparatively small frequency range. Relations such as (2.3.11) can be used e.g. with I.R. phonon absorption data to give an idea of the oscillator strength of that phonon branch.

2.3.6 Anisotropy and Dispersion Theory

Anisotropic crystals have differing I.R. phonon spectra for different polarisations. In this region, in contrast to the visible, very large anisotropy can exist, because for a classical oscillator whose damping tends to zero, optical constants tend to 0 or ∞ at certain frequencies.

For light directed along an axis of a uniaxial crystal, the situation is easily understood. If the axis is the c axis the two possible polarisations are degenerate and the spectrum shows the properties of perpendicular polarisation. If the axis is the a (or b) axis, the light is split into two components polarised parallel to the b (or a) and c axes respectively. The resulting spectrum is the sum of the spectra due to the two components.

In a uniaxial crystal there are only the two independent spectra, and for polarisation not parallel to an axis the optical properties can be derived from the optical properties of the two indepeendent directions (the optic axes). Obtaining the properties of spectra involving propagation not along an axis has led to some confusion, as different approaches appear to give differing results. The question is fairly important, because some important data for SnO_2 are transmission spectra on films (presumed to be without special orientation) and reflection spectra on material of uncertain orientation.

The work of Cochran and Cowley (1962) and Cochran (1965) indicate that whatever the direction of the light wave, the only dispersion (resonance) frequencies (i.e. ω_o in (8) and (9), or the frequency for which 2nk becomes large) are the basic dispersion frequencies which show up for polarisations along an axis. These frequencies are related to the inter-atomic forces.

On the other hand standard optics text books appear to contradict this. Born and Wolf (1965) equ 14.3.4, extended to include absorption by 14.6.9, shows that one polarisation is always the standard ordinary wave, but the other has optical properties given by

$$\frac{1}{\underline{\epsilon}} = \frac{\cos^2\theta}{\underline{\epsilon}_\perp} + \frac{\sin^2\theta}{\underline{\epsilon}_{//}}$$

where ϵ is the complex dielectric constant of a wave whose wave normal makes an angle θ with the c axis. It can be seen that when $\underline{\epsilon}_\perp$ or $\underline{\epsilon}_{//}$ are large, $\underline{\epsilon}$ is mainly determined not by the large one but the small one. Resonance for $\underline{\epsilon}$ therefore does not occur at the same frequencies as for $\underline{\epsilon}_\perp$ or $\underline{\epsilon}_{//}$. Because the real part of $\underline{\epsilon}_\perp$ or $\underline{\epsilon}_{//}$ can be negative, resonances of $\underline{\epsilon}$ can occur, but at frequencies dependent on θ .

A third approach is given by Loudon (1964) who studied the phonon spectrum. The absorption at resonance can be viewed as the creation of a (partly) transverse phonon. In a uniaxial crystal in which there is a single optically active phonon for both parallel and perpendicular polarisations, Loudon obtained for the phonon frequencies

$$\omega = \omega_\perp \quad \text{ordinary phonon}$$

and the solutions of $$\left(\frac{\omega_{//}^2 \epsilon_{s//} - \omega^2 \epsilon_{\infty//}}{\omega_{//}^2 - \omega^2}\right)\cos^2\theta + \left(\frac{\omega_\perp^2 \epsilon_{s\perp} - \omega^2 \epsilon_{\infty\perp}}{\omega_\perp^2 - \omega^2}\right)\sin^2\theta = 0 \qquad (2.3.12)$$

for the extraordinary phonons. $\omega_{//}$ and $\omega_{\perp}$ are the respective resonant frequencies and ϵ_s and ϵ are the low frequency and high frequency dielectric constants respectively. The two extraordinary phonons are in general both partly transverse and partly longitudinal, and so should both interact with light. The solutions of (2.3.12) vary with θ so they appear to contradict Cochran and Cowley. An exception to this which is of importance in SnO_2 is when a phonon is optically active for one polarisation but not for the other. In this case we effectively have $\epsilon_{s//} = \epsilon_{//}$ in (12). The "extraordinary phonon" solutions then become $\omega = \omega_{//}$ (which is presumably purely transverse) and

$$\omega = \omega_{\perp} \left(\frac{\epsilon_{//} \cot^2 \theta + \epsilon_{s\perp}}{\epsilon_{//} \cot^2 \theta + \epsilon_{\perp}} \right)^{\frac{1}{2}} \qquad (2.3.13)$$

(which is presumably purely longitudinal). (2.3.13) varies continuously from $\omega_{\perp}$ to $\omega_{\perp} \sqrt{\frac{\epsilon_{s\perp}}{\epsilon_{\perp}}}$ as θ varies from 0 to $\pi/2$. This would appear to agree with Cochran and Cowley and disagree with Born and Wolf.

The apparent differences in the results of these approaches would presumably be resolved by a very close examination of precisely what situation each theory is referring to. In SnO_2 these problems are most important when the condition described at the end of the last paragraph applies. In this situation it is assumed later that resonance only occurs at the resonances for polarisation parallel to an axis. It is also assumed that the longitudinal phonon frequencies (ω_L), which essentially occur when $\epsilon = o$, vary with the direction of the wave. This seems the most reasonable assumption, because the transverse phonon frequencies, ω_T, are essentially determined by atomic forces, while the ω_L are displaced from the ω_T because of long range coulomb forces. The steep increase in the reflection spectrum occurs around ω_L.

2.4 Free Carrier Absorption

2.4.1 Classical Theory

The classical formula for free carrier absorption can be obtained by considering free electrons as the limiting case of bound electrons as the natural frequency tends to zero. We now obtain a pair of equations similar to (2.3.8) and (2.3.9) but with $\omega_o = 0$. We get

$$n^2-k^2 = -\frac{Ne^2/m\epsilon_o}{\omega^2+g^2} + \epsilon \qquad (2.4.1)$$

$$2nk = \frac{gNe^2/m\epsilon_o}{(\omega^2+g^2)\omega} \qquad (2.4.2)$$

g (which equals $1/\tau$ where τ is a mean time between collisions) can be related to the mobility, μ, by $g = e/\mu m$ and so (2.4.2) becomes

$$2nk\omega = \frac{Ne\mu}{\epsilon_o(1+(\omega/\mu m/e)^2)}$$

For electrons in SnO_2 in the near I.R. $\omega/\mu m > e$, so we get

$$\frac{2k\omega}{c} = K = \frac{\lambda^2 e^3 N}{4\pi^2 c^3 n m^2 \mu \epsilon_o}$$

This is the well known result that K varies as λ^2.

From (2.4.1) we can derive what is known as the plasma frequency, i.e. the frequency for which $n^2-k^2 = 0$. It is similar to ω_L for lattice absorption and shows the same sharp rise in reflectivity. If $g \ll \omega$, it is

$$\omega_p = \sqrt{\frac{Ne^2}{m\epsilon\epsilon_o}} \qquad (2.4.3)$$

(2.4.3) has been calculated purely from classical concepts. An additional

assumption was that the lifetime, τ , was independent of energy. The classical approach can be extended a little farther by assuming $\tau \propto E^{+p}$ where E is the electron energy and p is a constant depending on the scattering mechanism. If this is done, and the carriers are not degenerate, a mathematical constant factor has to be inserted into (3). In some circumstances, discussed below, for optical phonon scattering $p = +\frac{1}{2}$ and the constant factor is 1.13. For ionised impurity scattering $p = +\frac{3}{2}$ and the factor is 3.4.

For optical phonon scattering (in the continuum approximation) the electron-phonon interaction varies as $\frac{1}{k^2}$ where k is the phonon wave vector. If the energy, E, of an electron is large compared with the optical phonon energy, then the average phonon wave vector for phonon absorption or phonon emission varies as $E^{\frac{1}{2}}$ and the density of states varies as $E^{\frac{1}{2}}$. The probability of scattering therefore varies as $E^{-\frac{1}{2}}$ and τ as $E^{+\frac{1}{2}}$, (so that $p = \frac{1}{2}$). If the electron energy is not large compared with $\hbar\omega_L$, then big differences occur between phonon emission and absorption, and in addition the averaging of the phonon wave vectors is more complex.

A requirement for classical theory to apply is that the photon energy is small compared with kT, i.e. that the act of absorbing a photon does not significantly change the position of an electron in the thermal distribution. ~~Durney~~ Dumke (1961) showed that for some types of scattering the errors in the classical approach are very small up to several kT and also that classical theory is true for degenerate material if the photon energy is small compared with E_F, the height of the Fermi level above the band edge.

2.4.2. Perturbation Theory for Optical Mode Scattering

When the classical calculation does not apply, it might be

possible to use second order pertubation theory, which requires $\omega\tau \gg 1$. If phonons are involved, both phonon emission and phonon absorption must be considered, and the electron can interact first with either the phonon or the photon. This means there are 4 processes to be calculated.

These calculations have been done for optical mode scattering by Visvanathan (1960) and Gurevich, Lang and Firsov (1962). The result is a complicated mathematical function involving Bessel functions, but which simplifies in certain limiting cases. Visvanathan obtains for $\hbar(\omega - \omega_L) \gg kT$ (where ω is the photon frequency).

$$K = \frac{4\pi}{nc}\frac{\sqrt{2}}{3}\frac{Ne^4}{\sqrt{m^*}}\left(\frac{1}{\epsilon_\infty} - \frac{1}{\epsilon_s}\right)\frac{\hbar\omega_L}{(\hbar\omega)^{5/2}}\left(\frac{e^{\left(\frac{\hbar\omega_L}{kT}\right)}+1}{e^{\left(\frac{\hbar\omega_L}{kT}\right)}-1}\right)\left(1 - \frac{4}{(\pi\beta)^{\frac{1}{2}}} + \frac{11}{4\beta}\right) \qquad (2.4.4)$$

where we have changed the notation a little (and corrected the omission of the square root sign for m^*) and $\beta = \hbar\omega/kT$. Examination shows, however, that (4) is only true if $\omega \gg \omega_L$, and that a more accurate result, assuming $\left(\frac{\omega-\omega_L}{\omega+\omega_L}\right)^{\frac{1}{2}} \times \exp\left(\frac{\hbar\omega_L}{kT}\right) \gg 1$, is

$$K = \frac{4\pi}{nc}\frac{\sqrt{2}}{3}\frac{Ne^4}{\sqrt{m^*}}\left(\frac{1}{\epsilon_\infty} - \frac{1}{\epsilon_s}\right)\frac{\hbar\omega_L}{(\hbar\omega)^{5/2}}\left(1 - \frac{\omega_L}{\omega}\right)^{\frac{1}{2}}\left(\frac{e^{\left(\frac{\hbar\omega_L}{kT}\right)}+1}{e^{\left(\frac{\hbar\omega_L}{kT}\right)}-1}\right)\left(\frac{1-4}{\sqrt{\pi}\left(\beta-\frac{\hbar\omega_L}{RT}\right)^{\frac{1}{2}}} + \frac{11}{4\left(\beta-\frac{\hbar\omega_L}{RT}\right)}\right)$$

The factor $\left(1 - \frac{\omega_L}{\omega}\right)^{\frac{1}{2}}$ can be checked by comparing Gurevich, Lang and Firsov's similar equation (27). It is important even when $T = 0$; when the last bracket equals unity. Gurevich, Lang and Firsov also plot their results in the range $\omega \sim \omega_L$ and

obtain an interesting peak in nK. These calculations are only valid for the electron-phonon coupling constant (see 2.7) $\alpha \ll 1$, although one might hope they will still be fairly accurate for $\alpha \sim 1$. (Visvanathan applied his results to the III - V compounds, for which $\alpha \ll 1$).

2.4.3. Perturbation Theory for Impurity Scattering

Visvanathan also calculated free carrier absorption for impurity scattering, for certain energy ranges. The result of most application in SnO_2 is

$$K = \frac{8\pi}{3\sqrt{3}} \frac{N_i\, Ne\, Z^2 e^6 (1-e^{-\left(\frac{\hbar\omega}{kT}\right)}) 4\pi^2}{m^{*2} c\, \hbar\omega^3 n\, (2\pi m^* kT)^{\frac{1}{2}} \epsilon^2} \qquad (2.45)$$

although it would not seem strictly to apply for large ω, when $\omega \gtrsim \frac{Z^2 e^4 m^*}{2\hbar^3}$. Here Ze is the charge on an ionised impurity, Ni is the number of ionised impurities and Ne the number of electrons in the band. Visvanathan does not define exactly what dielectric constant ϵ is, but it would seem that when the photon energy is large compared with the impurity Rydberg, R_i (c.f. 2.6), then the effective value of ϵ should tend to ϵ_∞. The result would only seem to be valid for comparatively low values of Ne, because no account appears to have been taken of shielding of the ion by other electrons.

Optical mode and impurity scattering are the two most likely mechanisms in SnO_2.

2.4.4. Polaron Effects

We end this section by mentioning polaron effects. If the optical mode interaction is strong, and the coupling constant $\alpha \gtrsim 1$,

then the interaction can no longer be handled by considering separate scattering events in phase space by using the Boltzman equation. Polaron properties (see 2.7) can lead to resonances, as is shown by Platzman (1963). His fig. 6 shows that for $\alpha = 3$ there are noticeable humps in the absorption, while his fig. 7 for $\alpha = 5$ shows considerable peaks.

2.5. Band to Band Absorption

The absorption coefficient for absorption of light by an electron making a transition from the valence band to the conduction band (and leaving a hole in the valence band) can be calculated assuming the electron and hole are independent. Modifications of the results due to electron-hole interaction will be considered in 2.6.

Band to band transitions can be divided into two types. "Direct" transitions are those which involve only a photon and an electron. "Indirect" transitions are those in which at least one phonon is emitted or absorbed. In both types momentum must be conserved. For all types of particle the momentum is given by $\hbar$ times the wave vector. Thus for "direct" tranistions the difference in wave vectors of the final and initial electron states must equal the light wave vectors (in the crystal). For light of frequency equal to or less than the near U.V. this light wave vector is small compared with Brillouin zone dimensions. For this reason direct transitions are often called vertical, because on an E-k diagram the transition is almost vertical. Because phonon wave vectors cover the whole of the Brillouin zone, there is no restriction on the indirect transitions.

The indirect transition requires an intermediate state so that the phonon transition can still take place "vertically". The magnitude of the indirect absorption is then related to the reciprocal of the square of the difference between the energy of this intermediate state and the conduction or valence band state, and also to the square of the electron-phonon matrix element connecting the intermediate state with the conduction or valence band state. There may be many alternative intermediate states.

In non-ionic materials the electron-phonon matrix element is small, and indirect absorption is much weaker than direct absorption. However in ionic materials like SnO_2 this may not be so.

Another distinction between types of transition near an absorption edge is important. If, as is often the case, the states involved in the absorption near the edge lie near a special symmetry point in the Brillouin zone, the optical matrix element at that point may be zero. The transitions are then said to be "forbidden". Otherwise they are "allowed". The matrix element for forbidden transitions is assumed to vary as $\underline{k} - \underline{k}o$ where $\underline{k}o$ is the symmetry point and $\underline{k}$ is the wave vector at which the "vertical" transition occurs.

Absorption in the four possible situations is briefly discussed. Features of (2), (3) and (4) are at least approximately involved in SnO_2.

(1) Allowed direct transitions

In the region of the absorption edge the optical matrix element is assumed to be constant. The main variable factor is then the density of states available for direct transitions at the appropriate energy. This is proportional to $\mu^{3/2} (E - Eg)^{\frac{1}{2}}$ where E is the photon energy and μ is the reduced mass $= \frac{m_c m_v}{m_c + m_v}$, with m_c and m_v being the conduction and valence bands density of states effective masses. In addition the absorption coefficient, K varies with the reciprocal of the refractive index, n, and the reciprocal photon energy. The former can be viewed as resulting from the basic quantity being the imaginary part (2nk) of the complex dielectric constant.

(2) Forbidden direct transitions

These transitions occur in SnO_2. The dependence of the matrix element on $(\underline{k} - \underline{ko})$ results in an extra $(\underline{k} - \underline{ko})^2$ factor. When converted to energy terms this is $\propto (E - Eg)$ making the absorption proportional to $\frac{\mu^{5/2} (E - Eg)^{3/2}}{n\omega}$

(3) Allowed indirect transitions

Because of the removal of the "vertical" requirement, the density of states factor now involves an integral. This results in a factor $m_c^{3/2} m_v^{3/2} (E - Eg \pm Ep)^2$, where Ep is the phonon energy involved, and + is to be taken for phonon emission and - for phonon absorption. Another factor contained in the probability of phonon emission or absorption is n + 1 or n respectively, n, here, is the phonon occupation number, and is not to be confused with the refractive index. After allowing for the changed threshold energy, the ratio of absorption branches with phonon emission and absorption, (for a particular type of phonon) depends almost solely on n. With corrections for electron-hole interaction the longer wavelength absorption edges in germanium and silicon have been interpreted very accurately as being due to transitions of this type. The electron-phonon matrix element is more likely to vary with energy than the optical matrix element.

(4) Forbidden indirect transitions

An extra factor in this case is, similar to (2), $(E - Eg \pm Ep)$. There is also a density of states effective mass factor, but which effective mass depends on the details of what part of the transition is forbidden and in which band the phonon interaction occurs. The total "energy above threshold" factor is thus $(E - Eg \pm Ep)^3$.

Parabolic bands are assumed in all the above cases. Whenever an individual contribution becomes negative it is to be taken as zero.

2.6 Excitons and their Influence on Band to Band Absorption.

2.6.1 Excitons.

Elementary semi-conductor theory deals with "one-electron" energy states i.e. the effect of all other particles in the solid is approximated by an average potential within which the electron moves. One step beyond this is to consider states that can be produced by the interaction of an electron and a hole. Such states are not states of a single electron but excited states of the crystal as a whole.

The electron-hole attraction leads to bound states. These states, or excitons, have two extreme types, depending on whether the dimensions of the wave function is very large compared with, or is approximately the same size as, a unit cell dimension. The former are known as Wannier excitons and the latter as Frenkel excitons. Wannier excitons resemble a hydrogen atom, except that the reduced mass μ replaces the electron mass and the coulomb force is moderated by a dielectric constant, ϵ, of the material. The hydrogen wave functions are envelope functions multiplying the normal wave function inside a unit cell. The ground state binding energy varies as $\frac{\mu}{\epsilon^2}$, so that if e.g., $\epsilon = 10$ and $\mu = 0.1$ m the energy is only .0136 e.v. The "Bohr radius" of the ground state varies as $\frac{\epsilon}{\mu}$, so that with the above figures the radius is 53Å. If the radius calculated in this way turns out to be of the order of the lattice dimensions, then the assumption in the Wannier theory, that the effect of all other particles can be averaged by taking an effective mass and a

dielectric constant, breaks down. A first approximation as the radius becomes small might be to assume the effective masses tend to m and the dielectric constant to 1, but this cannot be carried very far. Frenkel exciton theory is more difficult and has to take into account the many body nature of the problem from the start.

As well as the ground state, there are excited bound states. The Wannier theory can often be pictured as applying to higher states, even if it fails for the ground state. The ground state, however, is always the most important, and the properties associated with the higher bound states always merge smoothly with the properties of the unbound states. The properties of the unbound states, however, can be strongly affected by the electron-hole interaction.

2.6.2 Energy band diagrams for Excitons

The usual one-electron energy band plots are inadequate to represent exciton states. For the exciton we need a diagram showing states of the whole crystal. The two types of plot are compared in fig. 2.6.1.

The left diagram is a normal one, in which direct transitions are represented by almost vertical lines and diagonal lines represent indirect transitions. The hole and electron states are represented by the ends of the lines. The right diagram is for representing electron-hole pair (exciton) states, with K as the total wave vector (K is unfortunately also the symbol for absorption coefficient). All transitions (if the crystal is initially in the ground state) on this diagram start at the origin. All direct transitions have $K \approx 0$. The bound exciton states are represented as bands with a line on the E - K plot. The continuum is represented by the cross-hatched part.

FIG 2.6.1.

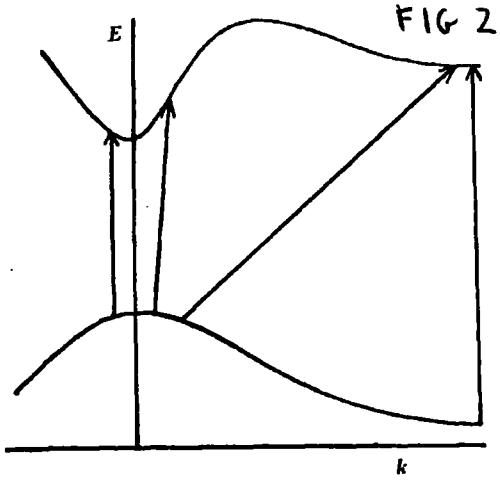

FIG. 1

Energy-band plot of one-particle states. Vertical lines direct, diagonal indirect transitions.

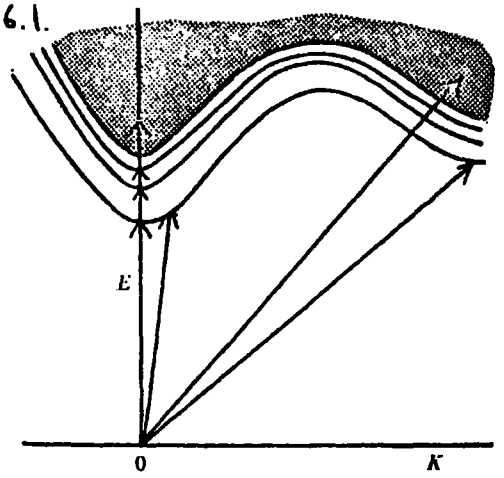

FIG. 2

Exciton bands. Ground state is at origin. Direct transitions vertical on axis, indirect diagonal.

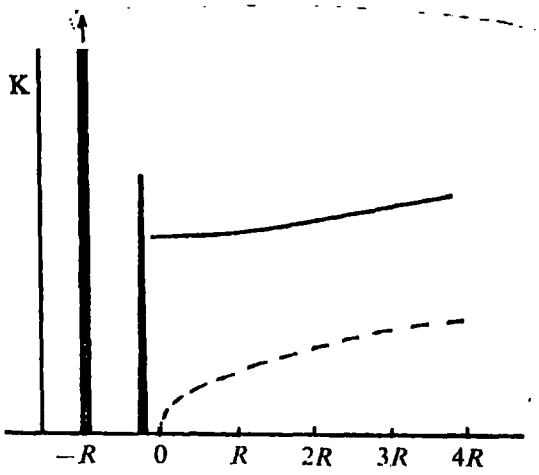

FIG. 2.6.2.

Direct allowed absorption near edge. $n = 1$ and 2 lines only shown. Free-pair absorption dotted.

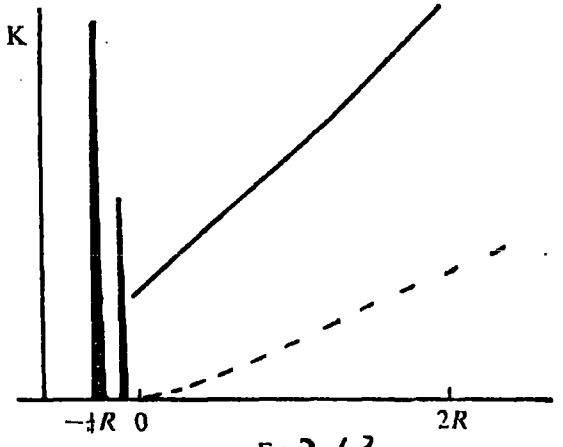

FIG. 2.6.3.

Direct forbidden absorption near edge. $n = 2$ and 3 lines only shown. Free-pair absorption dotted.

FIG'S. 2.6.1-3 after Elliott (1963)

2.6.3 Optical Absorption to Wannier Excitons

This is dealt with by Elliott (1957 and 1963). As in 2.5 four types will be considered.

(1) Allowed direct transitions

The strength of absorption to bound states has an interesting interpretation. The value of the (hydrogenic) wave function describing the exciton at its central point can be related to the probability of the electron and hole being found in the same unit cell. The oscillator strength for the transition to a bound exciton turns out to be the value it would be, in a molecule consisting of one unit cell, for a transition between the molecular levels corresponding to the valence and conduction bands, multiplied by the above probability. If the radius of the exciton is visualized as getting larger and larger, then the above probability gets smaller and smaller and more and more of the oscillator strength can be thought of as being transfered from exciton absorption to continuum absorption.

The S states on the hydrogen model are the only ones for which the wave function is not zero at the centre. For these the probability of finding the electron and hole together varies as $\frac{1}{(a_o n)^3}$ where a_o is the Bohr radius and n is the hydrogenic principal quantum number.

The wave functions of the unbound states are still affected by the electron hole interaction, in a similar way to unbound hydrogen atom states. The result of this is to increase the probability of finding the electron and hole in the same unit cell. The increase in absorption compared with the result obtained ignoring the electron-hole interaction is given by a "Sommerfeld factor", which Elliott gives as $2\pi\alpha(1-e^{-2\pi\alpha})^{-1}$

with $\alpha^2 = R/(E - E_g)$ and R the Rydberg of the exciton series (i.e. the binding energy of the ground state).

For large n, the bound states have an energy spacing proportional to $\frac{1}{n^3}$. As their individual integrated absorption varies as $\frac{1}{n^3}$, when the individual absorption peaks are no longer resolvable the absorption is independent of energy. This "plateau" is of equal height to the one at the tail of the continuum, so there is no discontinuity at the continuum edge. The absorption is shown in fig. 2.6.2.

(2) Forbidden direct transitions

In spite of the fact that for direct transitions the wave vector, K, of the exciton as a whole is equal to the wave vector of the photon, and is therefore small, appreciable transitions can take place to bound excitons. This is because the states from which the exciton is formed cover a range of $\underline{k}$ values. In general sense k_x is related to $\frac{d\Psi}{dx}$ because $\hbar\underline{k}$ gives momentum, and the momentum operator includes $\frac{d}{dx}$ (in one dimension). Thus the matrix element that was proportional to $(\underline{k} - \underline{k_0})$ is proportional to $\nabla(\Psi(o))$, where $\Psi(o)$ is the value of the hydrogenic wave function at the central point. $\nabla(\Psi(o))$ is non-zero only for p states on the hydrogen model. For p states. $[\nabla(\Psi(o))]^2$ varies as $\frac{n^2 1}{a_0 n^5}$

There is thus no n = 1 line for forbidden transitions.

The Sommerfeld factor for the continuum is $\frac{2\pi\alpha(1 + \alpha^2)}{1 - e^{-2\pi\alpha}}$ and this merges smoothly with the higher bound states. The absorption is shown in fig. 2.6.3.

(3) Allowed indirect transitions

Transitions to bound states now form continuous bands rather than lines. The density of states factor is obtained from the exciton band on the E - K diagram for states of the whole crystal. It is proportional to $M_x^{3/2}$ $(E - Eg + (R/n^2) \pm Ep)^{\frac{1}{2}}$ where

$M = m_c + m_v$ is the exciton mass. The probability factor is still proportional to $\frac{1}{(a_o n)^3}$.

The continuum absorption involves an integral which includes the Sommerfeld factor (see Mclean 1960) and which does not seem to have a solution in terms of elementary mathematical functions.

However for energy just above threshold it varies with a 3/2 power law and for large energies it varies as a square law.

(4) Forbidden indirect transitions

The forbidden aspect again adds a factor proportional to energy above threshold, for both bound and continuum contributions. Bound contributions thus vary as $(E-E_g + R/n^2 \pm Ep)^{3/2}$ and the continuum starts as $(E-E_g \pm Ep)^{5/2}$.

All transitions

For all situations when the energy above threshold $\gg R$, the modifications introduced by electron-hole interaction become small.

Even when absorption is absent or small according to the above description, absorption may occur due to a rather different mechanism - quadrupole absorption. The most conspicuous place where this can occur is the n=1 exciton for forbidden spectra. This is thought to occur in SnO_2. Here the symmetry conditions that forbid transitions can be slightly violated by the finite wave vector, q, of the light. What is required is that the hydrogen function should not change greatly in a distance of the order of the reciprocal wave vector. A measure of this is $a_o q$, where a_o is the Bohr radius.

2.6.4 Urbach's Rule

An empirical relation discovered by Urbach (1953) for the silver holides which covers a wide range of temperatures and absorption

coefficients is

$$K = K_o \exp \left[\sigma (E_o - E) / kT \right].$$

Here σ is a constant of order unity and E_o is an energy, which for materials with a strong exciton absorption is close to the energy of the lowest exciton peak. At low temperature, T is replaced by a fixed T_o. Urbach's rule applies to a wide range of compounds (Knox 1963) and a number of authors have attempted to give theoretical explanations. Most of these involve perturbations due to lattice vibrations blurring the band edge. Eagles (1963) gives a somewhat similar explanation except that phonon absorption and emission are considered on a model of the electron-phonon interaction that includes localised phonons. SnO_2 does not obey Urbachs rule, although it has some similarity. The similarity is a featureless rise in absorption over many orders of magnitude. The differences are a shallower slope (i.e. higher apparent T) not very dependent on temperature and the slope of the log K plot not being constant over wide ranges of K. Eagles suggests that his model used to explain Urbach's rule is more likely to apply to exciton absorption, and examination shows it to be most applicable when exciton interaction is strong (i.e. large exciton binding energies). The latter is not the case in SnO_2 (exciton binding energy $\sim$ .033 e.v.) and also exciton absorption is not of overwhelming importance. We interpret the SnO_2 absorption edge by using as a starting point the results of Eagles based on another model of electron-phonon interaction. This theory is treated in 2.8.

2.7 Polaron Theory

2.7.1. Introduction

In ionic materials the interaction between the electrons or holes and the ions of the lattice is important. This is considered in polaron theory. The measure of ionicity that enters polaron theory is $\frac{1}{\epsilon_\infty} - \frac{1}{\epsilon_s}$, where ϵ_s and ϵ_∞ are the static and high frequency dielectric constants. For SnO_2 this quantity is larger than for most compound semi-conductors (e.g. CdS, TiO_2 and much larger that in the III - V compounds). It turns out that most phenomena involving electrons or (even more especially) holes cannot be explained without the aid of some kind of polaron theory.

After a short introduction we discuss how polarons are classified into different types, for which different theories are required. We then briefly discuss some of the properties of the different types.

In many problems concerning electrons in solids, it is possible to get electron states which are fairly well defined and from which an electron occupying that state is only occasionally scattered by imperfections of some sort. The interactions can then be treated in a straight - forward way by perturbation theory. However in ionic crystals the interaction between the electrons and particularly the longitudinal polar phonons can become so strong that the picture breaks down. (For example it is doubtful how far the Boltzmann equation can be applied (~~P.M.~~ Platsman 1963 ~~"Polarons and Excitons"~~ p. 150 and ~~T. D.~~ Schultz 1963 ~~ditto~~ p. 112). The difficulty here is that the position of the electron in phase space is doubtful because the time between collisions is so short that the collisions cannot be thought of as independent). The problem is generally made easier by considering states of the combined electron-lattice system. These states

are known as polarons, and in some circumstances the interactions between polarons are small, thus avoiding considering the system as a many body problem. However there is still only an incomplete understanding of many properties of polarons, even in the relatively simple cases studied by theoreticians.

2.7.2. Types of Polaron

Polarons are classified by two criteria. The first is the strength of the dimensionless coupling constant α, defined by $\alpha = \frac{1}{\sqrt{2}} e^2 \left(\frac{m}{\omega\hbar^3}\right)^{\frac{1}{2}} \left(\frac{1}{\epsilon_\infty} - \frac{1}{\epsilon_s}\right)$. ϵ_∞ and ϵ_s are the high frequency (i.e. above the phonon frequencies, but below the electronic frequencies) and static dielectric constants respectively. m is the so-called "bare" electron mass, i.e. the effective mass the electron would have if the material had zero ionicity or if the lattice were held rigidly and not allowed to vibrate. ω (throughout this section) is the phonon frequency, and in all theoretical work the author has seen only one phonon branch is considered, and, in most, the dispersion of phonon frequencies is ignored. However Eagles 1964, in his study of Rutile, considers three branches.

For $\alpha \ll 1$, $\alpha \sim 1$ and $\alpha \gg 1$ the coupling is known as weak, intermediate and strong respectively.

The second criterion concerns the size of the polaron compared with a lattice distance. The extreme types are known as large and small respectively. Published small polaron theories are based on strong coupling. For weak and intermediate coupling the best measure of the size of a polaron is the "characteristic length" $(\hbar/2m\omega)^{\frac{1}{2}}$. When this is of the order of a lattice distance, large polaron theories can be somewhat extended in validity by using a cut-off in phonon wave vector, but eventually large polaron theory fails completely and a small polaron

theory must be used. When the coupling is too strong for intermediate coupling theory to apply, the polaron radius may be estimated by means of the Feynman model of the polaron. Schultz (1959 and 1963) gives the radius in the strong coupling limit as $\frac{3}{\alpha}\left(\frac{\pi}{2}\right)^{\frac{1}{2}}\left(\frac{\hbar}{2m\omega}\right)^{\frac{1}{2}}$, and tabulates values for smaller values of α.

The only factor in the above expressions for α and polaron radius that can vary from band to band is m. Thus the same crystal can have different types of polaron in different bands.

2.7.3. Some Properties of Polarons

2.7.3.1. Weak coupling large polarons

For $\alpha \ll 1$ the polaron properties are almost the same as the properties of a 'bare' electron. The interaction with phonons can be treated as separate scattering events, and perturbation theory can be used. Howarth and Sondheimer (1953) use perturbation theory on 'bare' electron states, and their results are supposed to apply at all temperatures. Perturbation theory on polaron states gives the same results as intermediate coupling theory for small energy and small α (D. Pines 1963 "~~Polarons and Excitons~~" p. 33)

2.7.3.2. Intermediate coupling large polarons

Pines (1963) (or the original paper of Lee and Pines (1952)) considers low energy polaron properties using a variational calculation or a series of canonical transformations. The two main results are that the 'bare' effective mass m should be replaced by a polaron effective mass m* given by

$$m^* = m\left(1 + \frac{\alpha}{6}\right)$$

and that the energy of the lowest energy state in the band is lowered by

$$E(o) = -\alpha\hbar\omega$$

These results should apply with small error for $\alpha < \sim 3$.

The main deficiency of this and several other polaron theories is that only low energy ($\ll \hbar\omega$) states and low temperatures are considered. This is particularly important for dealing with optical effects, as transitions are not confined to low energy states.

2.7.3.3 Strong coupling large polarons

An adiabatic approach to strong coupling theory gives results in descending powers of α. An account is given by Allcock (1963), though most of the original work appears to be Russian (that of Pekar et.al.) With some assumptions this results in

$$m^* = m(0.02\,\alpha^4 + O(\alpha^2))$$

$$\text{and } E(o) = (\alpha^2 W_o - \tfrac{3}{2} + O(\alpha^{-2}))\hbar\omega$$

where Wo is some parameter. By comparison with results (particularly effective mass) from the Feynman polaron it would appear that α must be very large for the results to be correct (Schultz 1959). In SnO_2 if the effective mass is imagined to increase steadily, by the time such large values of α have been reached, we have entered the small polaron domain.

2.7.3.4 The Feynman Polaron

More recently work on the Feynman model of the polaron (R.P. Feynman 1955) has produced more comprehensive results. It is based on Feynman's path-integral formulation of quantum mechanics. The Feynman model essentially replaces the effect of the lattice by a

second particle connected to the electron by a spring (Schultz 1959 p.528). The results apply to all coupling strengths and the method can be applied to finding properties such as the mobility at all temperatures and frequencies. It is, however highly complicated mathematically and involves a lot of numerical computation. It would appear that results have only been worked out for certain cases.

Schultz (1959 or 1963) gives numerical results, for specified values of α, of m*, E(o) and the previously mentioned polaron radius ρ. The values of m* and E(o) show the continuous transition from intermediate to strong coupling theory.

An account of transport properties is given by Platzman (1963) and Feynman, Hellworth, Iddings and Platzman (1962), in which the results of machine computation are given for some conditions.

2.7.3,5 Small Polarons

If the polaron radius predicted by any of the above theories, which are based on the continum approximation (with or without a cut-off), is much less than a lattice distance, then the theory breaks down. If small polaron theory applies, the properties are then quite different. It is no longer useful to start with Bloch-type electron states spread over many unit cells, but rather to consider states centred on one site.

One of the main works on the theory is Holstein (1959). He studies the highly simplified model of a one dimensional molecular crystal, in which a linear chain of diatomic molecules is considered. The individual molecules can vibrate and the electrons states are expressed in the tight binding approximation as the linear superposition of molecular wave functions, with coefficients depending on nuclear

positions. In spite of its simplifications, this model is thought to have many of the features that occur in real crystals.

His criterion for small polaron theory is equivalent to $2J \ll E_b$, where J is the overlap integral between neighbouring molecular wave functions, and E_b is the polaron binding energy for zero J. This is given in the continuum approximation by $\frac{1}{\pi}\left(\frac{1}{\epsilon_\infty} - \frac{1}{\epsilon_s}\right) e^2 w_{max}$ where w_{max} is the cut-off phonon wave vector defined as $w_{max} = 2\pi \times \left(\frac{3}{4\pi V_c}\right)^{\frac{1}{3}}$ where V_c is the volume of a unit cell. (The B.Z. has been approximated by a sphere of the same volume) (Eagles 1963).

The effect of the above condition applying is that the polaron is well localised on a single molecular site. There are two methods that an electron can use to move from site to site. It can tunnel between the potential wells, or it can jump the potential barrier with the aid of energy from phonons. The former gives a mobility variation at most temperatures which is exponentially falling with rising temperature, and the latter gives a mobility which is exponentially rising with rising temperature. The transition temperature, Tc, that separates the regions dominated by the two types of mechanism, is within 20% of $\frac{\hbar\omega}{2k}$ (or $\frac{\theta}{2}$) for a wide range of parameters (Holstein 1959 p.366).

If the tunnel effect dominates (i.e. $T > Tc$), then a more or less traditional band picture applies, but with a bandwidth of $4 J e^{(-S/2)}$ where $S \approx \frac{E_b}{\hbar\omega}$ but depends on direction (see sec. 3.3).

2.7.3.6. Nearly Small Polaron Theory

Recently a new polaron theory was published (Eagles 1966) that we consider to be the theory most applicable to the top valence band in SnO2. The theory has many of the features of small polaron theory, but an adiabatic rather than perturbation approach is used for transitions

from site to site. The conditions required for the theory are stated as

$$\left(\frac{1}{Z}\right)\left(\frac{1}{2}\,Wr/Eb\right)^2 \ll 1 \qquad (2.7.1)$$

$$2J \gg \hbar\omega \qquad (2.7.2)$$

$$W \ll \hbar\omega \qquad (2.7.3)$$

where Z is the number of nearest-neighbour lattice sites, Wr is the rigid lattice (i.e. without polaron effects) bandwidth, Eb is the polaron binding energy for zero bandwidth, J is an electron overlap energy and W is the polaron bandwidth found in the theory. For a primitive cubic crystal Wr = 12J.

(2.7.1) can be thought of as roughly the condition for small polaron theory. The left side of (2.7.1) is approximately ϵ_1, a parameter used in the theory, and the theory is only worked out to first order in ϵ_1. (2.7.2) is the condition for an adiabatic rather than perturbation approach being better. (2.7.3) appears to be the condition for the applicability of the approach used to calculating certain properties such as the bandwidth. The effect of it not being valid is not clear.

Because atomic displacements in small polaron theory can be of the order of a tenth of the nearest neighbour distance, Eagles introduced two further parameters, ϵ_2 and ϵ_3, to account for second order terms in the electron-phonon interaction and anharmonic terms in the lattice potential, respectively. Terms proportional to ϵ_1, ϵ_2 or ϵ_3 can produce changes in the local atomic forces around a polaron, and so can lead to localised normal modes of lattice vibration. The theory considers the results of this, but these effects are ignored in this thesis. There is no evidence of them being important in SnO_2. Without localised modes optical absorption can be

calculated by a similar theory to Eagles (1963) but with a modified parameter D (See 2.8).

2.8 Eagles' Theory of Optical Absorption

Eagles (1963) gives a theory of optical absorption involving small polarons. The theory can be extended to cover some departure from the strict conditions required for small polarons by the theory of nearly small polarons (Eagles 1966 A and B).

When electron-phonon interaction is fairly strong the method of calculating the absorption by treating both the electron-phonon interaction and the electron-radiation interaction as perturbations and using pertubation theory becomes unrealistic. It is necessary to treat the electron-phonon interaction first (to obtain polarons) and then to use perturbation theory for the radiation. When small polaron theory applies, the theory is similar to earlier work on F centres.

The theory used here is that for linear electron-phonon interaction. (Quadratic interaction can lead to Urbach's rule, see 2.6). Eagles worked out two extreme cases: (1) transitions between a small polaron band and a wide band in which coupling is neglected and (2) transitions between two small polaron bands. Because the conduction band in SnO_2 is fairly wide, the best starting point is (1), which is now considered.

The absorption is divided into parts $K_p(E)$ in which there is a net emission of p phonons. (A single phonon branch is assumed). Eagles then shows that

$$\int n K_p(E)\, E dE = AR_p$$

$$\text{where } R_p = \sum_{m=m_1}^{\infty} \frac{D^{2m+p}(\bar{n}+1)^{m+p}(\bar{n})^m}{(m+p)!\ m!} \exp\left[-(2\bar{n}+1)D\right] \qquad (2.8.1.)$$

and m_1 is zero if p is negative and equals -p if p is positive. A is a constant, D is a parameter of the theory (see later) and $\bar{n}$ is the mean thermal occupation number of the phonon branch. n is the refractive index and will vary (slowly) with E. Each term in the summation can be thought of as the contribution with m phonons absorbed (and, of course, p + m phonons emitted). It is straightforward to show that

$$\sum_{p=-\infty}^{\infty} R_p = 1 \quad (2.8.2), \qquad \sum_{-\infty}^{\infty} pR_p = D \quad (2.8.3) \qquad \sum_{-\infty}^{\infty} (p-D)^2 R_p = D(2\bar{n}+1) \qquad (2.8.4.)$$

(2.8.2.) shows that the total integrated absorption (or more precisely n KE) is independent of the phonon interaction. The latter enters the theory through D. (2.8.3) shows that the mean net number of phonons emitted is D and (2.8.4) shows that absorption which would have occurred at a particular energy in the absence of phonon interaction is spread into a root mean square energy width of $D^{\frac{1}{2}}\hbar\omega$. ($\hbar\omega$ is the phonon energy). (2.8.1) shows that absorption involving no phonons is reduced by the final exponential factor due to the phonon interaction. Thus if $D \gtrsim 2$, zero phonon absorption plays a very small part in the overall picture of band to band absorption.

So far we have only talked of integrated absorption. To obtain the shapes of the absorption parts we consider the K_{pm} part. Except for the zero phonon part, Eagles shows

$$nEK_{pm}(E) \propto \int \rho_c(E^1)\rho_v\ (E-E_g-p\hbar\omega-E^1)B_{pm}\ (E,E^1)dE^1 \qquad (2.8.5)$$

where ρ_c and ρ_v are the density of states in the (wide) conduction band and (narrow) valence band respectively and $B_{p,m}(E,E^1)$ is an average quantity that can be reduced to simple form in some circumstances. Two alternative such circumstances are when 2m+p is large and when the narrow band bandwidth is negligible. In either circumstance $B_{p,m}(EE^1) \propto Q^2(E^1)$ where $Q^2(E^1)$ is proportional to the (average) optical matrix element to conduction (wide) band states an energy E^1 above the band edge. The absorption shapes can now be found from (2.8.5).

The form of $Q^2(E^1)$ can be related to the allowed and forbidden transitions of 2.6 and 2.7 and to the Sommerfeld factor of 2.7.

The parameter D is evaluated by Eagles (1963), by using a continuum polarisation model, as

$$D = \frac{1}{\pi}\left(\frac{1}{\epsilon_\infty} - \frac{1}{\epsilon_s}\right)\frac{e^2 w}{\hbar\omega}\ \text{max} \qquad (2.8.6)$$

where w_{max} is defined by

$$\frac{4\pi}{3}\left(\frac{w\ \text{max}}{2\pi}\right)^3 = 1/V_c$$

and V_c is the unit cell volume

An interesting feature of (2.8.6) is that $D\hbar\omega$ depends solely on dielectric constants and the unit cell size. It might be an interesting line to investigate why the theory gives different D values for two similar compounds, one of which has, say, twice as many atoms in its unit cell.

(2.8.6) only applies when small polaron theory strictly applies, and is modified for nearly small polarons (see 3.5).

One further factor discussed by Eagles will be mentioned here. The lifetime τ of the small polarons will smear the absorption at any energy into an energy width of the order of $\hbar/\tau$. This will be of more importance for nearly small polaron theory, because the lifetime of the localised states reduces for reductions in the electron-phonon coupling. (The lifetime of "bare" electron states increases). The lifetime of the localised states is longer at low temperatures, and this would explain why sharp zero phonon excitons have been observed in SnO_2 at low temperatures but not at higher temperatures (e.g. liquid air). Acoustic phonons might also be responsible for this disappearance of sharp peaks.

2.9 Defect Absorption

So far (except for free carrier absorption) we have discussed perfect crystals (unless phonons and excitons are counted as imperfections). All real crystals have imperfections. These may be structural defects such as vacancies or dislocations, or else foreign atoms. These defects can lead to electron states in the forbidden band, which in turn lead to absorption below the band edge and which are exceptionally important in luminescence.

Levels is the band gap can be roughly divided into shallow and deep levels. These are roughly analagous to Wannier and Frenkel excitons. Shallow defects are most easily produced by substitutional impurity atoms with a position in a column of the periodic table neighbouring that of the displaced atom. A high dielectric constant also encourages shallow states. Sb doped crystals produce such states close to the conduction band. Optical transitions in or into the conduction band from electrons in such states are considered together with free carrier absorption (see 2.4) and ~~although~~ optical transitions from the valence band are changed by these states, ~~the absorption spectra we took of the absorption edge in these crystals have not yet been analysed in detail~~.

The defect absorption that has been analysed is believed not to be due to foreign atoms and is considered in ~~3.6 and~~ 6.2.

FIG. 3.11.

Rutile structure unit cell.

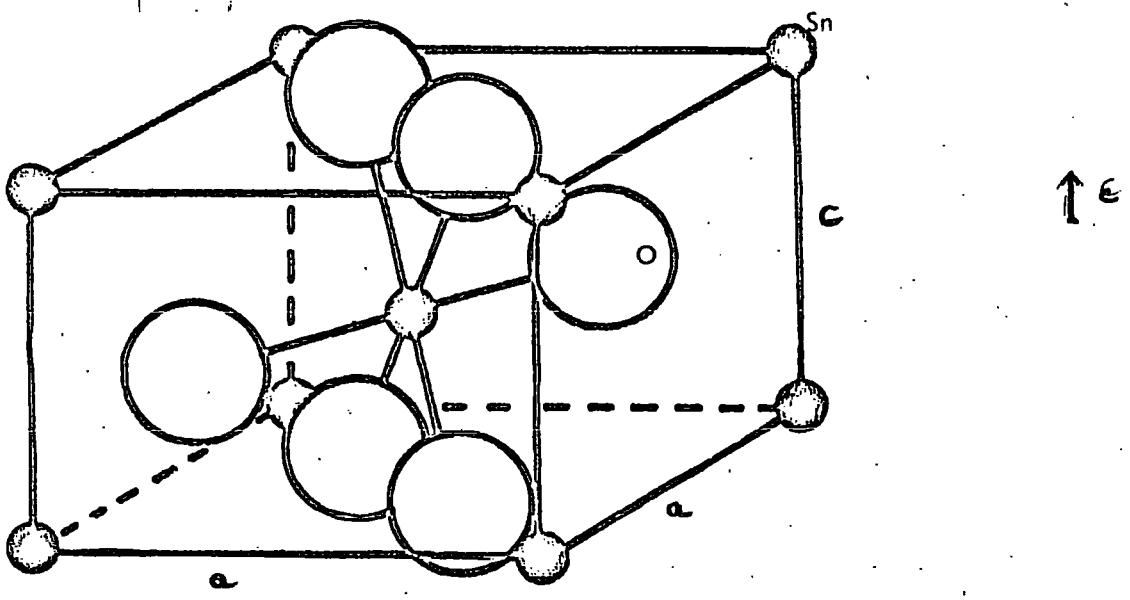

3.1 Crystal Structure and Expected Band Structure

3.1.1 Introduction

In this section we shall look at some of the known facts about SnO_2 and compare it with some other materials, with the object of building up a general picture of what is important and what is not.

Although the possibility was looked into of doing a simplified LCAO type of calculation and also building up a picture of the symmetry and optical absorption selection rules for different bands, it was abandoned. One of the factors was the comments of Slater and Koster (1954) concerning the number of mistakes other people had made who had attempted this.

We first discuss the crystal structure and then go on to consider the band structure, drawing on comparisons with $SrTiO_3$ and TiO_2. Next we comment on a proposed bonding model. We finally draw together some work on the band edge and high temperature electrical conductivity measurements, in order to obtain evidence on the valence band effective mass.

3.1.2 Crystal Structure

SnO_2 crystallises in the rutile structure. This is illustrated in fig.3.1.1. As more is known about Rutile (TiO_2) than SnO_2, a comparison between the two is instructive.

The lattice is simple as compared with many compounds, but, of course, not as simple as the lattices of elements and very simple compounds. It has 2 molecules (6 atoms) to the tetragonal unit cell, which is primitive. All atoms of the same type have the same coordination, and the same environment except for rotations about the c axis.

The main difference in the lattice between TiO_2 and SnO_2 is that the ionic radius of Sn^{++++} is 0.71 Å (Pauling, 1960) and Ti^{++++} is 0.68 Å (Pauling) or quoted as

0.64Å and 0.60Å elsewhere. This causes the two types of Ti-O distances in Rutile (1.988 and 1.944Å) to rise to the Sn-O distance in SnO_2 of 2.055Å. ~~for both types~~ (Data from Bauer 1956). The change in $\frac{c}{a}$ ratio from .644 (TiO_2) to .672 (SnO_2) can be explained on this basis as follows.

If calculations are done on the rutile structure assuming perfectly ionic binding, and ignoring repulsive forces due to overlap between like atoms, a $^c/_a$ ratio of .721 is obtained. (Pauling 1960). However, if the metal ion is small, this ratio would cause the O - O distance in a (110) direction to be less than the O^{--} ionic diameter. Thus a compromise must be reached between the O - O repulsion and the maximising of the Madelung constant for the structure. If this is taken into account, the value of $^c/_a$ calculated for TiO_2 (for ionic binding) agrees with experiment (Pauling 1960). This is contrary to the deduction drawn e.g. by Grant (1959) that the departure of the $^c/_a$ ratio indicates a degree of covalent bonding. The observed relevant O - O distance in TiO_2 is 2.52 Å compared with the normal ionic diameter of O^{--} of 2.80 Å. The larger Sn^{++++} ionic radius allows the O - O distance to rise to 2.58 Å, and explains the rise of the $^c/_a$ ratio.

3.1.3 Ionicity

Following Coulson (1952, page 134), a measure of the ionicity of an individual bond can be got from the electronegativity values of the elements concerned. It should perhaps be mentioned that the usefulness of the electronegativity approach is a matter of controversy among chemists (Cotton and Wilkinson). Coulson gives the formula:

$$\% \text{ ionic character} = 16 |x_A - x_B| + 3.5 |x_A - x_B|^2$$

where x_A and x_B are the electronegativity values of the two atoms A and B. Cotton and Wilkinson quote two sets of values for two different methods of calculation. They are:-

	1	2	Average
O	3.5	3.5	3.5
Ti	1.32	1.6	1.46
Sn	1.72	1.9	1.81

Taking the average values, the percentage ionic character for a Ti - O bond is $16 \times 2.04 + 3.5 \times 2.04^2 = 47\%$

and the Sn-Obond $16 \times 1.69 + 3.5 \times 1.69^2 = 37\%$

In a solid, however, the coulomb interaction with all the ions must be considered and this increases the ionicity (Coulson pages 266 - 267). A qualitative measure of this increase is the Madelung constant, ~~(see later),~~ which is large for the (ideal) rutile structure (4.816). It is interesting to compare NaCl (Coulson p.p. 266 - 268) for which (1) gives ~50%. The Madelung constant for this structure is only 1.75, and yet X - ray evidence shows that 17.85 electrons surround the Cl atom compared with 17 for neutral Chlorine (i.e. 85% ionicity).

From this evidence it would seem reasonable to conclude an overwhelmingly ionic character is to be attributed to Rutile and, to a lesser extent, to SnO_2. This is backed up by the considerable difference between ϵ_∞ and ϵ_s (see 5.6). No attempt has been made to relate this difference to the ionicity numerically, but this is possible and it would be interesting to do. It can certainly be said that this considerable difference between ϵ_∞ and ϵ_s shows considerable ionicity.

3.1.4 Band Structure

For strongly ionic crystals, the energy bands can be calculated with reasonable accuracy with the LCAO (linear combination of atomic orbitals) method (Cardona and Harbeke, 1965). The only material related to SnO_2 for which this has been done is $SrTiO_3$ (Kahn and Leyendecker, 1964).

The similarity between $SrTiO_3$ and SnO_2 lies in the fact that both have octahedra of oxygen ions surrounding a metal ion. In $SrTiO_3$ (and TiO_2) this ion is Ti^{++++} and in SnO_2 it is Sn^{++++}. Above the curie point, $SrTiO_3$ is cubic and the octahedra are regular whereas they are slightly distorted in tetragonal SnO_2 (and TiO_2). The reason for the change from cubic to tetragonal is that Sr has a valency of 2 rather than 4. This means that in the tetragonal case the different octahedra share fewer common oxygen ions, resulting in 4 oxygen ions to the unit cell rather than three. This change results in the squeezing together of each oxygen towards one of its neighbours (mentioned previously). In both cases the coordination and environment of each ion is identical, except for rotations. The "nearest" neighbour O - O distances,(together with the number of such neighbours in brackets,) in $SrTiO_3$ is 2.76 (8), in TiO_2 are 2.52 (1) 2.78 (8) 2.959 (2) in SnO_2 are 2.588 (1) 2.906 (8) 3.186 (2) (units are Å). The last distance for TiO_2 and SnO_2 is the unit cell dimension c. The Ti - O distance in $SrTiO_3$ is 1.95 (6), and in TiO_2 there are two, 1.944 (4) 1.988 (2). (The numbers in brackets are the number of such oxygen neighbours per Ti ion). In SnO_2 the Sn -O distances are all

the same, to within experimental error, at 2.055 A^{o} (Bauer 1956). This change from TiO_2 to SnO_2 is not in itself significant, but just reflects the different ionic radii.

The above mentioned work on $SrTiO_3$ assumed the valence and conduction bands were derived from the Oxygen 2p and the Ti 4d states. The authors then fitted as well as possible various parameters to known data before starting their calculations. For instance the approximately known energy gap of 3 e.v. was used to obtain the percentage ionicity (85%). See fig. 2.

Their results (fig. 3) gave 9 valence bands (3 (2p) states from the 3 oxygen ions in the unit cell) which degenerated to fewer levels at symmetry points in the Brillouin zone; e.g. to 3 levels at ($\underline{k}$ = 0,0,0). All the bands except one and in some directions two were narrow (spanning 0 - .4 e.v.). The conduction band is of less relevance to SnO_2, because it mainly derives from Ti d states.

Three differences are important in comparing $SrTiO_3$ and SnO_2. They are

(1) The extra oxygen ion in the unit cell in SnO_2 giving rise to the single closest "nearest neighbour".

(2) The larger values for the rest of the O - O distances in SnO_2 (this is a greater contrast in comparing TiO_2 and SnO_2).

(3) The Sn replacing the Ti.

For comparing TiO_2 and SnO_2 (1) does not apply.

We shall consider (1) first. The first point to note is that the extra oxygen ion would increase the number of possible valence bands

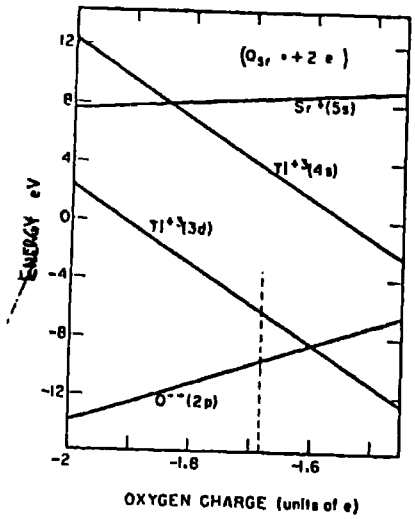

~~FIG. 2.~~ Plot of energies on the ionic model as a function of oxygen charge. The energy to excite an electron from an oxygen ($2p$) state to various states on cations is represented by the vertical distances from the O^{--} ($2p$) line.

FIG. 31.2.

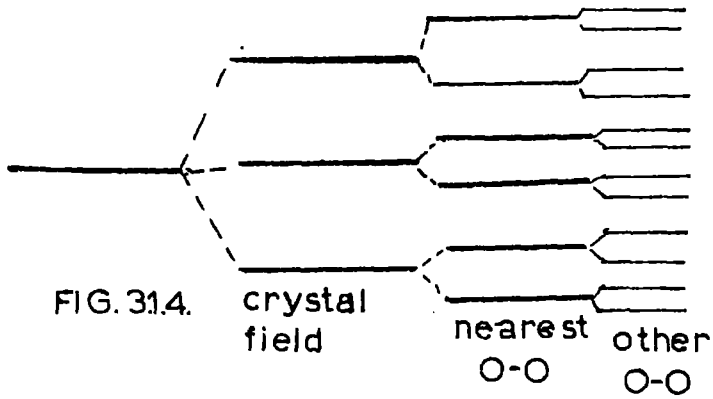

FIG. 31.4.

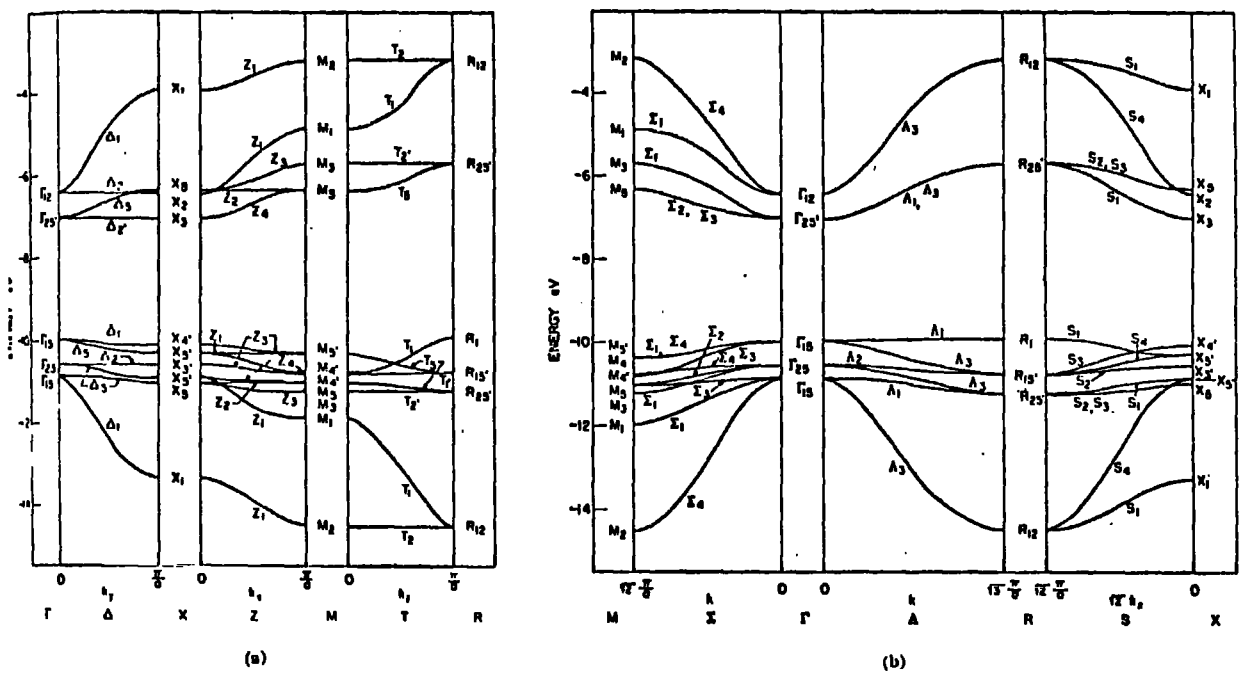

~~FIG. 3.~~ (a) and (b) Plot of energy versus wave vector for all lines of symmetry of the Brillouin zone.

FIG. 31.3.

from 9 to 12. Another effect is due to the single short O - O distance. This is $\sim .32\text{Å}$ less than the next batch of neighbours, (and $.22\text{Å}$ less than the generally accepted O diameter of 2.8).

This fact might be used in further theortical work as follows. If, as seems likely, the crystal field splitting of the oxygen p states is larger than the O - O and Sn - O overlap integrals, then the crystal field splitting should be considered first. It will split each oxygen's p states into 3 levels. The largest O - O overlap integral is then likely to be that between the single nearest neighbours, forming a sort of oxygen 'molecule' with two states where there was one previously. Finally the other overlap integrals between the two 'molecules' in the unit cell will split the states further. This may be shown diagrammatically (for k = 0) in fig. 3.1.4.

The neglect of the Sn - O (or sp) overlap integrals in the above description is possibly justified because Kahn and Leyendecker show that in $SrTiO_3$ at k = 0 those integrals are not operative.

We shall now consider difference (2), the larger O - O distances in SnO_2. The increase from 2.76Å ($SrTiO_3$) to 2.906Å (SnO_2) should significantly reduce that part of the width of the bands that can be attributed to direct overlap of oxygen ions.

Difference (3), Sn replacing Ti, shows its main effect in the conduction band, which should now be attributed mainly to Sn 5s. Another effect is that the (occupied) Sn 4d electrons are closer in energy to the Sn 5s than the Ti 3p electrons are to the Ti 4d.

Kahn and Leyendecker used the following parameters in their ($SrTiO_3$) calculation which may give a guide to what might be expected in

SnO_2.

	Electrostatic (crystal field) splitting of d orbitals		0.62 e.v.
	" " " " " " p "		0.48 e.v.
	overlap integral (resonance integral)	p d σ	2.1 e.v.
O - Ti	" " " "	p d π	.84 e.v.
	" " " "	p p σ	-0.16 e.v.
O - O	" " " "	p p π	0.062 e.v.

The comparison between TiO_2 and SnO_2 should be closer than between $SrTiO_3$ and SnO_2. All the O - O distances in SnO_2 being bigger should reduce the width of the p valence bands. Eagles (1964) quotes a total width of the valence bands in TiO_2 as 4 e.v., deduced from soft X-ray measurements.

The likelihood of the narrowest valence bands being near the top can be shown by considering what are likely to be the largest overlap integrals, the sp integrals. They will act so as to repel the respective energy levels from each other. Thus those valence bands in which they operate will be pushed down, leaving the narrower bands in which they do not operate near the top.

It must be pointed out that in this section we have been discussing electron bands without polaron effects (see section 3.3.).

3.1.5 Other Bonding Models

Morgan (1966) suggests considerable covalent bonding and discusses the role of hydridisation in SnO_2. The basis of this discussion was a paper by Mooser and Pearson (1956). In the view of the present author, the arguments given do not justify the conclusion of there being substantial covalent bonding.

It might be added in this context that the fact of good semi-conducting properties in the conduction band is not incompatible with highly ionic bonding. ~~This is because the conduction band is empty.~~

3.1.6 Band Gap and Electrical Evidence on Valence Bandwidth

One of the main arguments of this thesis is that the top valence band is fairly narrow. Strong support for this contention can also be obtained from high temperature electrical conductivity measurements on intrinsic specimens. Such measurements are available, but their interpretation involves consideration of the band gap and how it varies with temperature. No one else has published conclusions, based on intrinsic conductivity, about the effective mass. In conjunction with our own and other results from absorption edge measurements a general picture of how the band gap varies with temperature emerges, as well as support for the contention of narrow valence bands. For these reasons band gap measurements will now be considered.

Several workers have published figures for the band gap of SnO_2, either films or single crystal. They range from 3.2 - 4.0 e.v. The method of measurement has been mostly optical (e.g. Arai (1960) gives 3.7 e.v., Koch (1964) gives 3.45 e.v. (both films), E.E. Kohnke (1962) gives >3.54 e.v., R. Summitt, J. A. Marley and N. F. Borelli (1964) gives 3.93 e.v. (11^{11} to c axis) and 3.57 e.v. ($\perp$ c axis) and Nagasawa, Shionoya and Makishima (1965) gives 3.5 e.v. (single crystals)). The most important other method is intrinsic electrical conductivity (Marley and MacAvoy (1962) give 3.2 e.v., and T. Arai (1960) gives 3.4 e.v.). The only other method appears to be photoconductivity, for which Houston and Kohnke (1965) give 4.0 e.v.

Our own work on the absorption edge leads to 3.49 e.v. at room temperature and 3.59 e.v. at nitrogen temperatures (see 6.1). None of the published optical interpretation is to be trusted. Most of the writers use rough "rule-of-thumb" methods and don't claim accuracy. Summitt, Marley and Borelli completely fail to realise that in strongly ionic crystals like SnO_2, direct transitions with no phonons involved play a minor role. However they seem to be the only other workers to have measured in polarised light, and their crystals are purer than ours and their measurements, over most of the range, more accurate.

The electrical work is easier to interpret. Morgan and Wright (1966) show that for highly doped specimens the electron mobility only changes as $T^{-\frac{1}{2}}$ over the range where intrinsic conductivity can be easily observed (750 - 1300°K).

More recent results of Morgan (1966) show that for less highly doped specimens mobility varies as $T^{-0.6}$ and $T^{-0.9}$ for two different specimens. It seems that a variation of between $T^{-\frac{1}{2}}$ and T^{-1} is reasonable. For intrinsic specimens the holes because of their high mass will reduce

the mobility like ionised impurities, but concentrations are smaller than those of the donors in the above specimens.

As the number of intrinsic carriers varies by a factor of 10^5 over the temperature range the effect of the mobility variation is quite small and the conductivity roughly varies with the number of electrons (the holes, due to low mobility, can be ignored). More important however, the published values of band gap derived from conductivity have not taken into account the variation of band gap with temperature. They also seem to have ignored the $T^{3/2}$ factor which enters the formula for the intrinsic number of carriers. This is

$$n_i = p_i = 4.82 \times 10^{15}\, T^{3/2} \left(\frac{m_e m_h}{m^2}\right)^{\frac{3}{4}} \exp\left[-Eg/2kT\right] cm^{-3}$$

where m_e and m_h are density of states effective masses.

If $Eg = (Eg)_o - T\frac{\partial(Eg)}{\partial T}$,

then n_i varies as $\exp\left[\frac{(Eg)o}{2kT} - \frac{\partial(Eg)}{\partial T 2k}\right] = \exp\frac{(Eg)_o}{2kT} \exp\frac{\partial(Eg)}{2k\partial T}$. The second factor is constant to first order as T varies, and a conductivity measurement will measure $(Eg)_o$, the energy gap linearly extrapolated to 0^oK.

As far as the accuracy of the electrical results is concerned, those of Marley and MacAvoy only cover a limited intrinsic temperature range for any one specimen, and maybe not sufficient allowance has been made for the extrinsic effects. Such allowance would steepen the graph and raise Eg. Arai's results are on a film and one that has been oxidised from SnO, and so they may not be very reliable. The effects of the $T^{3/2}$ term and the mobility variation are quite small.

Valence Band Effective Mass from Electrical Measurements

The above formula for n_i contains only three unknowns, Eg, m_e and m_h. In order to get a rough estimate of m_h, approximately known values can be taken for Eg and m_e, and n_i can be estimated from conductivity and mobility for intrinsic specimens. For a temperature of 1250°K (the high value chosen to minimise extrinsic effects) an average value for σ from several sources seems to be 0.5 $(ohm/cm)^{-1}$, to an accuracy of about a factor of 3. A mobility of 45 cm^2/volt sec. seems about the best value (Morgan and Wright (1966) and Morgan (1966)). These figures give

$$n_i = \frac{\sigma}{e/u} = \frac{0.5}{1.6 \times 10^{-19} \times 45} = 7 \times 10^{16} cm^{-3}$$

Recently published results of Summitt and Borelli (1966) on the temperature dependence of the absorption edge are very interesting. It will be shown, when the absorption edge is interpreted, that their use of a fixed value of absorption at different temperatures does not accurately reflect the band gap at different temperatures. Also, their interpretation of absorption // to c axis as giving a second band gap we believe to be wrong. Our two points, however, agree quite well with their results for $\perp$ c axis. We shall, however use their value of band gap (for polarization $\perp$ c axis) at 1250°K. Their value works out at 2.33 e.v.

Taking m_e as $0.3m_j$ then the above formula gives

$$\frac{m_h}{m} = \left[4.8\times10^{15} T^{3/2}\right]^{-4/3} \left[0.3\right]^{-1} \left[\exp\left(2.33/2kT\right) \times 7\times10^{16}\right]^{4/3}$$

$$= 3.3 \left[\frac{\exp(10.8)}{3.03\times10^{3}}\right]^{4/3} = 140$$

This figure must only be treated as very approximate. An error in the intrinsic conductivity of a factor of 2 would change it by a factor of about 2.5. It should also be remembered that it is a density of states effective mass.

Such a large value of m_h leads one to examine the assumptions of of the formula used to obtain it. It is found that parabolic bands are assumed to hold up to energies of the order of kT from the band edge. A more informative viewpoint is to see, in the usual simplified band picture, what value of the effective valence band density of states, Nv, is required.

$$\text{Since } Nv = 4.8 \times 10^{15}\, T^{3/2} \left(\frac{m_h}{m}\right)^{3/2} \text{ cm}^{-3},$$

$$\text{for } T = 1250^{\circ}K \text{ and } \frac{m_h}{m} = 140,\ Nv = 3.6 \times 10^{23}.$$

This figure is not possible. There are 4 oxygen atoms to a unit cell and each has 6 p states. There should be no other states within an energy of many kT. There are 1.4×10^{22} unit cells / cm^3 so that there are only 3.4×10^{23} p states / cm^3, and this sets an upper limit to Nv. It is quite possible, though, that σ may in fact be half the above average value and an additional error of 30% in m_h due to errors in E, m_e and μ is quite reasonable. Allowance for these possible corrections gives $\frac{m_h}{m} = 43$ and $Nv = 0.6 \times 10^{23}$. This kind of figure is afforded a simple explanation. The crystal field splitting is likely to produce a splitting between the local p_x, p_y and p_z wave functions of the individual oxygen atoms of several kT. The combinations of these states within a unit cell and into bands of the crystal may well produce only quite a small energy spread (see earlier in this section, and the small polaron theory in 3.3).

The latter value of Nv is then roughly obtained if the top 4 of the 12 valence bands occupy a total energy spread of $\lesssim$ kT. If their maximum spread is taken as kT (and the band gap is taken as referring roughly to the middle of these bands rather than the top), then the minimum value of effective mass for each of the 4 top bands, if they are assumed degenerate, is about 20m. It should be emphasized that this is a minimum value. If $m_h' = \infty$, then the only electrical difference would be that the log of the intrinsic conductivity would differ, from the $m_h' = 20$ m case, by a factor of about $T^{\frac{3}{4}}$, which is barely noticeable. In the unlikely event of all twelve valence bands being effectively degenerate the value of m_h' for any one band would be about 9m for the latter value of Nv.

The gradient $\frac{\partial (Eg)}{\partial T}$ quoted by Summitt and Borelli is 1.2×10^{-3} e.v./^{o}K for high temperatures. This implies a (Eg)o of $2.33 + 1.2 \times 1.25 = 3.83$ e.v. at high temperatures. After this section was written, D.F. Morgan (1966B) showed me his results for the conductivity of apparently intrinsic specimens. For the high temperature range (900-1200^{o}K) the activation energy for the three most resistive specimens is $3.8 \pm .1$ e.v. This is very satisfactory agreement. The lower values quoted above presumeably arise from small extrinsic effects.

We conclude that there is strong electrical evidence for a large valence band (polaron) effective mass, of the order of, or larger than, 20m. // A note should just be added justifying our use of Summitt and Borelli's result for Eg and its temperature variation, at 1250^{o}C, after criticizing their method. We will show in section 3.5 that their method produces only fairly small errors for the temperature dependence

for polarization $\perp$ c axis. The errors will be shown to probably lead to a slightly too large value of gradient $\frac{\partial(Eg)}{\partial T}$. At 1250°K their figure for Eg is probably rather too small (2.4 e.v. might be better) . The gradient around 1100°K should, perhaps, be 1.15 e.v./ °K rather than 1.2 e.v./°C.

3.2 Phonons

3.2.1. Introduction

The ionicity of SnO_2 means that electron-phonon coupling is important and the maximum possible information on the phonon spectum is required. Especially important are the I.R. active optical modes.
The evidence will first be discussed, and then calculation of phonon parameters will be given.

Evidence concerning the I.R. active phonon branches comes from several sources:-

(1) Theoretical, by a consideration of the symmetry modes of the rutile lattice.

(2) I.R. absorption measurements.

(3) I.R. reflection measurements.

(4) Low frequency dielectric constant measurements.

(5) I.R. refractive index measurements.

(6) Recent low temperature absorption in the immediate vicinity of the absorption edge.

We consider these in order.

3.2.2. Theoretical

The first author to apply group theoretical arguments to the phonon spectrum of rutile was Dayal (1950). He found 5 Raman active modes (2 of which are degenerate), 9 I.R. active modes (6 of which doubly degenerate

in pairs) and one mode inactive in both. Later authors corrected this by removing two of the I.R. active modes and classing them as inactive in both. The 6 doubly degenerate I.R. modes have one mode from each pair with polarisation along the a axis and one mode with polarisation along the (symmetric) b axis, though, being degenerate, any pair of $\perp$ directions in the a b plane is equally good. These modes are of symmetry Eu and should give rise to three resonances in the I.R. spectrum for light polarised $\perp$ to the c axis. The remaining I.R. mode is A_{2u} and is polarised $//^{u}$ to the c axis, and should give rise to a single I.R. resonance for light polarised $//^{u}$ to the c axis.

3.2.3 I.R. Absorption Measurements

The Japanese workers Ishiguro, Sasaki, Arai and Imai (1958) and Arai (1960) have measured the I.R. transmission of powdered SnO_2. Both appear to be the same results presented rather differently, and Arai quotes his sample as being 2.5 mg/sq.cm., which means about 3.5 μ thick. The wavelength range is 25 μ - 200 μ, and the main conclusion to be drawn is that there are two absorption peaks, quoted as 33 μ and 39 μ.

Precise interpretation of transmission measurements around phonon resonances is not easy, because absorption, reflection and interference phenomena are all involved. For very thin films the situation is somewhat simpler because the interference is nearly zero order and reflection is not so important. In this case absorption predominates.

The Japanese films are barely thin enough to fall into this category. The peaks, however, can be taken as largely absorption peaks, particularly if the tip of the peak is used, as the absorption peaks are narrower than the reflection maxima.

An expression for the position of the absorption maximum was given in 2.3 as $\omega_0 + 0.29\ g$. It can be shown that the 33 and 39 μ peaks satisfy the conditions for the validity of this expression. g is estimated in 5.6 as being $\frac{\omega_0}{25}$ for the 33 μ peak and $\frac{\omega_0}{20}$ for the 39 μ peak, so it would seem that the ω_0 for each peak is $1 - 1\frac{1}{2}\%$ less than given by the absorption peaks.

Miloslavskii 1959 presents transmission measurements from 2 to 18 μ on conducting thin films. In addition to absorption due to impurities, the films show a peak, quoted as being at 16.4 μ. These specimens more nearly fulfil the thin condition than the above specimens. The peak is due to the most energetic $\perp$ phonon, and we shall use the measurements as a rough check on the magnitude and position of the absorption due to this phonon. We use the two specimens with the highest transmission and lowest conductivity, because these should minimise the effects of impurities and of reflection. Calculation indicates that on reasonable assumptions the apparent absorption is increased by a factor of very roughly two due to reflection. After allowance is made for a presumed zero error due to reflection, one obtains over the region of the peak (14 - 18 μ), $\int K d\lambda = 4.5$ for one specimen and 5.5 for the other. Calculation indicates that to allow for the unorientated nature of the films, these figures should be multiplied by about 1.25 to give the values for $\perp$ polarisation. Using (2.3.11) with $\lambda_a = \infty$, the phonons contribution to $n_s - 1$ for $\perp$ polarisation is given as .285 by the first film and .35 by the second. If this is to be compared to the contribution to ϵ_s found in sec. 5.6, the contribution of the

other phonons to ϵ_s is to be taken as their contribution to ϵ in the region of the peak ($\lambda \sim 16\mu$). This is about -1. In a similar way the impurity contribution to ϵ_s is to be taken as ~1.4 for the first film and 2.2 for the second. Thus taking our artificial parameters without the contribution of the phonons in question to be $n_s = \sqrt{\epsilon_s} = 2.1$ for the first film and 2.28 for the second (assuming $n_\infty = 2$) we get contributions to ϵ_s by the phonon of 1.3 (first film) and 1.7 (second film), which are to be compared with a value of 1.76 found in sec. 5.6.

More detailed study of the absorption peak indicates a larger value of g than is found in 5.6, especially if the contribution to ϵ_s is 1.76 rather than the rather smaller values suggested above. Perhaps $g = \frac{\omega_t}{15}$ is a fair estimate. Using $\omega_t + 0.29g$ given above as the maximum absorption, a 2% difference between the absorption peak and ω_t is obtained. The peak measured as 16.4μ is also influenced by reflection: reflection is decreasing quite rapidly with increasing λ in the region of the peak and this will shift the peak by perhaps another 1%. These two factors would make ω_t correspond to 16.9μ or 592 cm^{-1}. The value found in 5.6 is 577 cm^{-1}.

Finally, measurements were taken here of the transmission of films of powdered SnO_2 mixed with Nujol. This is a standard technique used by chemists for obtaining the spectra of solids. The spectrum was taken as far as 25μ, and its primary purpose was to bridge the gap between the Japanese and Russian work. This is described in section 5.6. The result is to broadly confirm the presence of phonon peaks around 16μ and 19μ.

3.2.4 Reflection

The results of numerical curve fitting work on this and other data has been put in 5.6.

Reststrahlen reflection measurements are the most general data for the analysis of I.R. active phonons. (Absorption measurements are probably best for determining the precise transverse phonon frequencies).

Reflection measurements have been made by Turner (1962) from 4 to 36 μ which are shown in fig. 3.2.1. The material is cassiterite (natural SnO_2), and no orientation is specified but it appears to be single crystal with orientation a little off $\perp$ polarisation. Summitt(1965) has measured the reflection for both polarisations from 1100-410 cm^{-1} (9-24 μ). This is shown in fig. 3.2.2. Summitt suggests his data is insufficient to do a Kramers-Kronig analysis in order to convert the reflection into absorption, and that Turner's data is less accurate than his. However it was felt that with the addition of other information the less exacting classical dispersion analysis was worth doing. To do this the phonon resonances are represented by damped harmonic oscillators and the limited number of parameters is adjusted to give the best fit to all the data.

The extra information consists of that given in other subsections of 3.2, and:

1. Liebisch and Rubens (1919) made polarised reflection measurements on cassiterite using the reststrahlen method. This method gives poor resolution and only isolated wavelengths, but they developed a lot of expertise.
2. The high frequency dielectric constants (see 6.5 or Reddaway 1966).
3. The low frequency dielectric constant for $\perp$ polarisation

MEASURED REFLECTANCE OF CASSITERITE (SnO_2)

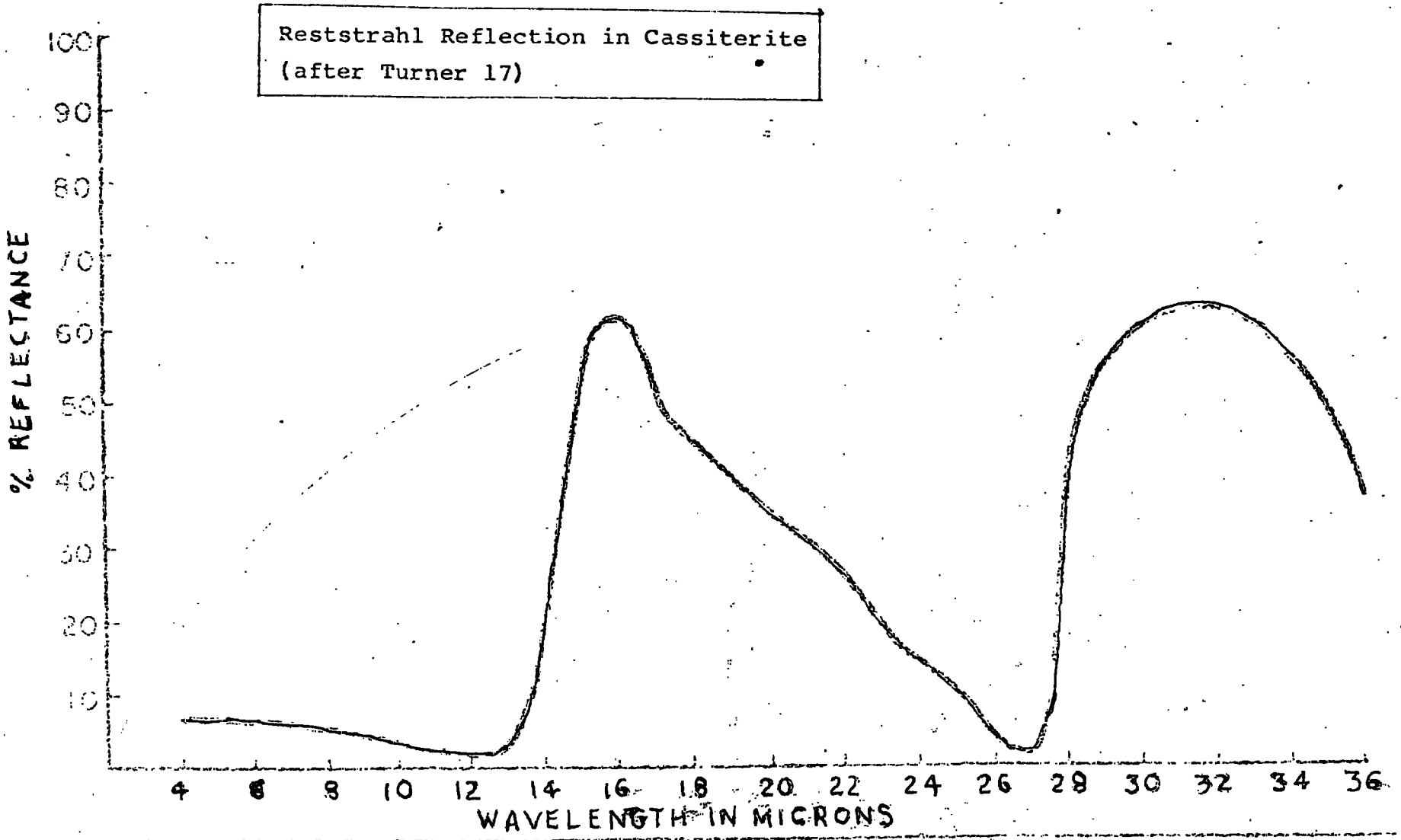

Fig 3.2.2.

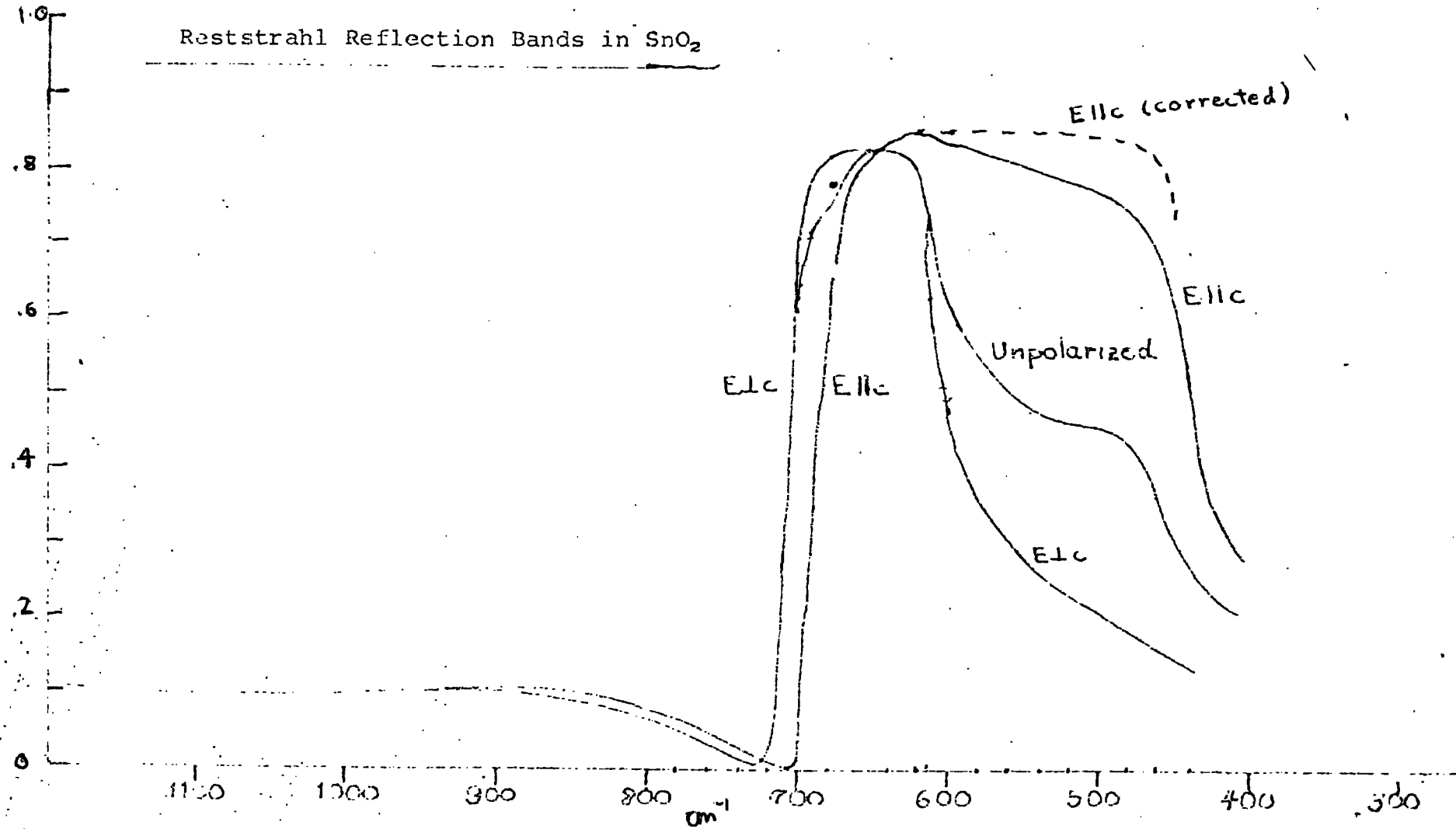
Reststrahl Reflection Bands in SnO_2
E⊥c (corrected)
E∥c
Unpolarized
E⊥c
E∥c
E⊥c
1.0
.8
.6
.4
.2
0
1100
1000
900
800
cm⁻¹
700
600
500
400
300

(Summitt 1965). At 1 M^c/s this is 13.6, a result to be preferred to the values of about 24 for both polarisations derived by Liebisch and Rubens from the reflections at 300μ, and quoted in the literature.

3.2.5 I.R. Refractive Index Measurements

I.R. dispersion is due to the phonon "reststrahlen" absorption. Thus in getting the best fit to the phonon spectrum, the phonon parameters must be made to also give a good fit to the I.R. dispersion. This has been done.

3.2.6 Absorption Edge

Nagasawa and Shionoya (1966) have detected a sharp exciton spectrum at 1.3°K. Just in the continuum there are two sharp increases in gradient. The most natural interpretation of these is phonon assisted transitions to the exciton ground state by the two lowest energy longitudinal phonons respectively. This is reinforced by the phonon energies (derived by measurement from their published graph) agreeing approximately with values previously derived. The two phonon energies measured from the graph are 290 cm^{-1} and 371cm^{-1}. These are, of course, the values at 1.3°K and available figures for other crystals indicate a few percent variation between low temperatures and R.T. However, the phonon energy in these other crystals is around half the values of the lower energy phonons in SnO_2, and so the variation is likely to be considerably less in SnO_2.

3.2.7 Calculation of Phonon Parameters Required in Polaron Theory

From the results of fitting the reflectivity and other data with classical oscillators (see 5.6) we shall now derive the very important strengths of the polarization of the different phonon branches. From the polarisation, the electron-phonon coupling strength of the phonon branches can be calculated. We shall be following Eagles 1964 work on rutile and Kurosawa 1961.

The transverse polarizations $P_{t/u}$ are given by

$$4\pi N P^2_{t/u} = 4\pi \rho_{/u} \omega_{t/u}$$

where subscript t stands for transverse, $/u$ (= 1,2,3 or 4) labels the phonon branch and N is the number of unit cells per unit volume. Values of $4\pi \rho_{/u}$ and $\omega_{t\mu}$ are given in 5.6, together with values of $\omega_{l\mu}$, the longitudinal frequencies. Eagles expands the longitudinal mode atomic displacements in terms of the transverse displacements,

$$x_{l\mu'} = \sum_{\mu} b_{\mu'\mu} x_{t\mu} \quad ,$$

and states that $\sum_{\mu} b^2_{\mu'\mu} = 1$, and

$$b_{\mu'\mu} = - \frac{4\pi N \; P_{l\mu'} P_{t\mu}}{\epsilon_{\infty a} (\omega^2_{t\mu} - \omega^2_{l\mu})} \; .$$

(Eagles gives $\omega^2_{l/u}$ instead of $\omega^2_{l/u'}$ which must be a misprint). Here $P_{l/u'}$ are the longitudinal polarisations and $\epsilon_{\infty a}$ is the value of ϵ_{∞} in the a or b direction.

These equations have been used to derive $4\pi N \times p^2_{1/u'}$ and, incidentally, $b^2_{/u/u'}$. Eagles tabulates these for rutile, but as no use is made of them we shall not bother.

From $p^2_{1/u'}$ we calculate the most important parameter, $f^2_{/u'}$, defined as $\dfrac{p^2_{1/u'}/\omega^2_{1/u'}}{\sum_{/u} p^2_{1/u'}/\omega^2_{1/u'}}$. This is given in table 3.2.1 where we have changed /u' to /u. Eagles shows that this is the factor with which to weight $\frac{1}{\epsilon_\omega} - \frac{1}{\epsilon_s}$ for each phonon branch in polaron theory. In rutile the dominance of the highest energy phonon is very great, which simplifies matters very much. In SnO_2 this is seen not to be the case to nearly such an extent.

In 5.6 we state that the last 'phonon' for each polarisation is a very dubious one put in to make the best of the experimental data. It does not affect the results very much.

Table 3.2.1

/u	$f^2_{/u}$	
	⊥ polarisation	// polarisation
1	.608	.881
2	.309	.119
3	.0224	
4	.0603	

3.3 Polarons in SnO_2

3.3.1 Introduction

The main difficulties encountered in applying polaron theory to SnO_2 (and TiO_2) are:-

(1) There are three theoretically allowed phonon branches that are infra-red active for polarisation $\perp$ to the c axis.

(2) Anisotropy.

(3) The lattice anharmonicity.

(4) The multiplicity of the valence bands.

(5) The lack of a good understanding of polaron properties for polarons with energies of the order of a phonon energy above the bottom of the band, for large polarons (Eagles 1963 p.1381). This difficulty is general and not confined to SnO_2. It is important for the optical properties.

(6) The lack of an adequate theory bridging the gap between small and large polaron theory. For the top valence band this is most nearly covered by nearly small polaron theory.

Several features of this account will be following Eagles 1964 treatment of polarons in Rutile.

These points will now be considered in more detail.

3.3.2 Multiple Phonon Branches and Anisotropy

Taking (1) and (2) together, Eagles 1964 showed that the large polaron coupling constant for the different phonon branches is given by:-

$$\alpha_{\mu} = \tfrac{1}{2} e^2 \left(\frac{2m}{\hbar^3 \omega_{\mu}}\right)^{\frac{1}{2}} \left\langle f^2_{\mu y} \left(\frac{1}{\epsilon_{\infty y}} - \frac{1}{\epsilon_{sy}}\right) \right\rangle_{av} .$$

Here $\mu = 1,2,3$ denotes the phonon branch and $\gamma = a,b,c$ denotes the three axial directions, $\langle\ \rangle_{av}$ denotes a simple average over those directions, $f^2_{\mu\gamma}$ is a weighting factor obtained from the I.R. phonon spectrum analysis (see 3.2) and ω_μ is an average over direction for each longitudinal phonon branch (at small wave vector), the average being weighted in favour of the most polar direction. (The phonon spectrum for wave vector $//^{a}$ c axis is to be thought of as consisting of 3 phonon branches, two of them with zero polarisation and unknown frequency.) It is clear that the above expression for α reduces to the usual one, in the case of an isotropic single-phonon-branch crystal.

The above expression still assumes a single effective mass m. In this thesis we assume an isotropic conduction band mass. The only evidence the author is aware of is first Morgan (1966) who measured mobility on different samples, some along the c axis and some the a axis. The results appear to show a somewhat lower mobility in the c direction, indicating a higher mass in that direction. The second bit of evidence is the free carrier absorption (see 6.3) which indicates a somewhat lower mass in the c axis direction. The third bit of evidence is the splitting of the n = 1 exciton peak dealt with in 3.4. This indicates $m_{c\perp} \approx 1.1\, m_{c//}$. An isotropic effective mass is thus probably only a moderate approximation for the conduction band. (It will be argued later that it is probably a very poor approximation for the valence band.) We therefore include a few remarks on anisotropy in large polaron theory.

The polaron binding energy is determined by α, and as polaron energy at k = o cannot depend on which direction the polaron moves, it is clear that for determining α an average value for m should be used. However

for finding the characteristic length or polaron mass, m^*, for a particular direction it would seem that the appropriate band mass should be used (not though in α). It would seem, too, that a polaron can show large polaron properties in one direction and small polaron properties in another. The question may be important, because even cubic $SrTiO_3$, (Kahn and Leyendecker 1964) shows large differences in effective mass with direction, and for tetragonal crystals the symmetry restrictions are further relaxed. It would seem that for large ratios in the effective masses, a single high effective mass would dominate α.

3.3.3 Lattice Anharmonicity

This was discussed in 2.2. It would appear that for some purposes it might be best to add a fourth phonon frequency at low energies, due to anharmonic effects. We only use the three 'proper' phonons in the polaron theory.

3.3.4 Valence Bands

These are discussed in 3.1. There are a total of 12 bands, some of which are likely to degenerate at symmetry points such as $\underline{k} = 0$. No small polaron theory of which the author is aware considers anything other that a single, well-isolated band. Both degeneracy and closeness of other bands appear bound up with some fundamental aspects of the theory, and these problems will not be solved in this theses.

Another aspect of this valence band multiplicity is that symmetry is likely to require, in other than very simple lattices, that some bands "stick together" at the zone boundary. These bands may not be horizontal at the boundary and from some points of view are best considered in terms of a larger B.Z. with fewer bands. It would seem that the approximation in small polaron theory that bands have a sinusoidal shape with a period equal to that of the B.Z. should be applied to this larger B.Z. in the case of these

bands that "stick together".

3.3.5. Conduction Band Polaron E - k curve

All polaron theories give $E \propto k^2$ for small k, and so each theory can define a polaron effective mass in this region. The most satisfactory theory for larger values of E (the polaron energy measured from the bottom of the polaron band) up to $E = \hbar\omega$ is given by Larsen (1966). His results show that as E approaches $\hbar\omega$ from below it bends over on the E - k curve and is actually horizontal at $E = \hbar\omega$, as sketched in fig. 3.3.1. However, as is made clearer in the earlier paper of Whitfield and Ruff (1965), at a certain value of k, the curve turns a sharp corner and E rises quite steeply away from $E \doteqdot \hbar\omega$, as is shown in fig. 3.3.1.. The present author has not come across a recent treatment of this region, $E > \hbar\omega$. It seems that it presents special difficulties because this region represents a quasi-particle with only a finite life-time before it emits a phonon and returns to a lower energy. The discontinuity of slope at $E = \hbar\omega$ can be thought of as a resonance effect, because the emission of a phonon first becomes possible at that energy. For $E > \hbar\omega$ we use the variatonal theory of Fröhlich et. al. (1950). They found

$$E = \alpha + k^2 - \frac{\alpha}{k} \times \frac{\pi}{2} \qquad (3.3.1)$$

(We have taken the units of energy to be $\hbar\omega$ and the units of k to be $(2m_c\omega/\hbar)^{\frac{1}{2}}$ and the polaron binding energy at k = o to be α). Unfortunately this does not intersect the line E = 1 at the same point as Larsen's solution, but the difference is not great and the consequent uncertainty does not affect the final result for the absorption edge very much. Larsen only evaluates his results for $\alpha = 1$, and the present author has not yet mastered the integrals required to make further evaluations for different α.

There is the additional problem in SnO_2 of several phonon energies. The method used to deal with this is given in 6.1.

3.3.6 Nearly Small Polaron Theory

This is the theory used for the valence band. One of the difficulties of applying the theory to SnO_2 is the anisotropy, which is not treated explicitly by Eagles (1966). We shall now calculate the bandwidths, binding energy and optical absorption parameter D in terms of the overlap integrals J for the SnO_2 lattice. We shall assume, as Eagles does in applying his theory to $SrTiO_3$, that all the different subscripted parameters J are equal (though not necessarily for the different crystallographic directions). For the rutile lattice Eagles' parameter, q, = 2Z where Z is the number of nearest neighbour lattice sites. Thus Eagles eq 3.2.1 and 3.2.4 gives the polaron bandwidth as

$$W = 2Z\ J\ \exp\left[-\tfrac{1}{2}\ (2\bar{n}+1)\ (So + S_1)\right]$$

where S and S_1 will be defined shortly, and $\bar{n}$ is the mean phonon occupation number. To account for anisotropy, consideration shows this should become

$$W = 8J_1\ \exp\left[-\tfrac{1}{2}\ (2\bar{n}+1)\ (S_{o1}+S_{11})\right] + 4J_2\ \exp\left[-\tfrac{1}{2}(2\bar{n}+1)\ (S_{o2}+S_{12})\right]$$

where the final suffixes 1 and 2 indicate $\perp$ and // polarisation respectively.

Combining several of Eagles equations we get

$$S_o = \frac{2B_o}{\hbar\omega}\left[1 - \frac{Si(w_o G)}{w_o G}\right]$$

where $Si(x) = \int_0^x \frac{\sin y}{y}\,dy$

$w_o \equiv 2\pi\left(\frac{3}{4\pi V_c}\right)^{\frac{1}{3}}$, V_c = unit cell volume. (The first Brillouin zone ($\equiv$ .938Å for SnO_2) has been replaced by a sphere of the same volume and of radius w_o).

G is a nearest neighbour lattice vector.

Using the continuum polarisation model Eagles gets

$$B_o = \frac{e^2 w_o}{\pi}\left(\frac{1}{\epsilon_\infty} - \frac{1}{\epsilon_s}\right)$$

S_{o1} and S_{o2} are obtained by inserting the appropriate lattice vectors. Using the unit cell dimensions for SnO_2 of a = b = 4.74Å and c = 3.186Å we obtain

$\hbar\omega S_{o1} = \left(\frac{1}{\epsilon_\infty} - \frac{1}{\epsilon_s}\right)$ 5.38 e.v. $\hbar\omega S_{o2} = \left(\frac{1}{\epsilon_\infty} - \frac{1}{\epsilon_s}\right)$ 3.28 e.v.

$B_o = \left(\frac{1}{\epsilon_\infty} - \frac{1}{\epsilon_s}\right)$ 4.30 e.v.

Combining several of Eagles equations and making what appear to be correct allowances for anisotropy we get

$$\hbar\omega S_{11} = -2\left[\hbar\omega S_{o1}\left(\frac{4}{\hbar\omega S_{o1}}\left(\frac{J_1}{\hbar\omega S_{o1}}\right)^2 + 2\left(\frac{J_2}{\hbar\omega S_{o2}}\right)^2\right) - B_o\left(\frac{J_1}{\hbar\omega S_{o1}}\right)^2\left\{8\frac{Si(w_o a)}{w_o a} - 4\frac{Si(w_o\sqrt{2}a)}{w_o\sqrt{2}a}\right.\right.$$

$$\left.\left. - 2\frac{Si(2w_o a)}{2w_o a} - 2\right\} - 4B_o\left(\frac{J_2}{\hbar\omega S_{o2}}\right)^2\left\{\frac{Si(w_o c)}{w_o c} - \frac{Si(w_o(a^2 + c^2)^{\frac{1}{2}})}{w_o(a^2 + c^2)^{\frac{1}{2}}}\right\}\right]$$

$$\hbar\omega S_{12} = -2\left[\hbar\omega S_{o2}\left(4\left(\frac{J_1}{\hbar\omega S_{o1}}\right)^2 + 2\left(\frac{J_2}{\hbar\omega S_{o2}}\right)^2\right) - 2B_o\left(\frac{J_2}{\hbar\omega S_{o2}}\right)^2\left\{2\,\frac{Si(w_o c)}{w_o c} - \frac{Si(2w_o c)}{2w_o c} - 1\right\}\right.$$

$$\left. - 8B_o\left(\frac{J_1}{h\,S_{o1}}\right)^2\left\{\frac{Si(w_o a)}{w_o a} - \frac{Si\,(w_o(a^2+c^2)^{\frac{1}{2}})}{w_o\,(a^2+c^2)^{\frac{1}{2}}}\right\}\right]$$

Inserting the lattice parameters for SnO_2 we get

$$\hbar\omega S_{11} = -\,(1.57\,J_1^{\,2} + .90\,J_2^{\,2})\left(\frac{1}{\epsilon_\infty} - \frac{1}{\epsilon_s}\right)^{-1}$$

$$\hbar\omega S_{12} = -\,(.67J_1^{\,2} + 1.22\,J_2^{\,2})\left(\frac{1}{\epsilon_\infty} - \frac{1}{\epsilon_s}\right)^{-1}$$

The optical absorption parameter D is given by (Eagles 1966B)

$$D\,\hbar\omega = Bo - Z\left(J/\hbar\omega S_o\right)^2$$

Allowing for anistropy, we get

$$D\,\hbar\omega = B_o - 4\left(\frac{J_1^{\,2}}{\hbar\omega S_{o1}}\right) - 2\left(\frac{J_2^{\,2}}{\hbar\omega S_{o2}}\right) \qquad (3.3.2.)$$

For the SnO_2 lattice we get

$$D\,\hbar\omega = 4.3\left(\frac{1}{\epsilon_\infty} - \frac{1}{\epsilon_s}\right) - (.744\,J_1^{\,2} + .61\,J_2^{\,2})\left(\frac{1}{\epsilon_\infty} - \frac{1}{\epsilon_s}\right)^{-1} \qquad (3.3.3.)$$

FIG. 3.4.1.

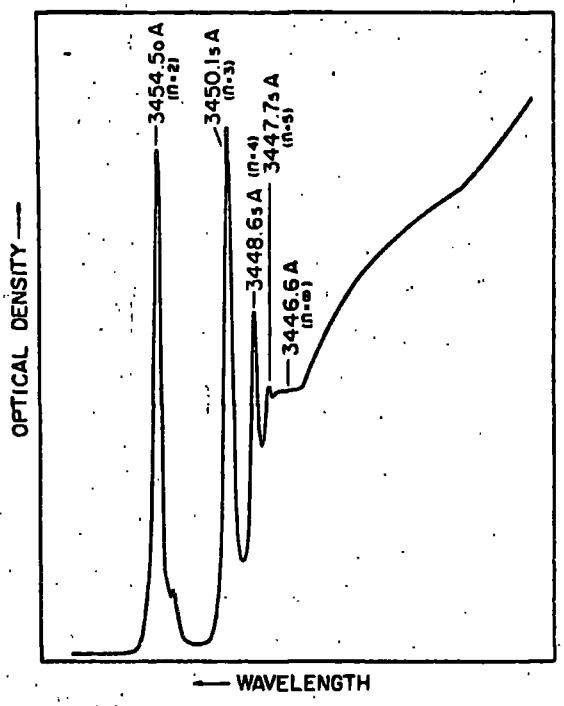

Fig. 1. Structure at the fundamental absorption edge of SnO_2 single crystals at 1.3°K.

Table 1
Observed and calculated exciton energy levels in SnO_2 at 1.3°K.

Quantum number (n)	$\lambda_{calc.}$ (Å)	$E_{calc.}$ (eV)	$\lambda_{obs.}$ (Å)	$E_{obs.}$ (eV)
1	3478.5	3.5641	3480.3	3.5622
2	3454.5	3.5888	3454.5_0	3.5888_5
	-	-	3453.5_0	3.5899_0
3	3450.1	3.5934	3450.1_5	3.5933_5
4	3448.6	3.5950	3448.6_5	3.5949_5
5	3447.8	3.5958	3447.7_5	3.5958_5
!	!	!	!	!
∞	3446.6	3.5971	–	–

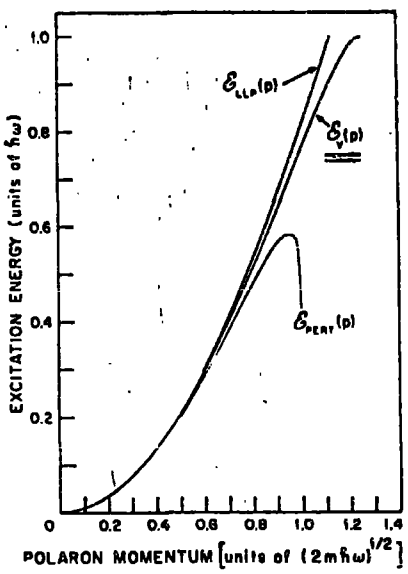

FIG. 1. Polaron excitation energy-versus-momentum curves for $\alpha=1$ as computed by three different methods. $\mathcal{E}_{LLP}(p)$ is the variational result of LLP. $\mathcal{E}_v(p)$ is the variational result of the present paper. $\mathcal{E}_{Pert}(p)$ is the result of Rayleigh-Schrödinger perturbation theory.

FIG. 3.3.1.

3.4 Excitons in SnO_2

3.4.1 Introduction

Indirect transitions to the ground state exciton are important in the absorption edge.// In SnO_2, as in other ionic solids, the treatment of excitons is made harder by the phonon interaction. From one viewpoint the difficulty becomes apparent if one tries to apply the simple formulae. The formulae contain the dielectric constant, and it must be decided whether to use the high or low frequency value, or some other value. The question is vital, because, e.g., the binding energy varies as ϵ^{-2}, and as $\frac{\epsilon_s}{\epsilon_\infty}$ is about 3 in SnO_2 the difference is large.

Unfortunately there are only simple answers in limiting cases, and in SnO_2 the problem is made worse by their being at least 3 phonon frequencies. The easiest starting point is that of Haken 1963 (in English) and earlier work (in German). He assumes the polaron wave functions of the two particles are known and derives the electron-hole interaction. He then substitutes the intermediate-coupling wave functions into that interaction and obtains the interaction energy:

$$-\frac{e^2}{\epsilon_\infty r}+\frac{e^2}{r}\left(\frac{1}{\epsilon_\infty}-\frac{1}{\epsilon_s}\right)\left(1-\frac{e^{-K_1 r}+e^{-K_2 r}}{2}\right) \qquad (3.4.1)$$

Here $K_1 = (2 m_c \omega/\hbar)^{\frac{1}{2}}$ where m_c is the electron 'bare' mass and K_2 is the equivalent function for the hole. For large values of r it can quickly be seen that (3.4.1) reduces to $-\frac{e^2}{\epsilon_s r}$, i.e. the static dielectric constant applies. Although the assumptions on which the above interaction is based are not all valid at small r, Haken states the formula provides a good qualitative interpretation between the large and small r regimes.

So far small r the interaction reduces to:-

$$\frac{-e^2}{\epsilon_\infty r} + \frac{e^2}{2}\left(\frac{1}{\epsilon_\infty} - \frac{1}{\epsilon_s}\right) \begin{matrix}(K_1 + K_2 - \text{higher terms}) \\ (K_1 + K_2 - \text{higher terms})\end{matrix}$$

In intermediate coupling theory the polaron binding energy is $\frac{e^2}{2}\left(\frac{1}{\epsilon_\infty} - \frac{1}{\epsilon_s}\right) \times (K_1)$, so the second term (which is independent of r) just represents the binding energy of the two separate polarons, and the effective interaction is $-\frac{e^2}{\epsilon_\infty r}$. The best effective masses to be used in the previous interaction for calculating orbits appear to be the polaron masses.

Physically speaking these results can be understood quite easily. At large distances each particle will be completely surrounded by its phonon cloud, the relative angular movement will be slow and so the lattice can follow all the motion. This implies the polaron effective mass and the static dielectric constant should be used. At small distances compared with the characteristic lengths $\left(\frac{\hbar}{2m\omega}\right)^{\frac{1}{2}}$ the electron and hole are inside what would be each others phonon clouds and move so rapidly that the lattice polarization cannot follow the motion, (but we assume the electronic polarization still can). This implies that there are no polaron effects and one should use the 'bare' effective masses and the high frequency dielectric constant for exciton calculations.

3.4.2 Hrivnak's Solution and its Modification

The only analytical solution for an intermediate type of exciton seems to be that of Hrivnak (1959) who took the special case $\epsilon_s = 2\epsilon_\infty$ and $m_e = m_h$, and assumed the exciton radius was less than $\left(\frac{\hbar}{2m\omega}\right)^{\frac{1}{2}}$. Examination shows that he also assumed a single effective mass for both large and small r, which will only be a good approximation for small α. His result for the wave function of the n = 1 exciton gives some interesting insights and is:-

$$\psi = \left[\frac{1}{4\pi}\left(\frac{4}{a_1^3} - \frac{K}{a_1}\right)\right]^{\frac{1}{2}} e^{-\left(\frac{1}{a_1} - \frac{K}{2}\right)r}\left(\frac{1 - e^{-Kr}}{Kr}\right) \qquad (3.4.2)$$

where in our notation $K = K_1 = K_2$. a_1 is the 'Bohr' radius for the high frequency dielectric constant. The bracket on the extreme right approximates to unity except for large γ and so the shape for small γ is that of a hydrogen ground state wave function, with a 'Bohr' radius of $\frac{1}{\frac{1}{a_1} - \frac{K}{2}}$. At large distances the wave function attenuates more sharply than a hydrogen one, and to ensure normalization the coefficient is larger than it would be for a hydrogen function of radius $\frac{1}{\frac{1}{a_1} - \frac{K}{2}}$. Elliott's theory shows that it is this coefficient that controls the magnitude of n = 1 exciton absorption.

For SnO_2 the case of interest is that of a large valence band mass and a small conduction band mass. In the limit, a large mass gives $K_2 = \infty$ and 3.4.1. reduces to

$$-\frac{e^2}{\gamma}\left(\frac{1}{\epsilon_\infty} + \frac{1}{\epsilon_s}\right)\frac{1}{2} + \frac{e^2}{\gamma}\left(\frac{1}{\epsilon_\infty} - \frac{1}{\epsilon_s}\right)\left(\frac{1 - e^{-K_1\gamma}}{2}\right) \qquad (3.4.3)$$

For small γ, the second term again reduces to a constant (the polaron binding energy) and the interaction is that of a dielectric constant $\frac{2}{\frac{1}{\epsilon_\infty} + \frac{1}{\epsilon_s}}$. (This result is confirmed by the result of Platzman 1962 who used the techniques of the Feynman polaron on the equivalent problem of shallow impurity states. His numerical results for non-limiting cases were obtained for the parameters of CdS).

If $\epsilon_s = 3\epsilon_\infty$ (which is nearly true in SnO_2) then we can define an effective ϵ_∞, let us call it ϵ'_∞, by

$$\epsilon'_\infty = \frac{2}{\frac{1}{\epsilon_\infty} + \frac{1}{\epsilon_s}} = \frac{\epsilon_\infty}{2}$$

and (3.4.3.) becomes $\frac{e^2}{\epsilon^1_\infty r} + \frac{e^2}{\epsilon_s r}(1 - e^{-K_1 r})$

which is the same as 3.4.1. with $K_1 = K_2$ and $2\epsilon_\infty = \epsilon_s$, except ϵ_∞ is replaced by ϵ^1_∞. We can therefore now use Hrivnaks solution, provided that for the purpose of calculating the orbit and binding energy we use m_c instead of the reduced mass $\frac{1}{2} m_c$ used for Hrivnak's case of $m_c = m_v$.

3.4.3. Sharp Exciton Spectra

Recently Nagasawa and Shionoya published some very important measurements. By going to 1.3^oK they observed a sharp exciton spectra with polarised light. They presented an example of their measurements, fitted a hydrogen series to the peaks, interpreted the series as that of forbidden transitions on Elliott's theory and pointed out the comparison with Cu_2O. It is possible to derive a considerable amount of important information from these results. Their published spectrum is shown in fig. 3.4.1.

In addition to the peaks visible in fig. 3.4.1., a line was observed at $\lambda = 3480.3\text{Å}$ "two orders of magnitude" smaller than the n = 2 line. It is this greatly reduced magnitude that leads to the "forbidden" interpretation. Although in forbidden spectra dipole transitions to the n = 1 exciton are absent, quadrupole transitions can still take place. These transitions have distinctive dependences on the polarisations of the light, and for Cu_2O Elliott (1961) was able to derive information about the symmetry of the valence and conduction bands because one possible symmetry situation predicted maxima when the light had its $\underline{k}$ vector and polarisation vector directed along crystal axes, and another possible symmetry situation predicted zero intensity for this type of light polarisation. In SnO_2 it would seem that light polarised $\perp$ to the c axis must be an intensity minimum, because Elliott gives the intensity ratio of the n = 1 and n = 2 lines as $32\ Z(ka_o)^2$ where k is the wave vector

of the light, a_o is the Bohr radius of the exciton series ($\sim 21\text{Å}$ in SnO_2) and Z is a number dependent on polarisation but whose average value is $^8/_{25}$. Evaluation shows that the average ratio of oscillator strengths is $\sim .07$. The n = 1 exciton having a radius smaller than predicted by the series it can be shown to increase the expected average ratio. It can therefore be seen that larger n = 1 exciton intensities are to be expected for orientations other than polarisation along an axis, and an expert in group theory should be able to derive information on band symmetries.

The ratio of oscillator strengths for the n=2 and n=3 exciton should be in the ratio $^{729}/_{256}$, but they are seen to be roughly equal. Speculation about this ~~will be reserved for section 7~~ can be made, but we will note here that this could be experimental error if the true line width were less than the resolution of the spectrometer. In that case a very large absorption coefficient in the spike, that produced almost zero transmission, would not show up as zero transmission and the integrated absorption would be underestimated, while a spike not large enough to produce near zero transmission anywhere would give an approximately correct integrated absorption.

The n = 2 line is apparently split into two. This can be understood as due to anisotropy. Hopfield and Thomas (1961) calculate the splitting to lowest order for a uniaxial crystal. Their results are that the hydrogen model s states are given by a hydrogen series with a mean reduced mass μ_o given by $\frac{1}{\mu_o} = \frac{2}{3}\frac{1}{\mu_\perp} + \frac{1}{3}\frac{1}{\mu_{//}}\frac{\epsilon_\perp}{\epsilon_{//}}$ and a mean dielectric constant ϵ_o given by $(\epsilon_{//}\epsilon_\perp)^{\frac{1}{2}}$. The P states are split, Po states having the s state energy multiplied by $\left(1 + \frac{4}{15}y\right)$ and for P $\pm$ 1 states the factor is $\left(1 - \frac{2}{15}y\right)$. The subscripts refer to units of angular momentum around the c axis, and y is the anisotropy parameter $\mu_o\left(\frac{1}{\mu_\perp} - \frac{1}{\mu_{//}}\frac{\epsilon_\perp}{\epsilon_{//}}\right)$. The binding energies of the two n = 2 excitons are

.0083 and .0072 e.v., so that y can be seen to be $\frac{15}{6} \times \frac{11}{78} = \pm .35$. (We do not know which peak is which). If we take $\epsilon_\perp = \epsilon_{//}$ then the ratio of effective masses is 1.5:1, but we do not know which is bigger. If we take $\epsilon_\perp = 1.24\epsilon_{//}$ (see 5.6), and assume $\mu_\perp > \mu_{//}$, then we get $\mu_\perp = 1.11\mu_{//}$ and y = -.35. (If $\mu_\perp < \mu_{//}$ then $\mu_\perp = \sim .55\mu$ which is an improbably large anisotropy for what is, in effect, the conduction band). Taking y = -.35, we obtain the 2s energy as .0079 e.v. and the 1s energy as .0315 e.v., rather than .033 e.v. found by ignoring anisotropy. (If y = +.35, the 1_s energy is .030 e.v.). Although these differences are quite small, they produce big differences in the deviation of the observed 1s energy (.035 e.v.) from the hydrogenic series.

The above identification of the larger binding energy exciton peak of the split n = 2 exciton with the $P_{\pm 1}$ hydrogen functions can be obtained more directly. Forbidden transitions to bound excitons depend on the gradient in the direction of polarisation of the hydrogen function at the origin. The gradient of the Po hydrogen function (which has lobes along the c axis) is zero in a direction $\perp$ to the c axis, while that of the degenerate $P_{\pm 1}$ functions is a maximum. The peak corresponding to greater binding energy has an intensity in Nagasawa and Shionoya's results for $\perp$ polarisation about ten times that for the other peak. The fact that the smaller peak is present at all indicates that either the crystal was slightly misorientated with respect to the light, or the crystal contained a spread of c axis directions, or the light was not perfectly polarised. Any of these causes could also explain why the n = 1 exciton was just present (in quadrupole radiation).

Using for $\epsilon_\perp$ and $\epsilon_{//}$ the values found in 5.6 for ϵ_s ignoring the dubious low energy extra phonon, we obtain $\mu_o = .276\ m_o$ from the s exciton series energy found above of .0315 e.v. For analysis elsewhere in the thesis

we have used a conduction band mass of $m_c = .29\ m_o$, a value derived using .033 e.v. (The derivation was performed before the above anisotropy analysis was performed). Allowance for the large valence band mass makes (the average) m_c ~1½% larger than μ_o. The uncertainty in $\epsilon_\perp$ and $\epsilon_{//}$ makes high accuracy ~~meaningless.~~ in m_c unimportant at present

The magnitude and shape of the continuum are used in 6.1 and 3.2.

3.4.4. n = 1 Exciton - Method Used to find the Phonon Coupling for the Absorption Edge.

There are several steps in the derivation.

Nagasawa and Shionoya (1966) measured the Rydberg for the large orbit excitons as .033 e.v., (but we think .0315 e.v. is better for s states), but the binding energy for the faint exciton line they attributed to the n = 1 exciton was .035e.v. This shift is an indication that the n = 1 exciton cannot be considered as formed from two independent polarons. Another indication is that the energy of .035 e.v. is of the same order as the conduction band polaron binding energy of ~ .1 e.v. Eagles (1963) considers the case of the polaron interaction when the instantaneous position of the electron or hole in the orbit is ignored. He obtains (equ 59) modified oscillator displacements d_w^1, which give for the continuum polarisation model

$$d_w^{1*} = -\frac{V_w}{\hbar\omega} \int \varphi_e^* (\underline{r}_1 \underline{r}^1)\ \varphi_e (\underline{r}_1 \underline{r}^1) \left[\exp (i\ \underline{w}.\underline{r}) - \exp (i\ \underline{w}.\underline{r}^1)\right] d^3\underline{r} d^3\underline{r}^1$$

where $\underline{r}$ is the hole coordinate, $\underline{r}^1$ the electron coordinate and $\varphi_e (\underline{r},\underline{r}^1)$ the exciton wave function. Because the instantaneous positions are ignored, we split $\varphi_e(\underline{r},\underline{r}^1)$ into $f(\underline{r})\ f^1 (\underline{r}^1)$ where, of course, the normalisation condition $\int f(\underline{r})\ d^3\underline{r} = 1$ holds for $f(\underline{r})$ and $f^1 (\underline{r}^1)$. We thus get

$$d_w^{1*} = -\frac{V_w}{\hbar\omega}\left[\int f(\underline{r})\exp(i\underline{w}\,\underline{r})\,d^3\underline{r} - \int f^1(\underline{r}^1)\exp(i\,\underline{w}\,\underline{r}^1)\,d^3\underline{r}^1\right] \qquad (3.4.4.)$$

The two integrals are the Fourier coefficients of the respective wave functions. The difficulty with using this expression is that we do not know what to use for $f(r)$, the hole wave function, when the hole is not perfectly localised. It will not be any wave function obtained directly from, say, nearly small polaron theory, because the surrounding electron reduces the magnitude of the lattice potential well, due to screening. The polaron binding energy for perfect localisation (B_o) is given by $\sum_w (d_w)^2$, so the new value (B_o^1) of this quantity due to the screening electron can be calculated by (3.4.4.) provided the electron wave function is known, because the first integral = 1 for perfect localisation. The method we have used to obtain the modified absorption parameters D^1 for the exciton is to account for the fact that the hole is not perfectly localised. We do this by using nearly small polaron theory (Eagles 1966) but with a changed value of B_o (approximately the perfectly localised polaron binding energy) and the other related parameters. We have no rigorous justification for this, but inspection of the expression below for D^1 shows that qualitatively both the direct reduction in D due to screening and the indirect reduction due to the 'nearly small polaron' being less localised have been taken into account. The expression for D^1 is thus similar to (3.3.2.).

$$\hbar\omega D^1 = B^1{}_o - 4\frac{J_1^2}{\hbar\omega s^1_{o1}} - 2\frac{J_2^2}{\hbar\omega s^1_{o2}} \qquad (3.4.5.)$$

In the continuum polarisation model with a spherical Brillouin Zone

$$B^1{}_o = \frac{e^2}{\pi}\left(\frac{1}{\epsilon_\infty} - \frac{1}{\epsilon_s}\right)\int_0^{w_o}\left[1 - \int f^1(\underline{r}^1)\exp(i\,\underline{w}\,\underline{r}^1)\,d^3\underline{r}^1\right]^2 dw \qquad (3.4.6.)$$

If $\phi^1(\underline{r}^1)$ is approximated by a hydrogen-like ground state wave function of 'Bohr radius' r_e thus:

$$\phi^1(\underline{r}^1) = \frac{1}{\sqrt{\pi r_e^3}} \; e^{\left(-\frac{r^1}{r_e}\right)}$$

The integral over $\underline{r}^1$ (which is just the Fourier coefficient with wave vector w) is found by making the element of integration $2\pi r^2 \sin\theta \, d\theta \, dr$, putting $\underline{w}.\underline{r} = wr\cos\theta$, integrating over θ and then integrating by parts. We get this integral equal to

$$\left[\frac{1}{1+\left(\frac{wr_e}{2}\right)^2}\right]^2$$

The integral over $\underline{w}$ in (3.4.6.) can either be done numerically or, if $\frac{w_o r_e}{2} \gtrsim 4$, the approximate result of

$$w_o - \frac{11\pi}{16 r_e} \qquad (3.4.7)$$

for the integration can be used with little error.

The problem now reduces to determining the best value for r_e. This is indicated by using Hrivnak's (1959) special case already mentioned. Even if Hrivnak's situation were exactly met and the exact wave function found, the above analysis would not apply rigorously because the wave function is not hydrogeneic. It can be seen from (3.4.2.), however, that for small r_e it approximates hydrogenic form because $\frac{1 - e^{-qr}}{qr} \approx 1$. However it departs from hydrogenic form in that when it is compared with the hydrogen wave function $(\pi r_e^3)^{-1} \, e^{-(r/r_e)}$, the 'Bohr' radius, r_e, obtained by comparing the normalising coefficients is smaller than that obtained by comparing the exponential factors. That the former is the superior value can be seen by noting that the factor $\frac{1 - e^{-qr}}{qr}$ attenuates the wave function for larger r, thus compensating for the larger 'Bohr' radius in the exponential.

The modification of Hrivnak's work required is that he assumed $m_c = m_v$ while we assume $m_c \ll m_v$. Inspection shows that in Hrivnak's expressions we require $m = m_c$ in q but $m = 2m_c$ in a_1 and E. Hrivnak's solution only allows for one phonon energy, so that we use a weighted average. The exact kind of average is somewhat arbitrary, but inspection shows that it is not very critical. We weighted each "proper" phonon energy proportional to its contribution to α, and obtain $\frac{\bar{\omega}}{2\pi} = 605\text{cm}^{-1}$. In determining q the 'bare' conduction mass should be used. Hrivnak' used the bare mass for a_1 and E also, but it would seem some allowance for polaron effects raising the mass should be made. (See, e.g., Platzman (1962) who considers bound polarons by the Feynman method for parameters appropriate to CdS). The allowance is smaller the greater the ratio of coulomb binding energy to polaron binding energy. A bare mass of $.29m_o$ is used and a mass of $.3m_o$ for a and E. Hrivnaks solution requires "ϵ_∞" $= \frac{1}{2}\epsilon_s$. Dielectric constants of 5.8 and 11.6 correspond, fortunately, very closely to the values (averaged over the three axes) for small r when $m_v = \infty$ and for large r (the static value ignoring the "dubious phonon") respectively. (The actual value for the latter is 11.35.) We obtain

$$a_1 = \frac{\epsilon_\infty \hbar^2}{e^2 m_c} = \frac{0.530 \times 5.8}{.30} = 10.25\text{Å} \qquad q = \sqrt{\frac{2m_c \bar{\omega}}{\hbar}} = 7.54\times10^{-6}\ \text{cm}^{-1}$$

From the normalising coefficient we obtain our pseudo 'Bohr' radius r_e

$$\frac{4}{r_e^3} = \frac{4}{a_1^3} - \frac{q^2}{a_1} = (3.7 - .55) \times 10^{-3} \, (\text{Å})^{-1}$$

$$\therefore r_e = 10.8 \text{ Å}$$

For completeness we calculate Hrivnak's binding energy

$$E = \frac{m_c e^4}{2\hbar^2 (\epsilon_\infty^1)^2} \left(1 - \frac{q \hbar^2 \epsilon_\infty^1}{2 m_c e^2}\right)^2 = \frac{13.6 \times .30}{5.8^2} \left(1 - \frac{.0754 \times 10.25}{2}\right)^2 = .0455 \text{ e.v.}$$

If this is compared with the experimentally observed binding energy .035 e.v. agreement is seen to be only fair. Hrivnak, however, did not consider any small polaron effects. The method should be more reliable for the radius than for the energy. So far we have taken $m_v = \infty$. The finite valence band polaron mass would cause the value of ϵ to be reduced for small r, thus reducing the radius and increasing E. Central cell corrections are likely to have a similar effect.

The most important result of this adaptation of Hrivnak's result is that it shows the exciton radius is much smaller than the value ($\sim$20Å) obtained using ϵ_s. This indicates considerable shielding of the hole by the electron.

We can now use the value of r_e to obtain D^1 with the help of (3.4.5.) (3.4.6.) and (3.4.7.). We obtain

$$B_o^1 = B_o \times .789 = .566 \text{ e.v.}$$

$$\text{and } \hbar\omega D^1 = .566 - \frac{4 \times .169^2}{.710} - \frac{2 \times .169^2}{.433} = .273 \text{ e.v.} \qquad (3.4.8.)$$

There are at least three sources of error in this method for obtaining D'. The first source is the errors in obtaining γ_e, mentioned above. The second source is the assumption that the phonon interaction is independent of the instantaneous position of the electron or hole. In reality the shielding of the hole by the electron will not be as big as indicated (thus raising D') and conversely the electron will have some phonon interaction of its own (thus giving a further contribution to D'). Third, the nearly small polaron approach adopted will be less valid for the n=1 exciton than for the free (hole) polaron, and ϵ_1^2 terms will be more important. The first two errors will work in opposite directions, but the second is probably larger. It is because of the second factor that we took the mass in determining a_1 and E to be slightly larger than the bare mass. The third error (which is related to the second) probably means D' is smaller than calculated. This can be seen by comparison with large polaron theory applied to the hole, where the nearest equivalent to D is closely related to α, and α is smaller than D.

Using the same ratio between D_1', and D_2' as for small polaron theory, we obtain from 6.1.1. and 3.4.8 the values

$$D_1' = 2.26 \quad D_2' = 1.57$$

For reasons given in the last paragraph these values are only a guide. The values actually used in obtaining the theoretical points were $D_1' = 2.33$ $D_2' = 1.58$. The reason for $\frac{D_1'}{D_2'}$ being larger than $\frac{D_1}{D_2}$ is that we are near the limit of applicability of nearly small polaron theory, and in large polaron theory the nearest equivalent to D appears

to be related to α , and the ratio of α_1 to α_2 is bigger(by a factor of $\sqrt{2}$) than the ratio of D_1 to D_2.

The above n = 1 exciton analysis probably applies best for small K. For larger K there are further difficulties. Because of the electron shielding, the exciton bandwidth (which is dominated by the heavy particle) is apparently~ 3 x larger than that for the n=2, 3 ... excitons. If this is taken literally, it implies that as we move away from K = 0, the n = 1 exciton energy level approaches and then exceeds first the position the n = 1 exciton would occupy if there were no shielding (.0315 e.v. below the continuum) and later the n = 2, 3 ... excitons and the continuum edge. This must be false, because it would imply weaker binding, larger orbits and hence less shielding of the hole, which is what caused the apparently larger bandwidth in the first place. (It should be noted that changing the shielding alters the true bandwidth both by altering the apparent bandwidth and by changing the coulomb and polaron binding energies. The latter are likely to be just as important as the former). Presumably as K increases and the shielding reduces, D gradually changes from its value for K=0 towards that for free particles.

3.4.5 Energy Balance Concepts

This is perhaps the place to illustrate the kind of way the energy equation balances to give the observed exciton binding energy. This is shown in fig. 3.4.2 in which some of the numbers are given purely for illustration, and are not rigorously derived.

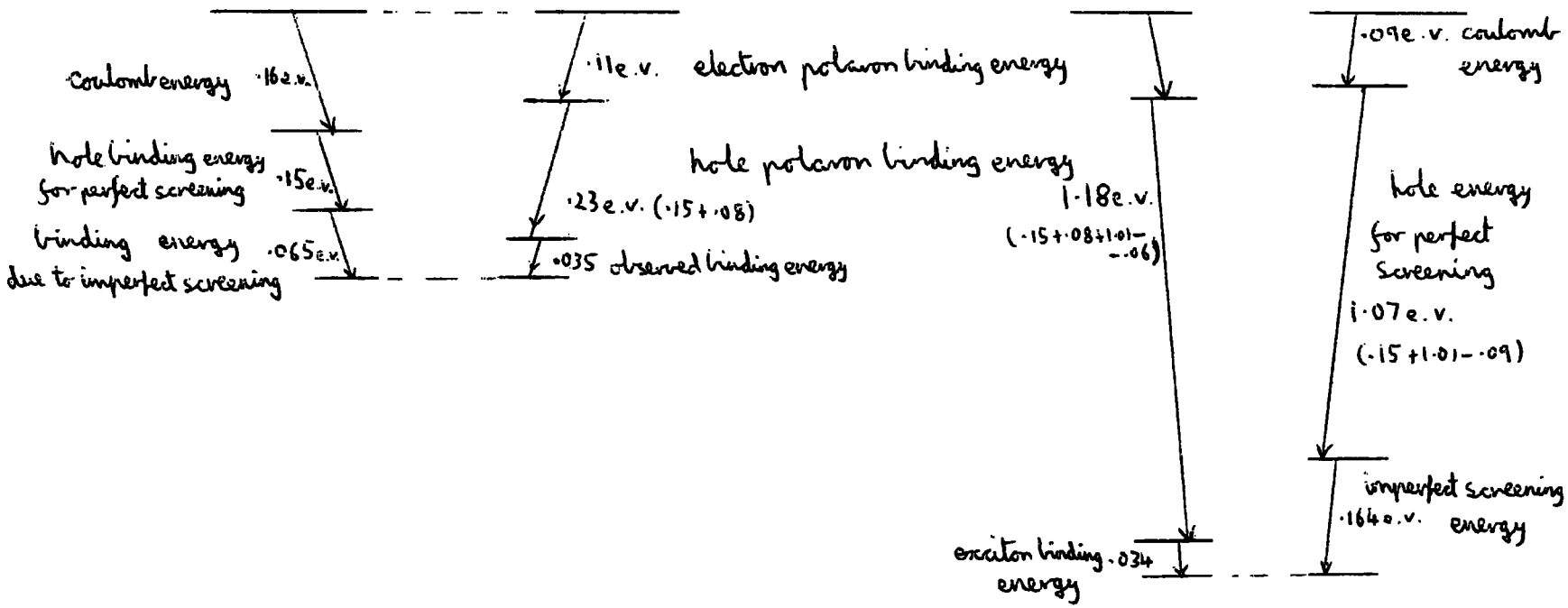
Coulomb energy ·16e.v.
hole binding energy for perfect screening ·15e.v.
binding energy due to imperfect screening ·065e.v.
·11e.v. electron polaron binding energy
hole polaron binding energy
·23e.v. (·15+·08)
·035 observed binding energy
1·18e.v. (·15+·08+1·01−·06)
exciton binding energy ·034
·09e.v. coulomb energy
hole energy for perfect screening
1·07e.v. (·15+1·01−·09)
imperfect screening energy ·164e.v.
K = 0
K = ½(π/a, π/a, π/c)

FIG. 3.4.2.

The left diagram is for K = 0 and the energy zero is the energy of the system with a free hole in a rigid lattice (i.e. no polaron effects). Two routes are shown for obtaining the exciton energy level. On the right are shown the binding energies for the two polarons (giving the actual energy of the band edge including polaron effects) together with the observed binding energy (.035 e.v.). The hole binding energy shown is roughly that given by large polaron theory. On the left the coulomb energy is shown first. This energy, if calculated using the radius found above of 10.8Å, an effective mass of .3 m_o and the formula $\frac{\hbar^2}{2a^2m}$ (found by eliminating ϵ from the hydrogen formula for E and a), is .11 e.v.. But as stated above this radius is probably an overestimate, and central cell corrections are also likely to raise E, so we have put E = .16 e.v. The next energy is an estimate of the hole binding energy assuming the shielding to be perfect. (For perfect shielding the electron interaction is zero). The final energy is a balancing term to obtain agreement with experiment. The ratio of this last energy to the sum of the binding energy of the free electron and the difference in binding energy of the hole with and without screening gives a picture of the degree of independent electron -phonon interaction and additional hole-phonon interaction on top of that indicated by perfect screening. With the numbers in the diagram this ratio is 6.5/19.

The right diagram of fig. 3.4.2. shows the same energy balance for K half way to the Brillouin zone boundary on all axes. (The much heavier hole wave functions that go to make up the exciton are drawn from k values around this K, but the light electron k values are still quite near k = o). The hole binding energy is now much larger because of the very small polaron bandwidth. The increase is $4\ J_1 + 2\ J_2 - \frac{1}{2}W$. The binding energy of the two polarons in

the exciton is not known, but is presumeably about .035 to .0315 e.v., the values for K = o, and for no screening, respectively. On the left the coulomb energy is reduced from the value for K = o, because of the larger exciton radius due to reduced screening. The value of W taken is not that which is predicted by the K = o screening (about 3 x the value for the free hole polaron), but is taken as 1.5 x the free value to allow for the reduced screening. The reduction in hole binding energy due to perfect screening is assumed to be the same as for K = o. The ratio defined above is now $\frac{16.4}{19}$ reasonably consistent with the lower screening assumed in estimating the values of W and the coulomb energy. This self consistency looks increasingly unrealistic if more screening is assumed. This larger ratio than for K = o indicates that the D^1 have increased from their K = o values, fairly nearly to the values for free particles.

3.5 Absorption Edge

3.5.1. Introduction

While trying to interpret the absorption edge it has become clear that, for both theoretical reasons and because of observed phenomena, many effects are involved. Not all of these effects are amenable to simple theories, and in some places simplifying approximations have to be made.

The most important evidence to date is the experimental work of Nagasawa and Shionoya (1966) who measured the absorption edge at $1.3^{o}k$ (see fig. 3.4.1.). This showed (for $\perp$ absorption) a discrete exciton spectrum with the n = 1 line almost missing, indicating that the transitions are 'forbidden' at k = 0. The only other material which has been established as having a similar spectrum is Cu_2O. There is however a big difference between Cu_2O and SnO_2. In Cu_2O, but not in SnO_2, the continuum at energies above the discrete spectrum can be explained by Elliott's theory. The explanation is that in SnO_2 the phonon coupling is large,

especially for the valence band. This means that the absorption with no phonons absorbed or emitted (which is the only type which exhibits a discrete exciton spectrum) only forms a small part of the total absorption. The most promising theory to use for SnO_2 is the optical absorption theory of Eagles (1963) applied to 'nearly small polaron' theory of Eagles (1966 (A and B)).

Using this theory it is still difficult to get a good fit to the whole spectrum. This is the first reason for looking for a second type of absorption. The second is that the 1.3°K spectrum quoted above shows a sharp rise in absorption just close to the beginning of the continuum. This rise cannot be explained as phonon assisted absorption (only phonon emission being possible because of the low temperature) to the continuum or to the n = 2 to ∞ exciton states, because, taking the most favourable case, the phonon energy if it were the n = 2 exciton would be only .0089 e.v. As mentioned earlier, the only likely explanation is phonon (energy .0356 e.v.) assisted transitions to the n = 1 exciton. However, the intermediate state cannot be the K = 0 n = 1 exciton, (reached by quadrupole absorption), because the ratio of the integrated intensity of the one phonon to that of the no phonon absorption is much too big. It must therefore be by some other intermediate state, possibly the states responsible for the most powerful absorption bands in the U.V., but the lower continuum and exciton states should not be overlooked. A similar state of affairs holds for phonon assisted transitions to the n = 1 exciton in Cu_2O. In both materials the shape is approximately $E^{\frac{1}{2}}$, indicating that the interband phonon matrix element is independent of K. Elliott (1961) indicates that in Cu_2O the phonon is not I.R. active, but for SnO_2 we have tentatively identified it with the lowest I.R. active phonon. A possible justification for this is that although the intensity of the one phonon absorption bands in the two materials is similar, in Cu_2O there is no evidence of two phonon absorption, while in SnO_2 we interpret the n = 1 exciton as still

interacting strongly with the optical phonons, and the total absorption as being much greater than the single phonon absorption alone: this greater total absorption indicates a stronger interband electron-phonon matrix element, and strongly interacting phonons are likely to be the polar (I.R. active) optical phonons.

We therefore consider phonon assisted transitions to the n = 1 exciton. The reason that this type of absorption can substantially change the shape of the absorption curve is because the electron shields the hole from part of the phonon interaction and the electron charge is almost neutralised by the hole inside its orbit. This gives smaller values of the parameter D in Eagles theory, for the exciton.

We consider the continuum first, and then the n = 1 exciton.

3.5.2. The Continuum

Eagles theory shows that when many phonons are involved the shape of each part of the absorption (assuming the conduction band is wide) is given by

$$\rho_c (E)\ \rho_v (E^1 - E)\ Q^2 (E)\ dE \qquad (3.5.1.)$$

where ρ_v and ρ_c are valence and conduction band density of states functions, $Q^2 (E)$ is proportional to the optical matrix element to the conduction band state of energy E, and E^1 is the excess energy above threshold. If a parabolic conduction band is assumed and electron-hole interaction is ignored $Q^2 (E)$ E varies as E for forbidden transitions. Electron-hole interaction adds a Sommerfeld factor $X = \frac{2\pi\alpha\ (1 + \alpha^2)}{1 - e^{-2\pi\alpha}}$ where $\alpha^{-2} = \frac{E^1}{R}$ (R = the Rydberg energy of the exciton series i.e. the apparent binding energy of the n = 1 exciton)

The non-parabolic nature of both bands still requires treatment. R varies as $\sqrt{\frac{\mu}{\epsilon^2}}$. μ is almost solely determined by the mass of the much lighter electron. The appropriate mass to use to determine R and hence $Q^2(E)$ is the value

of the conduction band mass in the region of the band around E above the bottom. This value is $\frac{\hbar^2 k}{dE/dk}$, which can be evaluated from fig. ~~3.3.2.~~ 6.1.1. The author has not seen a relevant treatment of the appropriate value of ϵ to take for different values of k (or E). The most natural interpretation would appear to be to assume the reduction in the electron-hole interaction (see 3.4) due to hole-phonon interaction is constant, but that the reduction due to electron-phonon interaction is proportional to the number of phonons around, or 'screening', the electron. Thus we take the effective value of ϵ to be given by

$$\frac{1}{\epsilon} = \frac{1}{\epsilon_\infty} - \frac{1}{2}\left(\frac{1}{\epsilon_\infty} - \frac{1}{\epsilon_s}\right) - \frac{1}{2}\left(\frac{1}{\epsilon_\infty} - \frac{1}{\epsilon_s}\right) F$$

where F is a factor equal to 1 at k = o and proportional to the average number of phonons in the cloud around the electrons. Pines (1963) shows that for intermediate coupling the variation of F with k is $1 + \frac{\hbar k^2}{4m\omega(1+\alpha/6)^2}$ for small k. The behaviour of F for larger k is not clear, but for large energies it probably varies as $\frac{1}{k}$ in the same way as the polaron energy is lowered compared with the rigid lattice electron. We therefore assume that F varies as given above for small k up to a polaron energy $\hbar\omega$ above the bottom of the polaron band and as $\frac{1}{k}$ at higher energies. We have no rigorous theory that this is the correct value of ϵ to take, but in order to proceed we need to adopt some theory. At k = o it is correct because large distances and small velocities are involved, and ϵ_s is the correct dielectric constant for these conditions. At large k the electron phonon interaction is small, and F = o appears to be correct. In between, the screening being related to the average number of surrounding virtual phonons seems the most plausible approach. A more rig-

orous theory would have to combine, for any energy, a good understanding of the unbound "hydrogen atom" wave functions with polaron theory. A point of interest is that the procedure we adopt could lead (though does not in SnO_2) to ϵ rising to ∞ and then going negative, corresponding to electron-hole repulsion. That this might be possible is supported by an analogous case considered by Schultz (1963) p. 110. He considers two polarons with the same charge interacting, and states that it has been shown that in some circumstances there can be attraction, rather than the normal repulsion. ϵ going negative would lead to no discontinuities in the optical absorption calculation. The detailed way ϵ varies does not have a very big effect on the absorption.

The non-parabolicity of the conduction band changes the value of E^1 used to determine α. The value should be that which would appear to an electron, with the appropriate value of k, to be the height above the band edge assuming a parabolic band with the local value of effective mass. Also for a non parabolic band the 'forbidden' aspect of $Q^2(E)$ gives a variation with k^2 rather than E.

The conduction band density of states is given by a term proportional to $k^2 / \left(\frac{dE}{dk}\right)$ and can be found from fig. ~~3.3.2~~ 6.1.1.. The valence band is fairly narrow (see 3.3) and when its width is small compared to E^1 the integral (3.5.1.) can be approximated as being proportional to

$$\rho_c(E^1 - \Delta E)\ Q^2\ (E^1 - \Delta E) \qquad (3.5.2.)$$

where ΔE is the average height of valence band states from the band edge. The shape is thus like that of forbidden direct transitions, but the band gap is increased

by Δ E. When E' is smaller than Δ E and only parabolic portions of both bands are involved, then (3.5.1) rises as E'^3 ignoring the Sommerfeld factor, and $E'^{5/2}$ with its inclusion. This absorption when E' is substantially less than Δ E is very small, and (3.5.2) is a fair approximation for all E'.

Eagles only proved (3.5.1) true when many phonons are involved. The zero phonon part is radically different because the final hole state in the valence band is confined to fairly small values of k because only vertical transitions are allowed. To a good approximation these states all have energies equal to the top of the valence band, so that (3.5.1) becomes $\rho_c(E')\, Q^2(E')$ instead of (3.5.2). This part is thus shifted Δ E to lower energies compared with the many phonon parts.

For one phonon absorption we can get a good idea of the shape by noting that the wave vector k of the electron is small compared with the dimensions of the Brillouin Zone, for the absorption region with which we are concerned. Therefore the wave vector w of the phonon involved is approximately equal to the wave vector of the final state hole. From Eagles (1963) equ 30 we find an extra factor inside the integral (3.5.1) proportional to $|d_w|^2$ where in the continuum polarisation model we have $|d_w| \propto 1/w$. If we assume for simplicity the valence band is parabolic with a sharp upper cut off then (3.5.1) becomes proportional to

$$\int_{E'-2\Delta E}^{E'} \frac{\rho_c(E)\, Q^2(E)}{(E'-E)^{\frac{1}{2}}}\, dE$$

where 2Δ E is the width of the valence band.

When $E' \gg 2\Delta E$, the variation of $\rho_c(E)\, Q^2(E)$ over the range of integration is small compared with the variation of $\frac{1}{(E'-E)^{\frac{1}{2}}}$ (which $\to \infty$ as $E \to E'$).

If $\rho_c(E)Q^2(E)$ is taken as constant, the weighted mean of $\frac{1}{(E'-E)^{\frac{1}{2}}}$ over the range of integration is found by integration to be $\frac{1}{3} \times 2\Delta E$. For a many phonon process with such a parobolic valence band the weighted mean is found to be $\frac{3}{5} \times 2\Delta E$, so the effective increase in band gap is nearly halved for one phonon processes compared with many phonon processes. (In small polaron theory a more realistic form for the valence band is that the energy varies like a sine wave with k_x, k_y and k_z. This results in a parabolic form near k = o, but its mean energy is half the bandwidth, rather than the factor $\frac{3}{5}$, even if the amplitudes of the three sine waves differ). When $E' \lesssim 2\Delta E$ the variation of $\rho_c(E)\,Q^2(E)$ becomes important, and for the almost parabolic region at the bottom of the conduction band, this weights still further the larger values of E in the integration, making the effective increase in band gap still less. The final tail of the one phonon absorption rises as $E'^{3/2}$, while the zero phonon part rises as E'+R and the multiphonon part as $E'^{5/2}$.

There is one further modification to (3.5.1) required to take account of phonon interaction with the conduction band (this is assumed to be negligible in Eagles theory). The most reasonable assumption is that the parameter corresponding to D in Eagles theory is the average number of virtual phonon surrounding the electron. Originally Eagles (1963) suggested phonon interaction in the wide band would reduce D, but it would seem that the phonon interaction of two unbound particles should be additive, and Eagles (1967) agrees that this is probably so, depending on whether there are any correlation effects. We assume the

effects are additive, and take the electron contribution to D as being proportional to F defined earlier in this section, and equal to $\frac{\alpha}{2}$ at k = o. The latter is the average number of virtual phonons around the electron (Pines 1963 p.41). This makes D depend on k and so the shapes derived from (3.5.1) are modified. The modification is achieved by applying the appropriate value of D to each region of absorption of each part.

3.5.3 Type of absorption to n = 1 exciton

The direct transition to the n = 1 exciton is forbidden. This rule includes both the zero phonon absorption (observed to be absent by Nagasawa and Shionoya) and phonon assisted absorption using the direct transition as an intermediate state. It does not, however, rule out phonon assisted absorption via another band with different symmetry. This absorption is certainly present in Cu_2O and is very strongly indicated in SnO_2 by the sharp rise in absorption .036 ev. above the very faint n = 1 exciton. (It would be interesting to obtain even more conclusive evidence by observing absorption starting .036 e.v. below the n = 1 exciton with the correct intensity. A temperature of about $80^{o}K$ might be the best).

The phonon coupling for the interband electron-phonon matrix element is likely to be small (so that only single phonon processes are important), and the relative strengths of the different phonons is not given by the normal calculations for intra band optical phonon interactions. (Indeed, the identification of the .036 e.v. phonon with an optically active one is not certain; we do, however, make this identification in the phonon analysis). It will be shown in 6.1 that the magnitude of absorption observed by Nagasawa and Shionoya starting

.036 e.v. above the $n = 1$ exciton is sufficient (to the low accuracy involved) to indicate the .036 e.v. phonon is probably the most important one involved in the interband matrix element. For simplicity (and ease of obtaining a good fit to the experimental points) we take it to be only phonon involved. The shape of the absorption is well fitted by an $E^{\frac{1}{2}}$ form, which indicates that the interband absorption is independent of K.

This is in contrast to the predictions for (intra-band) optical phonon coupling for excitons, which are that the matrix element varies as K for small K and $\frac{1}{K}$ for large K (the change-over being in the region $K r_e \sim 1$ where r_e is the exciton radius)

Because of the fundamental relation between phonon creation and annihalation the ratio between absorption with (single) phonon emission and (single) phonon absorption has the factor $\exp\left(\frac{\hbar\omega}{kT}\right)$. There will also be a factor $\frac{1}{(Ei - \Omega)^2}$ where Ω is the photon energy and Ei the (weighted) average energy of the possible intermediate states. Ω differs by $2\hbar\omega$ for phonon emission and absorption, so that only if $Ei - \Omega \gg \hbar\omega$ will this factor be negligible.

The big (intraband) optical phonon interaction associated with the creation of the exciton will be present in addition to the interband phonon interaction. The absorption to the n = 1 exciton is thus charactised by two superimposed groups of parts, each group having parts with absorption given by Eagles theory with the parameter D^1.

3.5.4. Temperature dependence of the absorption edge.

In polar semiconductors like SnO_2, the most important contribution to the temperature variation of the band gap is generally taken to be due to the electron-lattice interaction. For materials with only one I.R. active (longitudinal) optical phonon, the change in band gap, ΔE_G is taken as proportional to

$$\bar{n} = \frac{1}{\exp(\hbar\omega_{\perp}/kT)-1} \qquad (3.5.3.)$$

This expression was applied to SnO_2 by Summitt and Borrelli (1966) to interpret their absorption edge measurements over the range 20°K - 1300°K. They adjusted the phonon temperature to obtain a best fit for $\perp$ and // absorption. They found $\theta_{\perp}$ $(= \frac{\hbar\omega_{\perp}}{k})$ = 414.7°K and $\theta_{//}$ = 195.8°K . It is one of the purposes of this section to show this interpretation to be wrong, and that different phonon temperatures are not required for the two polarisations.

Contribution of the three phonons

A simple extension of (3.5.3.) to cover three phonons is

$$\Delta E_G = c_1 \bar{n}_1 + c_2 \bar{n}_2 + c_3 \bar{n}_3 \qquad (3.5.4)$$

where the $\bar{n}$ are given by (3.5.3) with the appropriate energies, and the c_1 c_2 and c_3 are constants. Eagles (1966) discusses atomic displacements in the neighbourhood of a polaron due to a particular phonon branch. He obtains (equs 5.19, 5.20 and 5.18) the displacements as being proportional to

$$\frac{1}{\omega^{\frac{1}{2}}}\left[\frac{1}{\hbar\omega}\left(\frac{1}{\epsilon_\infty}-\frac{1}{\epsilon_s}\right)\right]^{\frac{1}{2}}$$

The natural extension to 3 phonons is to use our weighting factor for the contrubution to $\frac{1}{\epsilon_\infty} - \frac{1}{\epsilon_s}$ by each phonon. For small amplitudes, energy is always a quadratic function of displacement. We therefore take

each phonon contribution as being proportional to

$$\frac{1}{\omega_\mu^2} \left\langle \int_\mu^2 y \left(\frac{1}{\epsilon_{\omega y}} - \frac{1}{\epsilon_{s y}} \right) \right\rangle_{av}$$

where the definition of the big bracket is given in 3.3. We thus obtain

$$c_1 : c_2 : c_3 = 1 : 8.3 : 6.8$$

288 371 722

where the numbers under the c's are the phonon energies in cm^{-1}.

To obtain reasonable agreement with the high temperature data of Summitt and Borrelli and with the change in band gap between R.T. and $1.3^{\circ}K$ found to give best agreement with experiment, the following values of the c's are taken

$$c_1 = .048 \text{ e.v.} \qquad c_2 = .40 \text{ e.v.} \qquad c_3 = .327 \text{ e.v.}$$

Substituting in (3.5.4.) we get $\Delta E_G\ (296^{\circ}K) = .0157 + .0792 + .0101 = .105$ e.v.

This agrees with the value found in 6.1 We require in 6.1, $\Delta E_G\ (90^{\circ}K)$. This is .0016 e.v.

Summitt and Borrelli only published their actual results as far as $550^{\circ}K$,

but from their fitted theoretical curve their results to 1300°K can be estimated. We therefore evaluate ΔE_g at 550°K and 1300°K.

$$\Delta E_g\ (550^\circ K) = .0425 + .244 + .0581 = .345 \text{ e.v.}$$
$$\Delta E_g\ (1300^\circ K) = .128 + .790 + .267 = 1.185 \text{ e.v.}$$

If the measured shift in the absorption edge of Summitts and Borelli is equated with ΔE_g, then they measured:

	$\perp$	$\parallel$
$\Delta E_g\ (296^\circ K)$	.155	.225 e.v.
$\Delta E_g\ (550^\circ K)$	.44	.53 e.v.

and it can be inferred

$\Delta E_g\ (1300^\circ K)$	1.36 1.42 e.v.

We shall now qualitatively discuss why these measured values differ from each other and from our theoretical ones. We have not yet done the numerical calculations for 550°K and 1300°K. They would best be done by computer.

Summitt and Borrelli measured the energy where the absorption was $\sim 75\ cm^{-1}$. This will shift with temperature for two reasons. First the band gap changes and second the magnitude and shape of the absorption changes. The latter is completely worked out for 296°K, 1.3°K and 90°K in 6.1. The largest factor causing the magnitude to change is the increase of phonon absorption as the temperature rises. For the continuum this shifts absorption to lower energies while leaving the integrated absorption constant. For the (n=1) exciton it increases the total integrated absorption (though presumeably slightly

reducing the absorption around the energy of the intermediate states). It is this increase of exciton absorption that is the biggest factor in shifting the apparent absorption edge faster than the band gap.

The reason for the bigger shift of the $//^{u}$ edge can be seen to be due to its smaller slope on the log absorption plot. An equal increase in absorption magnitude would shift the 75 cm^{-1} point on the $//^{u}$ curve more than twice as far as on the $\perp$ curve. The apparently different phonon temperatures of Summitt and Borrelli can be accounted for in this way.

Absorption Edge at 1300°K

Without doing the full calculation for the highest temperature (1300°K) we can use an approximation for $\hbar\omega < kT$ given by Eagles (1963). He stated the dependance of R_p on p is given by

$$R_p \propto \exp\left[-(\hbar\omega/4DkT)\ (p-D)^2\right]$$

Elsewhere Eagles states $\sum R_p = 1$, so that it can be seen by integration that at high temperatures

$$R_p = \frac{K}{kT} \exp\left[-(\hbar\omega/4DkT)\ (p-D)^2\right] \qquad (3.5.5)$$

where K is a constant indepeendant of T. This shows the maximum R_p only varies slowly with T, i.e. as $T^{-\frac{1}{2}}$. Consideration shows that as an order of magnitude the absorption parts with a major contribution at the energy where total absorption is 75 cm^{-1} have a value of R_p which is about 1/100 of the maximum value of Rp (i.e. the value at p=D) if only a single phonon branch were involved). From (3.5.5) Rp is 1/100 its

maximum value when

$$\hbar\omega(p - D) = 2.15\sqrt{4\, D\, \hbar\omega\, k\, T}$$

As it is $D\,\hbar\omega$ that appears, we shall take $\Sigma D\hbar\omega$ to allow for the 3 phonons. Although the integrated exciton absorption increases as $(2\bar{n} + 1)$ it seems that this is more than compensated (at high temperatures) by the smaller smearing out effect of a smaller D. We therefore substitute $\Sigma D\hbar\omega = .53$ e.v. as a typical continuum value, $kT = .112$ e.v. and get

$$\hbar\omega(p - D) = .99 \text{ e.v.}$$

At $0^{o}K$ Rp is $^{1}/100$ of its maximum value when

$$\hbar\omega(p - D) \sim .5 \text{ e.v.},$$

and the exciton absorption shifts the 75 cm^{-1} point about .05 e.v. to lower energies. The approximate calculation therefore gives the shift of the 75 cm^{-1} point with respect to the band gap as .44 e.v. The figures given earlier yielded a shift of .18 e.v. ($\perp$ edge) and .24 e.v. ($/\!/^{a}$ edge). More careful consideration would probably show that the $T^{-\frac{1}{2}}$ term in (3.5.5.) would lead to a larger fraction at high temperatures than the assumed $^{1}/100$. This would reduce the .44 e.v. figure. The main object of the calculation was to illustrate that a shift of the absorption at a particular value of K does not give a good measure of the shift of the band gap, and that our assumed values of c_1 , c_2 and c_3 are reasonable.

Polaron bandwidth

It should be said finally that we have neglected any specific consideration of the change in the valence band polaron bandwidth. The bandwidth is at a maximum (of $\sim$ .24 e.v. with our figures) at $0^{o}K$, reducing increasingly rapidly as the temperature rises (It is $\sim$ .12 e.v. at R.T. with our figures). The position in the hopping region ($T > \sim \frac{1}{2}\hbar\omega$) is not so clear.

If the shifts of band gap given by (3.5.4.) apply to the centre of the top valence band then the changing bandwidth would contribute a term which <u>increased</u> the true band gap with increased T. The term would not be linear in $\bar{n}$, but would be $\sim .12 \exp -\left[\sum 2\,\bar{n}\ (S_{02} + S_{12})\right]$, the sum being over the three phonons.

4.1. Crystal Growth

SnO_2 is a compound refractory material which, as far as is known, has never been satisfactorally liquified, and sublimes, or dissociates, into gaseous SnO and O_2, when heated to temperatures $> \sim 1600^{\circ}c$. This effectively rules out growth from the melt and although various other methods, such as growth from a solution, have been investigated by, among others, J.A. Marley and T.C. MacAvoy (1962), growth from the vapour has been the most successful so far. It is also a method with very wide application in crystal growth in general.

SnO_2 growth at Durham was started using the general techniques developed there for CdS under Dr. J. Woods. Of vapour methods, the two obvious alternatives are to use SnO_2 powder as starting material or to use metallic tin and form SnO_2 by a vapour phase reaction with O_2. The difference between the two is not likely to be very great, as the controlling reaction at the point of crystal growth is thought to be the same for both (see e.g. Marley and MacAvoy 1962):-

$$SnO + \tfrac{1}{2}O_2 \rightleftharpoons SnO_2 \qquad (4.1.1)$$

where the SnO is gaseous.

The most successful group at growing SnO_2 from the vapour has been that at the Corning Glass Works, U.S.A. (Marley and MacAvoy 1961 and 1962). Generally speaking

the scale of their effort has been larger and their results better than ours. Several comparisons and references will be made with their work. They used SnO_2 powder as starting material and we used tin.

Crystal Growing Apparatus

The main apparatus used at Durham is sketched in fig. 4.1.1, and a typical temperature profile given in fig. 4.1.2. The limiting factors are mostly those imposed by the heating element. This is made of SiC (manufactured by Morgan Crucible Co. Ltd.). This has an overall length of 62 cms. and has a cylindrical shape of 6 cms. dia. It is a semi-conducting resistance element with a spiral cut central region of 30 cms. length, which dissipates most of the heat. The hot spiral cut region was not allowed to touch anything, so the ceramic tube immediately inside the element was suspended clear. This tube was made of alumina and had to be of substantially smaller diameter than the element to allow clearance even after a certain amount of bending at high temperatures. Its diameter was 4.2 cms. It was advised, as a safety measure, that actual crystal growth should take place inside yet another tube. This was so that the growing tube could be inserted and removed without fear of damaging the expensive (~ £50) element, and so that if the growing tube cracked open, the element would, again, be spared. This inner tube was made of Mullite, an

FIG. 4.1.1 AND 4.1.2 (BOTTOM)

(After Morgan 1966B)

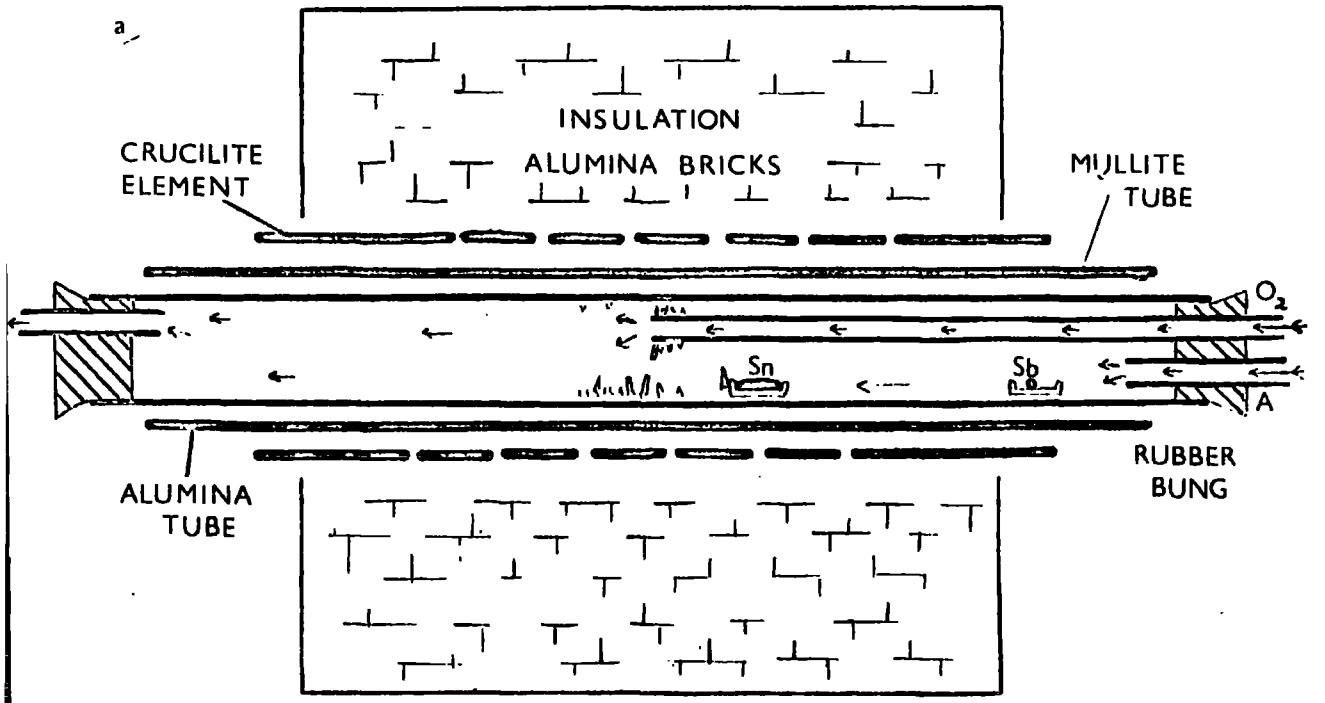

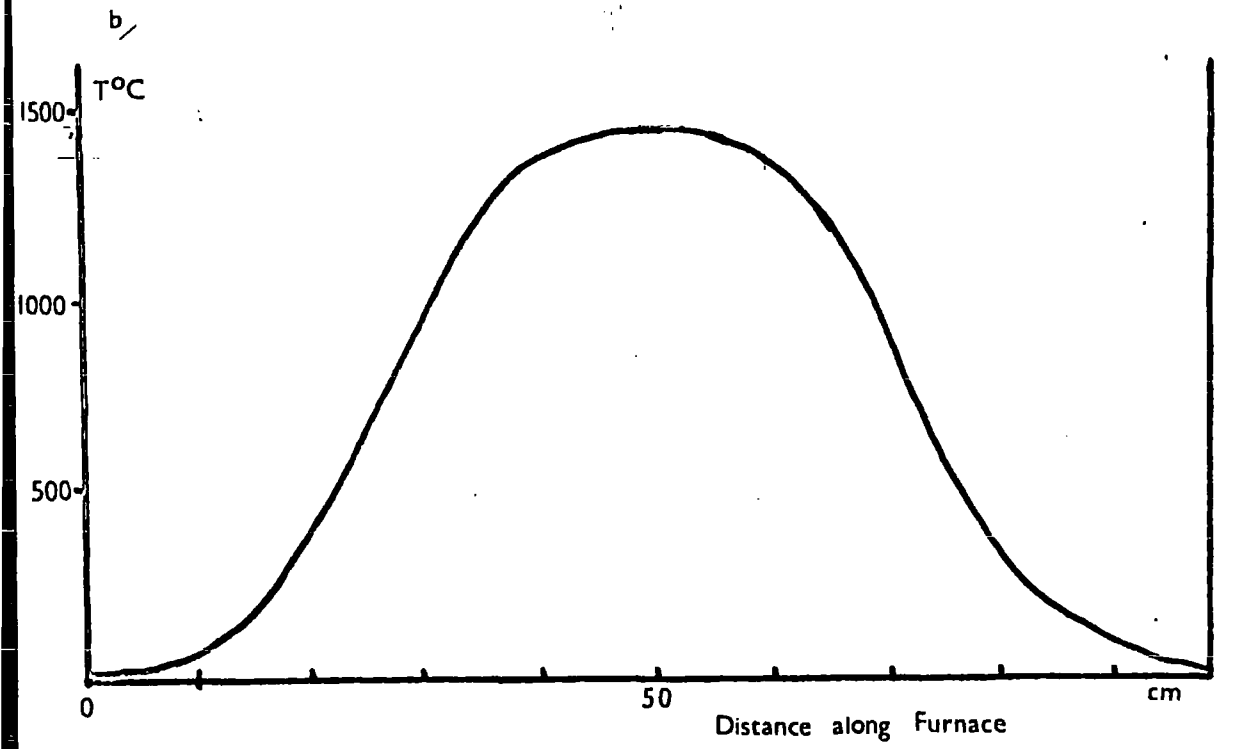

aluminium silicate (again by 'Morgan Crucible'), and of length 97 cms. and internal diameter 2.5 cms. Again, because of bending, the diameter could not be chosen to be too tight a fit.

The element also restricted the temperature profile to one basic shape, with temperature as the only variable. Marley and MacAvoy, using a tapped Pt-Rh element were able to achieve a variety of profiles, and in particular used one with a steady, low temperature gradient of $< 15^{\circ}C$/in.

Finally, the element restricted the temperature available. The lifetime of the element was quoted as varying rapidly with temperature. A maximum temperature of $1500^{\circ}C$ was recommended for short periods only, and considerably less for long periods. A related difficulty was that high temperatures produced a rapid increase of the resistance of the element. It may be that the mass of crystal produced in the lifetime of an element is roughly independent of the temperature used, as the vapour pressure of tin roughly doublesevery $40^{\circ}C$, which is roughly how the lifetime varies.

The inert gas (Argon) is introduced through a short small bore mullite tube and the oxygen is introduced at, or just beyond, the hottest point by another mullite tube. The choice of Mullite for the growing tubes was lucky, as

Marley and MacAvoy found that it anchored the crystals much better than alumina.

The boat (made of alumina) for holding the tin was placed about 10 cms. behind the tip of the oxygen tube, at what was considered to be a compromise between obtaining the maximum temperature for the tin and not allowing appreciable quantities of oxygen to come in contact with the tin. The tip of the oxygen tube could not be moved too far to the right as then growth would take place in a region of steep temperature gradient and lower absolute temperature. The former produces large numbers of nucleation centres because most of the SnO vapour is swept slightly beyond the theoretical equilibrium point for crystal growth, and, due to the steep temperature gradient actually condenses at a point where there is considerable supersaturation. The lower temperature is considered bad because diffusion coefficients are smaller and defects are more likely to be frozen in.

The power supply for the element consisted of a multi-tapped auto-transformer. The furnace required about 1.5 kW to reach 1450°C and as the element resistance was ~ 2 Ohms (varying with age) the transformer supplied ~ 30 Amps at ~ 60 Volts. Initially the furnace was run direct from the transformer, but this was found to have three disadvantages:-

(1) The power supplied varied as the square of the mains

voltage, which varied a few percent (in addition to voltage reductions during January 1963 due to cold weather, when some of these early runs were taking place).

(2) The ageing of the elements caused a steady reduction in power.

(3) It took about 8 hrs to get fully up to steady temperature.

For these reasons, a control circuit was installed consisting of an 'Ether' 'Transitrol' 'anticipatory' temperature controller which switched a mercury relay and used a Pt-Rh (5% - 20%) thermocouple. In an attempt to obtain finer control, only about 20% of the power was switched by means of the circuit in fig. 4.8.3.

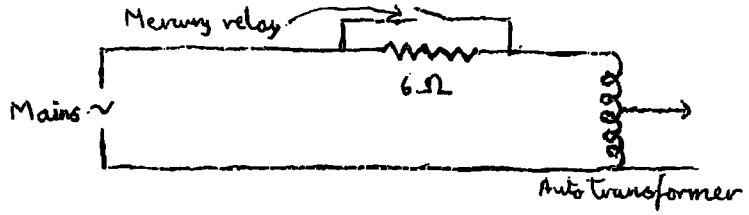

Fig. 4.8.3

The resistor dissipated about 300 watts and was made of Kanthol wire wound on a ceramic former.

Sometimes the anticipatory action would not work properly and the temperature would oscillate 5 - 10°C with a period of a few minutes. This may have been due to the time between the 'Transitrol' switching and a significant change occurring in the correct direction at the thermocouple, being too long for the 'anticaptory' circuit. The result was

probably worse than if a simple on-off type of controller had been used. In spite of the attention of the 'Ether' service engineer this was never properly cured. The thermocouples were placed between the alumina tube and the growing tube, and so the temperature oscillation would be less inside the mullite tube than at the thermocouple.

Argon was mostly used as the carrier gas. This was claimed by the manufacturers to be 99.995% pure, and so oxygen contamination from this source should be minimal. Because, however, the oxygen is introduced $< \sim 10$ cms beyond the tin boat, there is a chance some oxygen may find its way back. For perfectly uniform flow down the tube, and for the flow rates used, only a negligibly small amount of oxygen should diffuse back a distance of that order. However when eddy currents and turbulent flow are considered the possibility of appreciable oxygen finding its way to the tin boat cannot be excluded, although no calculations have been done. That this is likely is shown by the fact that sometimes the tin boat after a run was found to be partially covered with white very thin SnO_2 needles, and even more by the fact that crystals could sometimes be seen forming on the tin boat during growth.

It was partly because of this, but mainly because of difficulty in evaporating Cr for doping purposes, that at one stage the argon was passed through a drying tower

and over hot copper to remove water and oxygen. It was suspected that an oxide layer was forming on the Chromium (which was placed just inside the tip of the Argon tube).

At the time of crystal growing it was believed that the vapour pressure of SnO_2 was much lower than Sn, and that therefore the formation of SnO_2 on the Sn was bad. The analysis below shows that the transport rate should be a maximum when SnO_2 is just growing in the region of the boat.

One incidental observation which shows that there is very little oxygen in the argon and that very little leaks in, was the effect of turning off the oxygen flow during the heating up period. When the temperature was ~ 1200 - 1300°C a curious growth took place at the far end of the tube in quite a cool region estimated at 900 - 1000°C. It had a furry or fern like appearance as in fig. 4.4 and grew quite rapidly until the whole cross section of the tube was

fig 4.4 

filled with it. When removed and analysed it turned out to have very little mass, but x-ray powder photographs showed it to be a mixture of SnO_2 and β-tin. The two facts, namely that the growth region was comparatively cool and that there was tin in at least comparable quantities to SnO_2 showed that there can be very little

oxygen present. Growth rates varied considerably, but typically 2 - 3 grms of SnO_2 would be grown in a run of up to a week. Flow rates were widely varied, but the argon was generally 100 - 250 c.c./min. and the Oxygen 40 - 100 c.c./min.

Growth Theory

The following pages will discuss various factors affecting growth.

The choice between using Sn and SnO_2 as the starting material affects the process of evaporation and its rate. Marley and MacAvoy (1962) calculate from published thermodynamic data the vapour pressure of SnO_2 as being about 50 times that of metallic tin for the relevant temperatures (i.e. $\sim$1500°C, the temperatures at which the vapour pressures are becoming appreciable, or $\sim$1 mm Hg). This calculated vapour pressure of SnO_2 only applies when there are the exact stoichiometric proportions of Sn and O at equilibrium in a container. In practice this condition may not be valid, and any excess of oxygen will tip the balance of the above reversible reaction (4.1.1.) (which controls both the evaporation and condensation of SnO_2), to the right, as discussed further below. This lowers the vapour pressure of SnO and hence reduces the rate of evaporation and transport. If tin is used as the starting material, direct evaporation of tin will control the rate of transport of tin, unless appreciable quantities of oxygen are present.

In the latter case, the controlling reaction will once again be the above chemical reaction (4.1.1).

To get some idea of the effect of the oxygen pressure on the different processes, the equilibrium equation for the above reaction is of the form:-

$$\left[P(O_2)\right]\left[P(SnO)\right]^2 = K(T)$$

where $P(O_2)$ and $P(SnO)$ are the partial pressures of oxygen and SnO respectively and $K(T)$ is an equilibrium constant which is strongly dependent on T. If SnO_2 is being evaporated in an inert atmosphere, then $P(O_2) = \frac{1}{2} P(SnO)$ and so:-

$$P(SnO) = \left[2K(T)\right]^{\frac{1}{3}}$$

$K(T)$ can be calculated from thermodynamic data, but this will not be done here for the sake of brevity, and because of the doubtful accuracy of the data and the possibility of other chemical reactions (involving e.g. Sn or SnO_2 vapour) playing a significant part. From such thermodynamic data, Marley and MacAvoy calculate their graph of the vapour pressure of SnO_2. It can be seen from (4.1.1.) that if the ambient pressure of oxygen is $>$ $P(SnO)$, then $P(SnO)$ will be reduced and will be given by:-

$$P(SnO) = \left[\frac{K(T)}{P(O_2)}\right]^{\frac{1}{2}}$$

$$= \frac{\left[P(SnO)\ (\text{inert gas})\right]^{5/2}}{\left[2\ P(O_2)\right]^{\frac{1}{2}}}$$

where P(SnO) (inert gas) is the pressure of SnO over SnO_2 when stiochiometric ratios of SnO and O_2 are present.

Thus if P(SnO) (inert gas) = 10 mm Hg, and $P(O_2)$ = 760 mm Hg, then P(SnO) is reduced by a factor of 12.5 by the presence of oxygen (Marley and MacAvoy calculate a reduction of 13.2 at 1525°C, and observe one of about 10). At lower temperatures (and hence pressures) the reduction is, of course, more. As the graphs of log p against $1/T$ are roughly parallel for Sn and Sno_2 (neutral gas), and are approximately a factor of 50 apart, it would seem that the rate of growth from SnO_2 in an oxygen atmosphere and from Sn in a neutral atmosphere should be about equal for P(Sn)O) (neutral gas) ~ 1mm Hg, or T ~ 1400°C. This is roughly the temperature for evaporating Sn used at Durham, see fig. 2 (the temperature is hard to assess, as the cooling effect of the flow of neutral carrier gas on the tin in the evaporating boat is an uncertain quantity). It is illuminating to consider what happens, for temperatures of this order, as the presence of oxygen in the carrier gas is gradually increased. Provided the flow rate is slow enough (see below), every oxygen molecule passing the tin boat will take part in this reaction

$$Sn + \tfrac{1}{2}(O_2) \rightleftharpoons SnO,$$

which thermodynamic data suggests is heavily weighted to go to the right. So, as the oxygen pressure is increased,

the rate of tin leaving the boat area is increased, and when, e.g., the oxygen pressure equals half the vapour pressure of tin the flow of tin should be nearly double its initial value. This should continue until the pressure of oxygen entering equals half the equilibrium pressure of SnO_2 (neutral gas) at that temperature. At that point solid SnO_2 will begin to form, and as the oxygen pressure is increased further the transport of tin will be reduced as discussed above until for 100% oxygen the rate will be back to roughly the initial rate (for the temperatures considered). It would thus appear that the transport rate can be increased by more than one order of magnitude over that for a completely inert carrier gas by introducing small, controlled amounts of oxygen. The expected result is sketched in fig. 4.5.

These predictions have not been systematically verified at Durham, and if further crystal growing work is done using this method it would form an interesting study. The prediction that small quantities of oxygen would increase the transport rate depends, of course, on the accuracy of the thermodynamic data.

A sketch of the pressures of different vapour species is shown in fig. 4.6.

The Effect of Flow Rate

The above theory concerning transport rates is only directly applicable if the flow rate is low. It assumes

FIG. 4.1.5.

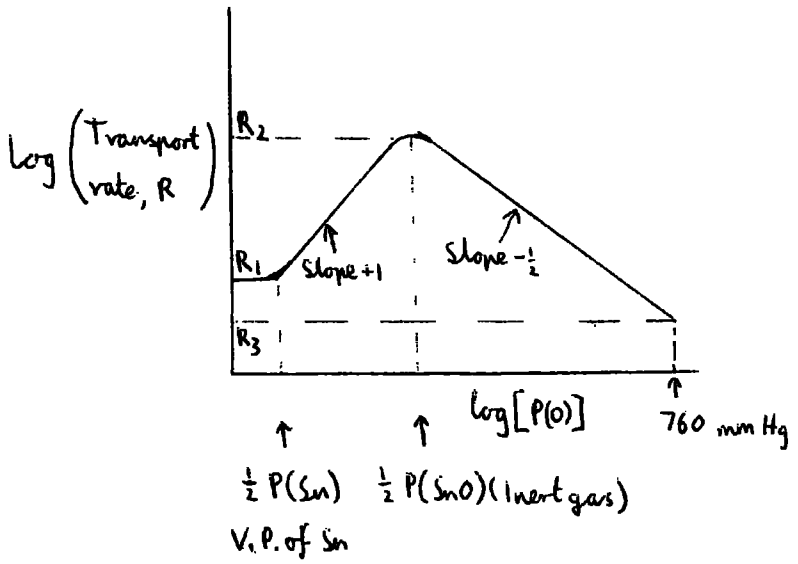

$$\frac{R_2}{R_1} = \frac{P(SnO)\,(\text{inert gas})}{P(Sn)}$$

$$\frac{R_3}{R_2} = \frac{P(SnO)\,(100\%\ \text{Oxygen})}{P(SnO)\,(\text{inert gas})} = \left(\frac{P(SnO)\,(\text{inert gas})}{2 \times 760}\right)^{1/2}$$

FIG. 4.1.6.

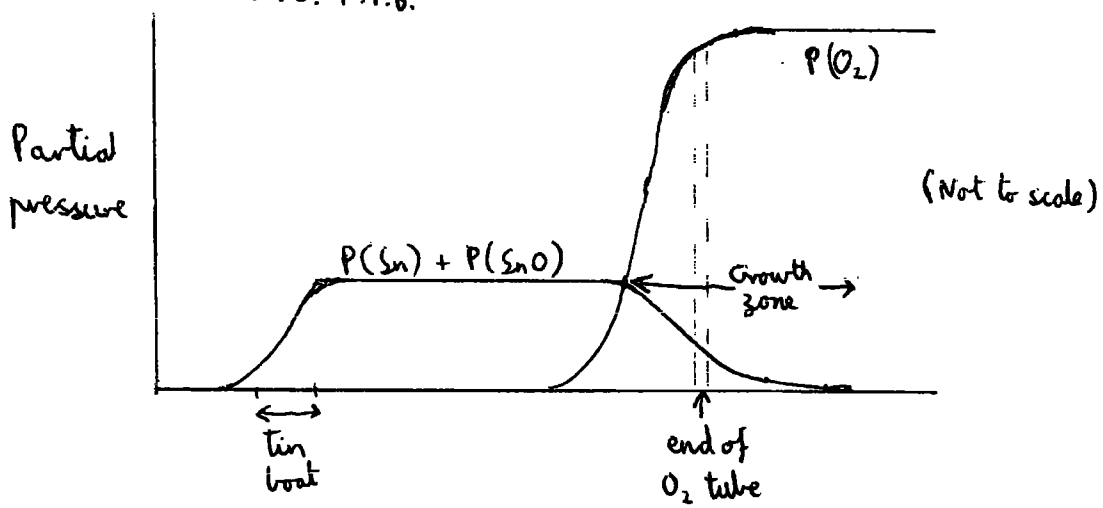

in growth region $[P(SnO)]^2 [P(O_2)] = K(T)$

$P(Sn) + P(SnO)$ is of the order of magnitude of the vapour pressure of tin.

a kind of pseudo-equilibrium is obtained above the tin boat across the cross section of the tube. If this does not occur, the theory should still be qualitatively true. The validity of the assumption can be roughly seen by comparing the time an atom takes to diffuse across the tube, with the time the general flow takes to pass the tin boat area. The diffusion time can be roughly obtained from the general principal in diffusion that the distance travelled varies as the square root of the time. The basic unit of distance is the mean free path, and the basic unit of time is the time taken to travel the mean free path. The mean free path in air at $0^{\circ}C$ is 6×10^{-6} cms, so that at $1700^{\circ}K$ it is $\sim 4 \times 10^{-5}$ cms. The velocity of the heaviest (and therefore slowest) atoms involved, Sn, is $\sim 2 \times 10^{4}$ cm / sec at $0^{\circ}C$ and so is $\sim 5 \times 10^{4}$ cm/sec at $1700^{\circ}K$. Therefore the basic unit of time is $\sim 8 \times 10^{-10}$ secs. The distance we are interested in is $\sim 5 \times 10^{4}$ mean free paths, therefore the time is $\sim 8 \times 10^{-10} \times (5 \times 10^{4})^{2} = \sim 2$ secs. If the length of the tin boat area is taken as 4 cms, a maximum speed of 2 cms/sec is arrived at. If the area of cross section is 5 sq cm a flow of 600 c.c./min at $1700^{\circ}K$ which corresponds to 100 c.c./min at R.T. Flow rates actually used were of this order, and so calculations based on pseudo equilibrium are likely to give transport rates that are ~~appreciably~~ approximately right, but a little too high, especially for higher flow rates.

Comparison between transport rates achieved by Marley and MacAvoy and at Durham are too difficult and involve too many unknowns to be able to say whether our rate corresponds to the vapour pressure of liquid tin or solid SnO_2. Their higher temperature ($1650^{\circ}C$) is certainly the biggest factor in their transporting more material in less time.

Their low thermal gradient probably allows them to get fewer and bigger crystals, and their use of helium they claim gives them more perfect crystals. The latter is said to be due to the high thermal conductivity of helium which keeps the crystals at more constant temperatures and prevents local hot spots and re-evaporation.

(4.1 continued)

Growth using the vertical furnace

A variation on the above method of crystal growth was tried in which a vertical furnace of broadly similar construction was used. The furnace element manufacturer claimed a slightly higher (1550°C rather than 1500°C) 'maximum' temperature for this design, which was one of the attractions of using it. The idea was to use a closed-end Mullite tube in the bottom of which the starting tin material was to rest, and when the working temperature was reached an equilibrium was to be established between the Sn or SnO vapour diffusing upward and the oxygen diffusing downward after passing through cracks round the edge of an alumina lid. An alternative was to do away with the lid and have a narrow bore mullite tube passing down the tube to within an inch or two of the bottom and through which argon could be passed. A small flow of argon was passed during warming up to prevent the oxidation of the tin and at working temperature this is reduced or stopped to allow oxygen in. If, during trial runs, a skin of SnO_2 forms on the tin surface this can be broken with the argon tube.

It was hoped that this method would increase the

rate of growth by working at a higher temperature and having a larger surface area of tin (the tube internal diameter was 4 cms). The variation of method might also produce changes in crystal habit and perfection.

Theory, and comparison of rate of transport in the two furnaces

A picture of what should happen in the vertical furnace when dynamic equilibrium is established (with no argon flow)is as shown in fig 4.1.7.

There is a background of almost atmospheric pressure of nitrogen, and the picture assumes that only vapour diffusion (rather than convection) is important and that the reaction $Sn + \frac{1}{2}O_2 \rightleftharpoons SnO$ is heavily weighted to the right. The flow of oxygen atoms down the concentration (and hence pressure) gradient to the right of the region of SnO_2 growth is twice that to the left of that region because of the two stages in the oxidation of tin. The atomic flow down the tin vapour gradient equals that down the final oxygen gradient because they combine to form SnO. The pressure gradients are roughly equal because the oxygen molecules have about twice the velocity of tin atoms, but there are two oxygen atoms to an oxygen molecule. The SnO gradient between the two

reactions roughly equals the Sn gradient because both represent the same atomic tin flow. An estimate of the parameters can be obtained as follows. Assuming the length of the tube is 20 cms, the vapour pressure of tin is 2 mm and the partial pressure of oxygen is 200 mm at the tube mouth, then the point of SnO formation is about $^{1}/_{50}$ of the tube length, i.e. 0.4 cms, from the tin surface. This distance has been used in an approximate theory (not given here) used to compare the flow rates in the two furnaces. The theory is based on the general approaches used in this section. It estimates that the vertical furnace should produce SnO_2 at about 30 x the rate for the horizontal furnace for the experimental arrangements described. One interesting feature of the vertical furnace arrangement is that the transport rate is independent of temperature. The effect of lowering temperature is to shift growth closer to the tin surface and so increase the probability of forming a skin of SnO_2 on the tin surface. The partial pressure of SnO is obtained from the reaction formula $\left[P(SnO)\right]^2 \left[P(O_2)\right] = K(T)$ in the region of crystal growth. If the vapour pressure of SnO_2 (inert gas) (i.e. the pressure of SnO and O_2 above SnO_2 in the presence of an inert gas only)

is, say, 10 x that of tin, then the region of SnO_2 growth starts nearly 10 x further from the tin surface than the point of formation of SnO.

Practice

Only about two experimental runs with the vertical furnace were done at Durham which produced in about 12 hours crystals of similar size to those requiring about a week with the other method. There seemed to be a tendency to form a skin of SnO_2 on the tin, presumably because of the presence of too much oxygen at too low a furnace temperature, or because of eddy currents of oxygen. The comparison of flow rates is complicated by the presence of the skin of SnO_2, and the agreement with theory must count as satisfactory in the circumstances. However, not nearly enough was done to establish a coherent experimental picture. The work was discontinued because the tin attacked the mullite and the bottom fell out of the tube. Tin had been placed in direct contact with mullite in early work on the horizontal furnace without disastrous results, so the difference is presumably due to the higher temperature (the early work was done at a temperature over 100°C lower) or greater weight of tin.

The account of this method is presented here largely

as a possible help to future experiments in choosing a method of crystal growth. The method has several advantages, but one disadvantage not already mentioned is the difficulty of introducing controlled amounts of impurity.

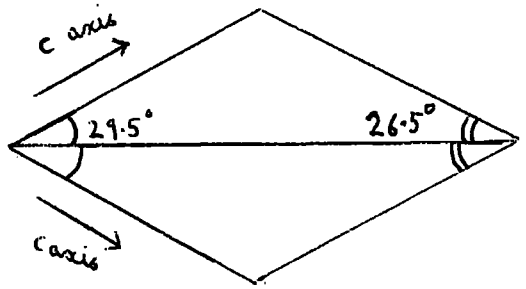

FIG. 4.2.1.

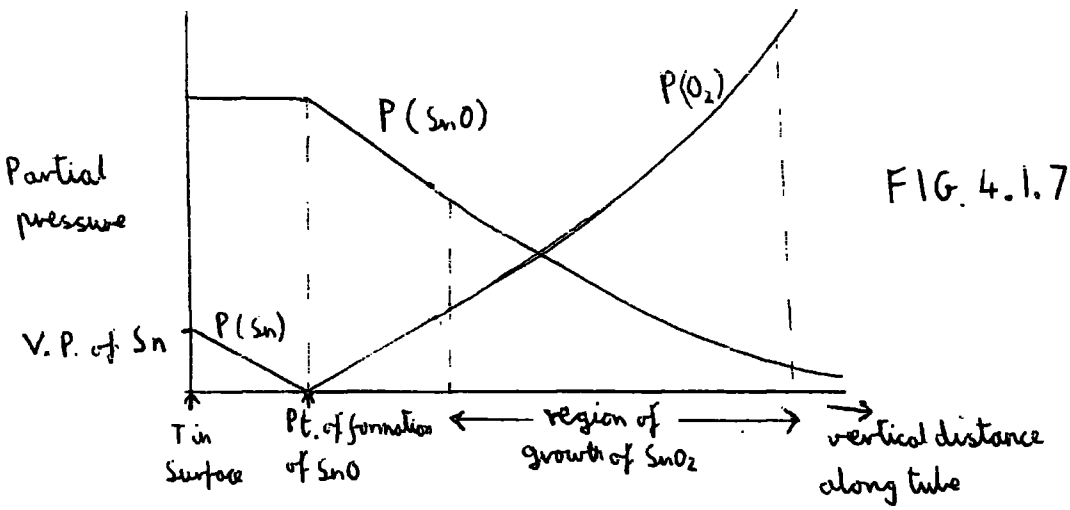

FIG. 4.1.7.

4.2. Crystal Habit

Three major different habits were produced: rods, plates and needles. Determining the exact location of different growth zones was difficult because most of the growth occurred on the inside wall of the main mullite tube. The bigger and better crystals fell out quite readily when the tube was tilted. The smaller crystals required to be knocked out and so gave some indication of position. Some crystals, predominantly rods, grew on the end of the oxygen mullite tube, and the rest started a little farther downstream.

Needles grew during lower temperature ($\sim 1350^{\circ}C$) runs and in some circumstances during warming up. Plates were the major growth habit, but there were nearly always some rods, perhaps rather more during higher temperature runs.

These facts largely agree with Marley and MacAvoy (1962) who found three distinct growth zones:-

rods	$1620 - 1570^{\circ}C$
plates	$1570 - 1460^{\circ}C$
needles	$1460 - 1300^{\circ}C$

The disagreement is over the temperature. At no time was any part of our horizontal furnace above $\sim 1500^{\circ}C$ and certainly not $1570^{\circ}C$. The explanation that comes to mind,

apart from possible error in temperature measurement, is that the degree of supersaturation is important as well as the temperature. The facts would best be fitted if a high degree of supersaturation caused a lowering of the transition temperatures. Marley and MacAvoy used a low temperature gradient and should have had a low degree of supersaturation. In our arrangement, close to where oxygen is admitted, there will be a rapid change in oxygen pressure, and hence in the equilibrium pressure of SnO. This will result in a high degree of supersaturation, as will the higher temperature gradients.

The needles and rods both had their C axes along their length and the plates were nearly always diamond shaped twinned crystals as shown in fig 4.2.1. The twin plane is demonstrated by the observed equivalence of angles when the crystal is reflected in the long diagonal and the agreement to within experimental accuracy ($\sim \frac{1}{3}^{o}$) between observed and calculated angles if it is assumed that the twin plane is (013) and the sides are (100) and ($\bar{8}$11). Further confirmation comes from the polarising microscope which showed the optic (c) axis to be (ambiguously) either parallel or perpendicular to the sides neighbouring the sharper end. The angle between the two optic axes was also measured as 53^{o}.

The twin plates were used most for optical work. Their C axis edges often had (110) faces at 45° to the plane of the plate, which reduced their useful area for transmission measurements, but otherwise their outlines were often nearly perfect with maybe a very small part of a tip broken off where the crystal had been anchored to the tube. Apart from that, the plates were not perfect in at least three ways. The twin plane was often multiple, with the crystal orientation changing back and forth several times over a fraction of a mm. around the long diagonal: there was also fairly often an irregular shaped area of one orientation jutting into or overlapping the wrong half of the crystal, with the consequence that it was impossible to get these areas to extinguish between crossed polaroids. The thicker crystals particularly were not of absolutely constant thickness: this was shown up by interference methods and was a nuisance for transmission measurements. Many crystals, particularly the thicker ones, contained small macroscopic voids, or other imperfections, which prevented the uniform transmission of light.

These plates seem almost identical with those grown by Marley and MacAvoy(1962).

4.3 Crystal Purity

Initially the tin starting material was only of "Analar" grade. Later purer metal was used. However, the method of crystal growing should considerably increase the purity due to distillation. The oxygen and argon were usually taken straight from the commercially supplied bottle.

Elsewhere in the thesis it is shown from the defect absorption, and from the absence of free carrier absorption, that the defect concentration is probably not very high ($\lesssim 10^{17}$ cm^{-3}). It is argued in 6.2 that the predominant defect is probably not a foreign atom, so the impurity concentrations should be considerably less than the above figure.

Two externally done analyses were made. The first was done using a mass spectrometer owned by British Titan Products Co. Ltd. The results are shown in table 4.3.1, in p.p.m. by weight. The results were considered accurate to within a factor of 3. Before submitting the material, it was ground to a powder. Care was taken not to introduce impurities, but this may not have been sufficient. The first three samples were taken from different early undoped growth runs, the fourth and fifth were heavily and lightly doped with Sb, respectively, the sixth was Cr doped and the seventh In doped.

The Al and Si are likely contaminants from the mullite tube, and the Fe may be a contaminant from tweezers. Sb crystals give concentrations of about 10^{20} and 2×10^{19} cm^{-3}, in reasonable agreement with measurements on free carrier absorption. The Cr and In crystals both have about 10^{19} cm^{-3}.

The second analysis was performed by chemical means at the Chemical Inspectorate, Royal Arsenal, Woolwich. Both powdered material (prepared in a similar way to that sent for the first analysis) and single crystals were sent. The results are shown in table 4.3.2. The single crystals were reported to have been powdered solely with the aid of plastic material. The results are in p.p.m., and it is apparent that our powdering method introduced impurities.

Table 4.3.1.

Samples

	1	2	3	4	5	6	7
Na	150	500	150	15	150	150	150
Al	1000	1000	500	100	100	100	100
Si	1000	3000	1000	250	1000	1000	1000
K	100	300	100	300	100	100	100
Va	10	30	10	3	30	10	10
Cr	< 30	< 30	< 30	< 30	< 30	85	< 30
Fe	300	500	100	300	1000	300	300
Cu	60	< 5	< 5	10	10	< 5	< 5
In	< 10	< 10	< 10	< 10	< 10	< 10	200
Sb	50	< 10	< 10	2000	400	100	< 10
Hg	10	< 5	< 5	< 5	30	< 5	< 5
Pb	10	10	< 10	< 10	10	< 10	< 10
Zr	50	50	50	50	50	50	50

All other elements < 10

Table 4.3.2.

	Crystals	Powder
Na	trace .. 5	trace . 5
Ca	5	10
Al	20	200
Mg	trace 5	trace 5
Si	trace 20	300
Fe	trace 50	50
Ga	n.d. 20	30
Hg	n.d. 50	200
Tl	trace 50	150

4.4 Grinding and Polishing

Although the as grown surfaces were generally good optical surfaces, there were three reasons for wanting to grind and polish crystals:-

(1) So that the same specimen could be measured at several different thicknesses.

(2) So that thinner crystals of a reasonable area could be obtained.

(3) So that parallel specimens could be obtained. This particularly applied to heavily antimony doped crystals of which only a few very non-uniform specimens were available. The removal of surface irregularities might also be included under this heading.

In fact not very many measurements were made using ground and polished specimens, largely owing to initial ignorance of techniques, lack of facilities and the break up of crystals.

The crystals were generally mounted with "Lakeside 70" cement, but "Shellac" and "Durofix" were also tried. Initially they were mounted on ordinary microscope slides, but later they were mounted on silica discs. The latter was with the object of possibly doing transmission measurements using the silica as a backing. The discs were also used in a jig originally built for E. Kahan of this department and shown in fig 4.4.1. The circular rim at the bottom keeps

the jig level, while pressure can be applied through the sliding central rod. The small steel piece at the bottom screws onto the central rod, and has a hole through its centre, so that the specimens can be examined in the polarising microscope at intervals. Several of these steel pieces were specially made.

Grinding was done on plate glass using successively finer SiC or alumina. The final polishing was done using diamond paste on a polishing pad mounted on plate glass. The grinding, being between two hard surfaces, cuts features of roughly the size of the particles, resulting in a mottled surface. It does, however, produce fairly good large scale flatness. Polishing, on the other hand, with the diamond particles embedded in a soft surface, only produces fine scratches by the just protruding particles. The softness of the surface, however, implies that less hard areas will be worn away more than harder areas and that sharp edges will become rounded. Tin oxide is quoted as having a hardness number of 7 (and is indeed used as a grinding powder) and is harder than "Lakeside 70". The result is that the cement around the crystal gets polished away and the edges become rounded. There was also a tendency for the edges of a crystal to break up when the crystal

thickness was $\sim 20\mu$, which progressively and quite rapidly destroyed the crystal.

Trouble was also experienced with removing the cement. This is because careful temperature control is necessary: if it is cooked too hot it 'burns' on and if it is too cold it won't flow easily and contains bubbles.

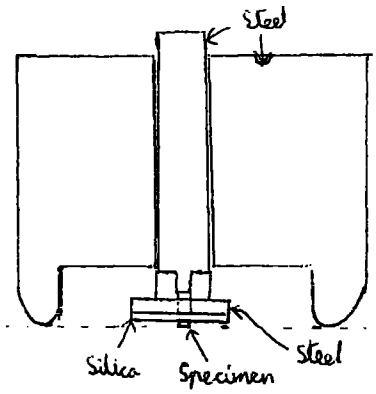

Fig. 4.4.1.

4.5 Spectrometers and Polarisers

4.5.1. Spectrometers

Seven different spectrometers were used for transmission measurements and in addition a small Hilger and Watts monochromotor was used in conjunction with a polarising microscope.

(1) Optica C F 4 DR

This machine, belonging to the Chemistry Department, was the one used most. It is a grating instrument, 800 mms focal length, with a double beam head used with a chart pen recorder, covering the range 2,000 - 10,000Å. Two sources are incorporated; a tungsten lamp (75 Watts) for the range 10,000 - 3,200Å and a hydrogen lamp for the range 3,600 - 2,000Å. The two photomultipliers are for the ranges 2,000 - 7,400Å and 7,000 - 10,000Å.

The principle of operation is that rotating mirrors alternately send a chopped light beam through sample and reference cells. Both beams fall on the same photomultiplier, whose output is amplified and the two signals are then separated by a relay which is synchronous with the rotating mirrors. A servo mechanism drives the slits so as to keep the final reference signal constant, causing the amplifiers and recorder to work with the same order of magnitude signals whatever the conditions of operation. The rectified reference signal then supplies the potential across the pen recorder slide wire, against which the sample signal is automatically balanced, giving a measure of the ratio of the light in the two beams. The light through the cells is nearly parallel. In order to increase the light through the small area occupied by a single crystal a special crystal holder was made with two quartz lens mounted on it to focus the light. This attachment, however, was not made to work fully satisfactorally.

In order to prevent the slits opening too far, thus giving poor resolution, the amplifier gain had to be turned high if only a small crystal was used. In

extreme cases the slits would be driven fully open by the servo mechanism. When the gain was high, instrument noise became important, especially when the crystal absorption coefficient was large. Initially it was assumed that the resultant output was given by the square root of the sum of the squares of the noise and the signal, and many results were worked out on this basis. Rather difficult measurements to check this were later carried out, and it was found not to be true.

(2) A second Optica machine with slight differences from (1) was later acquired by a group in the Applied Physics Dept. This was used in single beam mode for luminescence experiments.

(3) Spectromaster

This machine was acquired by the Chemistry Dept. and covers the range 0.6 - 25 μ, but has poor resolution $< 1\,\mu$. The principle of operation of this instrument is that the energy in sample and reference beam is kept equal by moving a "comb" in and out of the reference beam. The scale can be adjusted by a second comb in the sample beam. When the instrument is used with the small area of a single crystal, a small hole in a blank is required in the reference beam. Because this small hole has dimensions similar to those of the "teeth" of the comb, the absorption scale is not likely to be linear. For this reason this instrument was not much used for absorption measurements, but mainly for refractive index (interference) measurements.

(4) Another instrument somewhat similar to the Spectromaster was used in early work on refractive indices. If only covered the range $> 2\,\mu$.

(5) Hilger and Watts.

The Applied Physics Dept. posessed a Hilger and Watts prism monochromator. This was used with various prisms and detectors for absorption measurements.

(6) Barr and Stroud

The Applied Physics Dept. acquired a Barr and Stroud grating monochromator. Most of the later free carrier absorption measurements were made with this instrument.

(7) Unicam

An old Unicam spectrophotometer was used for some very early measurements. It was a single beam instrument with a built-in mechanism for inserting into the beam first the sample and then the reference object.

4.5.2. Polarisers

The first polarisers used were sheet polaroid. The chief drawback of this is its limited range. Around 4,000Å it has a complete absorption edge and above about 8,000Å it loses its efficiency as a polariser. In addition its polarising efficiency is not high just above the absorption edge, as is shown by white lights appearing blue when viewed through crossed polaroids.

Because of the limitations of polaroid a polarising prism was purchased from Hilger and Watts. Because of the expense only one was purchased. The prism polarised effectively over the range in which it was used, i.e. 2,900Å - 3/u. At shorter wavelengths it transmitted a progressively smaller fraction of the light. The prism was made of Calcite which absorbs strongly around 7/u.

Using the prism it was essential when doing absorption measurements to measure both with and without the crystal in the beam. The measurement without the crystal then acts as the "100%" line. This is also advisable when using polaroid because different pieces of polaroid absorb differently.

4.6 Crystal Holders and Cryostats

The Optica and other spectrophotometers are primarily designed for

liquids. To use small crystals some kind of holder is necessary and for polarised light it's design is important. A special holder was designed and built to fit into the Optica. The construction of it's central part is shown in fig. 4.6.1. With a plate crystal standing on the V notch (and resting, if necessary, on the vertical metal sheet) the twin line is almost horizontal and the horizontal edge can be varied in height so as to just block out the lower half of the twinned crystal. The top inverted V mask is adjusted so as to just frame the top half of the crystal. In this way nearly perfect diamond plates of any size can be mounted effectively. Also attached to the same stand of the holder is the polarising prism mounted at the correct height and at such an angle that the plane of polarisation is the same as that of the crystal. The holder was painted a matt black to minimise unwanted reflections.

An alternative central part of the holder was a rotating device whose centre of rotation was at the same height as the prism. The centre of the rotating device consisted of a hole over which a metal blank with a smaller hole could be placed. Over the smaller hole a crystal could be mounted. A pointer, which moved over a scale marked in degrees, was attached to the rotating device. This alternative arrangement was useful for plates that were not good twinned diamonds and which needed alignment with the plane of polarisation (see 4.7).

For low temperature work a cryostat was constructed. A diagram of the design is shown in fig. 4.6.2. It was designed to fit into the Optica, and also to use the central parts of the holder described above. (The holder was still used to support the prism). The cryostat could be evacuated and then detached from the vacuum pump so that it could be placed in the Optica. The evacuation serves two purposes: it improves thermal insulation and it

prevents condensation on the crystal. (The improved thermal insulation reduces condensation on the windows). The silica windows are sealed to the glass by wax. This seal sometimes gave vacuum trouble, as did the metal seal to the glass-to-metal seal and the glass-to-metal seal itself. If the vacuum was good, one filling with liquid nitrogen lasted 5 - 10 minutes.

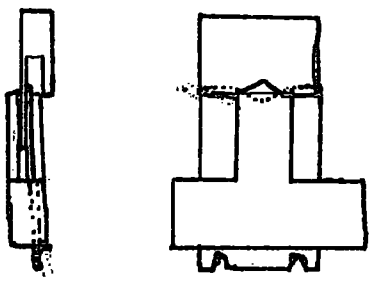

FIG. 4.6.1
(screws omitted for clarity)

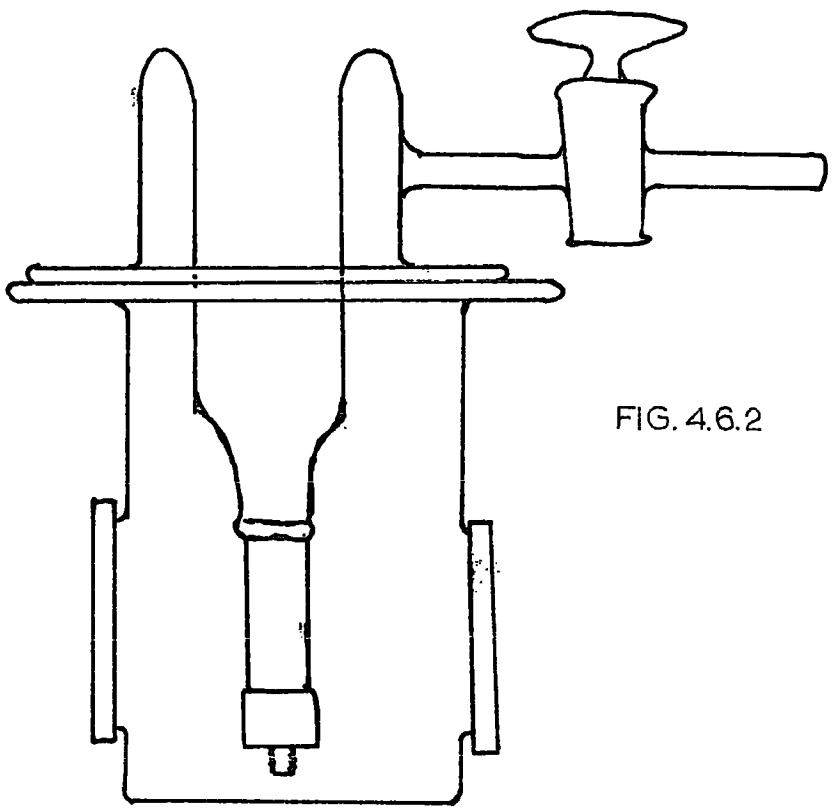

FIG. 4.6.2

4.7 Interference Methods

Interference fringes were first observed by accident while doing transmission measurements. They were then put to use in various ways for the following four purposes:-

(1) (Relative) refractive index measurements.

(2) Specimen thickness measurements.

(3) Specimen quality investigations.

(4) Lining up crystal axes with the axes of polarisers.

The methods can be classified as:-

(a) Multiple beam interference, in both polarised and unpolarised light.

(b) Birefrigent interference between crossed polarisers.

(c) As in (b) except using a polarising microscope instead of a spectrometer.

The details of the methods are as follows:-

(a) This method was used primarily for refractive index measurements. For almost parallel light passing through a specimen as in fig 4.7.1, fringes are produced with maxima given by $N\lambda = 2nt\cos\theta$ (4.7.1) where N is an integer and λ is the wavelength. If the bandwidth of the light beam satisfies the inequality

$$\delta\lambda > \frac{\lambda^2}{2nt\cos\theta}\left[\frac{1}{1-\frac{\lambda}{n}\frac{dn}{d\lambda}}\right] \qquad (4.7.2)$$

then the interference patterns due to different wavelengths cancel each other out and fringes are not seen. So high resolution and/or thin samples are required to observe the fringes.

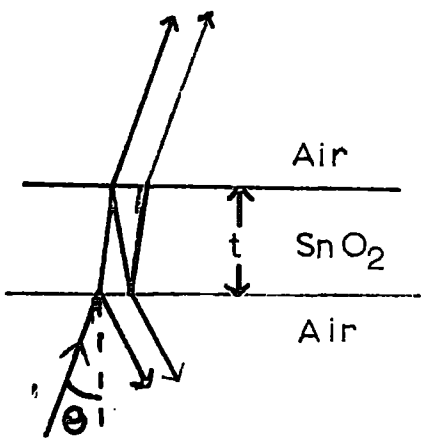

FIG. 4.7.1.

SnO_2 is tetragonal and therefore uniaxially birefrigent. So unless the direction of travel of the beam is along the c axis, the polarisation of the light must be considered. The component of light polarised with its E vector in the plane containing the c axis and the direction of travel will behave with one refractive index, and the other component polarised $\perp$ to the first (and to the c axis) will have another refractive index. The latter index is always the same, and the component of light is known as the ordinary ray. The former index varies from being the same as that for the $\perp$ (ordinary) ray in the limiting case of the c axis being in the direction of travel, to a maximum value (for a 'positive' material) or a minimum value (for a 'negative' material) when the c axis is $\perp$ to the light beam. This index is the one for the E vector $\parallel$ to the c axis and the component is known as the extraordinary ray. All except one of the samples had the c axis in the plane of the surface and normal incidence was used, so that the two indices involved are the extreme ones. The resultant interference pattern expected is therefore the sum of two, with different values of n in equation 1. If the two halves of a twinned crystal are both exposed to the

beam, this too must be taken into account and prevents a single pattern being observed, even when polarised light is used. When the two components are roughly equal in magnitude, a beat pattern is produced like the example in fig 4.7.2. If single crystals are used with polarised light, and the $\underset{\sim}{E}$ vector is $\perp$ or $//^{a}$ to the c axis a single pattern is produced, with maxima given by equation 1. Fig 4.7.2. is just the algebraic addition of two such patterns, and if fringes are counted in such a pattern an extra $\frac{1}{2}$ fringe is added on passing through each minimum for the component with small index, and $\frac{1}{2}$ a fringe subtracted for the component with large index. The fringe spacing through most of a group is the average of the two separate patterns.

Another requirement, for observing the fringes when the output is integrated as with a spectrometer, is that the specimen must be sufficiently uniform in thickness that fringes from different parts coincide. The criterion here is $\frac{\Delta t}{t} < \frac{1}{N}$ or $\Delta t < \frac{\lambda}{2n\cos\theta}$. (The low fringe contrast and the resolution requirements make observations difficult with a microscope).

The maximum to minimum ratio for a single pattern (or the highest such ratio in a beat pattern) is given by $\frac{(1+\alpha R)^2}{(1-\alpha R)^2}$ where α is the transmission in one traversal of the crystal. This does not allow for

FIG. 4.72.

thickness variation (see above) or resolution limitations. However, from observed ratios, an upper limit can be put on absolute absorption (assuming the refractive index) and a lower limit on refractive index.

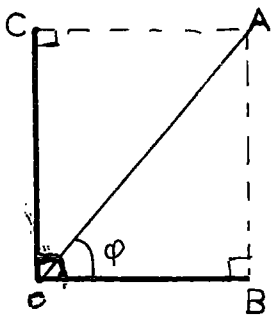

FIG. 4.7.3

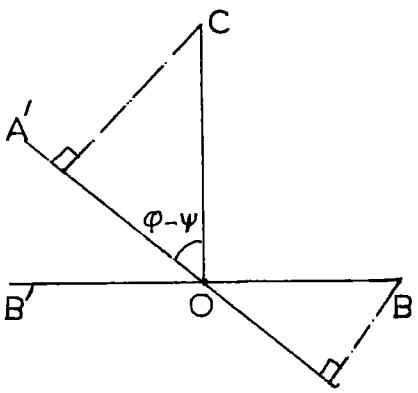

FIG. 4.7.4

(b) Two Polarisers.

This method was used mainly for determining thickness.

If two polarisers are used, one to polarise the light and one placed after the specimen to analize the emerging light, then a different kind of interference pattern can be produced, due to the ~~live~~birefrigence of the specimen.

Consider fig 4.7.3. OA represents the E vector of the polarised incoming light. OB and OC represent the directions of polarisation for the two beams in the crystal, their magnitudes being the resolved components of OA. Fig. 4 shows the emerging light. The relative phases of the two beams have changed due to differing refractive indices, so if OB now represents the E vector of that component at its maximum, then the E vector of the other component may be anywhere between OC and OC' depending on sample thickness, wavelength of light, and ~~live~~birefrigence. If a second polariser is placed $\perp$ to the first to accept light with E vector along OA', then by elementary geometry, the projection of OB and OC on OA' are equal, provided absorption, reflection and interference properties are the same, for the two components. The light

intensity is obtained by squaring the sum of these projections, and averaging over time. For given sample thickness and ~~fringe~~ birefrigence, the phase depends on the wavelength and sinusoidal fringes are produced with maxima given by

$$(N+\tfrac{1}{2})\lambda = \Delta n\, t \cos\theta$$

where N is as integer and Δn the difference in refractive indices. The minima have zero light transmitted and the maxima, ignoring losses, have a fraction $\sin^2 2\varphi$ of the light falling on the crystal, where φ is the angle between OA and (either) OB or OC. If $\varphi = 45^\circ$, $\sin^2 2\varphi = 1$ If the original light was unpolarised, then, of course, the first polariser absorbs half of it.

If the polarisers are not $\perp$ to each other, fringes of the form $1+A^2-2A\cos\delta$ are produced where A is a constant (=1 in the perpendicular case) depending on the angle ψ, $90-\psi$, between the polarisers, and δ is the phase difference. The maxima and minima occur at identical wavelengths for all values of ψ unless A is negative, when they are reversed. A is negative if the two polariser directions (OA and OA') lie in the same quadrant of the axes formed by OB and OC. There is only one direction of OA' other than $\perp$ to OA

that will give minima of zero intensity, and this direction depends on the angle of the crystal, unlike the case with the polarisers ⊥ . If either of the polarisers is only partly efficient, this will of course also reduce the contrast. Fig 5 was obtained using an efficient first polariser and no inserted second polariser, the mirrors and detector producing sufficient polarisation to obtain the fringes. This illustrates that instrument polarisation must always be borne in mind.

The same criterion regarding uniformity of specimen thickness and bandwidth of the light apply as in case (a), except 2n is replaced by Δn. This means that the thickness uniformity requirement is relaxed by a factor of rather over 40 and the bandwidth requirement relaxed by the same factor in the I.R., but an even larger factor towards the blue end of the spectrum where the dispersion term $\frac{\lambda}{\Delta n}\frac{d(\Delta n)}{d\lambda}$ from equation (4.7.2) becomes important. At a wavelength of less than 4000Å this term becomes >1 , and in the neighbourhood of this wavelength the fringe spacing, and hence maximum bandwidth requirement, becomes very large. (Fig 5, explained above, shows this. No second polariser was available for this wavelength). These differences enabled birefringent

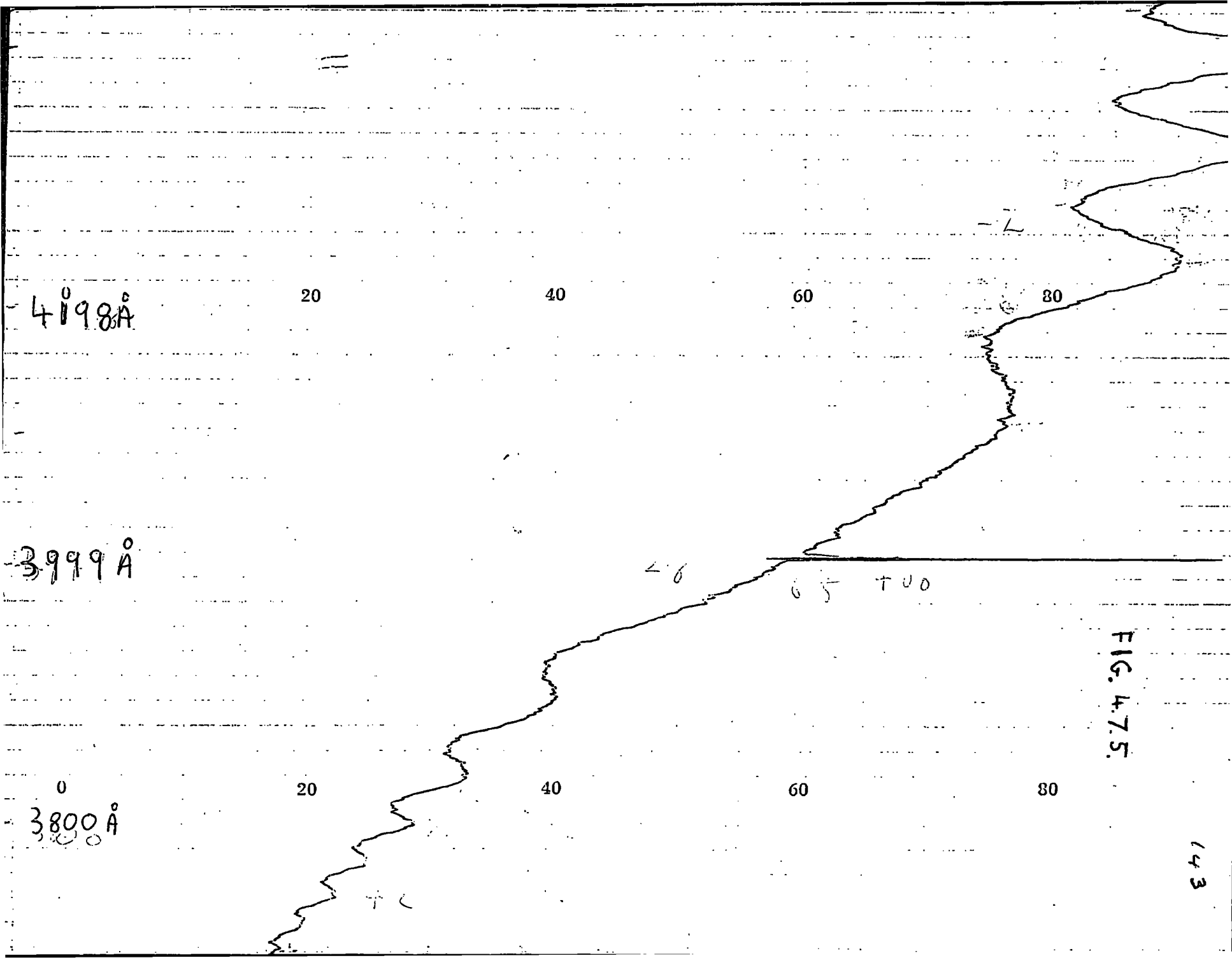

FIG. 4.7.5.

fringes to be observed in very much thicker and less uniform specimens than was possible for multiple beam fringes.

Observation of birefringent interference in crystals where multiple beam interference is also resolved, produces an unexpected effect (fig 4.7.6). If this is compared with Fig 4.7.2 it is seen that, as expected, birefrigent maxima and minima coincide with maxima in the beat pattern. The multiple beam fringe spacing is also the same, but the minima in the multiple beam beat patterns occur at different wavelengths. Fig 4.7.6 shows that these minima occur nearer the maxima in the birefrigent pattern, producing, for example, too few fringes in the group around the maxima. The explanation of this effect is as follows:

The expression for the $\underset{\lambda}{E}$ vector (assuming equal amounts of the two polarisations are transmitted) is:-

$$E \propto \frac{e^{i\delta'}}{1-Re^{2i\delta'}} - \frac{e^{i\delta''}}{1-Re^{2i\delta''}}$$

where δ' and δ'' are phase factors. The light transmitted, EE^*, $\propto$

$$\left(\frac{e^{i\delta'}}{1-Re^{2i\delta'}} - \frac{e^{i\delta''}}{1-Re^{2i\delta''}}\right)\left(\frac{e^{-i\delta'}}{1-Re^{-2i\delta'}} \quad \frac{e^{-i\delta''}}{1-Re^{-2i\delta''}}\right)$$

If this is multiplied out, and the denominators are expanded by the binomial theorem ignoring terms in R^2, we obtain after some further manipulation

$$2(1 - \cos\delta + 2R\cos(\delta' + \delta'')\cos\delta - 2R\cos(\delta' + \delta'')\cos 2\delta \quad)$$

where $\delta = \delta'' - \delta'$.

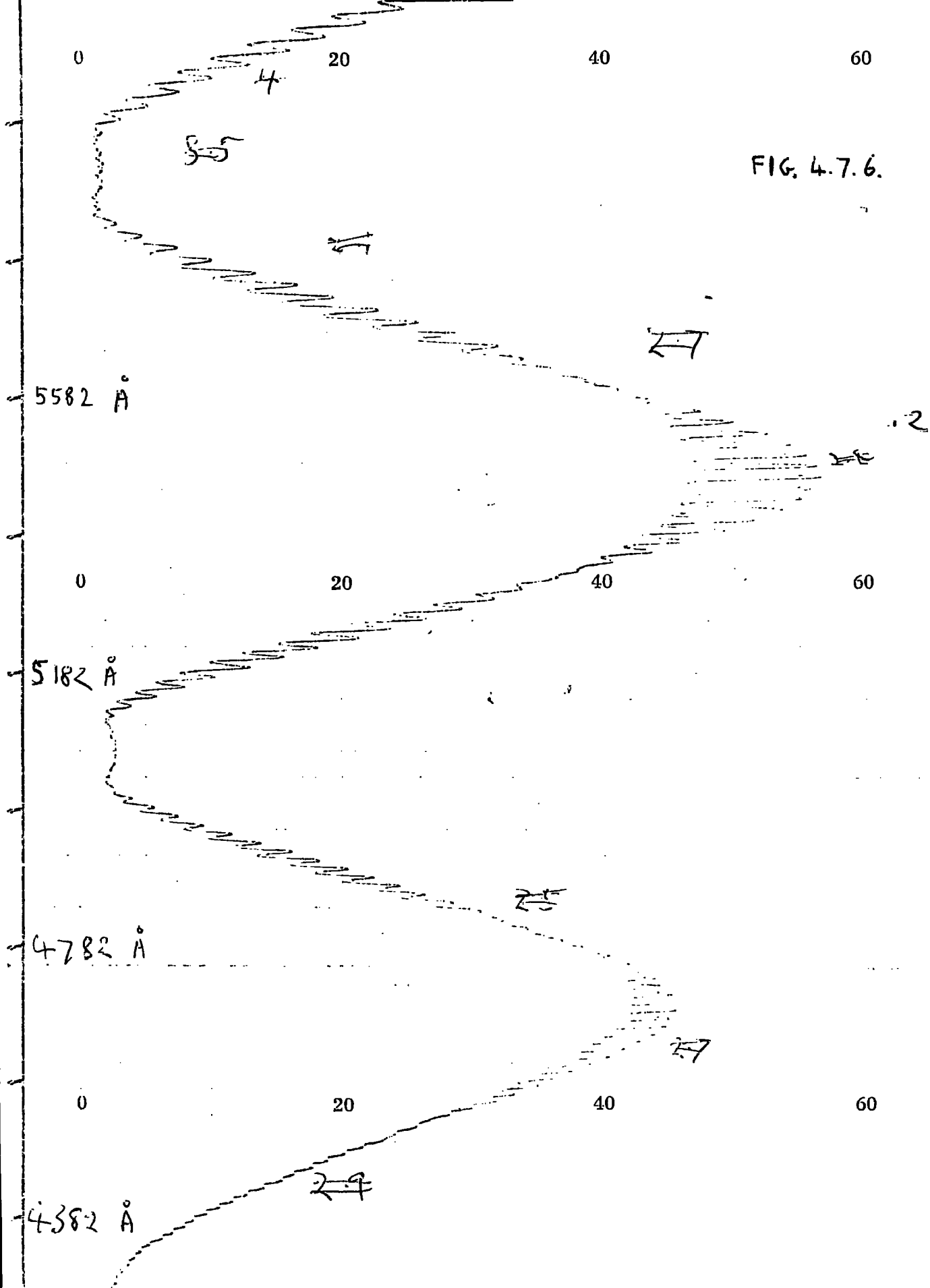

FIG. 4.7.6.

This formula is found to agree with experiment.

For aligning speciments, the case when OA and OB (fig 4.7.3) are nearly parallel is important. If the angle between them is φ, then $OB \propto \cos\varphi$ and $OC \propto \sin\varphi$. In fig 4.7.4 if OA' is $\perp$ to OA, then the output is the normal sinusoidal form with minima of zero intensity and amplitude $\sin^2 2\varphi$. If OA' makes an angle $90-\psi$ with OA, where ψ is small, then the maxima and minima of the output are

$$\left[\cos\psi \sin(\varphi-\psi) \pm \sin\varphi \cos(\varphi-\psi)\right]^2$$
$$\doteq \left[\varphi-\psi \pm \varphi\right]^2 \qquad (4.7.6)$$

If $\psi \doteq 90$, (OA nearly parallel to OA'), then the maxima and minima are

$$\left[\cos\psi \cos(90-\varphi+\psi) \pm \sin\varphi \sin(90-\varphi+\psi)\right]^2$$
$$\doteq 1 \pm 2\varphi\left[(90-\varphi)+\psi\right] \qquad 4.7.7$$

The output is, however, always sinusoidal (or constant) with maxima and minima at fixed wavelengths. These equations are used later.

(c) Polarising microscope.

This technique was mostly used to examine crystal quality.

The same principles apply as in the immediately preceeding section, except that here the output from individual parts of the crystal can be examined, and white light can be used.

With white light the fringe patterns are integrated. If the fringe number in the green is more than about 6 (i.e. fringe spacing $< \sim 1000 Å$) the light appears white and of intensity proportional to the average of the fringe maxima and minima. Thus for the case of crossed polarisers the intensity $\propto \sin 2\varphi$

If the fringe order is $< \sim 6$ (fringe spacing $> \sim 1000 Å$)interference colours are produced (c.f. Kerr 1959). Published colour charts are for Δn constant throughout the visible, but for SnO_2, Δn gets smaller towards the blue, shifting the fringe pattern a little towards the U.V. at the blue end. However, colour differences were not noticed. Presumably also the colour temperature of the source would change the colours. This, too, was not noticed.

Colours almost repeat themselves for different orders, and to be sure of colour identification,

either a "quarter wave" plate or a continuously varying 0 - 6 wave quartz wedge was used. These are birefringent materials introduced between the crossed polarisers, with φ , the angle between their c axes and the polarisation directions, equal to 45°. These add or subtract the phase difference indicated by the above numbers (which refer to the centre of the spectrum), provided the crystal also makes an approximately 45° angle. (The advantage of the $\frac{1}{4}$ wave plate is that its magnitude is definitely known, whereas the wedge varies across the field of view and its magnitude is difficult to know exactly. The wedge, though, gives a continuous range). The colour changes introduced by these devices help to identify uniquely the colour and hence optical path difference.

The microscope was also used with the small Hilger and Watts grating monochromoter (see section 4.5). The fringes give a contour picture of crystal thickness, and fringe order can be determined by varying the wavelength. Minimum bandwidth was ~ 30 Å , so the maximum thickness crystal whose fringes could be resolved at all was 0.9 mm , and then the intensity and contrast were very low and very great difficulty was experienced in observation (principally because of stray light). A convenient limit was 0.5 mm.

The above effects were used in the following ways.

1. Refractive indixes

Fairly early, one crystal (sample 6) was found giving multiple beam interference. For resolution reasons any crystal would have to be thinner than 0.4 mm (from equation 4.7.2) for the fringes to be resolved at all (assuming a resolution of 1.5 Å in the visible. This was about the best obtainable with the Optica and the surface areas of crystal available. In normal use, the time constant of the recording system put a lower limit on resolution of 3Å, giving a limit of ~0.2 mms.) Other crystals thinner than the latter limit did not exhibit interference and so presumably varied in thickness by more than $\frac{\lambda}{2n}$ or ~ .12 μ The interfering crystal was ~ 42 μ thick and so at 4000Å the fringe order was ~ 450 and fringe spacing ~ 10Å. The maximum to minimum ratio can, under certain conditions, be used as a check on the absolute value of the refractive index. The conditions used only permitted a rough check, which was quite satisfactory.

Part of the spectra obtained were shown in fig. 4.7.2 and single, rather than beat, patterns were produced in polarised light. The patterns were extended in unpolarised light using I.R. spectrometers out to ~ 9μ where the lattice absorption peaks make

interference peaks hard to identify. Water vapour peaks also cause some instrumental trouble at rather short or λ wavelengths. Here the fringe order is ~ 20, and the procedure originally adopted was to try different values for the fringe order, then count back and using equation 4.7.1. plot the relative refractive index against wavelength. Using various criteria from dispersion theory (e.g. that in non-absorbing regions n should always decrease with λ), the most likely plot was chosen. It was hoped that this would be confirmed by samples 7 or 8 of 55 μ and 120 μ thickness which began to give an interference pattern for wavelengths longer than 5 μ and 3 μ respectively, or sample 17 of 7 μ thickness which gave interference right through the visible. Unfortunately absolute experimental certainty, for a combination of reasons, has not yet been achieved in fringe identification. The method attempted was as follows. If the wrong order is chosen, the relative refractive index plots of different crystals cannot be made the same. An additional check on their thickness ratios came from ~~live~~ birefrigent interference. The fringe order identification can be shown mathematically as follows (assuming allowance has been made for the 'beat' effect which complicates matters in unpolarised light):

$$N\lambda = 2nt_1 \cos\theta_1 \qquad (4.7.8.)$$

$$N'\lambda' = 2n't_1 \cos\theta_1$$

$$M\lambda = 2nt_2 \cos\theta_2$$

$$M'\lambda = 2n't_2 \cos\theta_2 \qquad (4.7.9.)$$

where λ and λ' are wavelengths corresponding to maxima of order and N and N' (integers) in a specimen of thickness t_1 and M and M' are the corresponding (non-integral) fringe orders at the same wavelengths for specimen t_2

Then

$$\frac{N}{N'} = \frac{M}{M'} \qquad (4.7.10.)$$

and

$$\frac{N}{M} = \frac{t_1}{t_2} \left\{ = \frac{N'}{M'} \right\} \qquad (4.7.11.)$$

assuming the refractive indices for the two specimens are the same. $N - N'$ and $M - M'$ are known from counting fringes, and the possible choices for N or M only differ by integers. From this limited choice, only one will be found to satisfy (4.7.10.) and this can be checked at other fringe orders (The method only breaks down if $t_1 : t_2$ is very close to a simple ratio, e.g. 2:1. The less the initial uncertainty in fringe order, the

fewer the number of thickness ratios that could cause difficulty. In the present case the uncertainty was 2 or 3 orders). A further check comes from using (4.7.11) and the thickness ratio determined by ~~live~~ bire frigent interference (where there is no doubt about fringe order). Slight reservations were held. The main difficulty about using samples 7 and 8 was that their thickness variation (shown by only lower fringe orders being observed) led to uncertainty over their effective thickness for fringe production and for sample 8 the comparatively large thickness meant that high accuracy was required in dealing with high fringe orders. Sample 17 led to considerable experimental difficulties due to its very small area and the very broad low order fringes involved).

Then by counting fringes and using equations 4.7.1 a relative refractive index plot is obtained, limited ~~only~~ mainly by the wavelength accuracy with which the fringe maxima can be read and conceivably by a very small variation in effective thickness. ~~Unfortunately, at present the accuracy is also limited by lack of absolute certainty in fringe order~~. Both indices are obtained from the unpolarised'beat' patterns, and the indices are shown in fig 5.4.1 & 5.4.2. The large errors at the long wavelength end are due to uncertainty in the relative positions of the

peaks due to the two polarisations (or "how far we are along the beat pattern"). This is because there is not another 'beat' minima from which reasonable interpolation could be made of the birefrigence, and fringe magnitude is no guide to this because of lattice absorption. The error is of the type that the sum of the indices is better known than either individually. This error (which can only be crudely guessed) would be eliminated if polarised light were used, or more work done with more specimens with a different 'beat' pattern. Great care is required not to make a mistake in counting past a beat minima, particularly if this coincides with a change of instrument. The best check is to make a plot of refractive index and see that there is no sharp jump across the minima. For fringes not at the beat maxima, it is necessary to allow for the shifting of the peak by the other polarisation.

The short wavelength limit to the method is a combination of absorption at the absorption edge and resolution of the instrument. As fringes get smaller and noise increases (in order to maintain resolution), fringe indentification becomes impossible. Birefrigent measurements can be extended further but only by relying on instrument polarisation as only one polariser was available in this region below 4000Å.

To put ~~on~~ an absolute scale to fig 5.4.1. and 5.4.2., the values given by Kerr (1959) for natural Cassiterite in the middle of the visible were used. No range of values was quoted, unlike some minerals, and as natural Cassiterite occurs in a range of colours, presumably the value is not sensitive to impurity. Because only one figure was required to give a scale, the second acted as a check on the absolute value.

Great accuracy in the absolute values does not seem to be important, but two methods of check suggest themselves. A crude check was obtained by using the polarising microscope on a thicker specimen. From equation 4.7.2 $\Delta n\, t$ is obtained (finding N requires assuming the same value of Δn exists as in thinner crystals, where the order can be identified easily). By focusing the microscope on the top and bottom surfaces the apparent depth $\frac{t}{n}$ can be determined for either polarisation. Hence $\Delta n.n$ is obtained and so, too, an absolute value of n. This agreed with Kerr (1959) but accuracy was only ~1½% (because of focusing limitations).

The second method is to measure directly with a micrometer the crystal thickness. This is easiest for thick crystals, and the danger is from variations in flatness. However, with very careful crystal selection a value of t accurate to 3μ might be obtained, giving ½% accuracy for a 0.6 mm crystal. This would give Δn

~~firm~~ from $\Delta n\, t$ as above. This has not been done.

2. Specimen thickness measurements

This was mostly done with birefrigent interferenwe, either in the spectrometer or the polarising microscope together with a monochrometer. It could be conveniently done before or after taking an absorption spectrum. Equation 4.7.3 is used, different values of N being tried until the known relative variation of Δn is produced. Only for thicker specimens was exact identification of N not possible, but even then accuracy of 1% was attainable. If poor contrast was obtained, indicating thickness variation, greater reliability could be had with the polarising microscope where the thickness of a particular part of the crystal could be measured, but with rather less accuracy due to limited visual range ($\sim$ 4600 - 6300Å) and wavelength accuracy. For specimens less than $\sim 30\mu$ white light colours as described above can be used ~~i~~directly.

This method was also used for doped specimens. Further investigations ought perhaps to be made here to check that Δn does not vary significantly with doping.

When suitable, multiple beam interference described by equation 4.7.1. was also used.

3. Specimen Quality Investigations.

In looking for specimens the later procedure adopted was to spread out the material under the polarising

microscope and to search through, usually in white light, with or without the polarisers. Without the polarisers a picture of the general quality can be obtained from the outline, surface features, etc. Sometimes parts are dark, presumably because the light has been bent out of the acceptance of the microscope lens, by prism action. Similar features are seen when crossed polaroids are used, but the picture is confused because the intensity of a part of a crystal varies, depending on orientation. By rotating the stage of the microscope this effect is used to find out how single crystal a specimen is. If a region extinguishes all at the same angle, then it is single crystal. Twinning and grain boundaries are shown up. If a region will not extinguish at all, then there are two parts of crystal on top of each other with different crystal directions. This may either be two separate crystals or one piece as grown. In monochromatic light, if the bandwidth is small enough, the picture is further complicated by the fringes and also the lack of intensity. The contour pictures enable the most uniform specimens to be selected (and thickness measured as in the previous section by varying wavelength). Caution is required with the contours where they cross surface features as the contour order might jump. The only way to be sure is to vary the wavelength and note

fringes passing each side of the feature.

See section on crystal habit for results and observations.

4. Aligning Specimen Axes with Polariser

Thicker specimens, which could easily be handled loose and which had a good diamond outline (see section 4.2.) were aligned with sufficient accuracy with the special crystal holder (section 4.6). Other specimens were aligned by reducing the birefrigent interference to a minimum. ~~Details are given in section 4.6., but~~ The principle is to use two polarisers and rotate the crystal to eliminate the interference, as follows.

If the polarisers are approximately crossed, formulae 4.7.6. apply. The wavelength is set near a maximum and Ψ is varied and the output noted. It varies as $(2\Phi - \Psi + \varphi)^2$, so is symmetric about $\Phi = -\frac{\Psi}{2}$, a minimum of zero. (Here the 'maximum' of the fringe pattern has turned into a minimum, as the 'minimum' is constant at Ψ^2). So provided Ψ is small, the crystal is almost aligned if set for a minimum output. The drawback of this method is that very small outputs are involved, and these tend to get lost in noise. An alternative is to adjust Φ so that there is no fringe pattern. This gives the correct alignment (or $\Psi = \varphi$) whatever $\varphi\Psi$. If $\varphi\Psi$ is small ~~this~~ the output may be lost in noise

however if ψ is only moderately small, say 20^{o}, this is probably the most accurate method. A small error in ϕ will produce quite a large pattern, but care must be exercised to ensure $\varphi = o$ and not ψ . If ψ is increased to almost 90^{o}, formula 4.7.7 applies, which gives almost the same effects as with ψ small, except for a nominally constant large background. One is well clear of noise, but the 'constant' background will vary, making assessment of small fringe patterns difficult. With moderately small ψ the ratio of fringe pattern to background is much bigger.

4.8 Data Handling

In order to allow for reflection (2.3.6) is used as the starting point, and k is assumed $<<$ n. To find T the ratio of the measured transmission with and without the crystal is used. In order to do the arithmetic to obtain K a computer programme was written using ALGOL. The programme underwent a number of modifications, but one version of it is shown in fig. 4.8.1. Incorporated in the programme is a table of reflectivities at each wavelength for each polarisation. These tables were derived from the refractive index found by interference methods. (Extrapolation was used for the shortest wavelengths).

The data input includes a crystal identification, the polarisation, crystal thickness and the wavelengths at which the wavelength interval between points changes. The latter was designed with the absorption edge in mind and the longest wavelength points are separated by 100 $\mathring{A}$, the shorter ones by 50 $\mathring{A}$ and the shortest by 25 $\mathring{A}$. The bulk of the data input is then pairs of numbers corresponding to the specimen transmission and the " 100%" at each wavelength.

```
BEGIN INTEGER N,L1,L2,L3,L4,L5,P,NO'
REAL A,B,C,X,Y,K,D,E'
     ARRAY R(25:70)'
      SWITCH SS:= START'
      START: READ NO,P,A,B,C,E,L1,L2,L3,L4,L5,D'
      IF P=1 THEN
        BEGIN R(30):=.1447'R(31):=.1417'R(32):=.1393'
          R(33):=.1361'R(34):=.1335'R(35):=.131' R(36):=.1290'
          R(37):=.125' R(38):=.124' R(39):=.122' R(40):=.120'
          R(41):=.119' R(42):=.118' R(43):=.117' R(44):=.116'
          R(45):=.116' R(46):=.115' R(47):=.115' R(48):=.114'
          R(49):=.114' R(50):=.113' R(51):=.113' R(52):=.112'
          R(53):=.112' R(54):=.112' R(55):=.111'
        END
                ELSE
    BEGIN R(30):=.149' R(31):=.146' R(32):=.144' R(33):=.143'
          R(34):=.141' R(35):=.140' R(36):=.138' R(37):=.137'
          R(38):=.135' R(39):=.134' R(40):=.133' R(41):=.132'
          R(42):=.131' R(43):=.130' R(44):=.130' R(45):=.129'
          R(46):=.129' R(47):=.128' R(48):=.128' R(49):=.127'
          R(50):=.127' R(51):=.126' R(52):=.126' R(53):=.126'
          R(54):=.125' R(55):=.125'
    END'
        PRINT ££S?,SAMELINE,NO,P'
      FOR N:=L1 STEP -100 UNTIL L2,L2-50 STEP -50
UNTIL L3,L3-25 STEP -25 UNTIL L4 DO
      BEGIN READ X,Y'
       K:=LN((Y-E)/(C-E)*(B-A)/(X-A)*CHECKR((1-CHECKR(R(N/100)))**2
            /(1-CHECKR(R(L5/100)))**2))/D'
        K:=CHECKR(K)-CHECKR((LN((1-R(N/100)**2*(2.718**(-2*K*D))
                )/(1-R(L5/100)**2))))/D'
X:=12397.5/N'
          PRINT ££L??,DIGITS(4),N,PREFIX(££S3??),FREEPOINT(5),X,
IF K GREQ 0 THEN SQRT(K) ELSE -SQRT(-K),K,K*D,
X*K,IF X*K GREQ 0 THEN SQRT(X*K) ELSE -SQRT(-X*K)'
      END'GOTO START'END'

S.F.R. ABS. COEFF. NO.1'
BEGIN INTEGER N,L1,L2,
```

FIG 4.8.1

The output consists of a row for each point, with columns containing the wavelength, energy in e.v., K, $K^{\frac{1}{2}}$, $K\hbar\omega$, $\sqrt{K\hbar\omega}$ and Kd. The square root columns were included because when the program was written simple behaviour of the indirect transition type was being looked for.

4.9 Other Experimental Measurements

4.9.1. Luminescence

Luminescence was looked for but not observed. It has since been observed in some specimens at Durham by Morgan (1966B). The main experiment in the unsuccessful work consisted of using an Optica to scan the range 2800 - 5000 Å. The speciemen was illuminated with a high pressure mercury lamp which was passed through a liquid chemical filter to exclude the longer wavelengths. In spite of the chemical filter quite a lot of stray light from the mercury lamp got into the Optica. One method of checking if any luminescence was present was to take a spectrum at R.T. and then at nitrogen temperature. Any luminescence would almost certainly differ between the two measurements. There was no noticeable difference.

Another experiment was performed of using a darkened mercury lamp which emitted U.V. In a darkened room no luminescence was visible, either at R.T. or nitrogen temperature; this was still so when the lamp was focused onto the crystal using a quartz lens.

When Morgan later obtained luminescence it was found that the specimens we used did not give luminescence in the new experimental method.

4.9.2. Hall Effect

The little work done on the Hall effect, together with the reasons

why more was not done, are given in 5.3.

4.9.3. Faraday Effect.

The possibility was considered of measuring the Faraday effect, mainly with the object of finding the effective mass. The following considerations led to this experiment being considered unprofitable.

(1) Free carriers

The elementary (classical) formula for the free carrier Faraday effect is:

$\theta = BNe^3/2nc\,\epsilon_0 m^2\omega^2$ radians/metre.

The free carrier absorption is given by (6.3.1), $K=1.7 \times 10^{-18} N \lambda^3$. If we assume that the maximum thickness for practical measurements is given by 3/K, then the maximum angle of rotation (after adjusting for differing units) is $\left[3\omega Be^3/2nc^4\,\epsilon_0 m^2(2\pi)^3\right] \times 6 \times 10^3$ radians. The maximum value of B available was ~ 0.6 Weber/m^2. Taking $\omega = 10^{15}$ sec^{-1} ($\lambda \approx 2\mu$), n = 2 and m = 0.3 m_o we obtain the maximum angle as $\sim$ 0.08 radians. With simple measuring equipment the accuracy of measurement would probably be worse than 0.01 radians, so that the best accuracy obtainable would be about $12\frac{1}{2}\%$, and that at only one wavelength for each crystal.

(2) Intrinsic Faraday Effects

Moss (1961) shows that classically the rotation is related to the dispersion thus:

$\theta = (Be\omega/2cm)\, dn/d\omega$ radians/metre.

(The same relation holds for free carriers). m is the

mass of the charge carriers, presumably the valence or conduction band mass for the short wavelength dispersion and the ionic mass for the lattice dispersion. For crystals $\frac{1}{2}$ mm thick the angle of rotation in the maximum field is < 0.1 radians at wavelengths longer than the visible.

(3) Theoretical

A glance at the literature showed that the simple formulae were inadequate and obtaining a reliable effective mass would be difficult, even with perfect experimental results. One of the difficulties with using the intrinsic effect is to know what combination of valence and conduction band masses has been found. A difficulty with the free carrier effect is the error in the classical formula. In 6.3 the error in the closely related classical formula for the free carrier absorption is large. In that case the classical formula gives too big an effect, and, if the same is true here, the experimental error will become very large. Altogether, to achieve meaningful work on the Faraday effect appeared to involve a big programme of work.

4.9.4 Plasma Effects

In 6.3 we show that observation of plasma effects by transmitted light requires thinner crystals than we had. Plasma effects should be observable by reflection in highly doped samples and would make an

interesting study. This study was not carried out because we were not well equipped for reflection work, and because an erroneous calculation indicated the plasma frequency as being in the far I.R.

4.9.5 Conductivity Measurements

Early on considerable work was put into measuring conductivity. It was measured on undoped crystals at steadily higher maximum temperatures up to 500°C. As grown rod and needle crystals were used and silver "Dag" dispersion was used to make contact. Results were found to be not reproducible and to depend on thermal and electrical history. For example the current at constant voltage after heating was found to decay exponentially. Also observed was a form of hysteresis, in which as the voltage was raised above a certain point a large drop in resistance occurred, which only reverted back to higher resistance when the voltage was lowered to a point less than the first voltage. Another effect was change in the I-V characteristics, and in particular asymmetry between the two polarities, after passing current in one direction for some time. Photo-voltaic effects were also observed.

These effects were not fully explained, but Morgan (1966) et.al. achieved satisfactory measurements at higher temperatures by grinding off a surface layer. This layer was apparently a high resistance layer formed on cooling after growth.

5.1 The Absorption Edge and Defect Absorption

The absorption edge was measured on several as grown crystals on the Optica spectrophotometer. The transmission of free standing crystals was measured in polarised light and the data analysed, including the effects of reflection varying with wavelength and of multiple reflection, as indicated in 4.8.

The early results were presented in Reddaway and Wright (1965) for R.T. and are reproduced in fig 5.1.2. Results were later obtained at nitrogen temperatures, and the results at higher absorption levels are shown in fig. 5.1.1, on a log K plot. The results for lower absorption levels, where defect absorption is important, are shown plotted for S.8 in figs. 6.2.1. and 6.2.2. The differences in defect absorption for different samples was small (as shown in Reddaway and Wright). Unfortunately spectra on the thinnest crystals at nitrogen temperatures were not obtained. The R.T. results have been extended beyond the results published in Reddaway and Wright by use of the very thin crystal S.16 (7.3μ thick). These extended results are shown in 5.1.1. Unfortunately the largest measurable K has not been increased by the use of S.16 in inverse proportion to its thickness, because its very small area meant that the spectrophotometer had to be worked with a higher noise level.

Also shown in fig. 5.1.1. are results from a number of other sources, the most important being Summitt, Marley and Borrelli (1964). Their crystals were made with greater care and did not show the defect absorption. Their wavelength resolution appears to be rather better than ours, and their accuracy in measuring K may be better in some regions of the spectrum. However their maximum measured value of K is about 4 times less than ours.

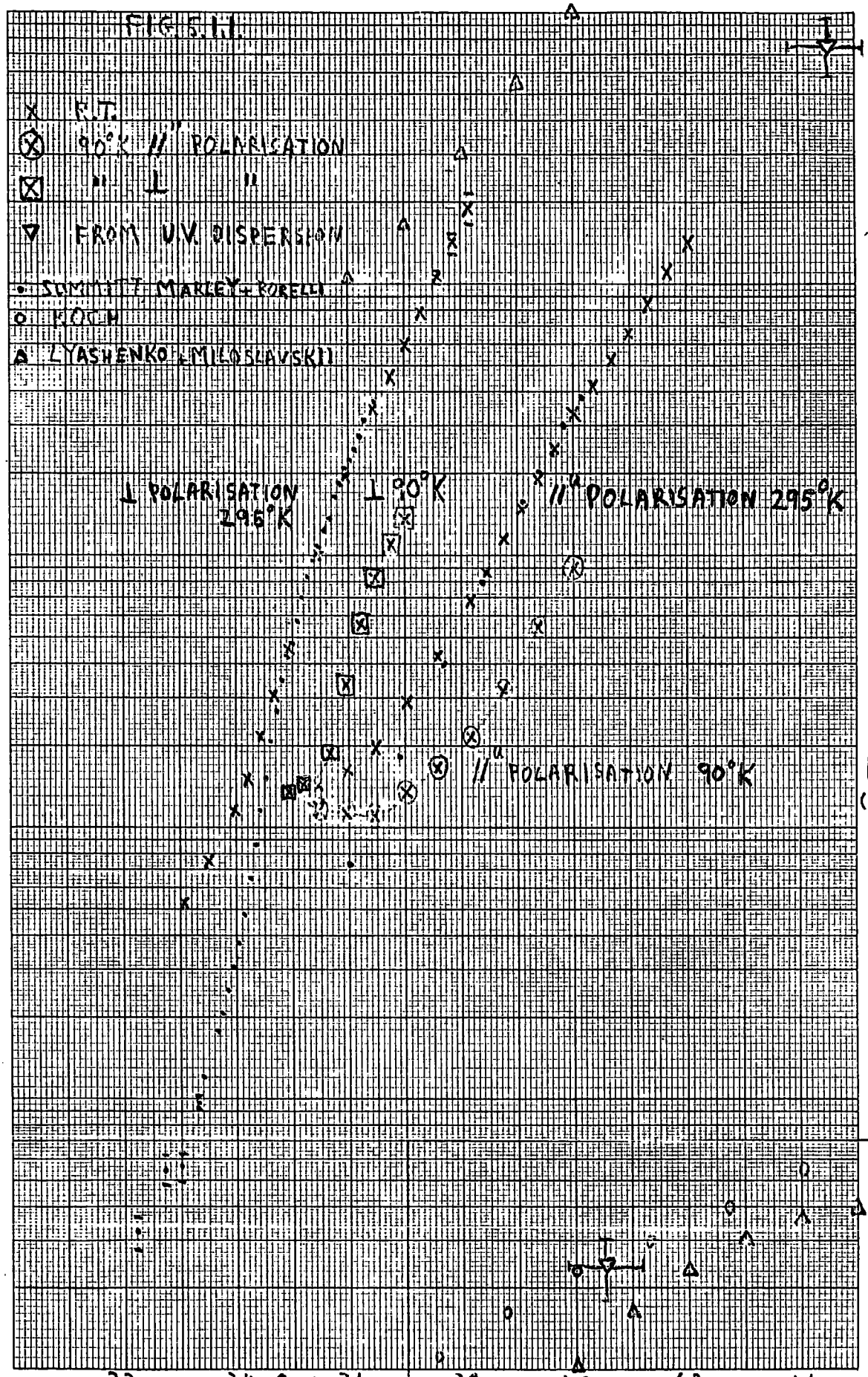
FIG. 5.11.
F.T.
90°K // POLARISATION
// ⊥ //
FROM U.V. DISPERSION
SOMMERFIELD, MARLEY + BORELLI
HOCH
LYASHENKO + MILOSLAVSKII
⊥ POLARISATION 296°K
⊥ 90°K
// POLARISATION 295°K
// POLARISATION 90°K
Kħω (e.v. cm⁻¹)
10⁵
10⁴
10³
10²
10
10⁵
3·2
3·4
e.V.
3·6
3·8
4·0
4·2
4·4

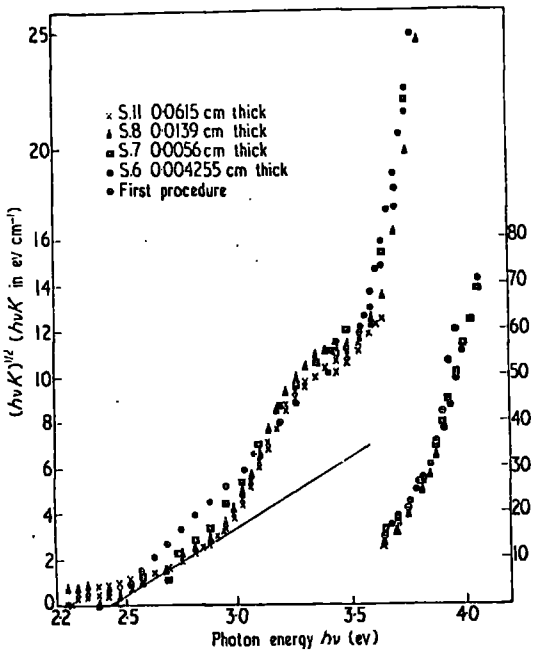

Figure 3. As figure 2; polarization parallel to c axis.

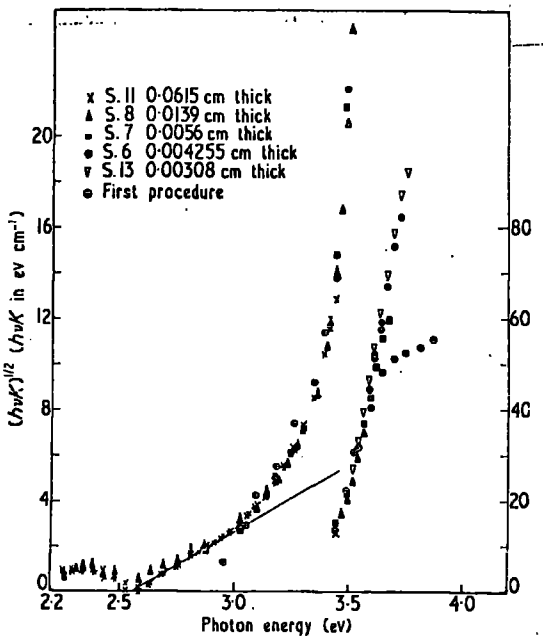

Figure 2. Variation of absorption $(K/h\nu)^{1/2}$ with energy near absorption edge. Polarization perpendicular to c axis.

Fig 5.1.2.

Also shown are the film results of Koch (1964) and of Lyashenko and Miloslavskii (1965). If these results are assumed to be randomly oriented, and if parallel absorption is neglected, it would seem that these should be multiplied by $^3/_2$ to give the perpendicular absorption. Also shown are the single very approximate points obtained from the U.V. dispersion analysis in 6.5.

Limited measurements of the absorption edge have also been made on Sb and Cr doped specimens, and these are given in 5.2 and 5.3.

5.2 Chromium Doped Crystals

Measurements were made on the Optica of Chromium doped specimens. The results are shown in fig. 5.2.1. Four graphs are plotted; $\perp$ and $//^u$ polarisation both as measured and with the absorption of S.8 subtracted (i.e. including the defect absorption, see figs. 6.2.1 and 2). That the defect absorption should be included is clear from the fact that the parallel absorption has a knee (beyond the range of fig. 5.2.1) around 3.4 e.v. similar to the defect absorption. This is indirectly clear from fig. 5.4.1 from the comparatively smooth curve after the subtraction including the defect absorption. However, the shorter wavelength subtracted points cannot be taken as reliable, both because they are the difference between two considerably larger numbers, and because the defect concentration may not be exactly the same as in S.8, (S.8 is rather on the high absorption side of the small spread between different crystals). The accuracy of the $\perp$ absorption gets steadily worse beyond, say, 3.25 e.v. and that of the $//^u$ absorption is uniformly rather poor between, say, 3.1 and 3.5e.v. and then gets worse.

FIG. 5.2.1.

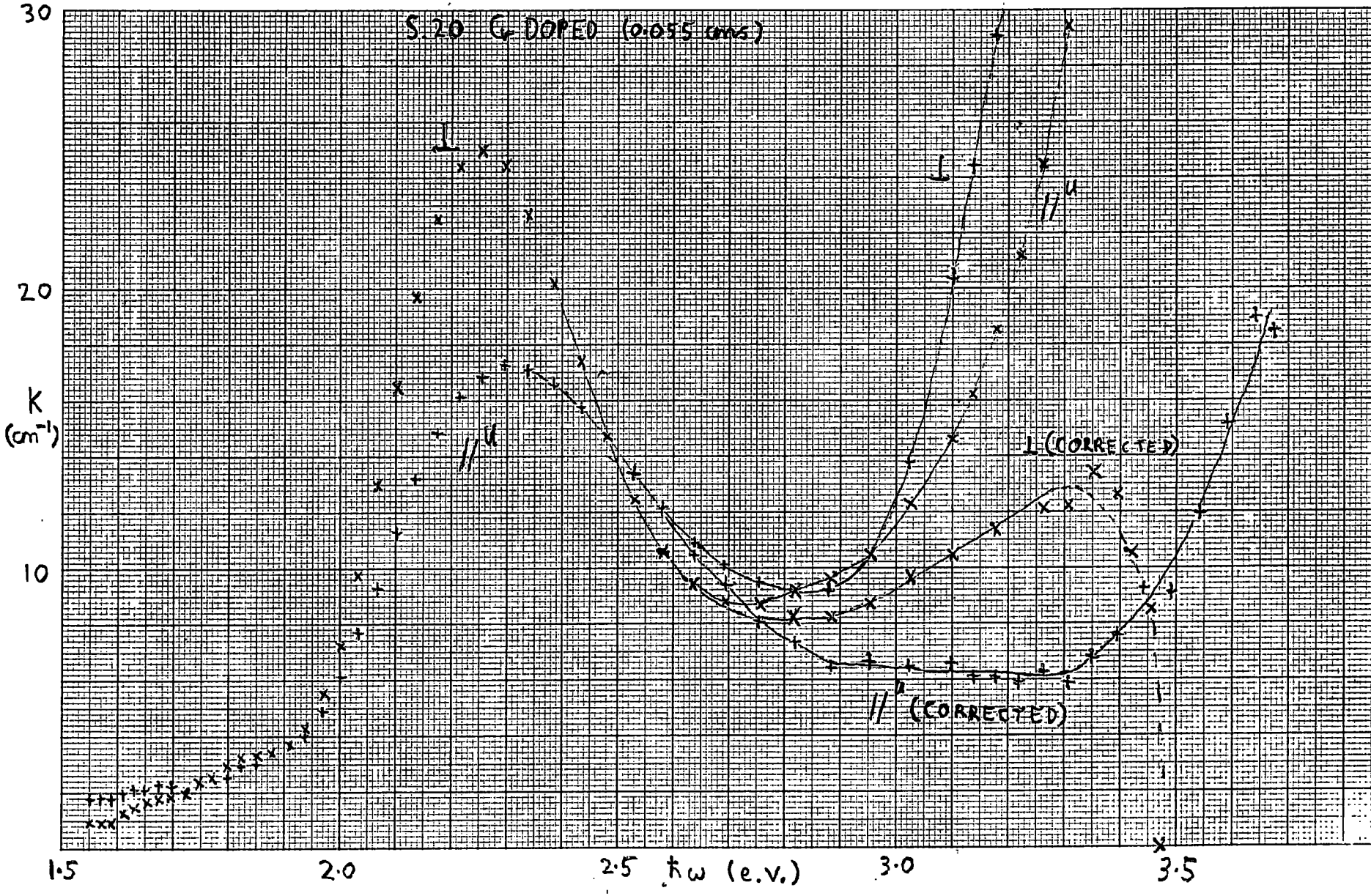
S 20 Cu DOPED (0.055 cms)
⊥
// u
⊥
// u
⊥ (CORRECTED)
// u (CORRECTED)
30
20
10
K (cm⁻¹)
1·5
2·0
2·5
ħω (e.v.)
3·0
3·5

5.3 Absorption in Antimony Doped Crystals

5.3.1 Measurement Errors

A number of measurements were made of free carrier absorption. The general quality of these measurements was not very high. The main reasons for this were specimen quality, specimen size and instrumentation.

Some of the ways in which poor specimen quality was a hindrance were microscopic voids or other defects that did not give a clear passage to the light inside the crystal. Together with surface irregularities and non-parallelism, these circumstances meant that a rather uncertain quantity of light was scattered or refracted out of the path of the light. How much of this light got collected and recorded depended on the details, such as how much (if any) focusing of the light there was. These factors led to two related types of error. The first was a systematic error in the zero for K and the second was the possibility of significant variations of the light lost at different wavelengths. The first made itself obvious by the fact that if the light transmitted through the crystal was compared with the light transmitted by a hole of the same area, then the light transmitted by the crystal was considerably less, even in wavelength regions where the absorption was thought to be small. The effect also often showed itself by the transmitted light sometimes being very sensitive to the exact angle at which the crystal was mounted. A third possible type of error from these imperfections is that some of the collected light may have been e.g., twice deflected from voids, and so have travelled through

a greater thickness of crystal.

Another type of specimen quality imperfection that would lead to errors is non-uniform doping. In regions of low absorption the value of K obtained will be representative of the average doping, but in regions of high absorption the average will be weighted towards the low doping regions. The specimens chosen mostly seemed uniform in colour, and this error is not thought to be very large.

No specimens were larger than about 3 mms across, and small size meant that high instrument gain had to be used and so high instrument noise resulted (in addition to any increased effects of stray light). The usual habit for plates was the twinned diamond shape, and so if measurements were required in polarised light, half the crystal could not be used. If, in addition, the twin plane was not perfect and part of one orientation extended across into the other "half" of the crystal, the area was reduced still further. The polariser itself transmitted only about 40% of the total light incident on it, and so the total reduction in available light for polarised light experiments was at least a factor of 5. For this reason, most of the experiments were done in unpolarised light. The smaller size was also a disadvantage because of the possible accuracy of positioning. Mostly single beam instruments were used, and in order to obtain transmission values, a reference measurement must be made without the crystal in addition to the measurement with the crystal. This can either be done by working right through a range of wavelengths with the crystal in and then right through again without the crystal, or the crystal can be inserted and removed at each wavelength. The former is subject to drift, and the latter is very sensitive to positioning the crystal in the same place each time.

There were certain instrument limitations. This was mainly because at times the only available instrument was the Barr and Stroud (see 4.5), and

with the accessaries used its sensitivily fell off rapidly around 3/u and in the (near I.R. and) visible. In addition to the reduced sensitivily, this meant that if the method was used of measuring over a range of wavelengths with the crystal in place, then in order to obtain reasonable accuracy very accurate wavelengths settings were required to make the reference measurement at exactly the same wavelength.

5.3.2. Results

Some of our results are shown in figs. 5.3.1. - 5.3.5. Fig. 5.3.1. shows samples 14, 18 and 19 plotted without the zero for K having been specially adjusted. The lower points on the graph could be made to fall more on the straight line by adjusting the zero for K, but their intrinsic percentage error is large. The fall away from the straight line at high K for S. 14 and 18 could be due to a number of errors such as non-uniform doping or thickness. The slope of the lines averages to a power law of about 3.3. Some polarised measurements on S.15, which comes from a much higher doping run, are also shown. The effect of changing the zero for K is shown to have a large effect on the slope. The plot with shallower slope can be seen to be curved, and hence possibly suspect, but the effect is not large. The steeper curve, which is perhaps the optimum for obtaining a straight line gives a power law of about 3.1, but this is very approximate. The measurements on S.15 were done on the Optica, and the longer wavelength limit was determined by a combination of high absorption and falling sensitivity. The lower wavelength limit was determined by uncertainty in allowing for absorption edge absorption.

Fig. 5.3.2. shows polarised measurements on S.18 in the I.R. There is less zero error for these measurements than for the polarised measurements on S.15, and so they are better for determining the ratio of the two

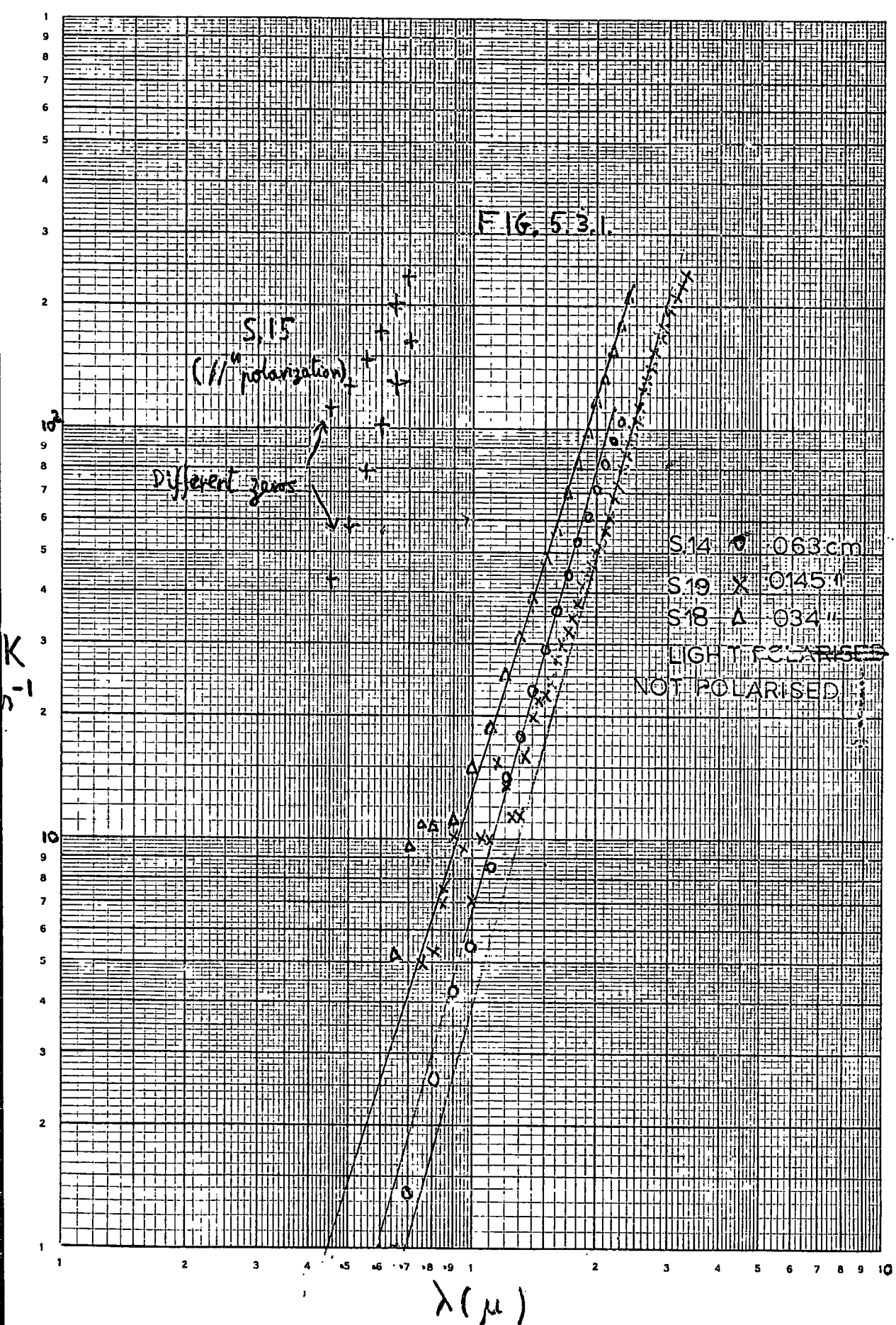
FIG. 5.3.1.
S.15
(// polarization)
different zeros
S.14 ○ .063 cm
S.19 X .0145 "
S.18 Δ .034 "
LIGHT POLARISED
NOT POLARISED
λ(μ)

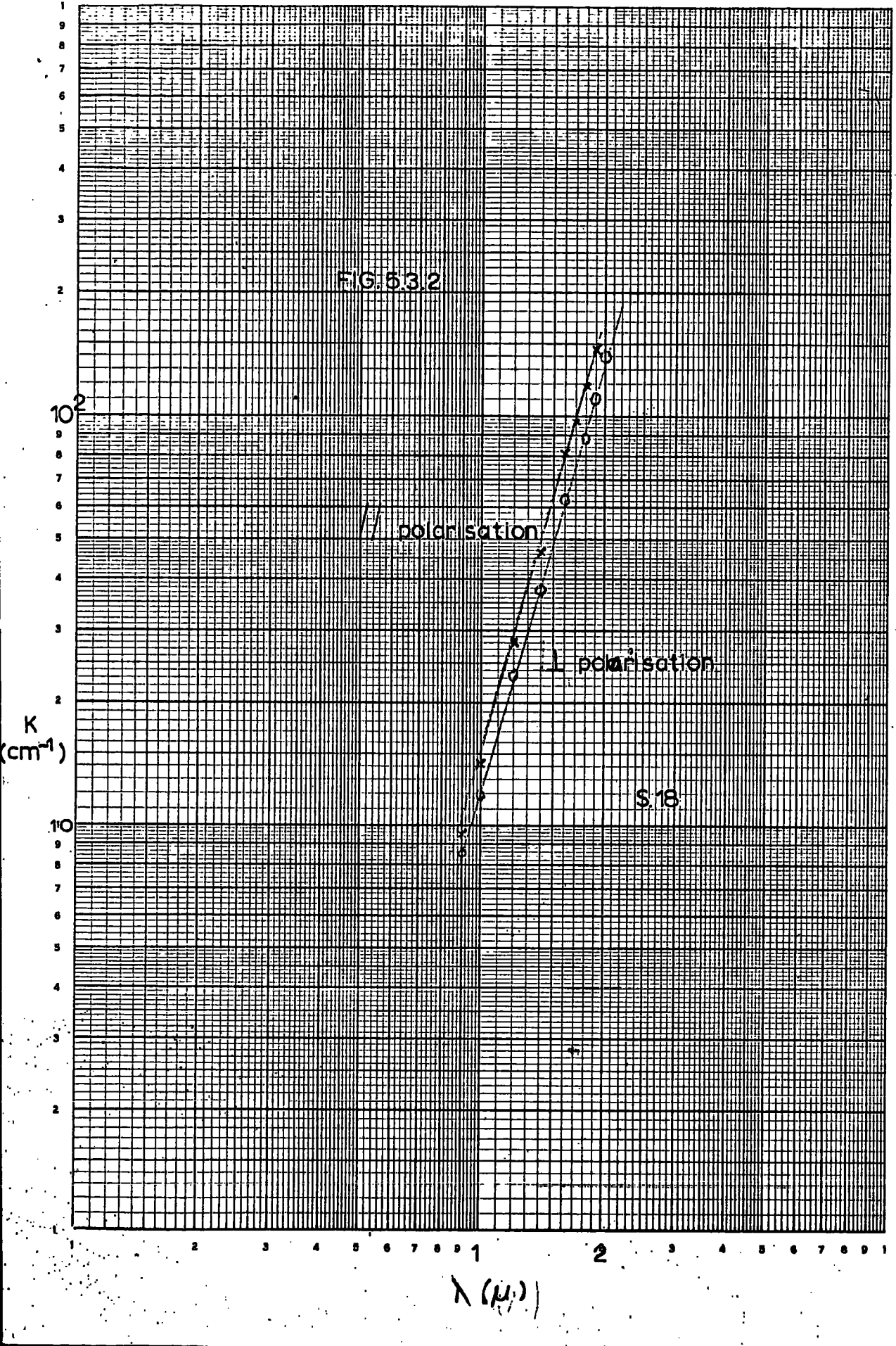
FIG. 6.3.2
// polarisation
⊥ polarisation
S.18
K (cm⁻¹)
λ (μ)
10²
10
1
2

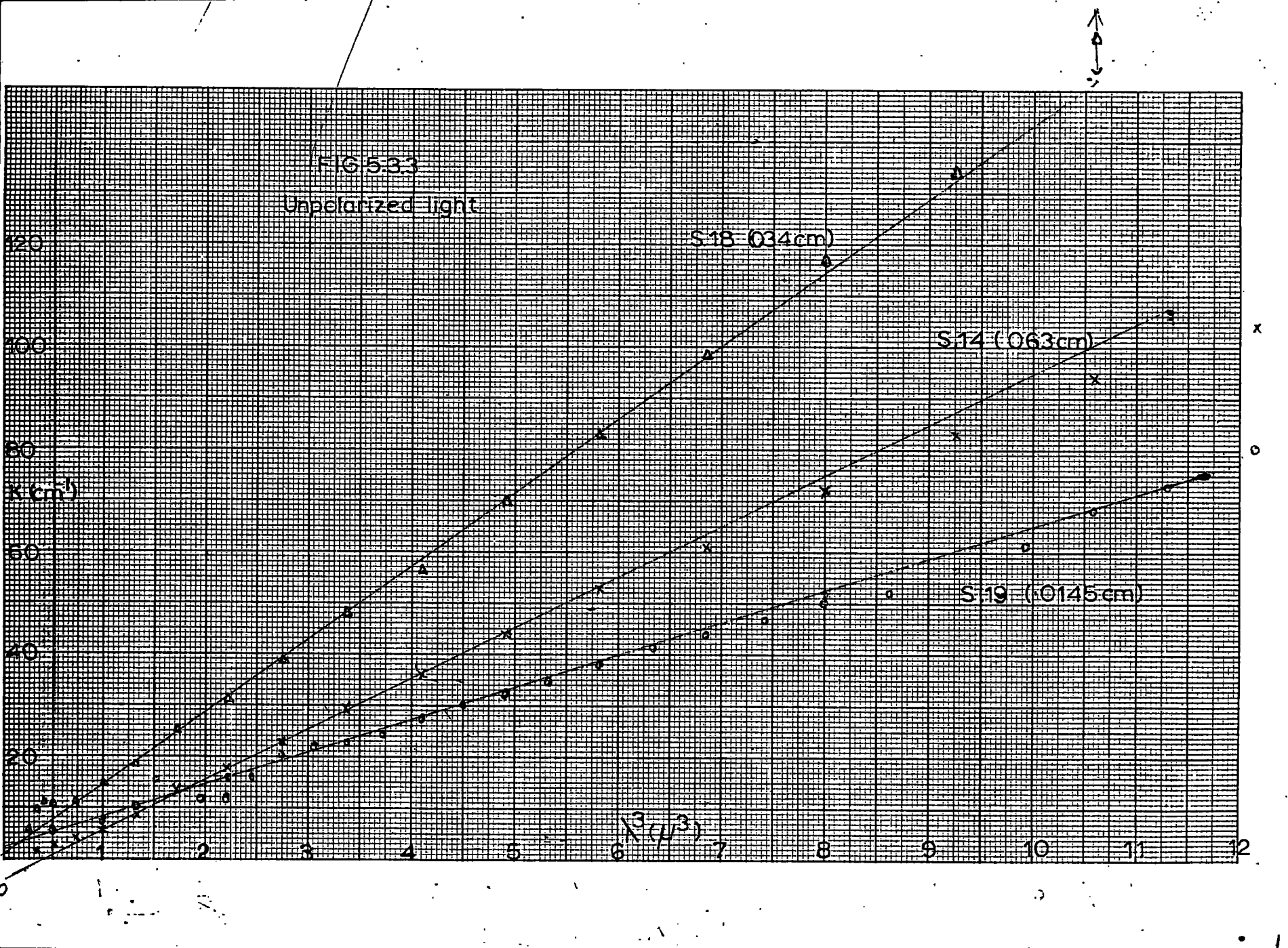
FIG 5.3.3
Unpolarized light
S.18 (.034cm)
S.14 (.063cm)
S.19 (.0145cm)
K (cm⁻¹)
λ³ (μ³)
120
100
80
60
40
20
0
1
2
3
4
5
6
7
8
9
10
11
12

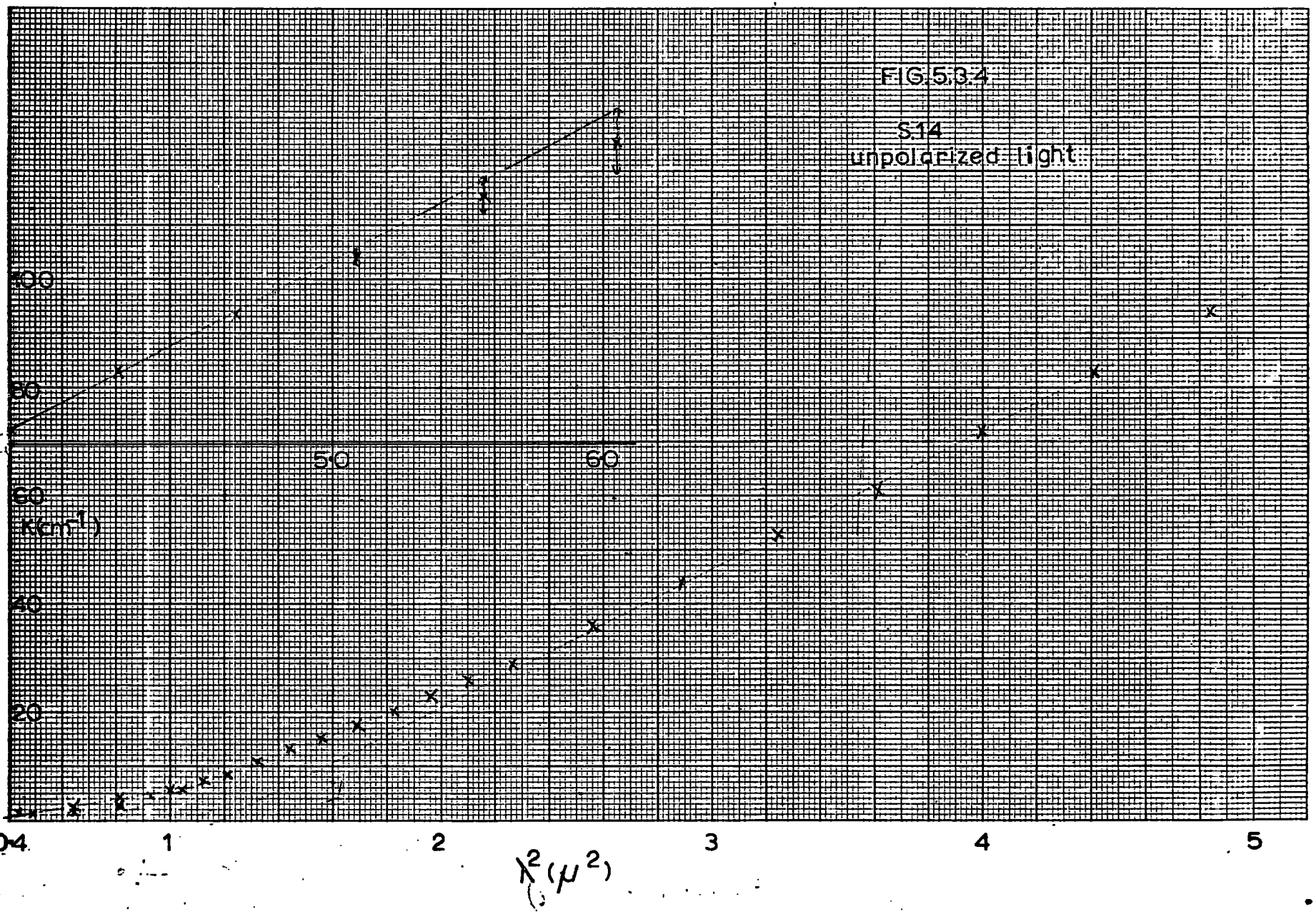
FIG.5.3.4
S.14
unpolarized light
100
80
60
K(cm⁻¹)
40
20
0
50
60
1
2
3
4
5
λ²(μ²)

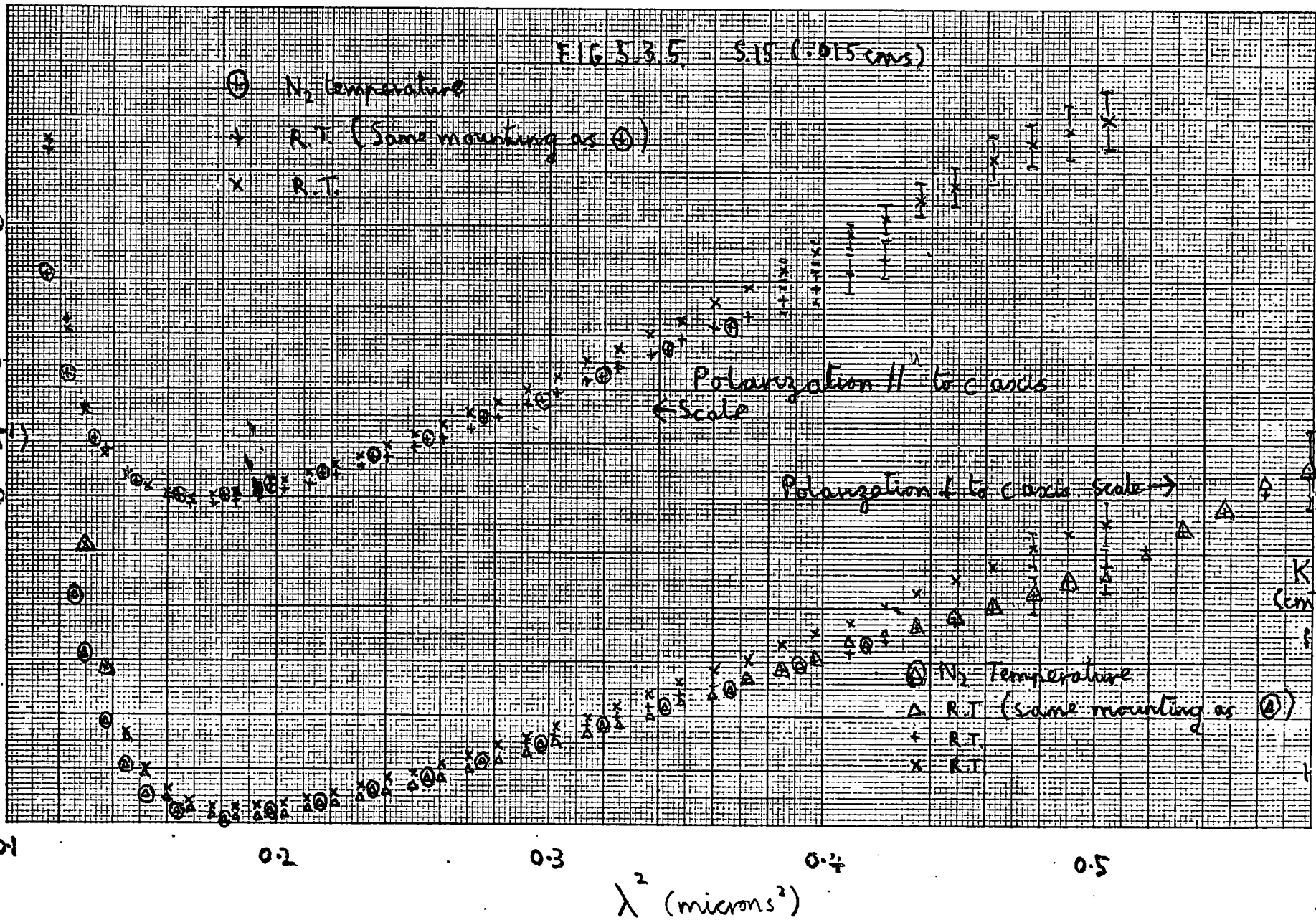
FIG 5.3.5 5.15 (·015 cms)
⊕ N2 temperature
+ R.T. (Same mounting as ⊕)
× R.T.
200
150
K (cm⁻¹)
100
Polarization // to c axis
← Scale
Polarization ⊥ to c axis scale →
K (cm⁻¹)
⊕ N2 Temperature
△ R.T (same mounting as ⊕)
+ R.T.
× R.T.
0·1
0·2
0·3
0·4
0·5
λ² (microns²)

polarisations. The ratio is

$$\frac{K_{//}}{K_{\perp}} = 1.25.$$

and the error is about 5%.

Fig. 5.3.3. using the same data as Fig. 1, shows K plotted against λ^3. How good a straight line is obtained does not depend on the zero of K. Reasonable straight lines are obtained in the range shown, except for S.14 at high absorption. The use of unpolarised light may account for this deviation because the light is being reduced by a factor of nearly 1000 at the highest point. At such reduction levels, much more $\perp$ polarised light is transmitted, and so that that absorption coefficient is effectively measured, rather than the average. This would change K by over 10% at the top, and a much better straight line is obtained. The reason for the same effect not being so apparent in S.18 may be that more of the light was polarised $\perp$ to the c axis because of polarisation occuring in the instrument. It can also be observed there is a fair degree of uncertainty in drawing the straight lines on Fig. 5.3.3.

As a check on a possible λ^2 law, fig 5.3.4 was drawn for S.14. It can be seen that large departures occur for $0.5 < \lambda^2 < 2.5$. If either S.18 or S.19 had been used, the graph would have curved up at longer wavelengths also. Fig. 5.3.5 shows measurements on S.15 taken on the Optica in polarised light at R.T., and at nitrogen temperatures. More than one set of R.T. measurements are shown, and their variation is an indication of error. A major source of error here, especially at longer wavelengths, arises from instrument noise. It can be seen that the nitrogen values equal the R.T. ones within experimental error. It might be mentioned that in one experiment the absorption was monitored (at fixed λ) as a crystal was cooled to nitrogen temperatures, and changes were noted but the net change was very small.

As can be seen from fig. 5.3.1 lowering all the K values by changing the zero looks more plausible, and no significance should be attached to the fact that fig. 5.3.5 is plotted against λ^2. λ^3 would give a better straight line. The slope of the // absorption is roughly 1.3 times the slope of the ⊥ absorption. This agrees with the ratio of 1.25 found above.

The absorption edge of some of the doped crystals was also measured. This is illustrated in Figs. 5.3.6 and 5.3.7. For the lightly doped S.14 no correction was made for free carrier absorption as this was almost negligible. For S.15, which is about 30 times more heavily doped, the free carrier absorption was extrapolated and subtracted. This was done by using the best possible λ^3 law fit to the data for K. This method is independent of the zero for K, and in fact a zero for K is found by the method. The assumption of a cube law for extrapolation may be a source of error, but any systematic experimental error that changes uniformly with wavelength will be largely corrected for. Two independent R.T. measurements of S.15 are shown, and also a measurement at nitrogen temperature. Also shown are (R.T.) measurements on our undoped S.8 and the results of Summitt, Marley and Borrelli on purer and better annealed crystals. The latter results for parallel polarisation at the lower absorption levels are obtained by dividing the perpendicular absorption by 30. When comparing figs. 5.36 and 5.37 it is essential to note the different energy scales. The figures cover the data range of S.14, but measurements on S.15, because it is thinner, are available to about 3 times the absorption shown. The R.T. highest point for perpendicular absorption, 760 e.v. cm^{-1} at 3.54 (2) e.v. is actually about 0.02 e.v. above the pure results, but

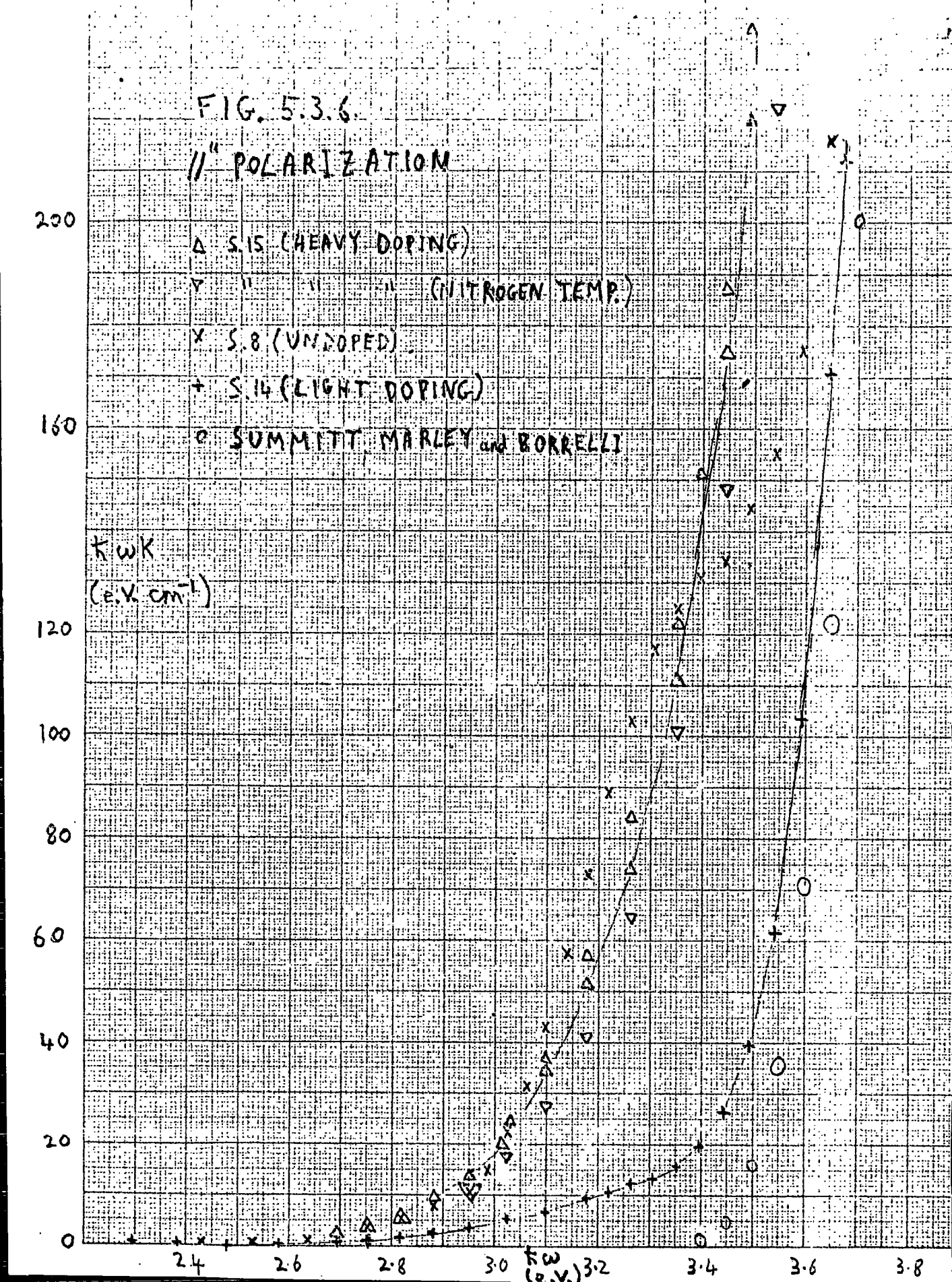
FIG. 5.3.6.
// POLARIZATION
△ S.15 (HEAVY DOPING)
▽ " " " (NITROGEN TEMP.)
× S.8 (UNDOPED)
+ S.14 (LIGHT DOPING)
○ SUMMITT, MARLEY and BORRELLI
ħωK (e.V. cm⁻¹)
200
160
120
100
80
60
40
20
0
2·4
2·6
2·8
3·0
ħω (e.V.)
3·2
3·4
3·6
3·8

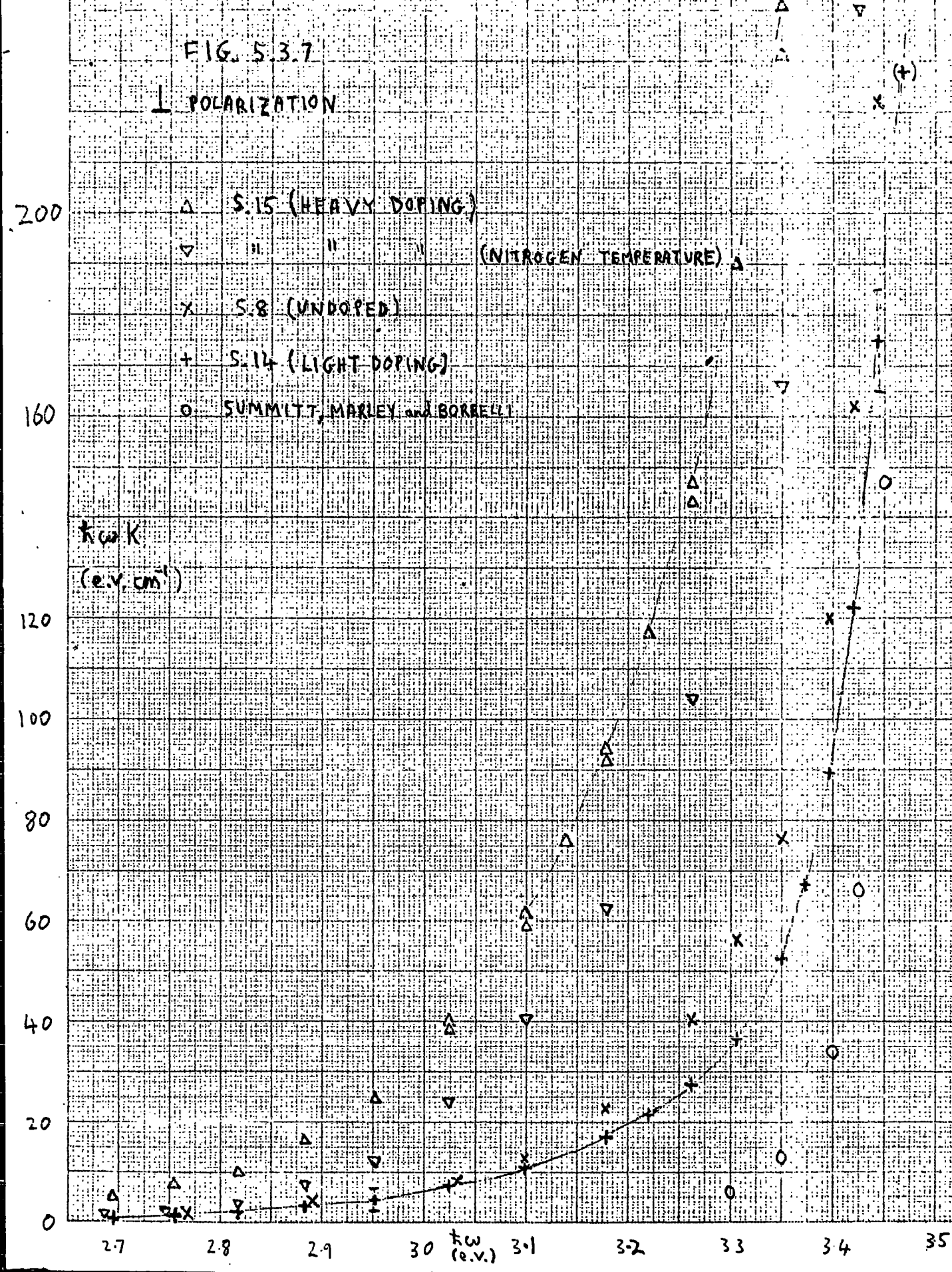
FIG. 5.3.7
⊥ POLARIZATION
△ S.15 (HEAVY DOPING)
▽ " " " (NITROGEN TEMPERATURE)
× S.8 (UNDOPED)
+ S.14 (LIGHT DOPING)
o SUMMITT, MARLEY and BORRELLI
(+) ∥
200
160
120
100
80
60
40
20
0
ħω K
(e.v. cm⁻¹)
2.7
2.8
2.9
3.0
ħω (e.v.)
3.1
3.2
3.3
3.4
3.5

this could be experimental error. The second highest point is about 0.01e.v. below the pure results. On the other hand the highest R.T. point for parallel absorption is still about .13e.v. below the pure results. At nitrogen temperature the highest perpendicular point almost coincides with the nitrogen results for S.8 while the second highest is about 0.025e.v. below. For nitrogen temperature parallel results the highest (S.15) point is still about 0.21e.v. below S.8.

new para. → In order to determine experimentally the zero of K for S.15 a program was started to grind it thinner. For S.15 this had the added advantage of the possibility of making it of more uniform thickness. The non-uniformity of the thickness of S.15 had either restricted the area available for use, or had introduced errors due to thickness non-uniformity. (The growth runs that produced the highly doped crystals produced nearly all needles, and very few plates. The plates were not of the usual twinned habit, and were not very uniform). Eventually the crystal broke up through grinding and polishing, but some measurements were taken before this happened. These have not been fully analysed, ~~and appear now to have been lost~~.

S.15 was also the only crystal on which a successful Hall measurement was made. The measurement was difficult due to instabilities in the contacts, and also the rather unsatisfactory shape of the crystal. The contacts were made with silver 'Dag' dispersion. The voltage on the Hall probes was unstable, and the difference in the voltage was recorded many times as the magnetic field was switched on and reversed. Because of the high doping the voltage was small, but a certain voltage difference occurred several times during switching, and this was taken

as the Hall voltage. Using the basic Hall equation of $R = \frac{1}{ne}$ a value of n of $1.5 \times 10^{20} cm^{-3}$ was obtained. No numerical constant was used in the Hall formula because the carriers were degenerate. The error on this figure is at least 20%.

The diamond shape, and the imperfections, of the other more lightly doped crystals made Hall effect measurements difficult, and these were not performed. One reason for this was that this doping range had been well covered by Summitt and Borrelli (1965).

5.4 Refractive Indices (and Multiphonon Lattice Absorption)

5.4.1 Infra Red Refractive Index.

Fairly early in the work good interference spectra in unpolarised light were obtained throughout the I.R. region with sample 6. This sample was known to have very parallel sides because it gave good fringes right into the U.V. where the fringe number was about 500, and also because of the uniformity revealed by the birefrigent interference in the polarising microscope. The interference peaks could therefore be relied upon to give an accurate measure of the relative refractive index (except for the birefrigence at long wavelengths) provided the correct fringe order could be determined. Considerable effort was put into doing this experimentally by the methods indicated in 4.7, but the results could not be made absolutely conclusive. This was mainly due to the not completely uniform thickness of other specimens. In particular for sample 8, the most promising thicker (139 μ) specimen, the following difficulties were encountered:-

(1) Specimen thickness varied by about 2 μ. To obtain fringes for $\lambda < \sim 4\,\mu$ required reducing the area of the crystal used, in order to reduce the thickness variation.

(2) For $\lambda > 7\,\mu$ multiphonon lattice absorption virtually destroyed the fringes because of the comparatively large crystal thickness.

(3) For $5\frac{1}{4}\,\mu < \lambda < 7\,\mu$ water vapour peaks showed up and confused the interpretation.

(4) For $\lambda < 5\,\mu$ the fringe order is > 100. This means that for fringe identification high wavelength accuracy is required. Possible change with wavelength in the effective thickness of the crystal also has to be considered. As well as being due to the variation

in crystal thickness this could be caused by the focusing of the light in the Spectromaster ~~(see 4.5)~~, combined with slight misalignment.

More work with this crystal might be successful, but after a considerable amount of time and effort complete confidence in fringe indentification was not achieved. Another attempt was made with S.16, whose thickness is only 7.35 /u. This speciment had a high thickness uniformity, but the problems encountered here were:

(1) Very small crystal area resulted in very small amounts of energy being available, and so very slow response of the instrument.

(2) Because of the small crystal size, the most convenient method of attaching the crystal to the specimen holder was a weak solution of nitrocellulose. Interpretation of the spectra led to the conclusion that a thin film of nitrocellulose was on the surface and was complicating the fringe pattern.

(3) The very low fringe orders meant that in order to identify the fringes of S.6, the fringe positions of S.16 had to be measured to a very small fraction of a fringe.

Another factor that might possibly spoil fringe identification is the possibility of two specimens not having identical refractive indices. The most obvious possible cause is free carrier absorption, and by using the fact that free carrier absorption is not detected calculation shows that this should have a negligible effect on the refractive index of the specimens used. However, other possible causes of refractive index variation cannot be ruled out for certain.

Because of the lack of absolutely conclusive fringe indentification, work on the I.R. refractive index was shelved for a time. However, after greater confidence had been gained by learning more about the phonon spectrum from other sources, the data derived from S.6 was re-examined. It was found that there was only one fringe identification that gave results that could be believed. If the fringes were assigned a fringe order one higher than the sensible identification the refractive index was virtually constant between 2 and 3 μ and at longer wavelengths its curvature downwards was comparatively large. The nearest approach to a reasonable interpretation with this fringe identification would be a comparatively weak lattice absorption at a small wavelength, say 12 μ and no powerful absorption at longer wavelengths. Even then the flat region between 2 and 3 μ would not be adequately explained and the postulated lattice absorption does not agree with observation. If the fringes are assigned a fringe order one lower that the sensible identification, the gradient of dielectric constant against wavelength squared is steeper, and the curvature considerably less. The only explanation of such a curve is powerful lattice absorption at long wavelengths only, again in disagreement with observation (expecially the substantial lattice absorption at $\sim$16 μ). An alternative way of illustrating the difficulty of either alternative identification is to attempt to obtain a good fit between the predicated refractive indices and values obtained from a lattice model based on the lattice spectra available, with only minor tinkering. Even when the models are forced to give approximate agreement, the shapes are wrong. // The results are shown in Table 5.4.1, and plotted in figs. 5.4.1 and 5.4.2. The data plotted have had the electronic (U.V.) dispersion subtracted, for $\lambda < 5\mu$.

Table 5.4.1.

Observed Peak λ (μ)	Corrected Peak λ (μ)	Fringe Order $\perp$ polarisation	$\perp$ Refractive Index squared $n_\perp^2$	Fringe Order $\parallel$ polarisation	$\parallel$ refractive index squared $n_\parallel^2$	U.V. Correction	λ^2 (μ^2)
11.25	11.23			11.44	2.228		126.1
11.025	11.00_5			11.93	2.327		121.1
10.56_5	10.54_5			12.92	2.506	.001	111.2
10.14	10.12			13.90	2.671	.001	102.4
9.68_5	9.66_5			14.90	2.800	.001	93.4
9.31	9.29	15.11	2.660	15.89	2.942	.001	86.3
8.92	8.90	16.08	2.765	16.92	3.061	.001	79.2
8.55_5	8.53	17.05	2.855	17.94_5	3.163	.001	72.8
8.21	8.19_5	18.03	2.947	18.97	3.263	.001	67.16
7.88_5	7.86	19.00	3.011	20.00	3.336	.001	61.8
7.58	7.56_5	19.98	3.084	21.02	3.414	.001	57.2
7.03_5	7.01_5	21.93	3.195	23.07	3.536	.001	49.2
6.55	6.53	23.88	3.282	25.12	3.632	.002	42.64
6.12	6.10	25.83	3.353	27.17	3.708	.002	37.2
4.628	4.626	35.11	3.561	36.89	3.932	.003	21.4
3.999	3.997	40.96	3.618	43.04	3.995	.004	15.98
2.814_3	2.811_9	59.01	3.717	61.99	4.102	.008	7.91
2.112_1	2.109_7	79.01	3.751	82.99	4.138	.015	4.45
1.675_0	1.673_5	99.98	3.780	105.02	4.170	.024	2.80
1.201_5	1.200	139.99	3.809	147.01	4.201	.046	1.44

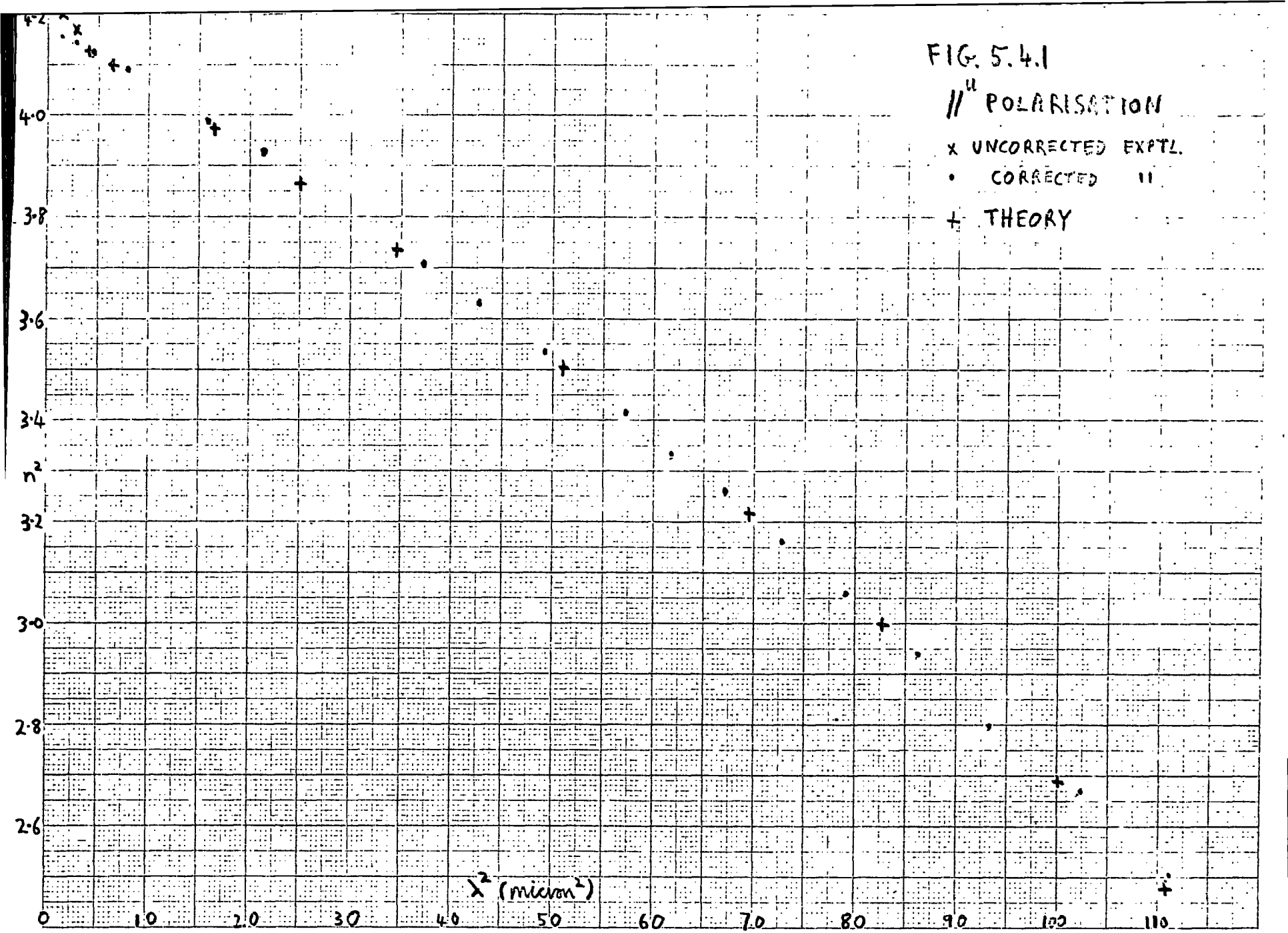
FIG. 5.4.1
// POLARISATION
x UNCORRECTED EXPTL.
• CORRECTED //
+ THEORY
4·2
4·0
3·8
3·6
3·4
n²
3·2
3·0
2·8
2·6
λ² (micron²)
0
10
20
30
40
50
60
70
80
90
100
110

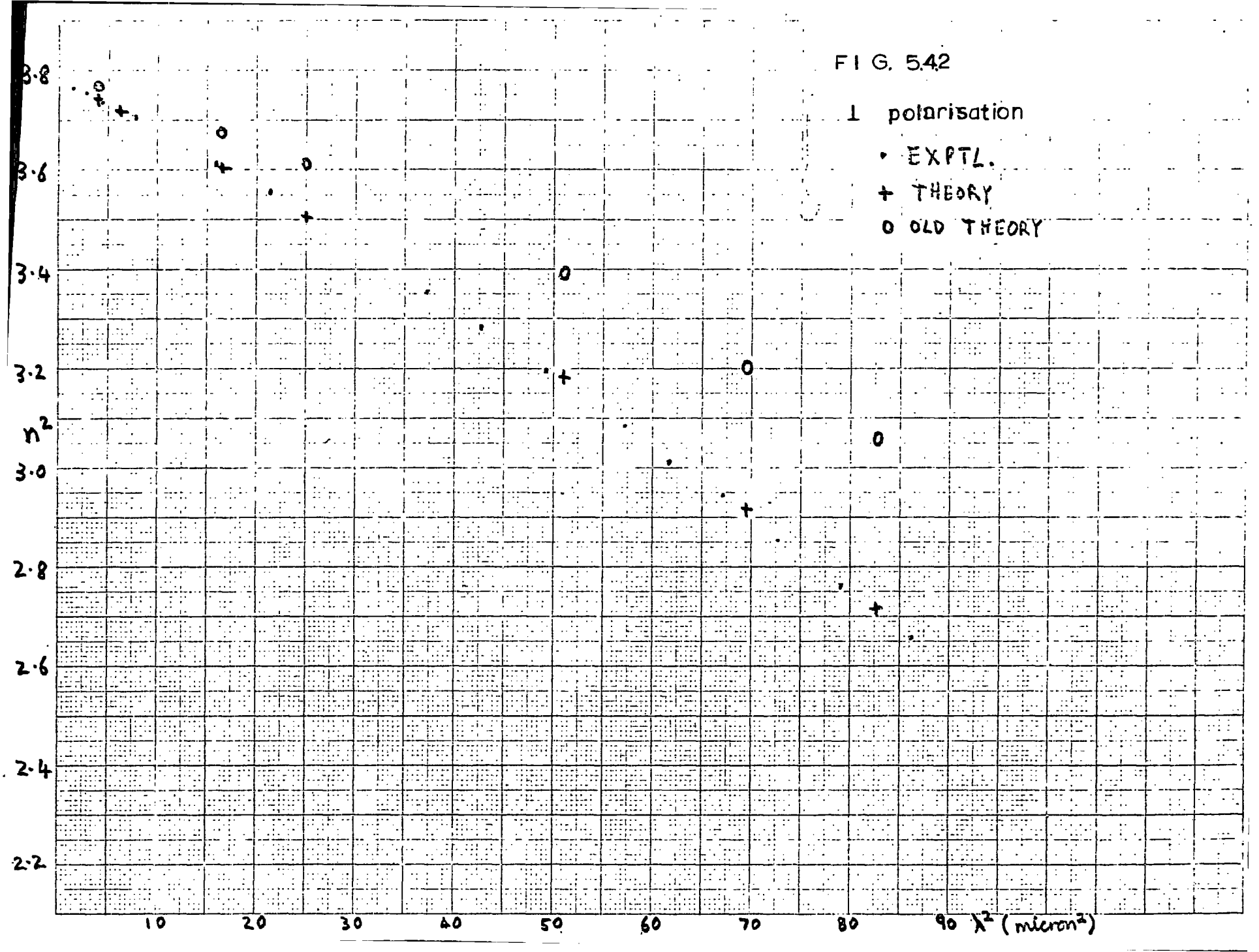
FIG. 5.42
⊥ polarisation
• EXPTL.
+ THEORY
o OLD THEORY
3·8
3·6
3·4
3·2
n²
3·0
2·8
2·6
2·4
2·2
10
20
30
40
50
60
70
80
90
λ² (micron²)

For $\lambda > 5\mu$ the birefrigence is largely obtained by extrapolation, because there are no usable 'beat' minima. For $\lambda > 9.3\mu$ the polarised absorption spectra of Summitt and Borrelli (1965) can be used to show that the dominant contribution to the interference pattern is due to the $//^{u}$ polarisation because of the higher absorption in the $\perp$ polarisation. The $\perp$ contribution cannot be completely ignored in estimating the effective fringe order, and the fringe orders shown in the table seem to be the most reasonable estimates.

The correction of the peak positions due to the lag of the spectrophotometer response is appreciable. The manufacturers have stated that this correction is approximately constant (in terms of λ) over each scanning range. The corrections used (see table 5.4.1) are considered to be the best estimates after studying data that include the reduction in amplitude of the interference fringes due to the lag and the differences in peak positions between the spectrum used and a spectrum taken at a faster scanning speed.

The accuracy of the results depends to a large degree on the wavelength accuracy of the "spectromaster". This is stated in the instrument manual as follows:

	Accuracy	Repeatability
0.6 - 5 μ	0.002 μ	0.001 μ
5 -15 μ	0.006 μ	0.002 μ

The makers have stated (private communication) that the quoted accuracy is conservative, and it would seem that for a well maintained machine like the Durham one, the accuracy is likely to be close to the limits quoted for repeatability. Even so, an error of .001μ at 1.2μ would give an error of .08% in refractive index and

.16% (or ~.007) in refractive index squared. This error could account for nearly half the discrepancy between ϵ_∞ found (for both polarisations) from U.V. and I.R. dispersion respectively (see 6.5) and an error of .002/u could account for most of it. Any error in the corrections (mentioned above) due to the lag of the instrument will be in addition to the basic wavelength error. A reasonable estimate for this error would be 1 in 2000 in the refractive indices and 1 in 1000 in their square.

An additional partial explanation of the discrepancies in ϵ_∞ can be found in the fact that the spectromaster passes the whole spectrum through the crystal before passing it through the monochromaster. This allows significant specimen heating, and the metal mask became very warm to touch, perhaps 40-50°C. The measurements for $\lambda > 1/u$ were made on the Optica machine in which the specimen temperature is very close to R.T., because very little energy is put into the spectrum. Ecklebe (1932) measured the refractive indices of cassiterite (at $\lambda = 5780$ Å) at several temperatures, and he found a temperature coefficient of $\frac{dn}{dt} \sim 5.5 \times 10^{-5} (°C)^{-1}$. A temperature rise of 25°C therefore raises n by $\sim 1.4 \times 10^{-3}$ or increases the refractive index squared by ~1 part in 700. Any thermal expansion would also cause an apparent increase in n.

The above four errors or effects could comfortably account for the discrepancies in ϵ_∞, but a further effect should be mentioned that works in the opposite direction. This effect is the reduction in the Spectromaster of the effective thickness of the crystal due to the focussing of the light. The angular size of the cone of light that is effectively used is not accurately known, but a reasonable figure might be 4° from the centre. The light on the edge of the cone would then

see a thickness reduced by cos4°, or .24%. Inspection shows that for a correctly aligned specimen the distribution of light energy is constant over the range of effective thicknesses, and so the average effective thickness would be .12% less than the actual thickness. This factor would increase the discrepancies about 50% and make their interpretation more difficult.

5.4.2 Multiphonon Lattice Absorption

Although not the logical place to mention multiphonon lattice absorption, it was studied for experimental reasons alongside the I.R. refractive indices. It was observed in all crystals measured, and S.8 is the best crystal (because of its appropriate thickness) for showing the absorption between 7 and 13 μ. The spectrum is shown in fig. 5.4.3. Unpolarised light only was used, and although with good spectra from crystals of differing thickness it is theoretically possible to separate the two polarisations, this was not done. This was partly because assumptions about the polarisation of the "unpolarised" light are necessary, and partly because the polarised spectra had already been measured by Summitt and Borrelli (1965). They also measured the unpolarised spectrum, and there were no obvious differences between this and fig. 5.4.3.

5.4.3 Visible and U.V. Refractive Index.

The sample S.6 was used to give useful interference peaks down to a wavelength of around 3600 Å where the absorption edge rapidly reduced the fringe contrast. The very thin S.16 (7.3 μ thick) was used to give results down to 3500 Å for perpendicular polarisation and to 3150 Å for parallel polarisation. ~~Some of the experimental difficulties~~

FIG. 5.4.3.

S.8

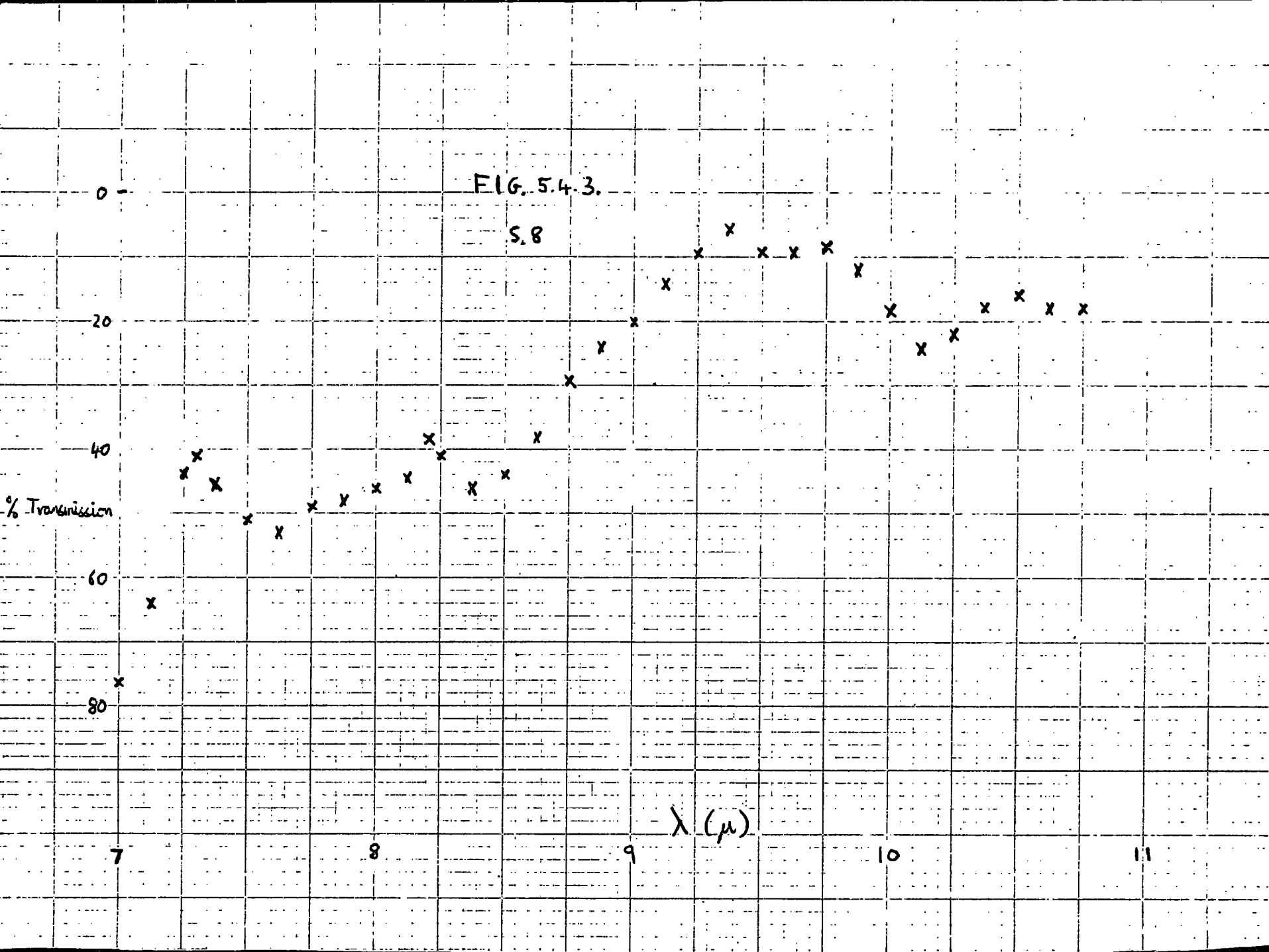

~~were mentioned in 4.5.~~ The results are shown in fig. 5.4.4 with n^2 plotted against $1/\lambda^2$. The small contribution of I.R. dispersion has been allowed for by substracting $0.01\,\lambda^2$ (with λ in μ) from n^2. The refractive indices have been normalized to the values given by Kerr (1959) for the middle of the visible.

Allowing for a wavelength error in using the Optica spectrophotometer of 3Å, the accuracy in n^2 varies from 1 in 1000 around 1 μ to 1 in 400 at 3200 Å.

Some interference spectra were obtained at nitrogen temperatures. This data was not analysed and might present difficulties without also having I.R. data to confirm fringe identification. The birefrigence, however, was unambiguous.

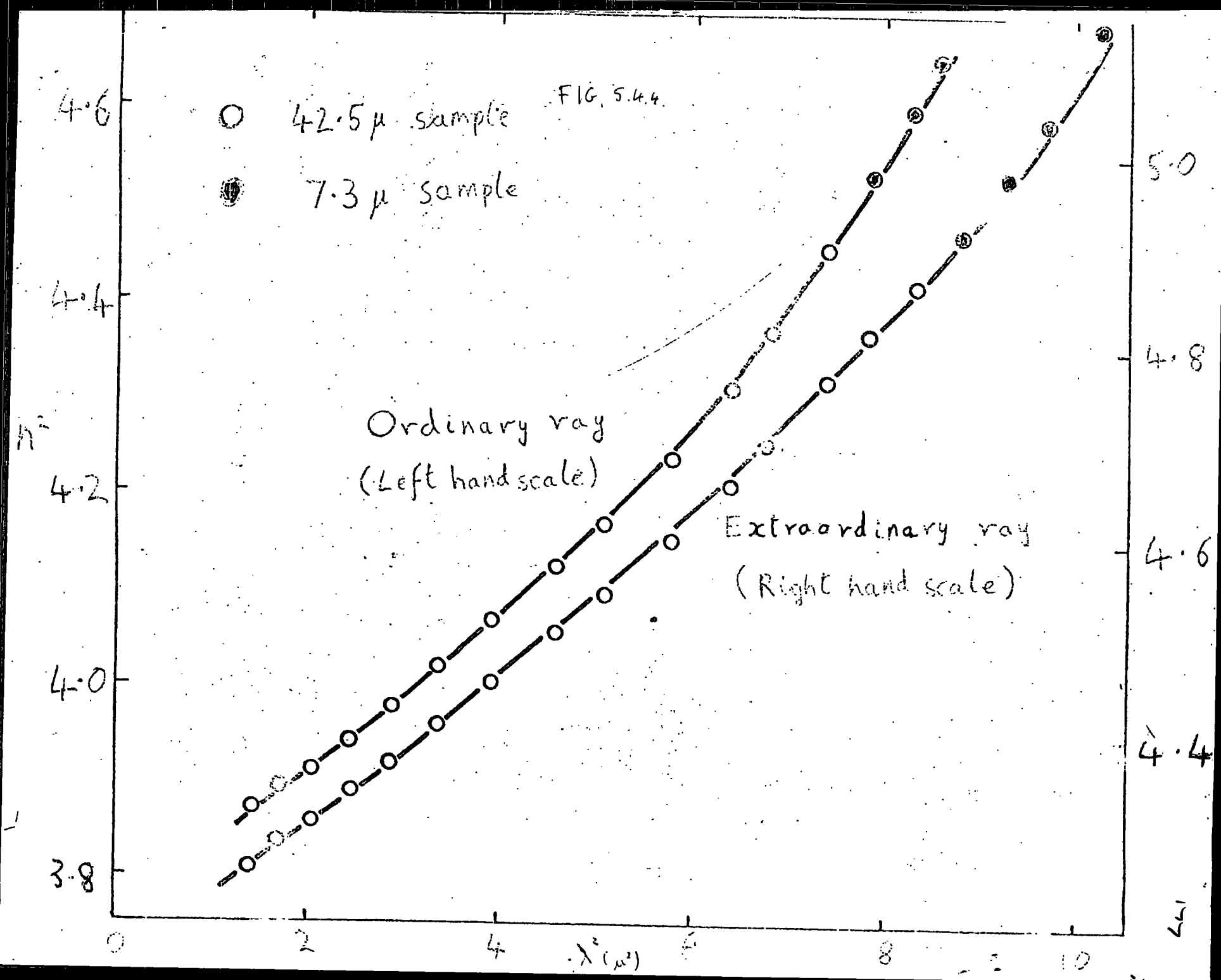
FIG. 5.4.4.
○ 42·5 μ sample
● 7·3 μ sample
Ordinary ray
(Left hand scale)
Extraordinary ray
(Right hand scale)
n
4·6
4·4
4·2
4·0
3·8
5·0
4·8
4·6
4·4
0
2
4
6
8
10
λ² (μ²)

5.5 Luminescence

For convenience in preserving a numbering system we shall briefly consider the interpretation of luminescence results here. Luminescence is generally carrier recombination via a defect level. This recombination in an ionic material will be accompanied by phonon emission in the same way as defect absorption. The phonons thus lower in energy the observed luminescence peak below the basic electronic transition energy. Thus the defect considered in 6.3 with a basic energy of 2.9e.v. might produce a luminescence peak of about 2.4e.v. Unfortunately similar crystals observed to luminesce in the visible by Morgan (1966B) were too faint to measure, and the only luminescence measured was in crystals grown by flame fusion. These contained most of their luminescence at the red end of the spectrum, but they did show a small peak around 2.8e.v. It would be interesting to observe defect absorption in these crystals or to measure luminescence in normally grown crystals so that absorption and luminescence could be correlated. One would not expect a luminescent peak at higher energies than about 2.4e.v. in crystals similar to ours. (Indeed the colour of the luminescence is described as yellow, as opposed to the "greenish white" of the flame fusion crystals).

5.6 Phonon Parameters

Before giving the results of our classical dispersion analysis, a few points will be mentioned.

(1) As was found by Spitzer et. al. (1962) for TiO_2, $BaTiO_3$ and $SrTiO_3$, so we also found that assuming a constant value of g for each oscillator did not perfectly fit the results. To prevent the reflection rising too high round ω_T required a g that was too large to give a good fit to the sharp reflection rise around ω_L.

(2) The Japanese results (see 3.2) showed considerable absorption at all wavelengths, that beyond 39 μ (including a shoulder at around 100 μ) having the most significance.

(3) Points (1) and (2) imply that we may be justified in not taking the exact wavelengths indicated by the absorption peaks as the values of ω_T.

(4) The results of Spitzer et. al. show excess absorption at long wavelengths in TiO_2.

(5) Liebisch and Rubens found increased reflection beyond 90 μ.

(6) With only 3 classical oscillators it is impossible to get a reasonable fit and also an ϵ_s as large as 13.6.

(7) The above points make it reasonable to assume a fourth "phonon" at about 100 μ for the purposes of the dispersion analysis.

(8) To have a significant effect on ϵ_s the absorption coefficients associated with this "phonon" need not be high, because the contribution to ϵ_s varies as $\int n K \lambda \frac{d\lambda}{\lambda}$, and both n and λ are large.

(9) The "explanation" of the extra absorption may be anharmonicity (see 2.2).

(10) The "phonon" near 100 μ is most likely to be a proper phonon rather than one of the others being the excess one. For brevity the arguments are omitted.

The classical dispersion formulaefound to give the best fit to the various data mentioned in 3.2 are:-

$\perp$ polarisation

$$n^2 - k^2 = 3.785 - \sum_{\mu=1}^{4} \frac{4\pi p_\mu (\omega^2 - \omega_{t\mu}^2)\omega_{t\mu}^2}{(\omega^2 - \omega_{t\mu}^2)^2 + \omega^2 g_\mu^2} \qquad 2nk = \sum_{1}^{4} \frac{4\pi p_\mu \omega g_\mu \omega_{t\mu}^2}{(\omega^2 - \omega_{t\mu}^2)^2 + \omega^2 g_\mu^2}$$

μ	$4\pi p_\mu$	$\frac{\omega_{t\mu}}{2\pi}$ (cms^{-1})	$\frac{g_\mu}{\omega_{t\mu}}$	and	$\frac{\omega_{l\mu}}{2\pi}$ (cms^{-1})
1	1.76	577	$1/32$		736
2	1	300	$1/25$		371
3	5.6	252	$1/20$		288
4	2.2	105	0.4		113

$\parallel$ polarisation

Similar equations but with $\epsilon_\infty = 4.175$ and

μ	$4\pi p_\mu$	$\frac{\omega_{t\mu}}{2\pi}$ (cm^{-1})	$\frac{g_\mu}{\omega_{t\mu}}$	and	$\frac{\omega_{l\mu}}{2\pi}$ (cm^{-1})
1	5.6	455	$1/30$		695
2	2.4	105	0.4		117

These parameters give the following values of ϵ_s

	with lowest "phonon"	without lowest "phonon"
$\perp$ polarisation	14.34	12.14
$\parallel$ polarisation	12.18	9.78

The lowest "phonon" is very dubious, and might be expected to be much reduced in effect at low temperatures.

The reflection calculated from n and k found from the above formula is plotted in figs. 5.6.1. and 2 together with the various reflection results. The most important deviation between theory and experiment is for the $\mu = 1$ phonon for $\perp$ polarisation (560 - 730 cm^{-1}). This deviation was necessary in order to fit the I.R. dispersion (see 6.4). A previous fitting ignoring the I.R. dispersion gave a better fit in that region. Further experimental work in that region is called for. Turner's results are too small compared with Summitt's for the $\mu = 1$ phonon, and so are likely to be too small in the longer wavelength region also. The effect of the probable small admixture of $//^{4}$ polarisation to Turner's results would be to shift the sharp rise around ω_{t2} to longer wavelengths, improving the agreement in that region.

Fig. 5.6.1. shows the I.R. spectrum of a powdered specimen in Nujol.

FIG. 5.6.1

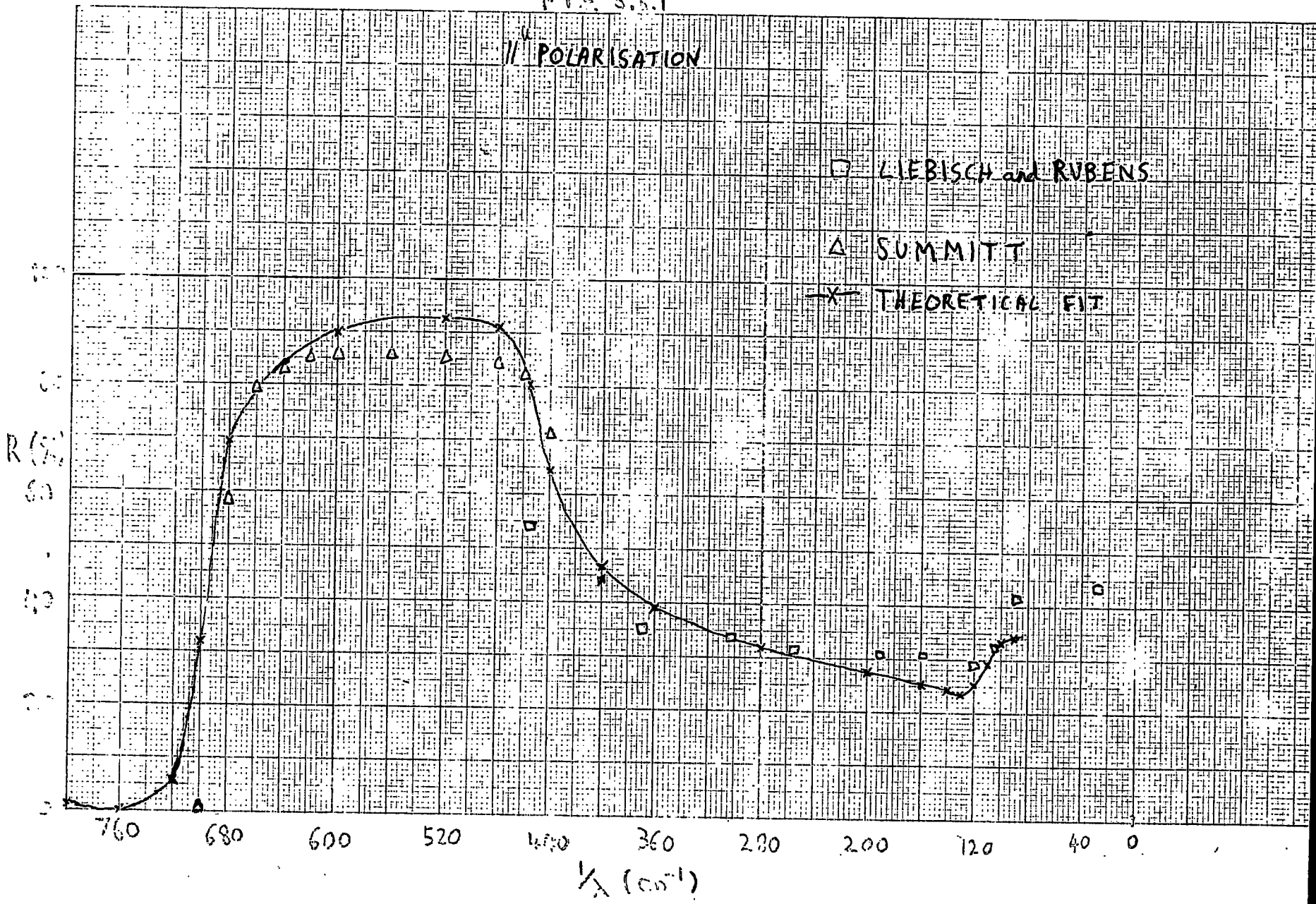
E ∥ POLARISATION
□ LIEBISCH and RUBENS
△ SUMMITT
—X— THEORETICAL FIT
R (%)
760
680
600
520
360
200
120
40
0
1/λ (cm⁻¹)

FIG. 5.6.2.

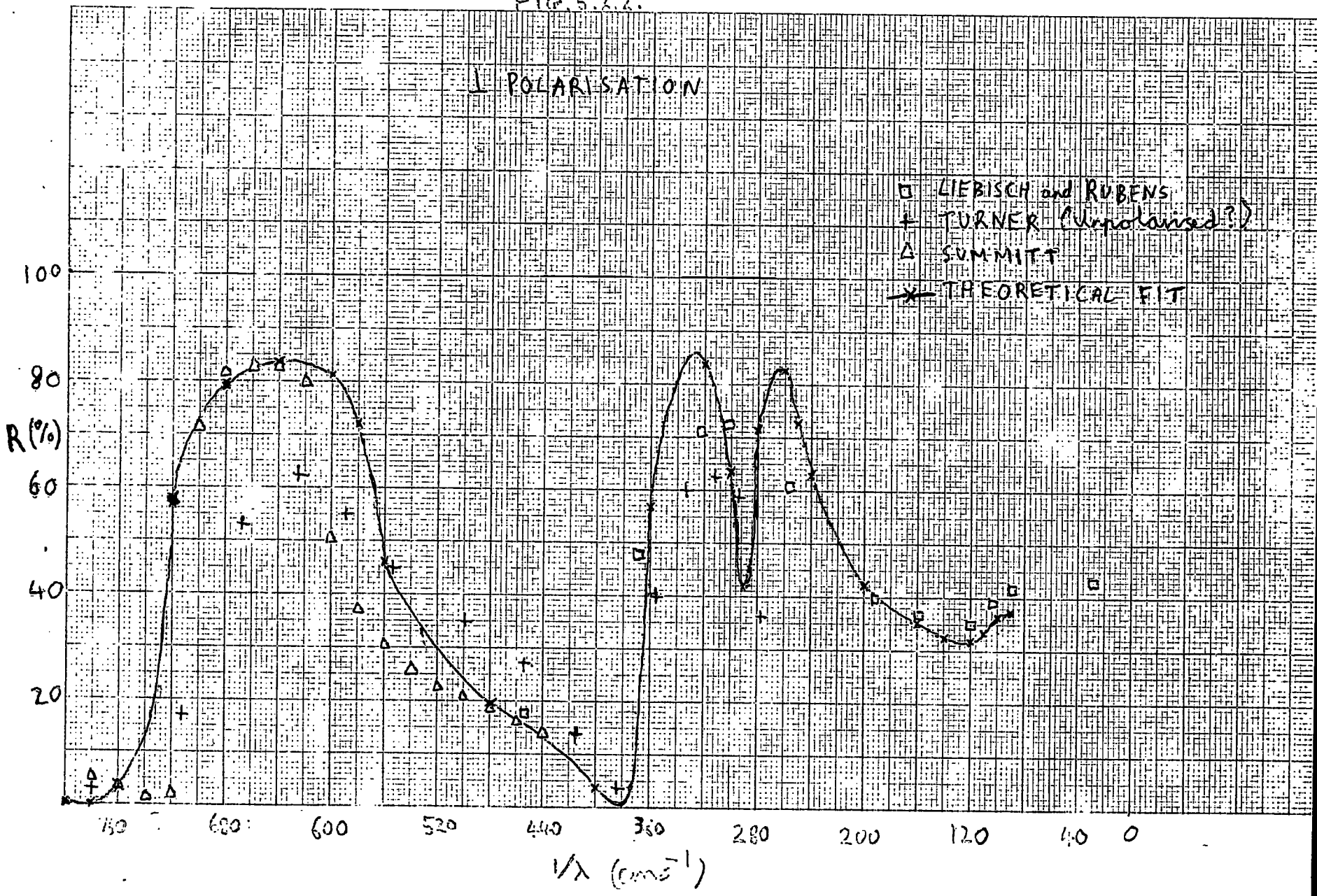
⊥ POLARISATION
□ LIEBISCH and RUBENS
+ TURNER (Unpolarised?)
△ SUMMITT
—×— THEORETICAL FIT
100
80
60
40
20
R(%)
680
600
520
440
360
280
200
120
40
0
1/λ (cm⁻¹)

FIG 5.6.3.

6.1 Absorption Edge

6.1.1. Introduction

The experimental measurements of the absorption edge cannot be plotted in any simple way to yield directly any information such as the exciton binding energy. The main reason for this is the phonon coupling, and a secondary reason is that the absorption to the n = 1 exciton involves a different mechanism from absorption to other states. Because of these complexities it is necessary to gather the maximum amount of information from other sources and adjust some of the other parameters until a good agreement between theory and experiment is achieved. Each evaluation of the theory with a given set of parameters is a tedious job, and the only practicable method of presenting the results is to assume the parameters that have been found to give the best agreement both with the absorption edge and with other evidence. With these parameters theoretical calculations will be made of the absorption edge and compared with experiment.

We start by calculating the large polaron coupling constants, followed by the conduction band E - k curve and then some nearly small polaron parameters for the valence band.

6.1.2. Large Polaron Coupling Constants

The coupling constant, α, defined ~~near the beginning of this section~~ in 3.3 will now be evaluated leaving the effective mass as a parameter. The parameters $f^2/u\gamma$ were derived in sec. 3.2 from (optical) data on phonons. Thus:

$$\alpha_1 = \frac{e^2}{2}\left(\frac{2m}{\hbar\omega_1}\right)^{\frac{1}{2}}\left[\frac{2}{3} \times .608\left(\frac{1}{3.78} - \frac{1}{14.34}\right) + \frac{1}{3} \times .881\left(\frac{1}{4.17} - \frac{1}{12.18}\right)\right]$$

$$= \frac{2.3 \times 10^{-19}}{2}\left(\frac{2 \times 9.1 \times 10^{-28}}{1.17 \times 10^{-81} \times 722 \times 1.88 \times 10^{11}}\right)^{\frac{1}{2}}\left[.0789 + .0463\right]\left(\frac{m}{m_e}\right)^{\frac{1}{2}}$$

$$= 1.53 \left(\frac{m}{m_e}\right)^{\frac{1}{2}}$$

Here m_e is the mass of an electron, m is the 'bare' effective mass and an average $\frac{\omega_1}{2\pi}$ has been taken of 722 cm^{-1}.

Similarly $\alpha_2 = 0.686 \left(\frac{m}{m_e}\right)^{\frac{1}{2}}$

and $\alpha_3 = 0.0564 \left(\frac{m}{m_e}\right)^{\frac{1}{2}}$

For these two phonons there is no contribution from polarization in the c direction. The fourth very dubius phonon gives:-

$$\alpha_4 = 0.426 \left(\frac{m}{m_e}\right)^{\frac{1}{2}}$$

Even if the phonon is genuine its effect in large polaron theory is doubtful because at R.T. $kT > \hbar\omega$, and polaron theory does not yet adequately cover this region.

6.1.3. Conduction Band E - k Curve

The method employed to obtain the E - k curve for the SnO_2 conduction band is to take the k = o binding energy as $\sum_i \alpha_i \hbar\omega_i$ and, when $E > \hbar\omega_i$ for any branch, to take its contribution to the phonon binding energy as $\frac{\alpha_i}{k} \frac{\frac{3}{2}\hbar\omega_i^{\frac{1}{2}}}{2\sqrt{2m_e}}$ (This is essentially what 3.3.1. states). Near k = o the shape is given by using an effective mass $m_c \left(1 + \sum_i \frac{\alpha_i}{6}\right)$. As the first phonon energy is approached, the curve is bent over and flattened in proportion to the corresponding α_i and qualitatively like Larsen's published curve for $\alpha = 1$. The point of discontinuity is determined by the intersection of $E = \hbar\omega_i$ and the energy curve given by the higher energy phonons alone (i.e. with an effective mass

and binding energy given without the lowest energy phonon) lowered by the energy given by the Fröhlich formula $\left(\frac{\alpha_i \hbar^{3/2} \omega_i^{\frac{1}{2}}}{\sqrt{2m_c k}} \frac{\pi}{2}\right)$ for the lowest energy phonon. A similar procedure is used as each phonon energy is crossed, until the polaron energy is given by the 'bare' energy lowered by a sum of Fröhlich terms, all proportional to $\frac{1}{k}$. If Larsen's theory were used to obtain the point of discontinuity, rather larger departures from parabolicity around the resonances would occur because the value of k at the discontinuity is bigger; this would lead to larger variations in effective mass. The treatment for $E > \hbar\omega$ would, however, be less clear.

For simplicity we have combined the second and third phonons and just used two. We have taken $m_c = .29$ m, and get $\alpha_1 = .83$, $\alpha_2 = .40$, $\Sigma\alpha_i = 1.23$ and $\Sigma \alpha_i \hbar\omega_i = 1.03\hbar\omega_1 = .092$ e.v. The resultant E - k curve is shown in fig. 6.1.1. where the energy units are $\hbar\omega_1$ and the k units are arbitrary (the points $\left(\frac{2m_c\omega_i}{\hbar}\right)^{\frac{1}{2}}$ for i = 1, 2 are marked). The largest value of $\left(\frac{2m_c\omega}{\hbar}\right)^{\frac{1}{2}}$ (for $\hbar\omega = .0895$ e.v.) is $.0825 \times 10^8$ cm^{-1}, while the nearest edge of the Brillouin Zone is $\frac{\pi}{a}$ or $.664 \times 10^8$ cm^{-1} from $\underline{k} = o$. Departures from parabolicity might be expected to begin about $\frac{1}{3}$ of the way to the zone boundary.

6.1.4. Nearly Small Polaron Parameters

To allow for the differing phonon energies, here we can simply put $\sum_{i=1}^{3} D_i \hbar\omega_i = D\hbar\omega$ etc., and use the figure for $\Sigma D_i \hbar\omega_i$ of .488e.v. found to give a reasonable fit to the absorption edge. We use values for ϵ_∞ found in 5.4 and values for ϵ_s (only taking into account the three main optical phonons) found in 5.6 and take an average of $\left(\frac{1}{\epsilon_\infty} - \frac{1}{\epsilon_s}\right)$ over the crystallographic directions of .167.

We first assume $J_1 = J_2$ and get

$$J_1 = J_2 = \left[\frac{(.719 - .488)\ .167}{1.35}\right]^{\frac{1}{2}} = .0285^{\frac{1}{2}} = .169 \text{ e.v.}$$

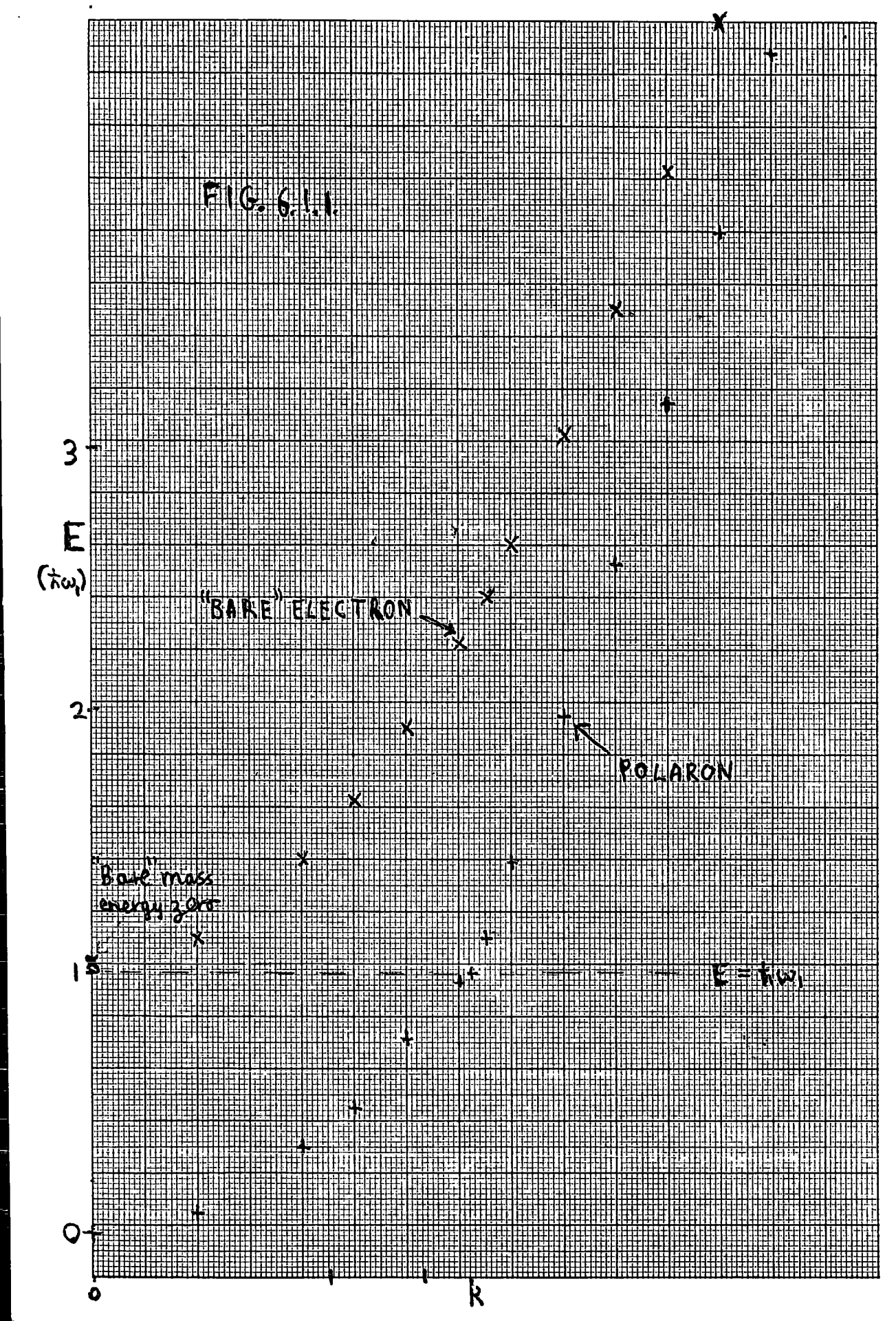
FIG. 6.11.
E
(ħω₁)
3
2
1
0
"BARE" ELECTRON
POLARON
"Bare" mass
energy zero
E = ħω₁
0
1
R

The main condition for small polaron theory is that a parameter of Eagles, $\epsilon_1' = Z\left(\frac{J}{Bo}\right)^2$, should be $\ll 1$. Including anisotropy appears to give

$$\epsilon_1 = 4\left(\frac{J_1}{Bo}\right)^2 + 2\left(\frac{J_2}{Bo}\right)^2$$

Using the above values for J we get

$$\epsilon_1 = .33,$$

so that the above condition is only moderately well satisfied.

Using the above values we obtain

$\hbar\omega S_{11} = -.421$ e.v. $\qquad \hbar\omega S_{12} = -.322$ e.v.

$\hbar\omega S_{01} = .900$ e.v. $\qquad \hbar\omega S_{02} = .548$ e.v.

$\hbar\omega(S_{01} + S_{11}) = .479$ e.v. $\qquad \hbar\omega(S_{02} + S_{12}) = .226$ e.v.

To find the total S values, we split these energies up among the different phonons by using the $f^2/u\,y$ (derived in 3.2.) in a similar manner to that used for large polarons earlier in this section. We obtain

1st phonon	$S_{01} + S_{11} = 3.98$	$S_{02} + S_{12} = 1.88$	$\bar{n} = .031$
2nd phonon	$S_{01} + S_{11} = 2.50$	$S_{02} + S_{12} = 1.18$	$\bar{n} = .20$
3rd phonon	$S_{01} + S_{11} = .23$	$S_{02} + S_{12} = .11$	$\bar{n} = .33$

where we have added the values of $\bar{n}$ for R.T.

$$\therefore \sum \tfrac{1}{2}(2\bar{n} + 1)(S_{01} + S_{11}) = 4.06 \quad \sum \tfrac{1}{2}(2\bar{n} + 1)(S_{02} + S_{12}) = 1.92$$

The bandwidth, $W = 4 \times .169\,(e^{-1.93} + 2e^{-4.06}) = .675\,(.146 + .035)$ $= .122$ e.v. Strictly speaking this result violates a condition of Eagles theory that W should be $\ll \hbar\omega$. It should be noted, however, that the c axis contribution to W (the first term in the above evaluation) is by far the biggest, and that the density of states in the band near the edge next to the band gap is much larger than it would be for a band of the same width with an isotropic effective mass. It should also be noted that this bandwidth

(.122 e.v.) is a factor of about 17 less than the rigid lattice width, and the polaron effective mass is very much bigger than anything predictable with large polaron theory. A further point is that a change of 1% in $\sum \hbar\omega D$ results in a change of about 7% in W and a change of 1% in $\left(\frac{1}{\epsilon_\infty} - \frac{1}{\epsilon_s}\right)$ results in a 4% change in W. It is thought that the lower energy phonons may be underestimated in strength (see 5.6). This would raise the S parameters and reduce W.

Another point is that Eagles theory is only to first order in ϵ_1, and with $\epsilon_1 = .33$ terms in ϵ_1^2 will be important (but small polaron theory should still be better than large polaron theory).

We have no direct evidence that $J_1 \simeq J_2$. One might suspect $J_2 > J_1$ because overlap might be greater in the direction of small lattice distance (c axis). $J_1 = J_2$ implies a large 'bare' effective mass anisotropy because $mJ = \frac{\hbar^2}{2G^2}$ where G is a lattice distance.. Hence $\frac{m_\perp}{m_{//}} = 2.2$ (with $J = .169$ e.v., $m_\perp = 1.00\, m_o$ and $m_{//} = 2.20 m_o$). A superficial arguement that $m_\perp \approx m_{//}$ because the valence band is mainly derived from Oxygen 2p orbitals, and the oxygen atoms are packed with very similar tightness in both axial directions appears to be false. This is because for electron states in a band the important factor is ease of movement from one unit cell to the next, rather that one atom to the next.

If $J_2 > J_1$, $m_\perp$ is larger, $m_{//}$ is smaller and W is bigger.

We finally calculate the polaron binding energy given be Eagles equ. 5.14

$$Ep = Bo + \frac{Z J^2}{\hbar\omega So} - ZJ\left(1 - \exp\left[-\tfrac{1}{2}(2\bar{n} + 1)(S_o + S_1)\right]\right)$$

Including anisotropy we get

$$Ep = Bo + \frac{4J_1^2}{\hbar\omega S_{01}} + \frac{2J_2^2}{\hbar\omega S_{02}} - 4J_1\left(\exp\left[-\tfrac{1}{2}(2n+1)(S_{01} + S_{11})\right]\right) -$$

$$\ldots - 2J_2 \left(1 - \exp\left[-\tfrac{1}{2}(2\bar{n}+1)(S_{02}+S_{12})\right]\right)$$

Substituting our values we obtain

$$Ep = .719 + .231 - .675\,(1-\exp(-4.06)) - .338\,(1-\exp(-1.92))$$

$$= .002 \text{ e.v.}$$

In other words J is so big that Ep has almost gone negative. If $\Sigma \hbar\omega$ D is increased 1% then Ep is increased about 70% and if $\left(\frac{1}{\epsilon_\infty} - \frac{1}{\epsilon_s}\right)$ is reduced 1%, Ep is increased about 3x. It should also be remembered that terms in ϵ_1^2 are likely to have considerable effect. If $J_2 > J_1$, larger values of Ep are obtained. If T is lower than R.T., then Ep is larger. However, the smallness of Ep throws doubt on the degree of applicability of nearly small polaron theory. Comparison with the binding energy given by weak coupling large polaron theory shows that the true Ep $\gtrsim$ .23 e.v.

As a final comment on the validity of the theory, it should be noted that most of the parameters in the theory were linked to observation by means of the continuum polarization model, which deals only with long range forces and which introduces ϵ_∞ and ϵ_s into the theory. Thus it is possible that nearly small polaron theory is more applicable than it appears to be if short range forces are ignored.

The different phonon branches are allowed for by weighting the contribution of each to $\left(\frac{1}{\epsilon_\infty} - \frac{1}{\epsilon_s}\right)$ in the same way as was done earlier for large polarons. In this way a value of D is obtained for each branch. In the calculation of the absorption, the second and third phonons are lumped together with an average energy and a total D. The justification for doing this is that the third phonon has very small weight and the energies of phonons two and three only differ by a factor of 1.29. The main motive is to take advantage of the coincidence that the weighted average energy is within experimental error exactly half the energy of the first phonon (the energies

being 361 and 722 cm^{-1}). We thus deal with only two values of D, D_1 and D_2. The ratio is found to be: $\frac{D_1}{D_2} = 1.45$ ~~(3.5.2)~~ (6.1.1)

6.1.5 Continuum Absorption at 296°K

The two factors that experimentally most determine the magnitude of D are the shape of absorption at high absorption levels (where n = 1 exciton effects are small) and the absolute magnitude of the 1.3°K absorption compared with the absorption at high levels. Each comparison of theory with the experimental points requires a very large amount of numerical work, so that accurately getting the best fit is a very long procedure. In any case, at present, the experimental accuracy at high absorption levels does not justify high precision, quite apart from theoretical approximations. For the purposes of conduction band calculations we have assumed $m_c = .29\ m_o$ and from this the changes in D with k (or E^1) have been calculated. With this assumption, the variable parameter was the valence band contribution to D, and the best values found to date are

$$D_1 = 4.05 \qquad D_2 = 2.8$$

their ratio having been found above. (The second and third phonons have been combined).

We shall now go through the steps in reaching the continuum (and n = 2 to ∞ exciton) contribution to the absorption. The method was outlined in 3.5. Substituting in (3.5.2) we can obtain for forbidden transitions that the shape of each part (ignoring the changes in D which are taken care of later) is proportional to $k^3 m_{ap} X$ where m_{ap} is the local effective mass and X is the Sommerfeld factor. Table 6.1.1 shows how this quantity is obtained for different values of $E^1 - \Delta E$ (this is taken to be equal to E for phonon assisted transitions), in conjunction with fig. 6.1.1. The energy units are the larger value of $\hbar\omega$ (.0895e.v.), the energy intervals are $\frac{1}{2}\hbar\omega$ and the first value of energy ($.157\hbar\omega$) is

Table 6.1.1.

$E^1 - \Delta E$	μ_{ap}	$E^1_{ap} - \Delta E$	ϵ_{ap}	R	$\frac{E^1_{ap} - \Delta E}{R}$	X	k	k^3	$k^3 \mu_{ap} X$
.157	1.205	.157	1.05	.334	.470	28.7	.274	.0206	.712
.657	1.207	.680	1.20	.256	2.66	5.5	.57	.185	1.22
1.157	.72	1.9	1.38	.115	16.5	2.13	.755	.431	.66
1.657	.75	2.4	1.15	.173	13.9	2.26	.845	.603	1.02
2.157	.815	2.75	1.02	.240	11.25	2.42	.935	.817	1.61
2.657	.85	3.06	.93	.300	10.2	2.51	1.02	1.06	2.26
3.157	.87	3.48	.875	.346	10.0	2.53	1.1	1.33	2.92
3.657	.89	3.88	.835	.39	9.95	2.53	1.175	1.62	3.65
4.157	.91	4.27	.805	.43	9.95	2.53	1.25	1.95	4.5
4.657	.92	4.75	.78	.462	10.3	2.50	1.323	2.32	5.34
5.157	.93	5.22	.76	.491	10.6	2.48	1.394	2.71	6.25

chosen so that it is $.25\hbar\omega$ above the n = 2 exciton (which can be regarded as the pseudo-end of the continuum). m_{ap} is measured in units of m_c, ϵ is measured in units of ϵ_ζ, k is in arbitrary units (from fig. 6.1.1) and X is found from $\frac{E^1_{ap}}{R}$. The values of m_{ap} and ϵ are approximately averaged over an energy interval, this being important and difficult near the sharp change in slope of fig. 6.1.1. Greater accuracy might be obtained by taking a smaller energy interval.

Each of these energy intervals has different average values of D. The calculation of the R_p for Eagles' theory is shown in Table 6.1.2 for the case $D_1 = 4.6$, $D_2 = 2.99$ and $T = 296^oK$ and assuming the shape of each part is the same (as discussed in 3.5 the one most seriously different is p = m = o). The first two parts of the table shown the distribution due to each phonon separately and in the third part each number is the product of values of R_{p1} and R_{p2} from the first two parts, the p_1 and p_2 being indicated by the diagonal and row. The total p designation indicated along the bottom is obtained by putting $2p_2 = p_1$, because ω_1/ω_2 was taken as 2. It is straightforward to show that this is the correct way to combine the two distributions. With a set of such tables for each pair D_1, D_2 it is now possible to obtain the absorption at each energy interval, as shown in table 6.1.3. The values of D_1 and D_2 for each row are shown. (In fact, to save time, tables were not worked out for each D_1, D_2 but only for two pairs, the other results being found by making appropriate percentage corrections).

The shifting of the zero and one phonon parts will now be allowed for. Taking $2\Delta E = .12$ e.v. the zero phonon shift (ΔE) is .06 e.v. and the one phonon shift ($\omega\frac{\Delta E}{2}$) is $\sim$.03 e.v. The results of this allowance is shown in

Table 6.1.2. Continuum Absorption at 296°K

$$R_p = \sum_{m=0} \frac{(D)^{2m+p} (\bar{n}+1)^{m+p} \exp -(2\bar{n}+1) D}{(m+p)!\, m!}$$

$D_1 = 4.6$ $\qquad \bar{n} = .0308$

p_1 =	-3	-2	-1	0	1	2	3	4	5	6	7
m = 0				1	4.75	11.25	17.4	20.6	19.6	15.5	10.5
1			.142	.674	1.60	2.47	2.9	2.8	2.2	1.5	.9
2		.0100	.048	.112	.17	.21	.2	.2	.1	.1	
3	.000472	.0022	.005	.008	.01						
4	.000079	.0002									
5	.000006										
R_{p_1}	.000557	.0124	.195	1.794	6.53	13.9	20.5	23.6	21.9	17.1	11.4

x exp (-1.062 x 4.6)

$D_2 = 2.99$ $\qquad \bar{n} = .21$

p_2 =	-4	-3	-2	-1	0	1	2	3	4	5	6	7
m = 0					1	3.62	6.55	7.9	7.15	5.17	3.12	1.61
1				6.28	2.27	4.11	4.95	4.5	3.25	1.96	1.01	.50
2			.197	.711	1.29	1.56	1.41	1.0	.61	.32	.15	.06
3		.0412	.149	.270	.33	.30	.21	.1	.07	.03	.01	
4	.00646	.0234	.042	.051	.05	.03	.02					
5	.00293	.0053	.006	.006								
6	.00052	.0006										
R_{p_2}	.00996	.0705	.0394	1.67	4.94	9.62	13.44	13.5	11.1	7.48	4.43	.2.2

x exp(-1.42x2.99)

Table 6.1.2. Cont.

P_1	0	1	2	3	4	5	6	7	P_2
-1	.0020	.008	.02						-5
	.00195	.018	.065	.14	.2	.2			-4
-2	.0138	.126	.46	1.0	1.4	2	2	1	-3
	.0049	.077	.705	2.57	5.5	8.1	9	9	7	4	-2
-3	.0207	.326	2.99	10.9	23.2	34	40	37	29		-1
	.0275	.061	.96	8.83	32.2	68.7	101	117	108	84	0
	.0054	.119	1.88	17.2	62.7	134	197	227	210		1
		.007	.16	2.56	23.5	85.7	183	270	310	288	2
		.008	.17	2.6	24.2	88	188	277	318		3
				.14	2.2	19.8	72	154	227	262	4
				.1	1.5	13	49	104	153		5
						.8	8	28	60	88	6
							4	14	31		7
								2	6	14	8
								1	3		9
$X \exp(-1.6(2 \times 4.6 - 1.42 \times 2.99))$	.01	.042	.163	.587	1.89	5.52	14.24	31.8	63.6	113	182	271	373	480	580	661	718	744	740	
Total P	-3		-2		-1	$-\frac{1}{2}$	0	$\frac{1}{2}$	1		2		3		4		5		6	

Table 6.1.3.

Continuum Absorption at 296°K

D_1	D_2	$E^1 - DE$	total p for top line: -2		-1		0		1		2		3	
4.48	3.03	.157	.132	.479	1.55	4.55	11.8	26.0	52.2	92	148	218	299	383
4.55	3.05	.657	.053	.218	.79	2.53	7.4	19.1	42.5	85	151	244	363	500
4.60	2.99	1.157	.006	.029	.12	.42	1.33	4.0	10.3	23	46	93	131	195
4.54	2.97	1.657	.002	.011	.05	.18	.67	2.2	6.4	16	37	73	129	208
4.49	2.95	2.157	~.001	~.006	.02	.08	.31	1.1	3.6	11	28	62	124	216
4.45	2.94	2.657			~.01	~.04	.11	.45	1.6	5	15	40	90	177
4.42	2.92	3.157					~.05	~.22	.6	2	7	20	52	119
4.40	2.91	3.657							~.3	~1	3	9	27	69
4.38	2.91	4.157									~2	~5	11	33
4.36	2.90	4.657											~6	~20
		5.157												
		5.657												
		6.157												
After allowance for the shifting of the zero and one phonon parts			.194	.743	2.54	7.8	21.7	53.1	117.5	235	437	764	1232	1920
			.194	.825	3.04	9.1	24.6	57.1	118.5	236	442	771	1240	1930
n=1 exciton absorption			.826	3.15	9.23	23.6	42.5	70.3	95	121	136	146	143	140
Total			1.02	3.97	12.3	32.7	67.1	127.4	213.5	357	578	917	1383	2070
$\hbar\omega$ (cm^{-1} e.v.)	Experimental absorption÷10		(1.7)	4.8	20	52	114	205	345	520	800	1300	2000	
ratio			(1.67)	1.21	1.63	1.59	1.55	1.61	1.62	1.46	1.39	1.42	1.45	
energy						3.505 e.v.								
Experimental	" absorption÷10							6.5	11.5	17.5	27	42	64	100
ratio								.051	.054	.049	.047	.046	.046	.048

Table 6.1.3. Cont.

Continuum Absorption at 296°K .

(Absorption scale reduced by a factor of 10)

total p for top line						
4		5		6		7
46	51	56	58	57	52	47
63	78	89	96	100	99	94
27	35	42	88	52	54	53
31	42	54	65	74	80	83
35	51	70	89	106	120	128
$31\frac{1}{2}$	50	74	100	128	152	168
$23\frac{1}{2}$	41	66	96	132	167	197
$15\frac{1}{2}$	30	54	86	125	169	215
$8\frac{1}{2}$	19	37	67	107	155	210
4	10	23	45	80	129	187
$\sim 2\frac{1}{2}$	~ 8	12	28	54	96	153
		~ 9	14	32	62	110
			~ 10	~30	37	70
					~31	~90
After allowance for the shifting of the zero and one phonon parts	288 289	415 416	586 587	802 804	1077 1079	1400 1402	1800 1802
n=lexciton absorption	13	11	9	6	3	2	1
Total	302	427	596	810	1082	1404	1803
$K_{tw}(cm^{-1})$ Experimental absorption ÷ 100			(1500)			(2600)	(3150)
ratio			(250)			(186)	(1.75)
Energy							
" Experimental absorption ÷ 10	15.2	22	32.5	45	62	84	118
ratio	.050	.0515	.0545	.0555	.057	.060	.065

table 6.1.3. We have not allowed for the tail of the absorption of each part (except the zero phonon part). Qualitatively this can be seen to shift the absorption slightly to lower energies, the shift getting progressively smaller as we move to higher energies.

The absorption in the column labelled p = o occurs .074 e.v. above the band edge.

6.1.6 Exciton Contribution at 296°K

We justified in 3.4 the use of α_n/λ increasing value of D as we move up the n = 1 exciton band. Associated with this will be a decrease in the sum of the absorption of all the parts compared with what would be expected from the density of states. This decrease is because the Sommerfeld factor varies as $\frac{1}{r_e^3}$, and r_e increases as we move up the band. The shape of the exciton band, and so also its density of states, closely follows that of the free polaron because the exciton binding energy is roughly constant. Because of the anisotropy of the polaron bandwidths, departures from parabolicity occur sooner than would otherwise be so, causing a higher density of states near the bottom of the band.

We evaluate the n = 1 exciton absorption at points .15 $\hbar\omega$ (i.e. .0135 e.v.) and .65 $\hbar\omega$ (i.e. .058 e.v.) above the bottom of each phonon part. These points can be taken to represent absorption from 0 - .4 $\hbar\omega$ and .4 - .9 $\hbar\omega$ respectively, and absorption above .9 $\hbar\omega$ is not very important. The change in Sommerfeld factor between these points is assumed to be 2.5, and the values of D^1 taken are $D_1^1 = 2.33$ $D_2^1 = 1.58$ for .15 $\hbar\omega$ and $D_1^1 = 4.1$ $D_2^1 = 2.8$ for .65 $\hbar\omega$. The number of states represented by each point is assumed to be in the ratio

1.3:1. For the anisotropic bands used here this can be shown to be roughly correct. Table 6.1.4. sets out the calculation of the R^1p of Eagles theory for the first of the points (and quotes the result for the second of the points) in a similar manner as for the continuum. Table 6.1.5. at the top shows the addition of the absorption derived for the two points, after allowance has been made for the relative Sommerfeld and density of states factors. Below this is shown the addition of the interband phonon emission and phonon absorption parts. To do this the .036 e.v. phonon has been approximated as $\frac{3}{8}\hbar\omega$ (i.e. .0336 e.v.) so that twice the .036 e.v. phonon becomes $1\frac{1}{2}$ energy intervals of $\frac{1}{2}\hbar\omega$. The factor $e^{\frac{\hbar\omega}{kT}}$ has been taken as 4, and the absorption half way between two evaluation points has been taken as the geometric mean of the absorption at the two points. The absorption in the p = 0 column (phonon emission) occurs .013 e.v. above the band edge.

The average intermediate state energy is taken as 5.4 e.v., which causes an increase of about 5% in the factor by which the absorption at one point is larger than the absorption at one energy interval lower. The figure of 5.4 e.v. is only a rough estimate; the reason for it being less than the estimated absorption peak obtained by the short wavelength dispersion analysis is that the term $\frac{1}{(Ei - \Lambda)^2}$ increases the effect of the lower energy transitions. The absorption to 5.5 e.v. is roughly known from film measurements, and the integrated absorption above that can be estimated from ϵ_∞ (see section 2.3.).

The exciton absorption with this factor included, as well as a constant factor chosen to give a good fit of the whole absorption with experiment, is shown in table 6.1.3. where it is added to the continuum absorption. Unfortunately the energy of the points at which the continuum and exciton contributions are calculated do not quite match, so that the exciton absorption

Table 6.1.4.

Exciton absorption at 2.96°K

$$R^1_p = \sum_m \frac{(D^1)^{2m+p}}{(m+p)!\,m!} (\bar{n}+1)^{m+p} (\bar{n})^m \exp -(2\bar{n}+1) D^1$$

1st Point $D_1^1 = 2.33$ $\bar{n} = .0308$

p_1 =	-2	-1	0	1	2	3	4	5
m = 0			1	2.4	2.88	2.3	1.38	.66
1		.0717	.17	.20	.16	.1	.05	.02
2	.00257	.0062	.01	.01				
3	.00015	.0002						
R^1p_1	.00272	.0781	1.18	2.61	3.04	2.4	1.43	.68

X exp (-1.062 x 2.33)

$D_2^1 = 1.58$ $\bar{n} = .21$

p_2 =	-4	-3	-2	-1	0	1	2	3	4	5
m = 0					1	1.91	1.82	1.16	.55	.21
1				.332	.634	.60	.39	.18	.07	.02
2			.0550	.105	.100	.06	.03	.01		
3		.00608	.0116	.011	.007					
4	.000505	.00096	.0009							
5	.000070	.00007								
R^1p_2	.00058	.00711	.0675	.448	1.74	2.57	2.24	1.35	.62	.23

X exp (- 1.42 x 1.58)

Table 6.1.4.

Exciton absorption at 296°K

Continued

P_1	1	2	3	4	5	P_2
0	.0007	.002				-4
	.0084	.019	.02			-3
-1	.0053	.080	.176	.20	.2	-2
	.0350	.529	1.17	1.4	1.1	-1
-2	.0047	.136	[2.05]	4.54	5.3	0
	.0070	.201	3.04	6.7	7.8	1
	.0001	.006	.175	2.64	5.8	2
		.003	.10	1.6	3.5	3
			.05	.7	1.6	4
					.3	5
						6

	-2	$-1\frac{1}{2}$	-1	$-\frac{1}{2}$	0	$\frac{1}{2}$	1	$1\frac{1}{2}$	2	$2\frac{1}{2}$	3	$3\frac{1}{2}$	4	$4\frac{1}{2}$	5	total p
Xexp(-1.062 x 2.33-1.42 x 1.58)	.0108	.0505	.224	.752	2.40	4.33	7.43	9.7	12.0	12.7	12.8	11.5	10	7.9	6.1	
Xexp(-1.062 x4.1-1.42 x 2.8)	.114	.415	1.39	4.06	10.6	23.4	45.6	78.2	122	174	229	281	323	351		

2nd point $D_1^1=4.1$, $D_2^1=2.8$

Table 6.1.5.

Exciton Absorption at 296°K(Cont.)(I)

p for top line	−2	$-1\frac{1}{2}$	−1	$-\frac{1}{2}$	0	$\frac{1}{2}$	1
1st point	.0108	.0505	.224	.752	2.40	4.33	7.43
2nd point	.0002	.0009	.003	.012	.035	.11	.20
phonon emission total	.0112	.0514	.227	.764	2.435	4.42	7.63
phonon absorption total	.013	.0568	.191	.608	1.105	1.91	2.52	3.18
	.0274	.1044	.341	.82	1.454	2.20	2.83
Total	.0386	.156	.568	1.584	3.89	6.62	10.46

Table 6.1.5.

Exciton Absorption at 296°K(Cont.)(II)

p for top line	$1\frac{1}{2}$	2	$2\frac{1}{2}$	3	$3\frac{1}{2}$	4	$4\frac{1}{2}$	5
1st point	9.7	12.0	12.7	12.8	11.5	10	7.9	6.1
2nd point	.4	.7	1.0	1.4	1.9	2.3	2.7	2.9
phonon emission total	10.1	12.7	13.7	14.2	13.4	12.3	10.6	9.0
phonon absorption total	3.42	3.55	3.35	3.1	2.6	2.2		
	3.30	3.5	3.45	3.2	2.8	2.4		
Total	13.4	16.2	17.15	17.4	16.2	14.7		

.013 e.v. above the band edge is added to the continuum absorption .029 e.v. above the band edge. This could be rectified in a straightforward manner, but the extra work is barely worthwhile. The exciton energy will be taken as the correct energy. Good agreement with experiment is obtained with the above absorption located at 3.505 e.v., giving the band gap as 3.492 e.v. with an estimated error of ± .015 e.v.

Underneath the total absorption is shown the experimentally observed absorption, the data coming from various sources (see 5.1). Below this is shown the ratio of the observed to the theoretical absorption (which is in arbitrary units). The high energy experimental points are from thin films and are not very reliable (see 5.1.) The ratio for the middle points is raised if the continuum energy is shifted .016 e.v. up to its true position. This reduces the scatter of the ratios, and makes a good average about 1.6. The most difficult feature of the experimental curve to reproduce is the rapid change of slope on the log plot around 3.5 e.v. This shows up in the second lowest point where the ratio falls to 1.21.

The change in band gap between 1.3°K and 296°K is thus .105 ± .015 e.v., since Nagasawa and Shinoya observed the band gap = 3.597 e.v. at 1.3°K.

6.1.7 Absorption Polarized Parallel to the c Axis.

The simplest assumption is that the absorption mechanism is the same as for ⊥ absorption, but that the optical matrix elements are reduced. If the intermediate states for the n = 1 exciton absorption are from the same valence and conduction bands as the continuum, then continuum and n = 1 exciton matrix elements will be in the same ratio for ∥ and ⊥ absorption. Otherwise different ratios will be expected.

The observed R.T. absorption is shown in table 6.1.3 and

examination shows that the ratio of the two matrix elements cannot be very different in the two cases. The ratio of the observed to the theoretical absorption is seen to be fairly constant, except that the observed points are rising faster at high energies. This could be explain by additional absorption possibly due to a different valence band. It could also be explained by departure of the conduction band from parabolicity at high energies, the only difficulty being that this should also apply to $\perp$ absorption.

No account was taken of absorption with this polarisation when adjusting the D or any other parameters; it is an entirely independent check.

The ratio of $\perp$ absorption to $//^{a}$ absorption is about 30. Elliott's approach to the theory does not give so much help in understanding this difference as the approach adopted by Knox (1963). He obtained "forbidden" transitions as being proportional to $|\sum_{\beta_c} Z_{nm}(\beta_o)|^2$ (equ. 9.26 and 9.29). Here β_c is a lattice vector in the direction of polarization (the Z axis), and $Znm|(\beta_o)|^2 = \left[\int a_{n\beta_c}(\underline{r})^* Z\, a_{mo}(\underline{r})\, d\underline{r}\right]^2$ where the a are Wannier functions. The suffix n or m indicates valence or conduction band, and the suffix β_o or 0 indicates the Wannier function is centred on the lattice point at a distance of β_o in the Z direction, or at the origin respectively. The Wannier functions are localised functions derived from the Bloch states for the band, and bear some resemblance to the atomic (or'molecular') functions from which the bands are derived, the resemblance being closer the more the tight binding approach applies. The β_o^2 accounts for a factor of 2.2 of the ratio of

the two absorptions, leaving a factor of about 14 to be accounted for by $|Z_{nm}(\underline{\beta}_o)|^2$, the two-centre matrix element. A fuller understanding of the symmetry of the top valence band might lead to an understanding of this factor.

6.1.8 Absorption Edge at Low Temperature

(a) Continuum at 1.3°K

We first compare the absorption obtained by using our parameters with the results of Nagasawa and Shionoya (1966) at 1.3°K. To a very good approximation we can put T = 0°K. Calculation from the Rp for total p = o shows that the total p=o absorption is reduced by a factor of 3.0 for the lowest energy point (in the continuum). From the fitting of theory with experiment the R.T. absorption of this type is about 54 cm^{-1}, so that our prediction for the absorption at this point at 0°K is about 18 cm^{-1}. This lowest point is .425 R above the band edge, so that the predicted absorption at the band edge is $\frac{18}{1.425}$ = 12.6 cm^{-1}. From the data of Nagasawa and Shionoya we deduce the measured absorption to be about 20 cm^{-1}.

Considering the large number of steps involved in getting the predicted value, the agreement is reasonable. The

most direct way of improving the agreement is to reduce D_1 and D_2 about 5% and reduce the ratio of exciton to continuum absorption a little; but there are many other possible ways.

(b) n = 1 Exciton at 1.3°K.

At an energy corresponding to p = o for the first point (.0135 e.v. above threshold) for phonon emission, the R.T. absorption for the n = 1 exciton is found to be 108 cm^{-1} from the comparison of theory and experiment. At 0°K the phonon absorption part is absent, and from the R^1p the phonon emission part is reduced by a factor of 1.09. The phonon emission part is proportional to $1 + \bar{n}$. For the present purpose we take the average phonon energy as .04 e.v. and a reduction factor of 1.26 results. These three effects together produce a reduction of 2.2, giving a "predicted" absorption of 49 cm^{-1}. Nagasawa and Shionoya's data indicate an approximately $E^{\frac{1}{2}}$ rise to .01 e.v. above threshold, at which point the exciton absorption appears to be rather under 20cm^{-1}. At this energy there appears a steadily increasing additional contribution above the $E^{\frac{1}{2}}$ shape. There are two possible explanations of this. It may be the start of absorption

with the .046 e.v. phonon providing the interband matrix element in which case it has a different shape from the .036 e.v. phonon assisted part. This matrix element might vary as k, giving an $E^{3/2}$ shape. It is interesting to observe that in Cu_2O a similar rise above the $E^{\frac{1}{2}}$ shape occurs about 600 cm^{-1} above the exciton, and that this has been attributed to a phonon of that energy, while the main "red" absorbtion is due to indirect transitions with 105 cm^{-1} phonons. The second plausible explanation is that the rise is due to the density of states factor. In 6.1 we found the bandwidth in the a or b axial directions to be $\sim$ .012e.v. at R.T. At $0^{o}K$ the figure becomes larger, $\sim$ .024e.v. The sinusoidal rather than parabolic form of the E-k curves therefore implies significant departures from an $E^{\frac{1}{2}}$ density of states at an energy of $\sim$.01e.v.

Considering the latter effect, examination shows that at .0135e.v. the absorption would be of the order of a factor of 1.2 higher than the $E^{\frac{1}{2}}$ curve. Because the range of absorption represented by the first point is $.4\hbar\omega$ rather than the $.5\hbar\omega$ tacitly assumed in the use of Eagles theory, the "predicted" absorption should be increased by a factor of 1.25. Because the parabolic part of the density of states factor has the term $m_1\, m_2^{\frac{1}{2}}$ (where m_1 is the polaron mass along the a axes and m_2 is that along the c axis) the "predicted" absorption should be reduced by a factor of about $2(1.4)^{\frac{1}{2}}$ to allow for the changing polaron masses between R.T. and $0^{o}K$. These factors bring the predicted value to 26 cm^{-1} at

.0135e.v. and 19 cm^{-1} at .01e.v. The experimentally indicated absorption at .01e.v. is about 16 cm^{-1}.

The above paragraph shows that the assumption that the .036 e.v. phonon is the only one with an appreciable interband matrix element leads to fairly reasonable results. The assumption was only made for simplicity and to aid agreement between theory and experiment in the shape of the R.T. absorption. The discrepancy between the absorption values of 16 and 19 cm^{-1} might really be considerably larger due to the many approximations used. This discrepancy can be accounted for by interband matrix elements other than the .036 e.v. phonon one. The .046 e.v. phonon might account for the sharp change of slope .01e.v. above threshold, and this was assumed in the phonon analysis to obtain a precise estimate of its energy.

6.1.9 Nitrogen Temperatures

Unfortunately the exact temperature of our "nitrogen" absorption measurements is unknown. Calculations indicate that it was probably of the order of 10°C above the B.P. of nitrogen (77°K) and probably somewhat variable. T= 90°K is assumed here. It is also unfortunate that the shape for the interesting part near the tail is distorted by the defect absorption. This is estimated (see 6.2) and subtracted but the errors are quite large, especially near the tail.

Theoretical Absorption

The calculation of the exciton part is shown in table 6.1.6. The interband phonon absorption part is averaged and added to the phonon emission part, as was done for R.T. The average intermediate state energy is assumed to have shifted by the same amount as the band gap, and the bottom line of the table includes the $\frac{1}{(Ei - \Omega)^2}$ factor as well as being converted to units of K (cm^{-1} e.v.) by a similar method as was used for 1.3°K. The band gap is taken as 3.590 e.v. (from 3.5 it should be 3.595e.v.) so the absorption in the total p=o column occurs at 3.603e.v. This is approximated as 3.600 e.v.

The calculation of the continuum part is shown in table 6.1.7 The $R_{\text{total p}}$ sums are split. The top line is the contribution with 2 or more phonons, the bottom line is the zero phonon part for total p=o and the one phonon part for the rest.

The zero and one phonon parts are very much more important than at R.T., as also are the 'tails' of the many phonon parts. Part of the reason for the latter is that the (hole) polaron bandwidth is larger, making the tails longer. This larger bandwidth also makes the differences between the positions of zero, one and many phonon parts bigger. All these facts make the accuracy of the theoretical prediction worse.

The fourth section of table 6.1.7 shows our calculation of the continuum absorption. The many phonon parts are shifted two energy intervals (i.e. .0895e.v.) to higher energies compared with the zero phonon part, and the one phonon parts are shifted one energy interval. These shifts (which are convenient for calculation purposes) correspond to a (hole) polaron bandwidth of .179 e.v., compared with a value of

Table 6.1.6.

Exciton at 90°K.

1st point $D_1^1 = 2.33$ $\bar{n} = 10^{-5}$

p_1 =	-1	0	1	2	3	4	
$R^1 p_1$ =	2.3×10^{-5}	1	2.33	2.7	2.1	1.2	X exp (-2.33)

$D_2^1 = 1.58$ $\bar{n} = .0032$

p_2 =	-1	0	1	2	3	4	
$R^1 p_2$ =	.005	1	1.58	1.25	.66	.26	X exp (-1.59)

p_1	0	1	2	3	4	p_2
[illegible]	.005	.01				-1
	1	2.33	2.7	2.1	1.2	0
	1.58	3.7	4.3	3.3	1.9	1
	1.25	2.9	3.4	2.6		2
	.7	1.5	1.8	1.4		3
	.3	.6	.7			4
	.1	.2	.2			5
		.1				6

^{1} total$_p$ X exp (-2.33-1.58)	.005	1	1.59	3.6	4.4	5.9	5.9	6.1	5.3	4.6	3.5
		0		1		2		3		4	total$_p$
^{1} total$_p$ X exp (-4.1-2.8)		1	2.8	8.1	15	27	40	56	69	81	2nd point $D_2^1 = 4.1$
	.005	1	1.59	3.6	4.4	5.9	5.9	6.1	5.3	4.6	1st point
			.02	.1	.2	.3	.5	.8	1.1	1.4	2nd point
nonon emission total	.005	1	1.61	3.7	4.6	6.2	6.4	6.9	6.4	6.0	
nonon absorption total	.01	.017	.04	.05	.1	.1	.1	.1	.1	.1	
Total	.018	1.03	1.65	3.8	4.7	6.3	6.5	7.0	6.5	6.1	
	1.3	75	127	310	405	570	620	710	690	690	cm^{-1} e.v.

Table 6.1.7.

Continuum at 90°K

$D_1 = 4.48$ $\quad \bar{n} = 10^{-5}$

p_1 =	-1	0	1	2	3	
Rp_1 =	4.5×10^{-5}	1	4.48	10	15	x exp (-4.48)

$D_2 = 3.03$ $\quad \bar{n} = .0032$

p_2 =	-1	0	1	2	3	4	5	
Rp_2 =	.01	1.03	3.09	4.7	4.7	3.6	2.2	x exp (-3.05)

p_1 \ p_2	-1	0	1	2	3	4	5	6
0	.01	1.03	3.09	4.7	4.7	4	2	1
1	.04	4.6	13.9	21	21	16	10	
2		10	31	47	47			
3		15	46					

R total p: .03 + .01 + 4.8 | 18.6 | 35 | 54 | 79 | 103 — x exp(-4.48-3.05)

total p: .01 | 1.00 | 3.03 | 4.5

total p	0	1	2	3	D_1	D_2	$E^1-\Delta E$
1.01	3.06	4.6	4.8	18.6	35	54	79	103	4.48	3.03	.157
1.65		5.0	7.6	8.0	31	58	90	132	4.55	3.05	.657
	.82		2.5	3.8	4	16	30	47	4.60	2.99	1.157
		1.4		4.2	6	7	26	49	4.54	2.97	1.657
			2.2		6	9	10	40	4.49	2.95	2.157
				3.1		9	13	15	4.45	2.94	2.657
					4		12	17			
								15			
						5	6	7			

		1.01	1.65	3.88	11.0	17.1	37.7	86	158	266	425	
continuum absorption		64	104	244	693	1080	2380	5050	10000	16700	26800	cm^{-1}
exciton absorption	1.3	75	127	310	405	520	620	710	690	690	600	e.v.
	1.3	139	231	554	1100	1650	3000	6280	10700	17400	27400	
experimental $\perp$ values	~12	210	630	1050								
experimental $/\!/^{\alpha}$ values		~7	18	44	71	110	165	250	410	600	~870	
experimental $/\!/^{\alpha}$ values	x30	~210	540	1320	2130	3300	4950	7500	1230	18000	~26100	
energy (e.v.)		3.600										

$\sim$.24e.v. (for $T < \sim 100^{\circ}K$) found assuming $J_1 = J_2$. The same values of D_1 and D_2 are shown as were used at R.T., but the same accuracy was not used. The absorption in the left hand column occurs at 3.604e.v., but this is approximated as 3.600e.v.

The absorption is then converted to cm^{-1} e.v. by a similar method as was used for $1.3^{\circ}K$, and the previously calculated exciton part is finally added. It should be emphasised that this prediction has contained no parameters to be adjusted in order to fit the $90^{\circ}K$ absorption, and the only parameter taken from the $1.3^{\circ}K$ absorption is the band gap. (The intensities at $1.3^{\circ}K$ have not been used). The experimental values for $\perp$ absorption are shown beneath the predicted absorption, and the values for $//^{a}$ absorption on a lower line. The bottom line shows the $//^{a}$ values multiplied by 30, the ratio of $\perp$ to $//^{a}$ absorption found for R.T.

The predicted values are seen to be too small at low energies and about right at high energies. Most of the discrepancy can be accounted for by the following.

(1) Neglect of the 'tail' absorptions. The tails would increase the low energy absorption, especially that at 3.645e.v. and 3.78e.v. which are two of the worst fitting points.

(2) The zero phonon continuum absorption comparison at $1.3^{\circ}K$ indicated that this was about a factor of 1.6 too small. It was pointed out that this could be improved by taking smaller values of D. The effect of thus adjusting D would be to raise the zero phonon part by a factor of 1.6 and the total $p=\frac{1}{2}, 1, 1\frac{1}{2}$ ... parts by progressively smaller factors. It was also suggested that the exciton contribution might be

lowered slightly (to retain a good fit at R.T.), but the net effect would be to raise the absorption at lower energies.

(3) If we had assumed the exciton intermediate states had not shifted their average energy, the exciton contribution would be raised about 12%, which raises the low energy absorption and hardly affects the high energy absorption.

There are also of course the many theoretical approximations and experimental errors, that are involved in the theoretical prediction, and could account for the discrepancy.

6.1.10. Evaluation of Matrix Elements

Knox (1963) expresses Elliott's results for the absorption coefficient at the edge of the continuum as:

$$K = 4\pi\omega\epsilon \frac{(2\beta_0 |Z_{vc}(\beta_0)|)^2}{3a^4cn} \qquad (6.1.1.)$$

The symbols should be interpreted as:

ω = angular frequency of the light

ϵ = dielectric constant for the electron-hole interaction ($= \epsilon_s$ for the continuum edge).

a α = Bohr radius calculated with the effective mass and dielectric constant for the exciton states at the continuum edge.

β_0 = lattice vector in direction of polarisation (Z axis)

$Z_{vc}(\beta_0)$ = The Z component of the "two-centre" matrix element between the valence and conduction bands.

n = refractive index at the frequency of the light.

Knox states earlier that he is calculating oscillator strengths

per electron. This means that if we are considering bands with spin degeneracy we should multiply (6.1.1.) by 2. We wish to use the intensity of the continuum edge for the zero phonon part at $0^{o}K$. Using our figures of $D_1 = 4.48$ and $D_2 = 3.03$ for that point, (6.1.1) should be multiplied by $e^{-(4.48+3.03)}$, to allow for phonon coupling.

From our R.T. fit we predicted for $\perp$ absorption a continuum edge absorption at $0^{o}K$ of $12.6cm^{-1}$. We therefore obtain

$$Z_{vc}(\beta o) = \frac{(12.6 \times 3 \times (21\times10^{-8})^4 \times 3\times10^{10} \times 2.2)^{\frac{1}{2}}}{4\pi \times 5.5\times10^{15} \times 11.3\times2\times e^{-7.51}} \frac{1}{2\times4.7\times10^{-8}} = 2.5 \text{ Å}$$

For $//^{u}$ absorption

$$(Z_{vc}(\beta_v) = .68 \text{ Å}$$

These are both quite reasonable two-centre matrix elements. The anisotropy of ϵ and a have been ignored, but should be fairly small (see sec. 3.4).

A similar calculation for Cu_2O yields $Z_{vc}(\beta o) \approx 0.1$ Å (The exponential factor due to phonon coupling is quite small in Cu_2O). (Knox (1963) p.122 obtains a value of .29Å but assumed an incorrect value for the unit cell volume). The difference between the magnitudes in Cu_2O and SnO_2 might be accounted for by a difference of symmetry of the atomic states from which the bands are derived. In SnO_2 the transition probably corresponds to oxygen 2p → tin 5s while in Cu_2O it is copper 3d to copper 4s (Elliott 1961), the latter being forbidden by the atomic spectra selection rules on Δl .

6.2 Defect Absorption

6.2.1. Nature of Defects Responsible

The object of this section is to build up the theory to explain the observed absorption at the tail end of the absorption edge, of our nominally 'pure' crystals and possibly also to help to understand the absorption of chromium doped crystals. For the 'pure' crystals, the necessity for some explanation of the absorption tail independent of the absorption edge was already suspected, especially for absorption $//^{a}$ to the c axis, but the publication of the results of Summitt, Marley and Borrelli (1964) made the conclusion inescapable for both polarisations. Their results agreed with ours for high absorption coefficients, but their 'tail' was much steeper, causing much smaller absorption coefficients in this region.

Earlier results of some of the above authors, Marley and MacAvoy 771 (AFCRL-62-1962), show results more similar to our own. Unfortunately in their later results they do not state the history of the crystals used. However study of a further paper by the Corning group(Marley and Dockerty 1965) is illuminating, in that it gives details of the treatment given to various crystals used in electrical measurements. The method of growth of their crystals is basically similar to ours (see 4.1), and so their results and conclusions relating carrier concentration, type of defect and crystal history in 'pure' crystals are probably relevant to us. They concluded (p. 307) that the defect responsible for their donor centres is probably Sn ion vacancies. This conclusion was based on their results that samples annealed in oxygen at successively higher temperatures contained successively more donors. They ruled out the possibility of oxygen interstitials because of "structural considerations" i.e. the large size of the oxygen ion. The conclusion also agrees with the explanation, to be outlined below, of our optical results and which was being formulated

before the above paper was published.

The principal arguments from the present work concerning the type of defect are:-

(1) The unlikeliness of impurities.

Different crystals, not all from the same batch, show remarkably constant extrinsic absorption. Contamination by impurity atoms would be more likely to vary from batch to batch. This argument is reinforced by the early Corning group results giving a similar absorption. There is even less likelihood of the same impurity arising in the two independent sources of crystal, and the purity of the Corning group's starting material is claimed as being very high (5p.p.m. Marley and Docherty 1965, 10 p.p.m. Marley and MacAvoy 1961 J. Appl. Phys. 32 2501).

(2) The presence of a peak in the absorption. (This actually occurs in the parallel polarisation at nitrogen temperatures, and can be inferred by substracting the absorption due to the absorption edge in other cases.) This implies that the conduction band continuum is unlikely to be involved, as, being a wide band, it would be unlikely to give rise to such a peak. (The analogy of band to band absorption with the photo-ionizing of the hydrogen atom is not valid here. The hydrogen absorption shows a peak at the continuum edge, but the photon energy is then equal to the ionization energy. In a solid the photon energy is much greater than the exciton binding energy).

(3) The absorption does not change its wavelength (within experimental error) between R.T. and liquid nitrogen temperatures whereas the absorption edge does. This implies that of the initial and final states, one cannot be closely related to the conduction band, and the other to the valence band (by way of e.g. being a shallow hydrogen-like donor or acceptor). If they were, the energy of the absorption would change in the same way as the change

of the energy gap.

(4) The difference in shape of the absorption for the two polarisations can be explained fairly well numerically on the theory to be outlined in 6.2.6. provided the absorption is not concerned solely with a single atomic site. (The latter would be the case, e.g. for an internal transition in an impurity ion). This argument is not conclusive, because in the case of chromium doping the two polarisations have different shapes and the transition is believed to be an internal one. In other words the agreement could be coincidental. However the reasonable quantitative agreement is still there for the defect absorption.

If these arguments are taken as valid, (2) shows that the conduction band continuum is not involved, and (4) that a single site is not involved. It would therefore seem that the valence band (or else a subsidiary defect level closely related it) must be one (the lower) of the states. (1) shows that there is no impurity and so all the relevant states must derive from atomic oxygen p states or atomic tin s states (in the tight binding approximation), i.e. they must be related to the valence or conduction bands. (3) shows that if the valence band is involved, states closely related to the conduction band cannot be involved. So it would seem likely that the transitions concerned are from the valence band to defect states probably related to the valence band.

The only other obvious possibility is that the transition might be from a deep lying conduction band defect state to a much shallower excited state. This possibility would seem most unlikely, because any excited defect state associated with the conduction band would almost certainly be hydrogenic with dielectric constant close to the static value and effective mass close to that of the conduction band. This would make it a very shallow state and over the energy range involved in the absorption (several tenths of an e.v.) it would

be inseperable from, and insignificant conpared with, the continuum states. Another feature of absorption to such an unlocalised state would be almost isotropic broadening, which is not observed. This type of absorption is thus ruled out.

6.2.2. Type of defect

Leaving aside groups of defects, (such as dislocations,) and impurities, simple defects are vacancies (anion or cation), interstial ions (anion or cation) and an anion in a cation site or vice versa. For compounds with a high degree of ionicity, the latter possibility is energetically most unlikely. Ion vacancies can either occur in pairs (Schottky defects) or as a result of non-stoichiometry. If the latter, over-all charge neutrality requires extra electrons in the vicinity of an anion vacancy and extra holes in the vicinity of a cation vacancy. In a similar way interstitial ions are either paired with a vacancy (Frenkel defects) or arise from non-stoichiometry. SnO2 has very high (but unknown) melting and boiling points. This probably implies large energies of formation of Frenkel and Schottky defects, and that even at the crystal growing temperatures of $\sim 1400^{\circ}C - 1500^{\circ}C$, these stoichiometric defects should have low concentrations. Schulman and Compton (1963) p. 12 state that at the melting point of alkali halides there are about 0.1% vacancies, and in Marley and Dockerty's air quenched SnO_2 crystals there are about 0.01% vacancies. Allowing for the rapid change in concentration with temperature, a short extrapolation from their growing temperature ($\sim 1550^{\circ}C$), would give a temperature for about 0.1% vacancies of $\sim 1700^{\circ}C$. This is considerably less than the estimated melting point. This might suggest that the concentration of stoichiometric defects (Frenkel or Schottky) would be considerably less than the carrier concentrations observed by Marley and Dockerty, and that therefore some other defect must be responsible for the free carriers. We have thus narrowed the likely defects

to single vacancies and single interstitial atoms. A tin interstitial or an oxygen vacancy would seem likely to lead to excess electrons and so to states linked to the conduction band. Thiswould be contrary to our previous analysis of the experimental evidence. An oxygen interstitial would seem unlikely because of the large size of the oxygen ion. (On the other hand an interstitial oxygen might be neutral). A tin vacancy would seem to be the most likely defect.

6.2.3. Defect Energy Levels

It will thus be assumed that the predominant defects are tin vacancies. In terms of colour centres this gives rise to trapped-hole color centers (Schulman and Compton 1963 p.139). These authors state (p.158) that apart from V_K and H centres very little is known about the confwiguration of the centres responsible for the trapped-hole absorption bands (compared with trapped electron (F centre) absorption bands). Their book is almost entirely about the alkali halides, so in spite of the vast literature on colour centres in alkali halides, it would appear not to be very fruitful to study this literature in detail and this has not been done. (For different reasons neither the V_K nor the H centre seem probable: X rays are required to produce the V_K centres and anyway in SnO_2 the high mobility conduction band would quickly make then disappear; the large size of the oxygen ion would make the H centre unlikely to occur).

A picture of the centre caused by the tin ion vacancy is as follows. Tin has essentially 6 oxygen neighbours (in fact 2 are slightly nearer than the other 4). In the neutral centre, therefore, these 6 ions between them will have 4 electrons too few (the valency of tin). The absense of the tin ion will raise all the oxygen p levels. (On a simple electrostatic picture the order of magnitude of the energy changes involved can be obtained by considering the quantity $\frac{e^2}{r}$ where r is an interionic distance. This equals about 7 e.v.)

This energy change probably means that all the p states of these oxygens should be considered as isolated levels, and not part of Bloch states. At the centre there are then 6 oxygens each with 6 (originally degenerate) p states. These wave functions will mix a little, forming up to 36 close levels. Of these 32 will be occupied and 4 unoccupied (at an unionised site). It is now easy to see how the same centre can give rise to both an optical impurity absorption band even at low T (with electrons from the valence band) and conduction electrons in the electrical work.

Optical absorption can thus be seen as putting one more electron into the p states of the centre and leaving a hole in the valence band. Alternatively it may be more accurate not to consider the hole as being in the valence band but as being trapped in a unit cell neighbouring the defect. In this case the accurate description of the transition may be as an internal transition within the centre, an electron transfering from a p state of a neighbouring unit cell into a (raised) p state of the unit cell containing the vacancy.

6.2.4. Relation between absorption and number of centres

Schulman and Compton (p. 56 - 57) quote the following relation due to Dexter, which is an improvement on the widely used classical relation:-

$$N f = 0.87 \times 10^{17} \frac{n}{(n^2+2)^2} \kappa_{max} W.$$

N = number of centres/c.c.

f = the "oscillater strength"

n = refractive index at peak absorption

W = the width of the absorption band at the points where the absorption is half the maximum, in e.v..

κ_{max} = the peak absorption coefficient in cm^{-1}

Taking the absorption // to the c axis, and putting (for our samples)

$n = 2.2$, $K_{max} = 40\ cm^{-1}$, $W = .5$ e.v.

$$N = \frac{0.87 \times 10^{17} \times 2.2 \times 40 \times .5}{(2.2^2+2)^2} = \frac{8}{} \times 10^{16}\ cm^{-3}.$$

(From the ratio calculated later the value for perpendicular absorption is $1.3 \times 10^{17} cm^{-3}$)

The oscillator strength, f, is a theoretical quantity which corresponds in classical theory to the number of electrons per centre involved. If there is more than one possible transition an electron can make then in many circumstances the sum of the f numbers for all the transitions equals one, and correspondingly if there is one predominant transition it will have $f \simeq 1$ (see Dirchburn "1952"). Calculations on F and other centres in the alkali halides generally give $f \simeq 1$. (Schulman and Compton). For our centres there are four possible levels to which an electron can jump, assuming an unionised centre. One can say there are four holes, any of which can jump into the valency band. Assuming an analogy between electrons and holes, one can say there are 4 electrons involved, and that therefore Σf should equal 4. Thus if the observed transition were the only important one,

$$N \simeq 2 \times 10^{16}\ cm^{-3}$$

However it is very likely that there are more transitions further into the U.V. due to transitions from lower lying valence bands or from the filled states of the centre. Also it may be that one of the unoccupied levels is considerably lower than the others, and that the transitions due to the others lie further into the U.V. So the above estimate of f is likely to be an upper limit, and the value of N a lower limit.

Comparison with the donor concentrations obtained by Marley and Dockerty shows that a donor concentration of the above figure corresponds to a sample equilibriated in oxygen at about 1200°C. Our crystals were grown at about ~1400°C, but the effective quenching temperature is unknown. 1200°C might

be a reasonable figure, the cooling rate being of the order of 10°C per minute. (A difficulty arises if the effective annealing temperature is much below the growing temperature, because it would then be reasonable to expect the effective annealing temperature to be thickness dependent. No significant thickness dependence of the defect absorption intensity was observed). Analysis of electrical measurements made on our crystals is called for.

6.2.5. Density of Defects from Electrical Measurements

A 'donor' or 'defect' density was used above that Marley and Dockerty derived from electrical measurements. Three assumptions used to derive there results should be investigated further before their density can be used with confidence. These will be briefly listed as:

(1) A degeneracy of 2 was assumed for the donor states. For the defect postulated here this would seem open to question. (A different degeneracy would also affect their density of states effective mass of 0.22 m).

(2) The theory they assumed of how the activation energy might vary with donor concentration seems dubious. No allowance is made for the varying number of donors that are ionised at different temperatures, which would seem likely to lead to an activation energy varying with temperature.

(3) They assumed a temperature independent activation energy. Quite apart from point(2), the defect considered here would seem to have its energy levels mainly linked to the valence band. Thus as the band gap varies with temperature, so would the activation energy.

6.2.6 Interpretation of Defect Absorption

The defect absorption overlaps the absorption edge, the maximum overlap being for perpendicular absorption and for R.T. (rather than lower temperatures). The most promising data to start interpreting is for parallel absorption at nitrogen temperatures, where the absorption actually goes through a maximum around 3.4 e.v. Following the above discussion we try an interpretation based on the idea that the main transition involved in the defect absorption is that of a valence band electron mainly localised in a cell neighbouring the cell containing the defect (probably a tin vacancy), to an excited defect state (probably a 2p state of an oxygen atom neighbouring the vacancy).

The theory we shall use is the theory developed by Eagles (1963) for transitions between two small polaron bands. The theory is similar to theories developed for defects such as F centres, and although it might be preferable to use such a latter theory, the present author is more familiar with Eagles' theory and it is thought to be essentially similar.

We shall start by applying the theory in its simple form and discuss complications later. The optical matrix element for a transition between states centred on neighbouring unit cells, $\varphi_\alpha(\underline{r}-\underline{R})$ and $\varphi_\beta(\underline{r}-\underline{R}-\underline{G})$ is given by Eagles equation (43) as being proportional to

$$\int \varphi_\alpha^* (\underline{r}-\underline{R}) \frac{\partial}{\partial x} \varphi_\beta (\underline{r}-\underline{R}-\underline{G}) \, d^3\underline{r} \qquad (6.2.1)$$

where G is the lattice vector between the neighbouring cells and the light is polarised in the x direction. For symmetry reasons it is likely that (6.2.1) will be zero when x is perpendicular to $\underline{G}$. If this is so, perpendicular polarisation will excite transitions between neighbouring cells with $\underline{G}$ along the a or b axes and parallel polarisation will excite transitions between cells with $\underline{G}$

along the c axis. Eagles shows that these transitions have different phonon coupling, and so different shapes, and his theory predicts the shapes (assuming the continuum polarisation model). Strictly speaking the parallel and perpendicular transitions might have a different basic energy difference for the transition, but this is only likely to be important for a very highly localised valence band in which the created hole stays for an "appreciable" time on the site it starts on. The results given below indicated there is no experimental evidence for any energy difference.

Eagles shows that the integrated absorption associated with m phonons absorbed and p+m emitted is proportional to

$$H_{p,m} = \frac{S^{2m+p}}{(m+p)!\ m!} (\bar{n}+1)^{m+p} (\bar{n})^{m} \exp\left[-(2\bar{n}+1)\ S\right]$$

which is the same situation as for transitions between wide and narrow bands considered previously, except that D has been replaced by S. S is the same parameter as occurs in Eagles (1966) nearly small polaron theory (dealt with in 3.3) as S_o. We called the parameter S_{o1} for perpendicular polarisation and S_{o2} for parallel polarisation and found in 6.1 their values to be given by $\sum S_{o1}\hbar\omega = .90$ e.v. and $\sum S_{o2}\hbar\omega = .548$ e.v. (The summations are over the phonon branches). Using the same method as before for determining the ratios for the S of the different phonon branches and for combining the two low energy phonons we arrive at S values for the individual branches and polarisations.

Table 6.2.1

Defect // Absorption 90°K

High Energy Phonon $S = 4.5$ $\bar{n} = 10^{-5}$

1 4.5 10.1 15.2 17.1 15.4 11.5 7.4 4.2 2.1

Low Energy Phonons $S = 3.1$ $\bar{n} = .0032$

1 3.1 4.8 5.0 3.9 2.4 1.24 .55 .2

.01

.01

	1	3.1	4.5		10.1		15.2		17.1		15.4		11.5		7.4		4	2
		3.1		14		31.4		47		53		48		36		23	13	
			4.8		21.6		48.5		73		82		74		55		36	20
				5		22.5		50.5		76		86		77		57	37	
					3.9		17.5		39.4		59		67		60		45	29
						2.4		10.7		24		36		41		37	28	
							1.2		5.6		12.5		19		21		19	14
								.5		2		6		8		9	9	
									.2		.9		2		3.		3	3
	.01	1	3.1	9.3	19	35.6	56	82	109	135	155	170	176	174	163	147	127	107	88	68
Scaling factor X.745		.7	2.3	6.9	14.2	26.5	41.7	61	81	100.5	115	127	131	130	121	110	95	80	$65\frac{1}{2}$	$51\frac{1}{2}$
Intrinsic absorption																	1	12	$25\frac{1}{2}$	
Total																	96	92	91	
Room Temp. Energy (e.v.)	.9	2.3	5.1	10.6	18.7	30.6	45	62.3	80	97	110	119	123	121	115	104	93	80		

3.165 3.39

6.2.7 Parallel Absorption

For parallel polarisation we used for the high energy phonon $S_{o2} = 4.5$ and for the combined lower energy phonons $S_{o2} = 3.1$ (These rounded numbers actually give $\sum S_{o2} \hbar\omega = .542$ e.v.- near enough to .548 e.v.). In a similar way as for the absorption edge we give in Table 6.2.1 the calculation of the combined H_p for $T = 90^oK$. For narrow bands, and provided there are not too many causes of broadening such as phonon dispersion, the individual $H_{p,m}$ should be fairly narrow. We assume they are just narrow enough to iron out any individual peaks. The shape of the absorption is then given by the H_p directly, with H_o being located at the basic energy difference for the transition. The curve obtained has been fitted to the observed absorption (for sample S.8) in fig. 6.2.1 (lower curves). The only two fully adjustable parameters are the intensity of the whole absorption and its energy. A third slight adjustment was made, and that was to substract a small absorption ($\hbar\omega K = 7$ ev.cm^{-1}) from all the experimental points, because at the low energy end there appeared to be another small absorption due to a different cause. Subtracting a constant amount was the simplest way of dealing with it - more refined methods might be possible. In any event the absolute zero of absorption is not an accurate experimental quantity.

The fit is seen to be good (mostly within experimental error) up to 3.45 e.v., especially considering the few "adjustable" parameters. Qualitatively the divergence above 3.45 e.v. can be explained by the intrinsic absorption edge, but in fact this would not seem to account for all of it. Unfortunately absorption measurements on purer crystals have

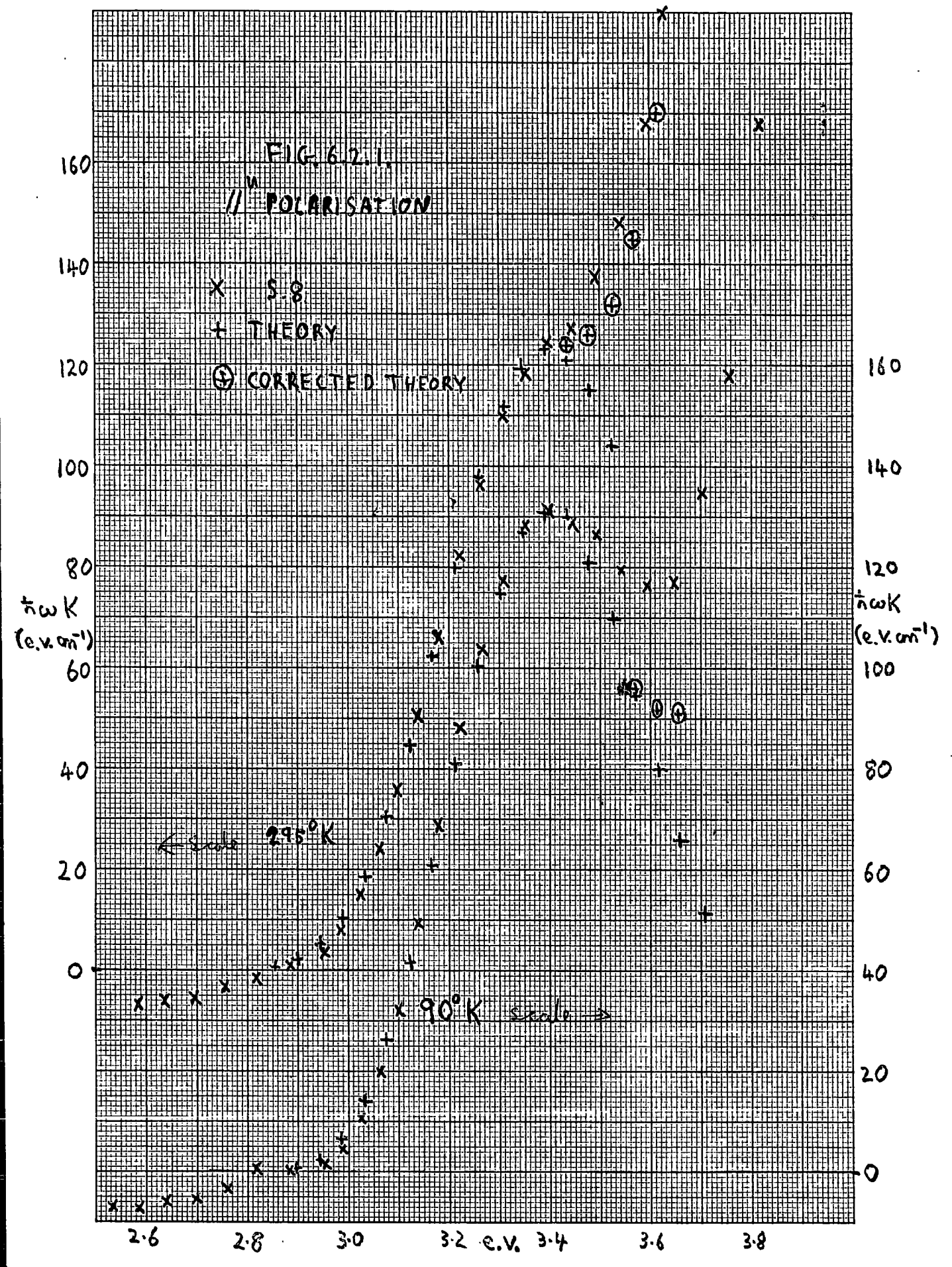
FIG. 6.2.1.
// POLARISATION
X S.S.
+ THEORY
⊕ CORRECTED THEORY
ħω K (e.v. cm⁻¹)
ħω K (e.v. cm⁻¹)
295° K ← scale
90° K scale →
e.v.
2·6
2·8
3·0
3·2
3·4
3·6
3·8
160
140
120
100
80
60
40
20
0

not been published for T below R.T., and so we cannot directly make numerical allowance for the intrinsic absorption. Neither are the theoretical results for the intrinsic absorption sufficiently accurate to give a meaningful numerical comparison. However, the 90°K perpendicular absorption can be made use of. If the best defect $\perp$ absorption theoretical fit is extrapolated and abstracted, and the result divided by 30 we have an estimate of the intrinsic parallel absorption. Extrapolation errors are not very important because they are divided by 30. This is done for three points as shown. The results indicate there is still some absorption unaccounted for. This will be commented on later.

At R.T. the general position, and to a lesser extent the magnitude, of the absorption is remarkably unaltered from 90°K. (The intrinsic absorption has changed considerably). The detailed shape has, however, changed. The absorption at low absorption levels has increased, and at high levels has reduced; i.e. the "wings" have grown at the expence of the peak. This is exactly what would be expected on Eagles' theory, which predicts an increase in optical absorption assisted by phonon absorption, while the integrated optical absorption remains constant. We have calculated the H_p for R.T. in the usual way in table 6.2.2 and put the results in table 6.2.1 for comparison. With the same scaling factor and basic energy difference as for 90°K, we plot the results together with the experimental points in fig. 6.2.1 (upper curves). In passing, it is interesting to note that although the theory gives results for most of the peak not very different from 90°K, the numbers in the calculations are very different;

Table 6.2.2

Defect // absorption R.T.

S = 4.5 $\bar{n}$ = .0308

		1	4.64	10.8	16.7	19.3	17.9	13.9	9.2	5.3
	.139	.64	1.50	2.3	2.7	2.5	1.9	1.3	.7	.4
.01	.045	.10	.16	.2	.2	.1	.1			
.002	.005	.01	.01							
.012	.189	1.75	6.31	13.3	19.6	21.9	19.9	15.2	9.9	5.7

S = 3.1 $\bar{n}$ = .21

			1	3.75	7.04	8.8	8.24	6.2	3.9	2.1	1
		.65	2.44	4.58	5.72	5.35	4.04	2.5	1.4	.6	.2
	.212	.79	1.49	1.86	1.74	1.31	.82	.4	.2	.1	
.046	.172	.32	.40	.38	.28	.18	.10				
.027	.052	.07	.06	.05	.03	.02	.01				
.008	.009	.01	.01								
.081	.445	1.84	5.40	10.62	14.81	15.6	13.2	9.1	5.5	2.8	1.2

Table 6.2.2. Cont'

	.5		1.1		.2		2		2		1		1					-
.78		2.8		6		9		10		9		7		4		2		1
	3.2		11.6		24		36		40		37		28		18		10	
1.02		9.4		34		72		106		118		107		82		53		31
	2.0		18.5		67		141		208		232		210		161		105	
.18		2.8		26		94		197		290		324		294		220		147
	.2		2.9		27		98		208		306		342		310		237	
.01		.2		$2\frac{1}{2}$		23		83		175		258		289		260		200
			.1		2		16		57		121		178		200		181	
						1		10		35		73		108		120		110
									5		18		37		55		61	
										2		8		16		20		26
													3		6		10	4
2	5.9	15.3	33.2	69	122	199	293	406	520	630	715	777	800	790	750	680	604	520

Scaling factor = exp(- .42 x 3.1 - .062 x 4.5) x .745 = .206 x .745

.3	.9	2.3	5.1	10.6	18.7	30.6	45	62.3	80	97	110	119	123	121	115	104	93	80
Intrinsic absorption													1	3	11	28	521	90
Total													124	124	126	132	145	170

e.g. the combined exponential factor differs by a factor of .206.

The fit up to 3.4 e.v. is seen to be remarkably good considering that there was not a single adjustable parameter. (The same small constant absorption was subtracted from the experimental points). At R.T. we can make a better allowance for the intrinsic absorption. Unfortunately the low level parallel absorption of Summitt, Marley and Borrelli (1964) on purer crystals is not available with sufficient accuracy, but we can assume a factor of 30 between the absorption intensities for the two polarisations and use either their results for perpendicular absorption, or (less accurately because of defect absorption) our own similar results or else our own theoretical results (fitted to the whole range of the edge). The differences are small, and we used Summitt, Marley and Borrelli's results and added the resulting absorption to our theoretical defect absorption and obtained the upper theoretical curve shown. It is seen to agree quite well with our experiment, but there is apparently still some absorption unaccounted for. (The amount is not much more than the likely experimental error in this particular part of the spectrum). The amount is less than, but of the same order as, the unaccounted part at 90°K.

The value of the basic energy difference in the transition is 2.90 e.v. An estimate of the error might be $\pm$ 0.05 e.v., and the same energy difference is used for perpendicular absorption.

6.2.8 Perpendicular Absorption

Less of this absorption is visible for two reasons. First the intrinsic absorption is thirty times as great, and, second, the

peak appears to be at higher energies. At 90°K there is enough that is not swamped by intrinsic absorption to make a numerical fit worthwhile.

We first used parameters derived from theory as before. (1st part of Table 6.2.3) We used $S_{01} = 7.3$ for the high energy phonons and $S_{01} = 5$ for the combined low energy phonons. (These numbers actually give $\sum S_{01}\hbar\omega$ = .88 e.v. instead of .90 e.v.). After applying a scaling factor the results are plotted in fig. 6.2.2 together with the experimental points (after subtracting 5 e.v. cm^{-1}). The same basic energy difference (of 2.90 e.v.) is used as for parallel absorption.

The fit can be improved, by taking $S_{01} = 6.8$ and 4.7 (2nd part of Table 6.2.3) for the high energy phonon and low energy phonons respectively, as shown in fig. 6.2.2. For the perpendicular absorption we cannot use the trick we used for the parallel absorption in order to allow for the intrinsic absorption edge. A qualitative estimate of the likely form of the intrinsic absorption indicates there may be some absorption unaccounted for, like there was for parallel absorption.

The R.T. perpendicular absorption has not been evaluated. The greater swamping by the absorption edge would lessen any information that might be obtained, but on the other hand intrinsic absorption can be well allowed for. It might just be worth doing for any further study. Qualitatively it appears to be related to the 90°K absorption in the same way as the parallel absorption.

Discussion

The departure of S values from Eagles' theory is small but

Table 6.2.3

Defect Absorption ⊥ Polarisation 90°K

S = 7.3

	1	7.3	26.5	64.8	113	159	193	200											
S =	5	$\bar{n}$ = .0032																	
.016	1	5	12.6	21	26.3	26.4	22	15.7	9.8	5.4	2.7								
	1		7.3		26.8		54.8		113		159		190		200				
		5		36.5		133		324		565		80800		960		1000			
			12.6		92		335		816		1420		2000		2430				
				21		153		558		1360		2370		3340		4000			
					26.3		192		700		1700		2970		4180				
						26		193		700		1710		2980		4200			
							22		161		585		1430		2480				
	1	5	19.9	58	145	312	594	16		115		420		1020		1800			
									10		71		260		640				
							1090	1800	2740	3940		40		140		350			
												5340	20		70				
													6870	10		30			
														8450	10,000	11,400			
	.0	.1	.3	.9	2.3	4.9	9.2	17	28	42.6	61.3	83	107	431	156	177			

Table 6.2.3 Cont'

	S = 6.8	1	6.8	23.1	52.5	89	123	140	136	116								
$\bar{n}$ =.0032	S = 4.7	1	4.7	11.1	17.4	20.5	19.3	15.1	10.2	6	3							
	1		6.8		23.1		52.5		89		123		140		136		116	
		4.7		32		109		247		420		580		660		640		540
		4	11.1		75.5		256		580		990		1370		1550		1510	
				17.4		118		402		910		1550		2140		2440		2360
					20.5		139.5		473		1080		1820		2520		2870	
						19		131		446		1010		1720		2380		2700
							15		102		350		790		1340		1860	
								10		70		240		540		910		1250
									6		40		140		320		530	
										3		20		70		160		[illegible]
													10		30		70	
	1	4.7	17.9	49.4	119	246	463	790	1250	1850	2580	3420	4270	5130	5900	6540	6960	7150
	0	.1	.4	1.2	2.9	6	11.2	19.2	30.4	45	62½	83	104	124½	143	159	169	174

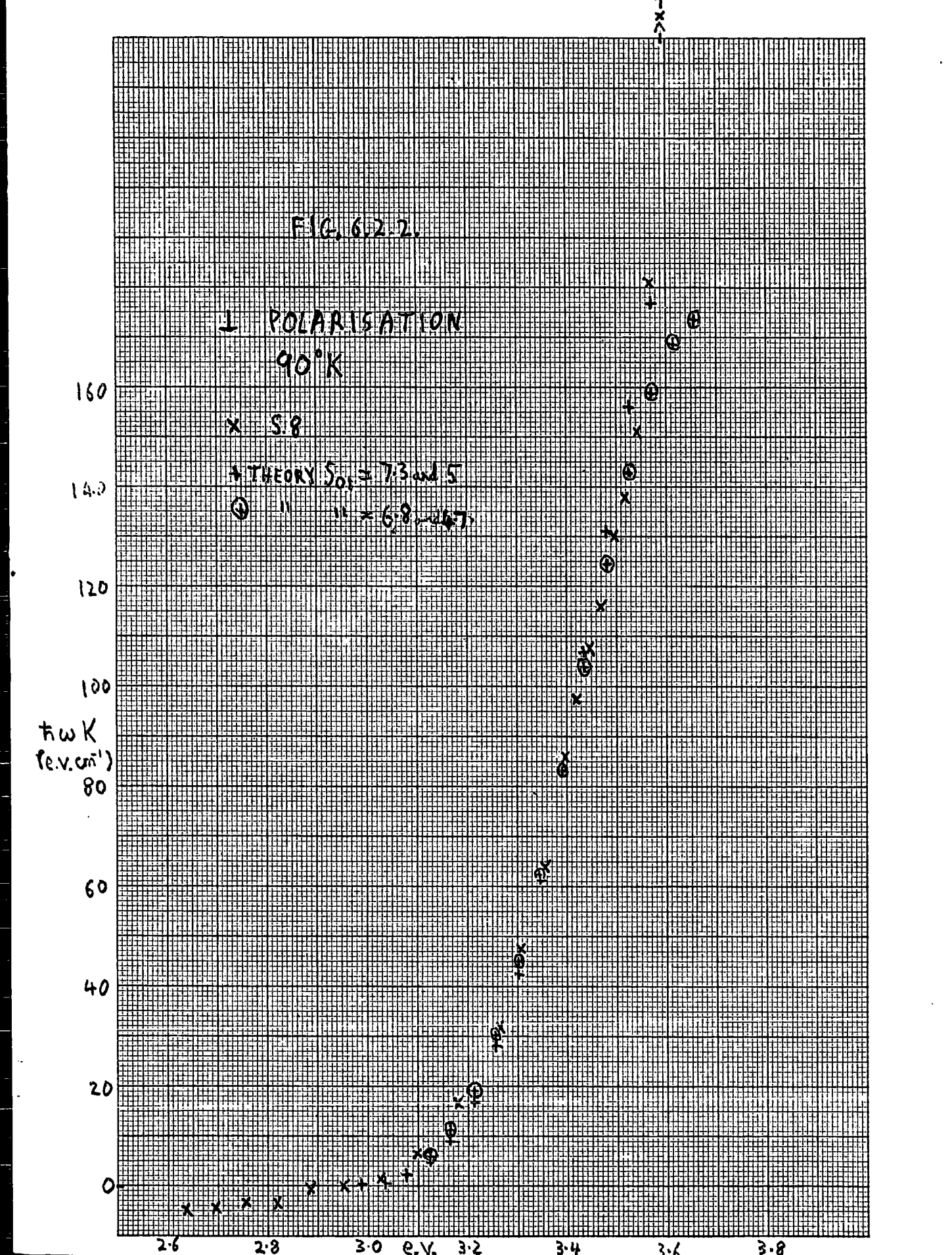
FIG. 6.2.2.
⊥ POLARISATION
90°K
× S·8
+ THEORY $S_{01} = 7·3$ and 5
⊕ " " $= 6·8$ ~4·7
160
140
120
100
80
60
40
20
0
ħω K
(e.v.cm⁻¹)
2·6
2·8
3·0
e.V.
3·2
3·4
3·6
3·8

significant. If the S for both polarisations were smaller than theory predicted, but they were in the correct theoretical ratio, then two simple explanations would be possible. Either the experimental parameters (derived from the phonon spectrum) used to obtain the theoretical magnitude could be in error, or the continuum polarisation model could be at fault. It might be that smaller S values for parallel absorption could lead to a sufficiently good fit that it would be reasonable for the ratio of the S values for the two polarisations to agree with theory, but it seems unlikely. (The theoretical ratio depends only on the axial ratio, $^{c}/a$). Assuming the ratio does not agree with theory, two types of explanation seem possible. First the continuum polarisation model may be at fault (although it would seem to lead more easily to magnitude errors). Second, the error may come from assuming a 'narrow valence band'. The valence band states in unit cells neighbouring the defect may either form discrete levels in the forbidden band close to the valence band, or else the defect may just distort the valence band in its neighbourhood without making discrete states. (It might be fruitful to investigate this point further, either theoretically or experimentally). If there are discrete states the "narrow band" theory should apply better than if there is a band. If there is a band, we have seen in dealing with the absorption edge that nearly small, rather than small, polaron theory should be used. Eagles has not considered transitions between small and nearly small polaron bands, so we cannot estimate the effect numerically. We can, however, look at the opposite extreme, and consider the effect on S if the valence band were "wide". In this case

S becomes D, and D is of the same order as S but is isotropic. Qualitatively, therefore, we can picture the experimentally observed departure of the ratio of the S values for the two polarisations from the theoretical value as being due to the finite width of the valence band making S more isotropic. On either the discrete or band picture of the valence states of the neighbouring unit cells, we can speculate that the unaccounted for absorption of the parallel absorption (which very likely also occurs for perpendicular absorption) is due to transitions from the lower parts of the top valence band (or even from lower valence bands) to the excited defect.

A final factor will be extracted from the analysis. This is the ratio of the integrated absorption for the two polarisations. From the "f sum rule" these might be expected to be roughly equal, but certainly not exactly so. We used the integrated absorption earlier to estimate the defect density, so the ratio indicates the difference in the estimate that would be obtained using the two polarisations. We obtain a rough figure for the ratio by assuming the integrated absorption is proportional to $S^{\frac{1}{2}}$ times the maximum height. We obtain:

$$\frac{\perp \text{ absorption}}{//^{n}\text{absorption}} = 1.65$$

The greatest experimental uncertainty arises from the best S values for perpendicular absorption. If these values are lowered, the ratio is substantially lowered.

6.3 Absorption of Antimony Doped Crystals

6.3.1. Power Law for Free Carriers

Summitt and Borelli (1965) performed rather more extensive measurements than we did in the wavelengths range $\cdot 5 < \lambda < 6\mu$ and carrier concentration range $10^{17} - 2 \times 10^{19}$ cm^{-3}. They found that, for each specimen, K varied as λ^{ν} where ν varied for different crystals from 2.9 to 3.3. At temperatures down to 50°K no detectable change was found, and at 900°K ν reduced by about 0.3 and the absorption magnitude increased by a factor of about two. They combined their measurements by plotting log (K/Ne) against λ, where N_e was found from Hall effect measurements using a formula with a constant factor of $\frac{3\pi}{8}$. A straight line through the points gave $K = 1.72 \times 10^{-18} N_e \lambda^3$ (6.3.1.), with most of the points lying within about 40% of that line. The ratio of $\parallel$ absorption to $\perp$ absorption is given as 1.25. The high carrier concentration samples had Sb doping, and the rest only had defects to provide the carriers.

Our own results are consistent with these results. Using (6.3.1.) our S.19 has a carrier concentration of 3.6×10^{18} cm^{-3} and S.18 has a concentration of 8.3×10^{18} cm^{-3}. Taking the lower of the two curves for S.15 in fig. 5.3.1. we obtain an absorption of 150 cm^{-1} at 0.7μ for the average of the two polarisations. (6.3.1.) then predicts a concentration of 2.5×10^{20} cm^{-3}, (which is 13 times the heaviest doping of Summitt and Borrelli), and this can be compared with our measured value of 1.5×10^{20} cm^{-3}. If the Hall factor of $\frac{3\pi}{8}$ were omitted from Summitt and Borrelli's calculation, the predicted value becomes 2.15×10^{20} cm^{-3}, which is moderately satisfactory agreement. Our measured ratio for the two polarisations agrees with Summitt and Borrelli, as does the absence of change at low temperatures.

Summitt and Borrelli applied Visvanathan's (1960) optical mode

formula (2.4.4.) at $\lambda = 3\mu$ and used $\omega_L = 3\Theta \times 10^{14}$ sec.$^{-1}$, $n = 2$, $\epsilon_\infty = 4$, $\epsilon_s = 25$ and $m^* = .14$ m. They appear to have done the calculation for low temperatures (where $\beta \gg 1$) and obtained $\alpha/N_e = 9 \times 10^{-17}$ cm^2, compared with 4.6×10^{-17} cm^2 from (6.3.1.). The straightforward formula cannot, however, be made to fit because it predicts a $\lambda^{2.5}$ law instead of λ^3; so that although we disagree with some of the parameters used, there is not much point in merely substituting better ones. We do, however, believe that optical mode scattering is the most important and we will return to it after discussing a number of factors. Impurity absorption will be considered at the end and shown unlikely to be important. The following points will now be discussed:

(1) The varying effective mass.

(2) The effect of electrons in donor states.

(3) The variation of refractive index, n.

(4) The corrections to the simple formula.

(5) Degeneracy.

(1) Effective mass

Examination of the origin of Visvanathan's formula (2.4.4.) shows that, although the absorption apparently varies as $\left(\frac{1}{m^*}\right)^{\frac{1}{2}}$, there are really three terms that depend on the E-k curve. Using the same definition of the effective m as previously of $\hbar^2 k / \left(\frac{dE}{dk}\right)$, then the terms are:

(a) density of final states varies as km

(b) phonon matrix element varies as k^{-2}

(c) photon matrix element varies as k^2/m^2 (provided the photon energy $\gg$ kT).

m and k refer to the final electron state. The product of these terms is thus k/m, which for a parabolic band varies as $(E/m)^{\frac{1}{2}}$. Therefore in order to correct (2.4.4.) it should be multiplied by a term proportional to $k/mE^{\frac{1}{2}}$,

which is constant for a parabolic band.

Two cases of non-parabolicity will be considered: first polaron effects (from fig. 6.1.1. and table 6.1.1.) and second the finite bandwidth which will be assumed to have a cosine variation (in a spherical Brillouin Zone). The energy range covered by the measurements is about 0.2 - 2.5 e.v. Within this range the polaron effects are important at the low energy end, and the finite bandwidth at the high energy end. The two regimes should merge smoothly to give a reasonably constant correction to the λ power law, except at high energies (say above 1.5 e.v.) where the correction is larger. For simplicity we shall calculate the average over the whole range. So far as the polaron effects are concerned $k/E^{\frac{1}{2}}$ does not vary very much in the range of interest and the main contribution is from m. From table 6.1.1. this is about .82 at 0.2 e.v. compared with nearly 1 at large energies.

The bandwidth (in a spherical brillouin Zone) that corresponds to an effective mass of about 0.3 m_e is about 4.5 e.v., $k/mE^{\frac{1}{2}}$ works out as $(1 - E/E\ max)^{\frac{1}{2}}$ where E max is the bandwidth. At 2.5 e.v. this is .667, and at .2 e.v. it is .98. The two factors together therefore produce a factor of about .56 between 2.5 e.v. and .2 e.v. This corresponds to an increase in the predicted power law of about 0.23.

A more accurate calculation taking into account the true shape of the Brillouin Zone would probably show a bigger effect, because in some directions in k space the bandwidth is considerably less than 4.5 e.v.

(2) Donor States

Marley and Dockerty (1965) showed that for donor concentractions up to about 3×10^{18} cm^{-3} a substantial number of donors were not ionised. (In deriving 6.3.1. Summitt and Borrelli used Hall measurements for N_e, which only measures free carriers). They obtained donor levels of the order of 0.1e.v.

below the band edge. For radiation of greater energy than this these electrons contribute to absorption, but the states to which they are excited are correspondingly lower than for the free carriers. The full effects of this have not been worked out, but a simple way of dealing with this is to use the number of donors, rather than the number of carriers, in the formula. (This should be accurate when the photon energy $\gg$ 0.1e.v.) The absorption measurements at the longest wavelengths are done on the crystals with fewest donors. Summitt and Borrelli's purest crystals had a carrier concentration of 1.1×10^{17}, and from Marley and Dockerty we would estimate about 0.4 of the donors are ionised. (This figure should be treated with caution). This would change the power law(for the whole collection of specimens, rather than individual crystals) by about 0.35.

This factor also explains why the absorption is unchanged at low temperatures, while the carrier concentration of the low donor concentration specimens falls substantially.

(3) Refractive Index

The variation in index over the range is fairly small for pure specimens. However, for doped specimens the free carriers will change ϵ ($=n^2$), and at longer wavelengths will produce plasma effects. The simplest method is to calculate the plasma frequency (for which $\epsilon = 0$) and then ϵ lies on a straight line on a λ^2 plot from $\epsilon = 4$ at $\lambda = 0$ to $\epsilon = 0$ at λ_p, the plasma frequency.

In M.K.S. $\omega_p = \sqrt{\frac{N_e e^2}{m \epsilon \epsilon_0}}$ (ϵ_0 is free space ϵ)

If $N = 10^{25} m^{-3}$, $m = 0.26 \times 10^{-30}$ kg and $\epsilon = 4$,

$$\omega_p = 1.66 \times 10^{14} \text{ sec}^{-1}$$

$$\text{or } \lambda_p = 11.4 \mu$$

Absorption from such a crystal is measured out to a wavelength of about 2 μ.

The refractive index is then about 2% too low, so this effect is small. (As, of course, are any other plasma effects). If very thin crystals were used it would not be so small.

The magnitude of the effect on the power law of this 2% change can be estimated by assuming that the absorption coefficient for any specimen is measured over a range of a factor of 10. The refractive index at the lower end will be about 0.4% low, so the change over the range is 1.6%. This corresponds to a change of about .020 in the power law for an individual specimen.

At the longer wavelengths the change in the power law due to the lattice dispersion may be roughly estimated. Between 3μ and 6μ the refractive index changes by about $4\frac{1}{2}\%$. The change in power law is then about .06. At wavelengths $< 1\mu$ there is a rather smaller change due to dispersion in that region. The intrinsic dispersion might produce an average change in the power law of about .035.

(4) Corrections to the Simple Formula

The term $\left(1 - \frac{\omega_L}{\omega}\right)^{\frac{1}{2}}$ reduces the predicted 2.5 power law. The average ω_L corresponds approximately to $\lambda = 20\mu$, so that at 6μ K is reduced by a factor of .84 and at $\frac{1}{2}\mu$ by a factor of .99. The average reduction in the power law is thus .07. The β terms in (2.4.4.) also reduce the power law, but they are small at R.T. and negligible at low temperatures. They would, however, explain the observed reduction in the power law at 900°K.

(5) Degeneracy

There are two possible effects here which might affect the more heavily doped samples which are degenerate. The first effect is that if the band shape is unchanged by the impurities most of the electrons lie substantially above the bottom of the band. The second effect is that the formula for the Hall effect for non-degenerate specimens contains a mathematical constant, while

for degenerate specimens it is considered to be absent.

The former effect is likely to be largely cancelled out by the impurity states for heavy doping merging with the bottom of the band to form a "strong" impurity band. These extra states will equal the electrons in number and are likely to prevent electrons from having appreciably large energies. The second effect means that the carrier concentration of heavily doped specimens has been over-estimated. The effect of this might be to reduce the "observed" power law by an average of about 0.08 (but not the power law for individual crystals).

Combined Effects

There are two comparisons between theory and experiment that can be made for the power law. The first is the overall power law and the second is that for an individual crystal.

For the overall comparison, effects (1), (3) and (4) increase the theoretical power law from 2.5 to 2.695. Effects (2) and (5) reduce the "observed" power law from 3.0 to 2.57, so that the corrections have been too big too obtain exact agreement between theory and experiment. However the biggest correction (2) is uncertain and might well be smaller. The agreement is satisfactory.

For the individual comparison the theoretical law is increased for effect (3), making a total of 2.715 (but with considerable variation for different parts of the spectrum), while the "observed" law is unaffected at around 3.0. The agreement here is seen to be worse. Two points should be made. Closer examination may show that effect (2) changes the individual law. Experimental error in measuring the individual power law is more than that in the overall law, because the zero error is more important and the wavelength range is less.

Clearly, detailed future work should provide interesting comparisons of theory and experiment.

6.3.2. Magnitude for Free Carriers

We will now compare theory and experiment using what we consider to be the best parameters. We assume the absorption due to the different phonon branches to be additive and obtain the result that the high energy phonon has about 5.8 times the effect of the two low energy ones combined. We calculate for $T = o$ that the high energy phonon contribution at $\lambda = 3\mu$ is about 2×10^{17} N cm^{-1} and adding 20% for the other phonons gives $2.4 \times 10^{-17} N_e$ cm^{-1}. We have used $m^* = .25m$. Summitt and Borrelli found 4.6×10^{-17} N experimentally, but if allowance is made for incomplete ionisation of donors, this becomes about 3×10^{-17} N which is satisfactory agreement, especially if allowance is made for other scattering mechanisms.

Provided T is fairly small and we consider photon energies for which the correction terms in Visvanathan's formula are small, the temperature dependence is given by $\frac{e^{\frac{\hbar\omega_L}{kT}} + 1}{e^{\frac{\hbar\omega_L}{kT}} - 1}$. The lower temperature phonons thus show the biggest increase with T, but their contribution is fairly small ($< 20\%$). For simplicity we thus take an average $\frac{\hbar\omega_L}{k} = 880^{\circ}K$. (The largest phonon has $1040^{\circ}K$). At $T = 295^{\circ}K$ the factor is about 1.1, and at $900^{\circ}K$ it is about 2.2. The theoretical ratio between $295^{\circ}K$ and $900^{\circ}K$ is thus in (exact) agreement with experiment. The exact agreement is fortuitons, because when T is very large, K varies at $T^{\frac{1}{2}}$ (Gurevich, Lang and Firsov equation (20)).

6.3.3. Impurity Scattering

One reason why this is unlikely to be very important is that K would be likely to vary with T at low temperatures. In some specimens the reduction in the number of ionized donors at low temperatures might roughly cancel the $(1/T)^{\frac{1}{2}}$ term, but this will not apply to all dopings. From (2.4.5.) the theoretical magnitude

for $N_i = N_e = 10^{18}$ cm^{-3}, Z = 1, T = 295°K, m* = .26m, $\lambda = 1/\mu$ and $\epsilon = 4$ is 0.2cm^{-1}, which is only 8% of the absorption. Larger dopings would raise this figure, but then screening would be important.

6.3.4. Polaron Effects

The total coupling coefficient $\Sigma\alpha$ for the three 'proper' phonons, with ω_c = .28 m, is 1.3. As mentioned in 2.4 calculations using the Feynman polaron have shown that when $\alpha = 3$ polaron resonances are distinctly visible. The reduction of α to 1.3 would seem likely to almost wash them out. The effect might be observable as slight variations in the power law at different wavelengths.

6.3.5. Classical Formula

The classical formula in 2.4.1. leads to $K = 40 \lambda^2 \times 10^{-18} N$ cm^{-1}, where λ is in microns, assuming a mobility of 100 cm^2/ volt cm (Morgan 1966). At $\lambda = 3/\mu$ this is about 8 times the observed value. At higher temperatures, where the classical formula might be expected to be better, the agreement is only a little better because the mobility falls. Higher mobilities or a higher effective mass would improve the agreement.

6.3.6. Absorption Edge

It can be seen from fig. 5.3.6. that the light doping ($\sim 5 \times 10^{18}$/c.c.) of S.14 has almost completely removed the defect absorption. Assuming the defect centres are still present, this can be explained by the defects capturing one or more electron each in an analogous way to the electron affinity of an atom.

One of the interesting points about the heavily doped (S.15) results is that at high absorption levels the $\perp$ polarisation returns to near its undoped position but the $\parallel^u$ polarisation does not. This might be explained as the breaking down of the forbidden nature of the $\parallel^u$ absorption when the lower conduction band states are being mixed with impurity states.

The shift of the absorption of S.15 to lower energies is interesting.

Koch (1964) gave results of film measurements which showed that at high absorption levels heavy doping shifts the absorption to higher energies. This shift was explained on the basis of the conduction band filling up and so reducing the number of empty states for interband absorption. The shift in the opposite direction at low energy might be due to the screening effects of the carriers reducing the long range coulomb interaction of the optical phonons. This would reduce the effective values of $\mathcal{D}$ and shift absorption to lower energies, especially at low absorption levels.

A final interesting point about the absorption edge is the small shift at nitrogen temperature (for S.15). The shift seems to get larger at higher absorption levels and may become the same as for undoped crystals above, say, 500 cm^{-1}. There does not appear to be an obvious explanation of the smallness of the shift.

6.3.7. Application to transparent Electrodes

SnO_2 films are used to make transparent electrodes. We shall now derive the minimum theoretical resistance per square of such films. We arbitrarily assume the minimum transmission permissable at 5000Å to be 1/e, i.e. that Kd is 1. The resistance per square is given by $(\sigma d)^{-1} = (dne/\mu)^{-1}$. From (6.3.1.) we derive $d\,n = \dfrac{10^{18}}{1.7 \times (0.5)^3}$ if Kd = 1. Assuming μ = 100 cm^2/ v. sec. (Morgan 1966) we obtain the minimum resistance as 0.013 ohms per square. Films are likely to have a lower mobility, so it would be difficult to obtain such a low resistance. Also very highly doped material is likely to have a lower mobility. If a film as thin as 0.01 cms is required, a doping of about 5×10^{20} cm^{-3} is needed for minimum resistance.

6.4 Chromium Doped Crystals

The first thing to notice about fig. 5.2.1. is that the peak around 2.3 e.v. is thinner for $\perp$ than $\parallel^{u}$ absorption, which is the reverse of the defect absorption. On the theory given in 6.2. this is an indication that the optical transition is an internal one and does not involve electron states in neighbouring unit cells. The widths of the peaks at half the maximum absorption cannot be accurately determined because of uncertainty about background absorption, but widths of 0.38 and 0.51 e.v. for $\perp$ and $\parallel^{u}$ absorption respectively appear reasonable. The slight differences in the position of the maxima may be related to these differences in widths. The width at half the maximum is, on Eagles' theory, roughly equal to $S\hbar\omega$ and also to the displacement of the peak from the zero phonon transition. Thus if the basic transition energy for the two polarisations is equal, or very nearly equal, the $\parallel^{u}$ peak should be at about 0.13e.v. higher energy. From fig. 5.2.1. this difference appears to be only about 0.055e.v., but it should be noted that if $K\hbar\omega$ had been plotted the $\parallel^{u}$ peak would shift about 0.04e.v. to higher energy while the $\perp$ peak would only shift about 0.015e.v. The observed difference would then become 0.08 e.v.

If the transition is an internal one it is likely to show similarities to chromium transitions in other materials such as ruby. (The colour is very similar to ruby). In that case two peaks would be likely, with one in the blue or near U.V. Fig. 5.2.1. shows some evidence of a second peak, especially for $\perp$ absorption. However, for $\parallel^{u}$ absorption it must be remembered that the defect absorption of S.8 has been subtracted, and that this is larger for $\parallel^{u}$ absorption in the region of interest. This absorption has a peak at around 3.4 e.v. of about 40 cm^{-1}; so that if S.20 has, say, 20% fewer defects then the $\parallel^{u}$ absorption will rise in a similar way to the $\perp$ absorption between 2.9 and 3.3 e.v. and join smoothly onto the points around 3.65e.v. The same 20% less defect absorption for $\perp$ absorption removes the downturn beyond 3.3e.v. (except for the final point, which, apart from any differences in defect absorption, has an exceptional experimental error).

6.5 Refractive Indices (and Multi-phonon Peaks)

6.5.1 I.R. Dispersion

The I.R. dielectric constants derived from the refractive index measurements were shown in figs. 5.4.2 and 5.4.3. Also shown are the theoretical points calculated from the phonon analysis of 5.6. The theoretical points are tabulated in table 6.5.1. The parameters were adjusted to give a good fit, and the fit is indeed seen to be satisfactory. A phonon analysis was first performed without using this data, and that analysis gave the points shown in fig. 5.4.2 for $\perp$ polarisation. It shows that there must have been considerable error in the earlier results; the error should be reduced by forcing agreement with the I.R. dispersion. The discrepancy between the first phonon analysis and the I.R. dispersion for $\parallel$ polarisation was small.

The remaining differences between theory and experiment can be reduced by allowing for the subsidiary (two phonon) peaks at energies higher than the highest energy phonon. The peaks with largest integrated absorption are those from roughly 8.8 to 10μ (see fig. 5.4.3). Fig. 5.4.3 shows our measurements in unpolarised light. Summitt and Borrelli (1965) shows that the absorption ~~for the two polarisations~~ is somewhat different ~~for~~ for the two polarisations, but the refractive indices were measured in unpolarised light, so the correction is probably best made with the unpolarised absorption. To allow for the absorption we use equ. 2.29b of Moss (1961):

$$n_a - 1 = \frac{1}{2\pi^2} \int_{\bar{\upsilon}}^{\infty} \frac{K d\lambda}{1 - \left(\frac{\lambda}{\lambda_a}\right)^2} \qquad (6.5.1)$$

Table 6.5.1.

Energy (cm^{-1})	phonon contributions 4	3	2	1	Total 1-4	$n_\perp^2$	correction	corrected $n_\perp^2$	phonons 2	1	total	$n_{//}^2$	correction	Corrected $n_{//}^2$
900									.03	1.925		2.220	+.006	2.226
950									$.02_7$	1.670		2.478	+.011	2.589
1000	.016	.378	.099	.88	1.373	2.412	+.017	2.429	$.02_4$	1.462		2.689	+.017	2.706
1100	.013	.310	$.080_5$	.666	1.070	2.715	(-.010)	2.705	.02	1.155		3.000	(-.010)	2.990
1200	.011	.259	.067	.529	.866	2.919	-.008	2.911	$.01_7$	.940		3.218	-.008	3.266
1400	.008	.187	.048	.360	.603	3.182	-.003	3.179	.012	.660		3.503	-.003	3.506
1700									.008	.432		3.735	$-.001_5$	3.736
2000	.004	.092	.023	.160	.279	3.506	-.001	3.505	.006	.305		3.864	-.001	3.865
2500	$.002_5$	.0575	.0147	.099	.174	3.611			.004	.192		3.979		
4000	.001	$.022_3$	$.005_6$	$.037_4$	.066	3.719			.002	$.073_5$		4.100		
5000	.0006	$.014_2$	$.003_6$	$.023_8$	.042	3.743			.001	.045		4.127		

Here we want to isolate the effect of a small part of all absorption, so we write 6.5.1 as

$$n_a = (n_o)_a + \frac{1}{2\pi^2} \int_{8.8}^{10} \frac{Kd\lambda}{1-\left(\frac{\lambda}{\lambda_a}\right)^2}$$

where $(n_o)_a$ is what n_a would have been at wavelength λ_a without the extra absorption. The change in dielectric constant (n_a^2) can be seen to be

$$\frac{(n_o)_a}{\pi^2} \left[\frac{\int Kd\lambda}{1-\left(\frac{9.4}{\lambda_a}\right)^2}\right]$$

where we have approximated the absorption to be concentrated at 9.4 μ. (This approximation must certainly not be used between 8.8 and 10 μ). K averages about 100 cm^{-1} in the region, so $\int Kd\lambda = .012$. These corrections are calculated and shown in table 6.5.1.

6.5.2 Multiphonon Lattice "Peaks"

Summitt and Borelli (1965) give an interpretation of some of the absorption "peaks" between 7 and 13 μ. This, however, seems very optimistic and tenuous. The "peaks" represent not fixed energies, but maxima in phonon density of states functions (as is corroborated by the broad and variously shaped "peaks"). There are not even any "van Hove singularities" clearly resolved to help pinpoint features. It seems to the present author that any interpretation of these "peaks" must wait until a much fuller understanding of the whole phonon spectrum is obtained, including phonons that are not I.R. active and the symmetries and selection rules.

However, the final rise in the absorption at 11-12μ ($\perp$ absorption) and $\sim$13μ ($\parallel$ absorption) can be related to the broadening of the highest energy main phonon peaks. The difference between the above wavelengths supports the interpretation (see 5.6) of the $\parallel$ peak being at a longer wavelength than the $\perp$ one.

6.5.3 Short Wave Length Dispersion

Absorption in the U.V. region would not normally be expected to be uniform, and fairly pronounced maxima would be expected, due perhaps to maxima in density of states functions. Maxima have been observed in other semi conductors (see e.g. Moss 1961). For this reason it is reasonable to try to explain the dispersion curve mainly in terms of a single oscillator in the U.V., although this will only be an approximation. In particular, the refractive index close to the U.V. absorption edge will be affected by the moderately large absorption nearby. So the model used to fit the results was a single large oscillator and a small one near the edge. Another factor to be born in mind is the multiplicity of valence bands. How good the model might be can be judged from the results. A little algebra makes the model clearer.

The model is

$$n^2 = A + \frac{B\lambda^2}{\lambda^2 - \lambda_1^2} + \frac{C\lambda^2}{\lambda^2 - \lambda_2^2} \qquad (6.5.1)$$

or, expanding, $n^2 = A+B+C+ \frac{1}{\lambda^2}\left[B\lambda_1^2 + C\lambda_2^2\right] + \frac{1}{\lambda^4}\left[B\lambda_1^4 + C\lambda_2^4\right] + \ldots$ (6.5.2)

This shows how the effect of the smaller oscillator (with λ_2) increases for smaller λ (if $\lambda_2 > \lambda_1$).

The five adjustable parameters A, B, C, λ_1, λ_2 of course give a lot of freedom and many combinations would give quite good fits. However for the model to be useful we want (1) C small and λ_2 close to the absorption edge so that it is only really a correction factor and (2) B to be large and A not very much greater than unity (A - 1 represents contributions at wavelengths much shorter than λ_1, e.g. transitions from inner electrons to the conduction band. These are usually small). The results of a little trial and error are shown in tables 6.5.2 and 3 and also plotted in Fig 5.4.4. (The experimental values for the longer wavelengths need correction for the small I.R. contribution). As can be seen there is a reasonable scatter of points, except around $\lambda = 3800\text{Å}$ where there appears to be a jump of about 1 in 400 (1 in 800 in n) which is more than double what the maximum error should be (for nearby points) and is difficult to explain physically for the extraordinary index where the absorption edge is farther away. (For that index it coincides with the rise of the hump in the absorption (see sec. 6.2). However that is only $K \sim 30\text{cm}^{-1}$ and using e.g. the formula given by Moss 1961 (equ. 2.29(b)) $n_a - 1 = \frac{1}{2\pi^2} \int_0^\infty \frac{K d\lambda}{1 - \frac{\lambda^2}{\lambda_a^2}}$ for the relation between K and n_a, a contribution of $\sim 10^{-5}$ only is obtained. n_a is the index at λ_a). So further wavelength calibrations are called for (about 3 - 4 Å is the discrepancy).

The model fits both indices fairly well, perhaps the extraordinary one better.

Extraordinary Index

This was fitted by

$$n^2 = 1.44 + \frac{2.7}{1 - \frac{.024}{\lambda^2}} + \frac{.015}{1 - \frac{.078}{\lambda^2}}$$

Table 6.5.2.

λ	$\frac{1}{\lambda^2}$	n^2(calculated)	n^2(observed)	Contribution from I.R.	Discrepancy (10^3) (n^2calc.-n^2obs.-I.R.)
1.0034	.993	4.231	4.218	.010	+3
.9681	1.067	4.237	4.229	.009	-1
.9308	1.153	4.243	4.224	.009	+10
.8374	1.425	4.263	4.253	.007	+3
.7610	1.727	4.284	4.281	.006	-3
.6972	2.05	4.308	4.301	.005	+3
.6352	2.48	4.340	4.335	.004	+1
.5894	2.88	4.369	4.364	.004	+1
.5456	3.36	4.407	4.405	.003	-1
.5056	3.91	4.451	4.449	.003	-1
.4670	4.58	4.507	4.500	.002	+5
.4434	5.09	4.551	4.540	.002	+9
.4165	5.76	4.610	4.597	.002	+11
.3959	6.38	4.668	4.654	.002	+12
.3840	6.78	4.707	4.700	.001	+6
.3690	7.35	4.763	4.763	.001	-1
.3588	7.79	4.809	4.810	.001	-2
.3475	8.285	4.862	4.861	.001	0
.3382	8.75	4.915	4.916	.001	-2
.3299	9.20	4.968	4.974	.001	-7
.3221	9.635	5.022	5.033	.001	-12
.3130	10.20	5.098	5.133	.001	-16

Table 6.5.3.

λ	$\frac{1}{\lambda^2}$	n^2calc.	n^2obs.	Contribution from I.R.	n^2calc.-n^2obs.-I.R.
	.993	3.838	3.828	.010	0
	1.076	3.844	3.839	.009	-5
	1.153	3.850	3.894	.009	+7
	1.425	3.869	3.861	.007	+1
	1.727	3.891	3.888	.006	-3
	2.05	3.915	3.908	.005	+2
	2.48	3.947	3.942	.004	+1
	2.88	3.978	3.972	.004	+2
	3.36	4.018	4.014	.003	+1
	3.91	4.065	4.062	.003	0
	4.58	4.126	4.118	.002	+6
	5.09	4.175	4.164	.002	+9
	5.76	4.244	4.231	.002	+11
	6.38	4.314	4.304	.002	+8
	6.78	4.365	4.363	.001	+1
	7.35	4.441	4.450	.001	-10
	7.79	4.508	4.517	.001	-10
	8.22	4.585	4.597	.001	-13
3433	8.50	4.643	4.651	.001	-9

λ being measured in μ. So $\lambda_1 = 1550\text{Å}$, $\lambda_2 = 2790\text{Å}$. The second oscillator is just a correction factor, and certainly does not mean there is a peak at 2800Å. Taking it to represent absorption from 2550-3000Å, the average absorption coefficient from Moss's formula given above is $K = \frac{.0037 \times 2\pi^2}{450 \times 10^{-8}} = 1.7 \times 10^4 \text{ cm}^{-1}$, which is in order of magnitude agreement with extrapolated values of the absorption coefficient (see 5.1) (Explanatory note:- the oscillator gives a contribution of .015 to n^2 at $\lambda = \infty$. This corresponds to a contribution of .0037 to n).

For the main oscillator, equ. 6.5.2 shows that the most accurately known parameter is $B\lambda_1^2$ (the coefficient of $\frac{1}{\lambda^2}$) However large departures from the values given for λ_1^2, and B separately give considerably worse fits, and if the model is roughly applicable, they should be right to within 10%. Although other more complicated models would give equally good fits, the fact that a single main oscillator fits fairly well shows that a single main peak is possible. Very little can be deduced about the shape of the peak. The value of A should be > 1, giving a maximum value of B of 3.1 showing that the minimum value of λ_1 is 1460Å (from the value of $B_1\lambda_1^2$).

Ordinary Index

This was fitted by

$$n^2 = 1.572 + \frac{2.15}{1 - \frac{.028}{\lambda^2}} + \frac{.050}{1 - \frac{.094}{\lambda^2}}$$

implying $\lambda_1 = 1670\text{Å}$ $\lambda_2 = 3070\text{Å}$. The model does not fit quite so well here, as the small oscillator is three times bigger than previously and the large one 25% smaller, leaving A bigger at 1.57(2). However,

the size of the small oscillator agrees with the larger extrapolated value of the ordinary ray absorption coefficient (see 5.1) and also with the thin film measurements. The film measurements are presumably determined by $\frac{2}{3} K_{\perp}$. If the small oscillator represents absorbtion from 2850Å to 3300Å, the average value of K is $5.5 \times 10^4 cm^{-1}$.

The fact that the main oscillator is considerably smaller than for the other polarisation and the value of A larger (in spite of being the smaller refractive index) indicates that the peak is less pronounced. This is also borne out by the larger small oscillator and fairly large thin film values down to 2400Å (assuming them to be due to this coefficient).

Both Polarisations

A more rigorouse use of the U.V. refractive indices would be as a check on U.V. absorption results by the use of integral formulae given in 2.3.

The position of the main peaks at about 7.4 and 8.0 e.v. can be correlated with m_c. The peak is likely to roughly correspond with the maximum in the density of states where the conduction band flattens off at the edge of the Brillouin zone. If the Brillouin zone is approximated by a sphere in the usual way then this maximum occurs about 4.2e.v. above the bottom of the band for $m_c = .028m$ and for a sinusoidal band. If the weighted mean energy of the valence band is 0.8 e.v. from top of the band, and the band gap is taken as 3.5e.v., then the conduction band width works out at 3.1 and 3.7 e.v. for the two polarisations, compared with the figure of 4.2e.v. given above. This agreement is satisfactory in the circumstances. (It should be noted that most values of m_c quoted in

the literature are smaller than 0.28m, and these would give worse agreement).

A curiosity is that the smaller refractive index belongs to the polarisation which has the absorption edge and main oscillator peak at longer wavelengths. This is the reverse of what is expected on simple ideas.

7.0 DISCUSSION

A reasonably consistent picture of many of the properties of SnO_2 has emerged from the work. Partly because a good understanding of some of the properties was not achieved until after the experimental work had finished, more experiments could be made to test specific parts of the theory. Also, a better understanding of some parts of the theory is needed. For brevity we shall only discuss a few points here, rather than repeating many points made earlier.

Quite a lot of filling out of the bare bones of theory and experiment presented here could be done by the same methods as used here. (Indeed, we still have some unanalysed results).

Somewhat different new approaches might be:

(a) An application of group theory to both the valence and conduction bands. For the conduction bands the effect of the two tin atoms in the unit cell should be clarified.

(b) A good appreciation of how far the valence electron wave functions should be treated on an atomic, and how far on a unit cell basis.

(c) Sharp zero phonon absorption lines at around 2.9 e.v. might be looked for in thick crystals with high defect concentrations.

(d) The distorting effect of polaron effects on the conduction band and hence on a range of other properties might be investigated. For example from I.R. work Lyashenko and Miloslavskii (1965) obtained an effective mass varying with (degenerate) carrier concentration

(e) The similarities and differences of SnO_2 and Cu_2O should be explored. Both have forbidden exciton spectra, but multi-phonon assisted transitions appear to be unimportant in Cu_2O, indicating low phonon coupling. The dielectric constants of Cu_2O are quoted as $\epsilon_\infty = 7.3$ and $\epsilon_s = 8.5$ by several authors, which would indicate surprisingly small ionicity. Brown (1963) quotes $\epsilon_\infty = 4.0$ and $\epsilon_s = 10.5$ which would give stronger coupling than is observed. The latter figures seem dubious as the reference quoted by Brown is irrelevant and so his source cannot be checked. Assuming the former figures to be correct the small difference between them compared with SnO_2 is surprising because Pauling (1960) quotes the relevant electro-negativity values as both being 1.9. A small factor that would make SnO_2 more ionic is that the Madelung constant of rutile is slightly more than that of cuprite. This factor would only be small, and so there would seem to be scope for further work here.

Finally, the references are not intended as a complete bibliography, but are generally only those that arise directly from the text.

REFERENCES

NOTE → "Polarons and Excitons" referred to several times below is edited by C. G. Kuper and G. D. Whitfield, published by Oliver and Boyd.

Allcock G.R. (1963) "Polarons and Excitons" p.45.

Avai T. (1960) J. Phys. Soc. Japan 15 916.

Baur W. H. (1956) Acta Cryst.. 9 515.

Brown F. C. (1963) "Polarons and Excitons" p. 325.

Cardona M. and Harbeke G. (1965), Phys. Rev. 137 A. 1467.

Cochran W. (1965)Private Communication.

Cochran W. and Cowley R. A. (1962) J. Phys. Chem. Solids 23 447.

Cotton F. A. and Wilkinson G. "Advanced Inorganic Chemistry".

Coulson V. A. (1952) 'Valence' O.U.P.

Cowley R. A. (1963) Advances in Physics 12 421.

Dayal B. (1950) Proc. Indian Academy Sc. A, 32 304.

Ditchburn R. W. (1952) "Light" Blackie, London.

Dumke W. P. (1961) Phys. Rev. 134 1813.

Eagles D. M. (1963) Phys. Rev. 130 1318.

Eagles (1964) J. Phys. Chem. Solids 25 1243.

" (1966A) Phys. Rev. 145 645.

" (1966B) Private Communication.

" (1967) Private Communication.

Ecklebe (1932), quoted in "System of Mineralogy" by Dana, 7th ed. (1944).

Elliott R.J. (1957) Phys. Rev. 108 1384.

Elliott R. J. (1961) Phys. Rev. 124 340.

" (1963) "Polarons and Excitons" p. 269.

Feynman R. P. (1955) Phys. Rev. 97 660.

" , Hellwarth R. W., Ikkings C. K. and Platzman P. M. (1962), Phys. Rev. 127 1004.

Fröhlich H., Petzer H. and Zienau S. (1950) Phil. Mag. 41 221.

Grant F. A. (1959)Rev. Mod. Phys. 31 646.

Gurevich V. L. Lang I.G., Firsov Yu. A. (1962) Soviet Physics - Solid State 4 918.

Haken (1963) "Polaron and Excitons" p. 295.

Holstein (1959) Annals of Physics 8 325 and 343.

Hopfield J. J. and Thomas D. G. (1961) Phys. Rev. 122 35.

Houston J. E. and Kohnke E. E. (1965) J. Appl. Phys. 36 3931

Howarth D.J. and Sondheimer E.H. (1953), Proc. Roy. Soc. A219 53

Hrivnak L. (1959) Czech. J. Phys. 9 685

Ishiguro K., Sasaki T., Arai T. and Imai I. (1958) J. Phys. Soc. Japan 13 296

Kahn A.H. and Leyendecker A.J. (1964) in Physics of Semiconductors, 7th Int. Conf. Paris and Phys. Rev. 135 A1321.

Kew (1959) "Optical Mineralogy" McGraw-Hill, New York.

Knox R.S.(1963) "Theory of Excitons" Academic Press

Koch H. (1964) Phys. Stat. Sol. 7 263

Kohnke E.E. (1962) J. Phys. Chem. Solids 23 1557

Kurosawa (1961) J Physical Soc. Japan 16 1298

Lee T.D. and Pines D. (1952) Phys. Rev. 88 960

Larsen D.M. (1966) Phys. Rev. 144 697

Liebisch T. and Rubens H. (1919) Preuss. Akad. Wiss. Berlin 48 876

Loudon R. (1964) Advances in Physics 13 423

Lyashenko S.P. and Miloslavskii V.K. (1965) Optics and Spectroscopy 19 55

Lyashenko S.P. and Miloslavskii V.K.(1965B) Sov. Phys. - Solid State 6 2042

McLean T.P. (1960) Progress in Semiconductors 5 53

Marley J.A. and MacAvoy T.C. (1961) J. Appl. Phys. 32 2501

Marley J.A. and MacAvoy T.C. (1962) U.S.A.F. Report AFCRL-62-771

Marley J.A. and Dockerty R.C. (1965) Phys. Rev. 140 A304

Miloslavskii V.K. (1959) Optics and Spectroscopy 7 154

Mooser E and Pearson W.B. (1956) J. of Electronics 1 629

Morgan D.F. and Wright D.A. (1966) Brit. J. Appl. Physics 17 337

Morgan D.F. (1966B) Private Communication

Morgan D.F. (1966C) Ph.D. Thesis, Durham University.

Moss T.S. (1961) Optical Properties of Semi-conductors" Butterworths, London.

Nagasawa M, Shionoya S and Makishima S (1965) Japanese J of Applied Physics 4 195

Nagasawa and Shionoya S (1966) Physics Letters 22 409

Nozieres P. and Pines D (1958) Phys. Rev. 109 1062

Pauling L (1960) "Nature of the Chemical Bond" 3rd Edition, Connell University Press.

Pines D. (1963), "Polarons and Excitons" p.33.

Platzman P.M. (1962) Phys. Rev. 125 1961

Platzman P.M. (1963A),"Polarons and Excitons" p.150

Platzman P.M. (1963B), "Polarons and Excitons" p.123

Reddaway S.F. and Wright D.A. (1965) Brit. J.Appl. Phys. 16 195

Reddaway S.F. (1966) Brit. J. Appl. Phys. 17 697

Schulman J. and Compton W. (1963) "Color Centres in Solids" Pergamon Press

Schultz T.D. (1959) Phys. Rev. 116 526

Schultz T.D. (1963) "Polarons and Excitons" p.112

Slater J.C. and Koster G.F. (1954) Phys. Rev. 94 1498

Spitzer W., Miller R, Kleinman D. and Howarth L. (1962) Phys. Rev.126 1710

Summitt R., Marley J.A. and Borrelli N.F.(1964) J.Phys. Chem. Solids 25 1465

Summitt R and Borrelli N.F. (1965) J.Phys. Chem. Solids 26 921

Summitt R. and Borrelli N.F. (1966) J. Appl. Phys. 37 2200

Summitt (1965) Private Communication.

Turner A.F. (1962) Third Quarter Report, Contract DA-44-009-ENG-4954, AD296457

Urbach F. (1953) Phys. Rev. 92 1324

Visvanathan S. (1960) Phys. Rev. 120 376 and 379

Whitfield G. and Puff R. (1965) Phys. Rev. 139 A338